LEABHARLANN CHOLÁISTE NA TRÍONÓIDE, BAILE ÁTHA CLIATH | TRINITY COLLEGE LIBRARY DUBLIN
Ollscoil Átha Cliath | The University of Dublin

Terms and Conditions of Use of Digitised Theses from Trinity College Library Dublin

Copyright statement

All material supplied by Trinity College Library is protected by copyright (under the Copyright and Related Rights Act, 2000 as amended) and other relevant Intellectual Property Rights. By accessing and using a Digitised Thesis from Trinity College Library you acknowledge that all Intellectual Property Rights in any Works supplied are the sole and exclusive property of the copyright and/or other IPR holder. Specific copyright holders may not be explicitly identified. Use of materials from other sources within a thesis should not be construed as a claim over them.

A non-exclusive, non-transferable licence is hereby granted to those using or reproducing, in whole or in part, the material for valid purposes, providing the copyright owners are acknowledged using the normal conventions. Where specific permission to use material is required, this is identified and such permission must be sought from the copyright holder or agency cited.

Liability statement

By using a Digitised Thesis, I accept that Trinity College Dublin bears no legal responsibility for the accuracy, legality or comprehensiveness of materials contained within the thesis, and that Trinity College Dublin accepts no liability for indirect, consequential, or incidental, damages or losses arising from use of the thesis for whatever reason. Information located in a thesis may be subject to specific use constraints, details of which may not be explicitly described. It is the responsibility of potential and actual users to be aware of such constraints and to abide by them. By making use of material from a digitised thesis, you accept these copyright and disclaimer provisions. Where it is brought to the attention of Trinity College Library that there may be a breach of copyright or other restraint, it is the policy to withdraw or take down access to a thesis while the issue is being resolved.

Access Agreement

By using a Digitised Thesis from Trinity College Library you are bound by the following Terms & Conditions. Please read them carefully.

I have read and I understand the following statement: All material supplied via a Digitised Thesis from Trinity College Library is protected by copyright and other intellectual property rights, and duplication or sale of all or part of any of a thesis is not permitted, except that material may be duplicated by you for your research use or for educational purposes in electronic or print form providing the copyright owners are acknowledged using the normal conventions. You must obtain permission for any other use. Electronic or print copies may not be offered, whether for sale or otherwise to anyone. This copy has been supplied on the understanding that it is copyright material and that no quotation from the thesis may be published without proper acknowledgement.

Bioenergetics and Mitochondrial Dynamics in Cancer Cells and Neurons

A dissertation submitted to Trinity College, University of Dublin,
in candidature for the degree of Doctor of Philosophy

Stephen Quinn

School of Biochemistry and Immunology
Trinity College Dublin

2012

TRINITY COLLEGE
2 5 SEP 2012
LIBRARY DUBLIN

Thesis 9618

Declaration

I declare that this thesis is entirely my own work and has not been submitted for any degree at this or at any other University. I agree that the library may lend or copy this thesis upon request.

Stephen Quinn

Acknowledgements

First and foremost, I must express my sincere gratitude to my supervisor, Dr. Gavin Davey, for giving me this opportunity, for his support, positive attitude and for his astounding patience. I would also like to thank Dr. Jeff O'Sullivan for being so supportive and so helpful (read: pushy!) when I needed it. I am indebted to Dr. Rashmi Upadhyay Pathak for her fantastic guidance and wisdom at the beginning of the project. I owe Dr. Orla Hanrahan a huge thank-you for getting me set up on the confocal and for all her great advice, confocal-related and otherwise! Of course, many thanks to Prof. Keith Tipton for the use of his lab facilities. I would also like to express my heartfelt gratitude to Dr. Derek Nolan, who was instrumental in securing the funding and time I needed to complete the final year of my project. In addition, I wish to thank my transfer viva examiners, Dr. Vinny Kelly, Dr. Colm Cunnigham and Dr. Daniela Zisterer, whose advice came at a critical point in the project and proved to be invaluable.

The best part of my Lab One experience has been getting to know its members, past and present, who have all been wonderful throughout my time there. Special thank-you to Jayne and Seán who helped me from when I was an annoying undergrad to when I blossomed into an annoying postgrad and of course to Martha for being a little lab mammy and looking after us. Super huge special thank you to my darlings Sonia, Laura, Emma and Susan, without whom I could never have got through this; the moanfests, the tired giddiness, the adventures to HazMat and the support were completely essential! I honestly couldn't have done it without you guys. Big thank-you to Kate (Special K) for being so much fun and for having such a brilliant attitude. How did we manage before you came along?! To all my other friends in Biochemistry, thank you all so much for the good times and for keeping me sane (especially those who brought me cakes and went for tea, you know who you are). To all my non-Biochem friends (I swear I have some), thanks for all the great nights out and the laughs. I definitely would have cracked without the comic relief. To the prep room staff, thanks for the chats and all the borrowed chemicals. Your relaxed and helpful attitudes made demonstrating a real pleasure. Many thanks to Bioresources for their essential service to the University. Of course, Mary Pat and Miriam surely deserve several rounds of applause (with standing ovations and flowers) for being the glue that keeps the School (and the desperate

students!) together. Thank you for all the chats and for re-teaching me how to use the fax machine every time I had to use it!

The support of my family was absolutely instrumental in allowing me to carry out this work. I can't possibly express in words my gratitude to my parents in giving me constant, unwavering encouragement throughout this entire process, even providing food and shelter in the last year! They have dealt with adversity in recent years with a courage that put me to shame for moaning about failed Western blots. Thank you so, so much. Also thanks for all the lovely dinners. To my ragamuffin brother John, thanks for always being optimistic and giving me a bit of perspective. I promise I will chill out now.

Finally, to my biggest support of all, Conor, who, more than anyone, had to deal with all the crazy hours and PhD madness everyday for the past four years and through it all, has been so patient, loving and supportive. I can't even put it into words. I promise I will do the same for you while you're becoming a doctor too! I would also like to thank Conor's family for their support and for allowing him to go out with a penniless graduate student.

I gratefully acknowledge the financial support of the Irish Research Council for Science, Engineering and Technology.

Summary

Mitochondria in mammalian cells exist as a highly dynamic and interconnected reticulum. This reticular ultrastructure is defined by the opposing forces of fission and fusion, mainly mediated by a group of large GTPases collectively known as mitodynamins. The regulation of fission and fusion is poorly understood but it is thought that bioenergetics and dynamics engage in a bi-directional crosstalk, such that disturbing one will have deleterious effects on the other. The pathophysiological hallmarks of mitochondrial dysfunction are evident both in cancer and neurodegeneration, implicating a role for disturbed mitochondrial dynamics. This study explores the effects of bioenergetic modulation on mitochondrial fusion rates in human cervical carcinoma HeLa cells and rat primary cortical neurons.

Cancer cells typically derive a disproportionate amount of ATP (~50% or higher) from glycolysis, owing to the Warburg effect. However, studies have shown that HeLa cells are capable of growth and proliferation when forced to derive ATP exclusively from oxidative phosphorylation (OXPHOS), a phenomenon that has been observed in large, aglycaemic tumours. In HeLa cells, this metabolic switch is accompanied by significant mitochondrial ultrastructural changes but it is not yet known if this corresponds to a change in fusion rates. Furthermore, it is not known if the sensitivity of fusion rates to bioenergetic modulation differs between these two metabolic phenotypes. Using live-cell confocal microscopy and HeLa cells expressing mitochondrially-targeted photo-activatable GFP, small regions of interest (ROIs) throughout the mitochondrial network were examined and mitochondrial fusion was compared under defined conditions.

Mitochondrial fusion rates in HeLa cells cultured in high glucose medium were impervious to inhibition of the electron transport chain (ETC) complexes. Fusion was significantly decreased following dissipation of the electrochemical gradient and inhibition of ATP synthase by oligomycin, but these effects were not linked to decreased cellular ATP levels. Inhibition of glucose metabolism by 2-deoxy-D-glucose (DOG) seriously compromised fusion rates, which correlated with a marked decrease in ATP. Fusion could not be restored by alternative energy substrates, such as L-glutamine and pyruvate, in the presence of DOG. In contrast, cells cultured in glucose-free, galactose/glutamine (OXPHOS-inducing) medium showed independence from sugar metabolism for maintenance of fusion at resting conditions. However, significant

sensitivity to mitochondrial inhibition was acquired; ETC/OXPHOS inhibitors blocked fusion, which correlated with decreased cellular ATP levels, increased recruitment of fission-mediating mitodynamin DRP1 and markedly higher cell death compared to glycolytic cells. Importantly, fusion could be restored in galactose-cultured cells if the ETC inhibitor was applied concurrently with a glucose bolus. Finally, early fusion inhibition across both substrates was predictive of complete fragmentation of the mitochondrial reticulum and cell death at later time points. Thus, HeLa cells exhibit substrate-dependent changes in mitochondrial dynamics in response to bioenergetic modulation.

Primary cortical neurons showed significant perturbation of fusion and complete fragmentation of the mitochondrial network within minutes of exposure to ETC/OXPHOS inhibitors, which correlated with significant reductions in mitochondrial membrane potential and cellular ATP levels. Significantly, the availability of glucose did not protect neuronal mitochondria from these effects, indicating a lack of metabolic flexibility in neurons that is detrimental to mitochondrial function. Titration of complex I activity using a piericidin A dose-response in non-synaptic rat brain mitochondria suggested that mitochondria of the neuronal soma could tolerate at least ~33% inhibition of the activity of this enzyme before fusion was seriously compromised. Thus, mitochondrial fusion was shown to be extremely sensitive to bioenergetic modulation in neurons, and subject to threshold effects. The differences between metabolic control in cancer cells and neurons in the context of mitochondrial dynamics are further discussed.

Table of Contents

DECLARATION i
ACKNOWLEDGEMENTS ii
SUMMARY iv
TABLE OF CONTENTS vi
ABBREVIATIONS xi

CHAPTER 1: General Introduction 1
1.1 Introduction 2
1.2 Mitochondrial Bioenergetics: An Overview 3
1.2.1 The Electron Transport Chain 3
1.2.2 Oxidative Phosphorylation 6
1.3 Mitochondrial Dynamics 10
1.3.1 Mitochondrial Fission 11
1.3.1.1 Regulation of Mitochondrial Fission 13
1.3.2 Mitochondrial Fusion 16
1.3.2.1 Regulation of Mitochondrial Fusion 21
1.4 Functions of Mitochondrial Dynamics 24
1.4.1 Maintenance and Sharing of mtDNA 26
1.4.2 A Role in Apoptosis 29
1.4.2.1 OPA1 in Apoptosis 30
1.4.2.2 DRP1 in Apoptosis 32
1.4.2.3 Mitofusins in Apoptosis 34
1.4.3 Mfn2 – Roles Outside of Fusion 35
1.4.4 Mitochondrial Dynamics and Bioenergetics 37
1.4.4.1 The Influence of Mitochondrial Dynamics on Bioenergetics 38
1.4.4.2 The Influence of Bioenergetics on Mitochondrial Dynamics 41
1.4.4.3 SIHF – Integration of the Bi-directional Crosstalk? 44
1.5 Conclusion 45
1.6 Aim of Thesis 47

CHAPTER 2: Materials and General Methods 48
2.1 General Methods 49

2.1.1 Antibodies and Reagents 49
2.1.2 Preparation of Solutions and Pipetting 49
2.1.3 Centrifugation 49
2.1.4 Electrophoresis 50
2.1.5 Experimental Animals 50
2.1.6 Cell Culture 50
2.1.7 Statistical Analysis 50
2.1.8 Image Processing 51
2.2 Protein Estimation 51
2.3 Western Blotting 51
2.4 Microscopy 53
2.4.1 Fluorescence Microscopy 53
2.4.2 Confocal Microscopy 50
2.4.3 Quantification of Mitochondrial Fusion Rates 53
2.4.4 Quantification of $\Delta\Psi_m$ 54
2.5 Immunocytochemistry 55
2.6 ATP Measurement 55
2.7 Molecular Biology 56
2.7.1 Transformation of Competent Bacterial Cells 56
2.7.2 Growth of Single Colonies and Miniprep 58
2.7.3 Restriction digest and Agarose Gel Electrophoresis 58
2.7.4 Glycerol Stocks and Maxiprep 58
2.8 Generation of DsRed-stable Clones 60
2.8.1 Neomycin Kill Curve 60
2.8.2 Transfection of Cells and Selection 60

CHAPTER 3: Bioenergetic Control of Mitochondrial Dynamics in HeLa Cells Cultured in High Glucose Medium 63
3.1 Introduction 64
3.1.1 Cancer Metabolism 64
3.1.1.1 The Warburg Effect 65
3.1.1.2 The Role of Mitochondria in Cancer 68
3.1.1.3 Mitochondrial Dynamics in Cancer 70
3.2 Aims of the Chapter 74

3.3 Methods 76
3.3.1 Cell Culture 76
3.3.2 Transient Transfection 76
3.3.3 Assessment of Mitochondrial Fusion Rates after Transient FCCP Exposure 76
3.3.4 Use of Krebs Buffer 77
3.4 Results 78
3.4.1 Mitochondrial Fusion Rates 78
3.4.2 Effects of Mitochondrial Inhibition on Fusion Rates 81
3.4.3 Effects of ETC Inhibition and Microtubule Disassembly on Mitochondrial Fusion Rates 89
3.4.4 Effects of Inhibition of Glucose Metabolism on Mitochondrial Fusion Rates 96
3.4.5 Effects of Inhibition of Oxidative Phosphorylation and Glucose Metabolism on Mitochondrial Membrane Potential 104
3.4.6 Effects of Inhibition of Oxidative Phosphorylation and Glucose Metabolism on Cellular ATP Levels 113
3.5 Discussion 116

CHAPTER 4: Bioenergetic Control of Mitochondrial Dynamics in HeLa cells Cultured in Galactose Medium 123
4.1 Introduction 124
4.2 Aims of the Chapter 127
4.3 Methods 129
4.3.1 Cell Culture 129
4.3.2 Transfection 129
4.3.3 Preparation of Whole Cell Lysates 129
4.3.4 Isolation of Mitochondria from Cells 129
4.3.5 Assessment of Mitochondrial Morphology after Six-Hour Inhibitor Exposure 130
4.3.6 Assessment of Cell Viability 130
4.4 Results 132
4.4.1 Effects of substrate Change on Mitochondrial Fusion Rates 132

4.4.2 Effects of Mitochondrial Inhibition on Fusion Rates in Gal-HeLa Cells 132
4.4.3 HeLa Cell Adaptation to Glucose-Free Environment and Independence from Sugars for Mitochondrial Fusion 137
4.4.4 Effects of Galactose Starvation and Inhibition of Oxidative Phosphorylation on Mitodynamins in Gal-HeLa Cells 150
4.4.5 Effects of Galactose Starvation and Inhibition of Oxidative Phosphorylation on Mitochondrial Membrane Potential in Gal-HeLa Cells 153
4.4.6 Effects of Galactose Starvation and Inhibition of Oxidative Phosphorylation on ATP levels in Gal-HeLa Cells 156
4.4.7 Effects of Longer Exposure to Mitochondrial Inhibitors on Mitochondrial Morphology and Cell Viability 156
4.5 Discussion 163

CHAPTER 5: Bioenergetic Control of Mitochondrial Dynamics in Primary Cortical Neurons 171
5.1 Introduction 172
5.1.1 Mitochondrial Dynamics in Neurons 172
5.1.2 Mitochondrial Dysfunction and Dynamics in Alzheimer's Disease 176
5.1.3 Mitochondrial Dysfunction and Dynamics in Parkinson's Disease 178
5.1.4 Mitochondrial Dysfunction and Dynamics in Huntington's Disease 181
5.2 Aims of Chapter 184
5.3 Methods 185
5.3.1 Primary Cortical Neurons 185
5.3.2 Transfection 185
5.3.3 Isolation of Rat Brain Mitochondria and Synaptosomes 186
5.3.4 Complex I Assay 186
5.3.5 Confocal Microscopy 188
5.3.5.1 Quantification of Mitochondrial Fusion Rates 188
5.3.5.2 Quantification of $\Delta\Psi_{m}$ 189

5.4 Results 190
5.4.1 Optimisation of Primary Neuron Culture 190
5.4.2 Effects of Inhibition of Oxidative Phosphorylation on Mitochondrial Fusion Rates in Primary Cortical Neurons 192
5.4.3 Effects of Inhibition of Oxidative Phosphorylation on Mitochondrial Membrane Potential in Primary Cortical Neurons 192
5.4.4 Effects Inhibition of Oxidative Phosphorylation on ATP Levels in Primary Cortical Neurons 204
5.4.5 Threshold Effects of Complex I Inhibition on Mitochondrial Fusion Rates in Primary Cortical Neurons 205
5.5 Discussion 222

CHAPTER 6: General Discussion 229
6.1 General Discussion 230
6.2 Future Work 232
6.3 Conclusions of the Thesis 236

BIBLIOGRAPHY 237

Abbreviations

ABC1	ATP-binding cassette protein 1
ADP	Adenosine diphosphate
ADOA	Autosomal dominant optic atrophy
AICAR	5-aminoimidazole-4-carboxamide-1-β-D-ribofuranoside
AMPK	Adenosine monophosphate-activated kinase
ANOVA	Analysis of variance
ANT	Adenine nucleotide translocase
Anti A	Antimycin A
Apaf-1	Apoptosis protease-activating factor-1
APC^{Cdh1}	Anaphase-promoting complex-Cdh1
Ara-C	Cytosine β-D-arabinofuranoside
ARJPD	Autosomal recessive juvenile Parkinson's disease
ATP	Adenosine triphosphate
BAR	Bin-Amphiphysin-Rvs
BAT	Brown adipose tissue
Bcl-2	B-cell lymphoma-2
BMI	Body mass index
BSA	Bovine serum albumin
CaMKIα	Ca^{2+}/calmodulin-dependent protein kinase Iα
CCCP	Carbonyl cyanide-*m*-chlorophenylhydrazone
CMTIIa	Charcot Marie Tooth Disease, type IIa
CoQ	Coenzyme Q
$CoQH_2$	Coenzyme Q, reduced
DAPI	4,6-diamidino-2-phenylindole
DMEM	Dulbecco's modified Eagle's medium
Dmfn	*Drosophila* mitofusin
DMSO	Dimethyl sulfoxide
dmn1	Yeast homologue of DRP1
DNA	Deoxyribonucleic acid
2,4-DNP	2,4 Dinitrophenol
DOG	2-Deoxy-D-glucose
DRP1	Dynamin related protein 1

DsRed	*Discosoma sp.* red protein
ER	Endoplasmic reticulum
ETC	Electron transport chain
$FAD(H_2)$	Flavin adenine dinucleotide (reduced)
FCCP	Carbonyl cyanide-*p*-trifluoromethoxyphenylhydrazone
FMN	Flavin mononucleotide
FRAP	Fluorescence recovery after photobleaching
Gβ2	Guanine nucleotide binding protein-β subunit 2
GED	GTPase effector domain
GFP	Green fluorescent protein
Gln	Glutamine
GPCR	G-protein coupled receptor
GTP	Guanosine triphosphate
G-6-P	Glucose-6-phosphate
G6PDH	Glucose-6-phosphate dehydrogenase
hFis1	Human fis1
HK	Hexokinase
H_2O_2	Hydrogen peroxide
HR	Heptad repeat
HSD	Honestly significant difference
HSF	Human skin fibroblast
HSP	Hereditary spastic paraplegia
IM	Inner membrane, mitochondrial
IMS	Intermembrane space
KCN	Potassium cyanide
LDH	Lactate dehydrogenase
LHON	Leber's Hereditary Optic Neuropathy
L-OPA1	Long form of optic atrophy 1
Mal	Malonate
MEF	Mouse embryonic fibroblasts
MELAS	Mitochondrial myopathy, encephalopathy, lactic acidosis, and stroke
MERRF	Myoclonic epilepsy and ragged-red fibres
Mff	Mitochondrial fission factor
Mfn	Mitofusin

MIB	Mitofusin binding protein
mTOR	Mammalian target of rapamycin
Mief1	Mitochondrial elongation factor 1
mK_{ATP}	Mitochondrial ATP-sensitive potassium channels
MOMP	Mitochondrial outer membrane permeabilisation
MnSOD	Manganese superoxide dismutase
MPP^+	1-methyl-4-phenylpyridinium
mtDNA	Mitochondrial deoxyribonucleic acid
MTP18	Mitochondrial protein, 18kDa
MTS	Mitochondrial targeting sequence
3-NP	3-nitropropionic acid
NAD(H)	Nicotinamide adenine di nucleotide, reduced
NADPH	Nicotinamide adenine dinucleotide phosphate, reduced
NMDA	N-methyl-D-aspartate
NSM	Non-synaptic mitochondria
$O_2^{-}\cdot$	Superoxide anion
$\cdot OH$	Hydroxyl radical
Oligo	Oligomycin
OM	Outer membrane, mitochondrial
OPA1	Optic atrophy 1
OXPHOS	Oxidative phosphorylation
PAGE	Polyacrylamide gel electrophoresis
PA-GFP	Photo-activatable green fluorescent protein
PBS	Phosphate buffered saline
PD	Parkinson's Disease
PEG	Polyethylene glycol
PFKFB3	6-Phosphofructo-2-kinase/fructose-2,6-bisphosphatase 3
PGC-1	Peroxisome proliferator-activated receptor γ coactivator 1
PH	Pleckstrin Homology
PHB	Prohibitin
PI	Pixel intensity
PINK1	PTEN-induced putative kinase 1
PMF	Protonmotive force
PPP	Pentose phosphate pathway

PTM	Post-translational modification
PTP	Permeability transition pore
Pier A	Piericidin A
RCR	Respiratory control ratio
ROI	Region of interest
Rot	Rotenone
SD	Standard deviation
SDS	Sodium dodecyl sulphate
SEM	Standard error of the mean
shRNA	Short hairpin ribonucleic acid
SIHF	Stress induced hyperfusion
SLP2	Stomatin-like protein
TCA	Tricarboxylic acid
RCR	Respiratory control ratio
tRNA	transfer ribonucleic acid
ROS	Reactive oxygen species
S-OPA1	Short form of optic atrophy 1
SNARE	Soluble N-ethymaleimide-sensitive factor attachment protein receptor
Tfam	Mitochondrial transcription factor A
TMRM	Tetramethyl rhodamine methyl ester
TSC1	Tuberous sclerosis complex 1
UCP	Uncoupling protein
VDAC	Voltage dependent anion channel
YME1L	Yme1-like protein
YY1	Yin-yang 1

CHAPTER 1

General Introduction

1.1 Introduction

Mitochondria are highly dynamic organelles with essential roles in energy production and apoptosis regulation in the eukaryotic cell. Thought to have arisen from endosymbiosis of an alpha-proteobacterium (Gray *et al.*, 1999, Gabaldon and Huynen, 2007), they are vital organelles in the production of adenosine triphosphate (ATP, the energy transfer molecule of the cell), catabolic and anabolic metabolism, calcium buffering and programmed cell death (Billups and Forsythe, 2002, Suen *et al.*, 2008). Given their essential roles across myriad cellular functions, there exists a significant number of human disorders associated with mitochondrial dysfunction, known collectively as 'mitochondrial diseases' including myoclonic epilepsy and ragged-red fibres (MERRF), Leber's Hereditary Optic Neuropathy (LHON) and Leigh syndrome (Wallace, 1999). Furthermore, mitochondrial dysfunction has been implicated in the pathophysiologies of a diverse number of other diseases, including cancer (Modica-Napolitano and Singh, 2002) and neurodegeneration (Schon and Przedborski, 2011).

The term 'mitochondrion', first coined in 1898 by German biologist Carl Benda (Bechtel and Abrahamsen, 2007), is derived from the Greek *mitos*, meaning 'thread' and *khondrion,* the diminutive of *khondros*, meaning 'granule' (Baloh, 2008). True to their name, these organelles exist in both tubular and punctate forms within the cell as part of an interconnected reticulum, owing to continuous fission and fusion events governing their shape. The field of mitochondrial dynamics in mammalian cells has become a major research interest in the past decade; continuous remodelling of mitochondrial structure in response to physiological and environmental cues is essential to accommodate different demands on mitochondrial function during growth, differentiation, and maintenance (Chen and Chan, 2009, Kageyama *et al.*, 2011) and during embryonic development, particularly in the central nervous system (CNS) (Chen *et al.*, 2003, Ishihara *et al.*, 2009). The balance of these opposing processes is tightly regulated by numerous mechanisms, and there exists a complex cross-talk between mitochondrial bioenergetic state and dynamics, the intricacies of which have yet to be fully characterised. The matter is obfuscated by several factors, not least by the functional and morphological heterogeneity in mitochondria across cell types (Sauvanet *et al.*, 2010). Moreover, it is not yet known if mitochondrial bioenergetics regulates dynamics, or vice versa, though there is evidence to support both hypotheses (Legros *et al.*, 2002, Rossignol *et al.*, 2004, Benard *et al.*, 2011, Gomes *et al.*, 2011). What follows is a brief overview of mitochondrial

bioenergetics, followed by a review of our current knowledge of mitochondrial fission and fusion. Several aspects of mitochondrial dynamics will be described, including the molecular mechanisms underlying and regulating these processes, their functional significance at the organellar and cellular levels, and their interaction with mitochondrial bioenergetics.

1.2 Mitochondrial Bioenergetics: An Overview

Mitochondria are responsible for the production of 80 - 90% of cellular ATP (Zablockaite *et al.*, 2007). Their double-membrane structure facilitates intra-organellar compartmentalisation with high functional specificity and the integration of multiple metabolic pathways. Through the oxidation of amino acids, β-oxidation of fatty acids and the tricarboxylic acid cycle (TCA), mitochondria can generate reduced forms of nicotinamide adenine dinucleotide and flavin adenine dinucleotide (NADH and $FADH_2$, respectively). These reduced equivalents are used as electron donors to the electron transport chain (ETC), a group of four enzymes (complexes I – IV) located on the mitochondrial inner membrane (IM). According to chemiosmotic theory (Mitchell, 1961), the free energy liberated from the passage of electrons from each enzyme of the ETC is harnessed by complexes I, III and IV to translocate protons (H^+) from the mitochondrial matrix into the intermembrane space (IMS) against their concentration gradient, thus establishing a protonmotive force (PMF). While the electrons are ultimately used to reduce molecular oxygen to water, the PMF is utilised by another IM enzyme, F_1/F_o ATPase (ATP synthase), to generate ATP from inorganic phosphate (P_i) and adenosine diphosphate (ADP, fig 1.1). Newly formed ATP is translocated to the cytosol by the adenine nucleotide translocase (ANT), an IM antiporter which exchanges ATP for ADP. This process of coupling respiration to ATP generation, called 'oxidative phosphorylation' (OXPHOS), is responsible for an estimated 90% of mammalian oxygen consumption (Benard *et al.*, 2011).

1.2.1 The Electron Transport Chain

The electron transport chain is composed of four enzymatic complexes and two electron carrier intermediates, coenzyme Q (CoQ) and cytochrome c. While the supramolecular structure of complexes I – IV in the mitochondrial IM is not fully understood, it is thought that single ETC complexes co-exist as supercomplexes – stoichiometrically

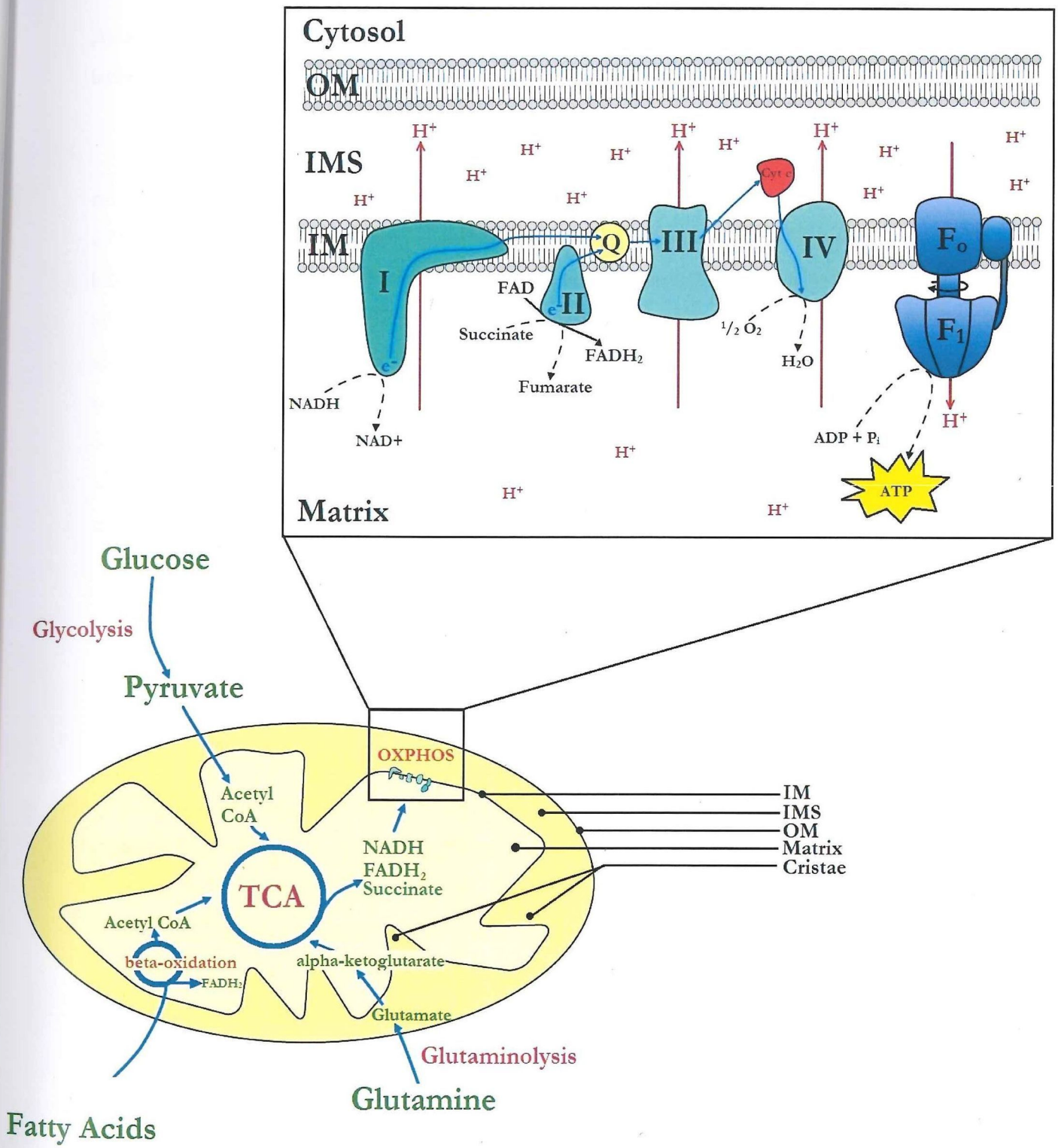

Figure 1.1: Selected pathways in mitochondrial bioenergetics. Multiple cellular catabolic pathways converge at the tricarboxylic acid (TCA) cycle, including glycolysis, amino acid oxidation (in this example, glutaminolysis) and β-oxidation of fatty acids. Reduced equivalents nicotinamide adenine nucleotide (NADH) and flavin adenine nicotinamide ($FADH_2$) donate electrons (e^-) to the electron transport chain (inset) to promote oxidative phosphorylation (OXPHOS). Complex I accepts electrons from NADH and uses free energy from the reduction of coenzyme Q (Q) to extrude protons (H^+) out of the matrix, thus contributing to the electrochemical gradient. Complex II oxidises succinate, whilst reducing FAD, which reduces coenzyme Q. Coenzyme Q passes electrons to complex III, which also translocates protons as it reduces cytochrome c (Cyt c). Complex IV accepts electrons from cyt c and reduces molecular oxygen to water, whilst translocating protons. Finally, ATP synthase (F_o/F_1 ATPase) utilises the protonmotive force generated by electron transport in the production of ATP. Protons travel through a channel in the F_o domain, with causes the rotation of a central rotary stalk, causing conformational changes in the β subunits of the F_1 region, leading to the sequential binding of ADP inorganic phosphate (P_i), ATP generation and ATP release. IM, mitochondrial inner membrane; IMS, intermembrane space; OM, outer membrane.

diverse assemblies of multiple ETC enzymes known as 'respirasomes' (Bianchi *et al.*, 2004, Boekema and Braun, 2007). The ETC machinery is enriched in mitochondrial cristae; large folds of the highly convoluted IM that project into the matrix.

Complex I (NADH dehydrogenase), the first and largest enzyme of the ETC, comprises 45 subunits that assemble into a hydrophobic membrane-spanning arm and a perpendicular hydrophilic matrix-facing arm. Within complex I, electrons from oxidised NADH are transferred to a non-covalently bound flavin mononucleotide (FMN) and thence, down a chain of several iron-sulphur clusters to the mobile CoQ, a quinone derivative with a hydrophobic isoprenoid tail. For every electron pair transported by complex I, four protons are translocated from the matrix to the IMS. Coenzyme Q also accepts electrons from complex II (succinate dehydrogenase), the only ETC enzyme that also participates in the TCA cycle but does not transport protons. Complex II oxidises succinate to fumarate, whilst reducing FAD to $FADH_2$, which, in turn reduces CoQ. Reduced CoQ ($CoQH_2$) then transfers electrons to complex III.

Complex III (cytochrome bc_1) contains two b-type cytochromes, a c_1 cytochrome and an iron-sulphur cluster, and mediates the reduction of cytochrome c by $CoQH_2$. This occurs through a process known as the Q cycle, in which $CoQH_2$ undergoes two cycles of reoxidation, the net result being the reduction of two cytochrome c proteins (one electron each) and the translocation of four protons for every $CoQH_2$ oxidised. Complex III does not function as a proton pump *per se* (as with complex I and IV), rather, it facilitates the redox of $CoQH_2$, which in turn facilitates the translocation of protons across the IM. Cytochrome c is a small, soluble and mobile electron carrier loosely associated with the IM in the IMS. It shuttles electrons from complex III to complex IV.

Complex IV (cytochrome c oxidase) is the terminal enzyme for the transported electrons and the site at which they are used to reduce molecular oxygen to water. It exists as a transmembrane dimer containing four redox centres – cytochromes a and a_3, a copper atom called Cu_B and a copper atom pair called the Cu_A centre. At the cytochrome a_3-Cu_B complex, four electrons from four individual cytochrome c proteins are used to reduce one molecular oxygen molecule to two water molecules. In addition to the four protons used to create water, another four are translocated across the IM. In total, for every

electron pair transported by the ETC, 10 protons are translocated and one molecule of water is generated.

1.2.2 Oxidative Phosphorylation

The PMF (alternatively called a pH gradient) that is generated by the active pumping of protons across the IM reaches a maximal value of ~180 – 220 mV (Brand and Nicholls, 2011) and confers a net negative charge to the mitochondrial matrix. It comprises two elements: an electric potential ($\Delta\Psi$) and a chemical potential ($\Delta\mu_{H+}$). At physiological conditions, mitochondria can alternate between two energy-production states; state 4, in which respiration is slow and there is little ATP production (creating a higher mitochondrial membrane potential ($\Delta\Psi_m$)) and state 3, in which respiration is fast and ATP is produced (creating a lower $\Delta\Psi_m$).

Discharge of the PMF is an exergonic process (energy-releasing), a property exploited by ATP synthase (also called complex V) to generate ATP. ATP synthase is both ubiquitous and unique; it is one of the most abundant and highly conserved proteins across species but also one of only two proteins known to use a rotary motion as a step of catalysis (the other being the bacterial flagellum) (Noji *et al.*, 1997, Yoshida *et al.*, 2001). The mechanism of ATP synthesis by this enzyme is called the 'binding change' mechanism, proposed by Paul Boyer (Kayalar *et al.*, 1977). ATP synthase is composed of a hydrophobic transmembrane portion (F_o) and a hydrophilic matrix portion (F_1), connected by a central rotor portion and an outer stator portion (which prevents movement of F_1 with the central rotor). As protons pass through F_o, a central set of F_o subunits rotate, leading to the rotation of the central rotor portion. This causes conformational changes in the β subunits of F_1, which leads to the sequential binding of ADP + P_i, ATP synthesis and release of ATP. Although it has not yet been definitively quantified, it is estimated that the synthesis of one ATP molecule requires the passage of four protons through F_o (Yoshida *et al.*, 2001).

The degree of coupling between ATP synthesis and respiration can be experimentally quantified in isolated mitochondria and intact cells by defining the ratio of oxygen consumption during state 3 and state 4 respiration, called the 'respiratory control ratio' (RCR) (Brand and Nicholls, 2011). A high RCR indicates a high degree of coupling and a low level of 'proton leak', i.e., the re-entry of protons to the matrix through routes

alternative to ATP synthase. *In vivo*, facilitated proton leak is regulated through the action of specific IM proteins, known as uncoupling proteins (UCPs), primarily UCP1 (Nicholls and Lindberg, 1973, Nicholls, 1977, Nicholls and Rial, 1999). Uncoupling protein 1 is most highly expressed in brown adipose tissue (BAT) of mammals and human infants, and its transport of protons across the IM induces mitochondrial uncoupling and the dissipation of the energy generated by electron transport as heat (Nicholls and Rial, 1999, Porter, 2008). This forms the molecular basis of non-shivering thermogenesis in mammals (Nedergaard *et al.*, 2001). While the exact mechanism of action of UCP1 is not fully understood, it is known to be inhibited by purine nucleotides and activated/stimulated by free-fatty acids (Porter, 2008, Brand and Nicholls, 2011). Thus, its activity is inherently regulated by metabolic cues. As the maintenance and regulation of the PMF is central to mitochondrial function, it follows that any change affecting overall mitochondrial function must affect the kinetics of one or more processes that contribute to the regulation of the PMF, i.e., substrate oxidation, electron transport, oxygen consumption, ATP production and proton leak (Brand and Nicholls, 2011).

Oxidative phosphorylation can be specifically inhibited using a number of chemical agents targeting individual enzymes of the ETC/OXPHOS machinery (fig. 1.2). Inhibition of the electron transport chain can have two downstream effects: (1) respiration rates are reduced as there are no electrons available for the reduction of molecular oxygen and (2) the F_1 portion of ATP synthase can consume ATP and turn in reverse, forcing the F_o portion to pump protons *out* of the matrix, thus maintaining $\Delta\Psi_m$. This latter effect is also seen in anoxia, when electron transport slows as oxygen is no longer available for reduction at complex IV (Takeda *et al.*, 2004). Inhibition of complex I with such compounds as rotenone, piericidin A or 1-methyl-4-phenylpyridinium (MPP^+) blocks the transfer of electrons to CoQ and, thus, respiration from NAD^+-linked substrates. Respiration is still possible through FAD-linked substrates via complex II. Conversely, inhibition of complex II with malonate or 3-nitropropionic acid (3-NP) inhibits respiration through FAD-linked substrates, but respiration is still possible through NAD^+-linked substrates. Inhibiting complex III with antimycin A, or myxothiazol, completely blocks respiration from all substrates, as does inhibition of complex IV with potassium cyanide (KCN) or sodium azide (fig 1.2). The F_o region of

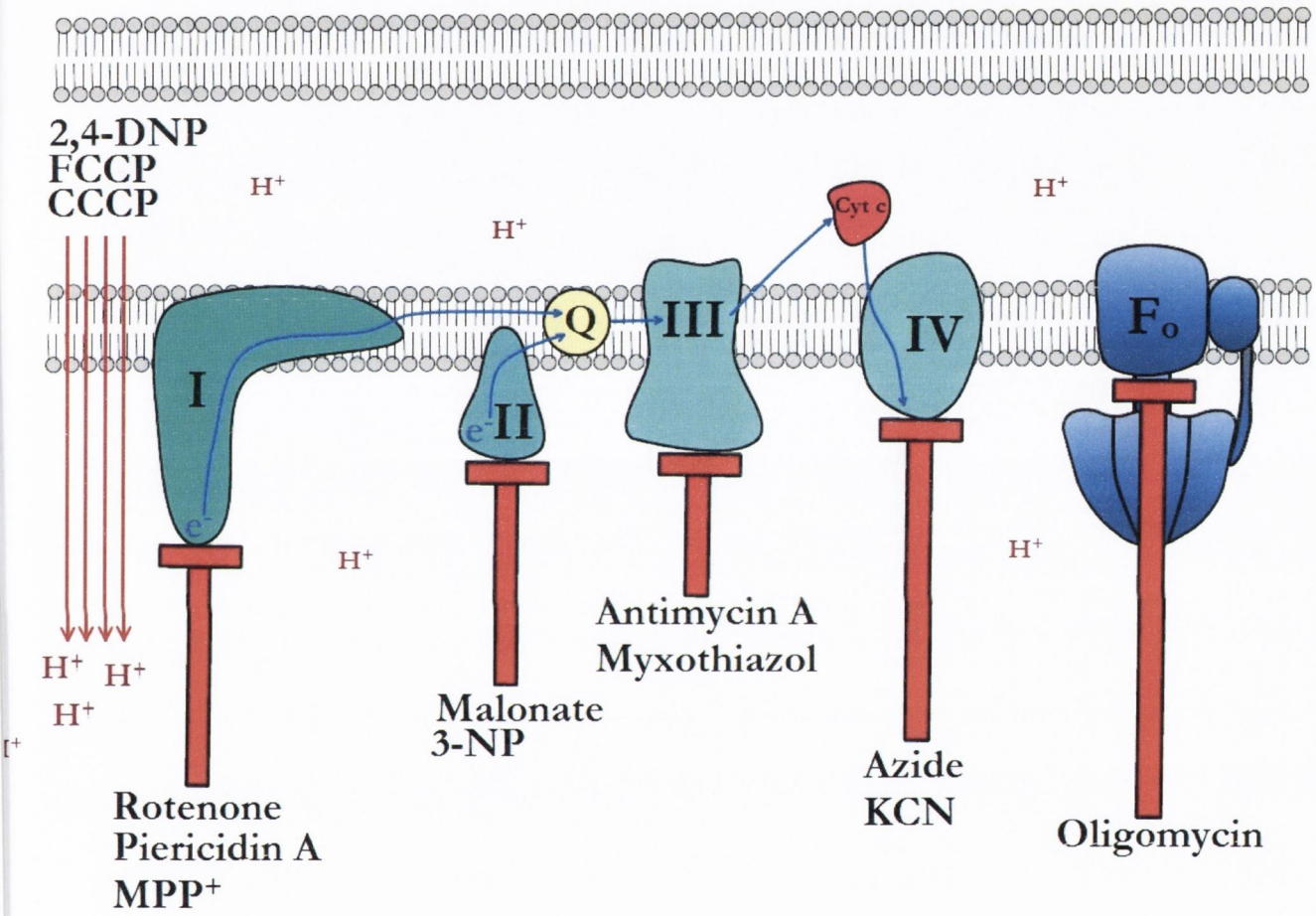

Figure 1.2: Selective inhibition of ETC/OXPHOS components. The electrochemical gradient can be dissipated with lipophilic protonophores carbonyl cyanide-*p*-trifluoromethoxyphenylhydrazone (FCCP), carbonyl cyanide-*m*-chlorophenylhydrazone (CCCP) or 2,4-dinitrophenol (2,4-DNP), which allow passive diffusion of protons (H^+) across the usually impermeable inner membrane. Electron transport can be inhibited at complex I with rotenone, piericidin A or 1-methyl-4-phenylpyridinium (MPP^+). Complex II and be inhibited by malonate or 3-nitropropionic acid (3-NP), while antimycin A and myxothiazol inhibit complex III and azide and potassium cyanide (KCN) inhibit complex IV. Finally, ATP sythnase can be inhibited by oligomycin.

ATP synthase can be inhibited by oligomycin (hence the subscript 'o' in its name, i.e., the oligomycin-inhibited fraction in fractionation procedures), which prevents proton translocation in either direction. If ATP synthase alone is inhibited, mitochondria can become transiently hyperpolarised, as the ETC continues to extrude protons from the matrix while none can re-enter through inhibited ATP synthase. Eventually, electron transport ceases at such high $\Delta\Psi_m$ as there is insufficient free energy available to translocate protons against their steep concentration gradient. Simultaneous inhibition of ATP synthase and ETC enzymes results in significant depolarisation, as proton flux is inhibited at both sites. Finally, the $\Delta\Psi_m$ can be completely dissipated with lipophilic 'uncouplers' such as carbonyl cyanide-*p*-trifluoromethoxyphenylhydrazone (FCCP), carbonyl cyanide-*m*-chlorophenylhydrazone (CCCP) or 2,4-dinitrophenol (2,4-DNP), which function as protonophores at the IM. As a result, respiration is increased (electron transport increases due to decreased $[H^+]$ in the IMS) but is uncoupled from ATP production.

Inhibition of ETC complexes can increase the generation of a partly reduced and highly reactive intermediate, superoxide anion ($O_2^{\cdot-}$). Its production can lead to the subsequent generation of hydrogen peroxide (H_2O_2) and the hydroxyl radical ($^{\cdot}OH$), all of which have been classified as 'reactive oxygen species' (ROS). Generation of ROS also occurs under non-pathological conditions; it is estimated that 1-2% of electrons escape the ETC (Chance *et al.*, 1979, Dlaskova *et al.*, 2010). Mitochondria have mechanisms in place to neutralise ROS, such as non-enzymatic scavengers CoQ and vitamin E (Ham and Liebler, 1995). Enzymatic scavengers include manganese superoxide dismutase (MnSOD), a matrix enzyme that catalyses the conversion of $O_2^{\cdot-}$ to H_2O_2, which is further neutralised by glutathione peroxidase or peroxiredoxins (de Moura *et al.*, 2010). Uncoupling proteins also play an important role in regulation of ROS production (Dlaskova *et al.*, 2010, Oelkrug *et al.*, 2010). Mitochondria isolated from BAT of UCP1 knock-out mice exhibit higher basal H_2O_2 production irrespective of ETC substrate, while mitochondria from wild type BAT show comparable increases upon purine nucleotide inhibition of UCP1 (Dlaskova *et al.*, 2010, Oelkrug *et al.*, 2010). Furthermore, UCPs have been shown to be activated by by fatty acid oxidation product 4-hydroxy-2-nonenal (Echtay *et al.*, 2003) and $O_2^{\cdot-}$ (Echtay *et al.*, 2002). It is hypothesised that the UCP-induced state 3-like respiration of mildly uncoupled mitochondria could decrease ROS production, as the likelihood of ROS production is higher when electrons dwell at

ETC enzymes for longer periods in state 4 respiration (Chance *et al.*, 1979, Turrens, 2003, Adam-Vizi and Chinopoulos, 2006).

While $O_2^{\cdot-}$ and ·OH are charged, and therefore cannot exit the matrix, H_2O_2 can freely diffuse across the mitochondrial membranes and enter the cell proper, where catalase is its most common neutralising enzyme. Complexes I and III are considered the sources of highest ROS production, although the latter produces ROS only when artificially inhibited, whereas the former does so under physiological conditions as well as when inhibited (Adam-Vizi and Chinopoulos, 2006). Although ROS have vital physiological signalling functions (Radak *et al.*, 2011), excessive production can overwhelm mitochondrial antioxidant defences and seriously compromise cell integrity, oxidizing proteins, lipids, and DNA. The result of an imbalance between ROS production and antioxidant action is called oxidative stress (de Moura *et al.*, 2010) and is cited as a significant contributing factor to myriad diseases, especially cancer and neurodegeneration. It is thought to particularly affect the heart and brain, in which the consequences of mitochondrial dysfunction are compounded by the high aerobic demands of these organs (Adam-Vizi and Chinopoulos, 2006).

Clearly, the regulation of mitochondrial function is of supreme importance for cellular survival. Mitochondria are not only sites of vital and efficient energy production, but also sources of toxic metabolic intermediates, which set in place destructive cascades of cellular damage if not controlled. The processes of fission and fusion are considered to be important in the regulation and maintenance of mitochondrial and cellular homeostasis and will now be discussed in detail.

1.3 Mitochondrial Dynamics

Contrary to the stereotypical depiction favoured by biochemistry textbooks of mitochondria as solitary spherical bodies, modern advances in high resolution confocal microscopy techniques have revealed mitochondria in many cells, particularly those in culture, to form a highly interconnected and tubular network, or groups of networks (Plecita-Hlavata *et al.*, 2008). Through the process of fission, a tubular mitochondrion of 2 – 25μm in length can divide into two or more smaller organelles of ~0.5μm or larger. Through fusion, a single organelle can combine with another to form a larger

mitochondrion. This process also allows a mitochondrion to integrate with the larger reticulum and become involved in cellular processes occurring in cellular regions distal to its own location. Mitochondria also make use of microtubules and actin filaments to redistribute and relocate, especially in axonal transport in neurons (Suen *et al.*, 2008, Cai and Sheng, 2009, Palmer *et al.*, 2011).

Fission and fusion are best characterised in yeast mitochondria (Nunnari *et al.*, 1997, Hermann *et al.*, 1998, Bleazard *et al.*, 1999), but mammalian equivalents to some of the protein machinery involved have been identified. As in yeast, mitochondrial fission and fusion are mediated mainly by a group of large (80 – 100kDa) dynamin-related guanosine triphosphatases (GTPases), often referred to as 'mitodynamins'. Fission requires dynamin related protein 1 (DRP1, Dmn1 in yeast), while OM fusion requires two mitofusins (Mfn1 and 2, Fzo1 in yeast) and IM fusion requires optic atrophy 1 (OPA1, Mgm1 in yeast).

1.3.1 Mitochondrial Fission

Dynamin-related protein 1 (also called dynamin-like protein 1) is a ~80kDa cytosolic, microtubule-associated protein containing a GTPase domain, an ill-defined middle domain, a putative pleckstrin homology (PH)-like domain and a GTPase effector domain (GED) (Cereghetti *et al.*, 2008, Zhang *et al.*, 2011). The elegant studies of Alexander van der Bliek's group at the turn of the last century shed much light on the importance of DRP1 in mitochondrial fission in mammalian cells. In 1998, they showed that DRP1 was involved in mitochondrial distribution, as COS-7 cells expressing mutant DRP1 with a defect in the GED exhibited excessively-clustered perinuclear tubules (Smirnova *et al.*, 1998). In 2001, they described the association of green-fluorescent protein (GFP)-fused DRP1 directly at mitochondrial division sites and that purified DRP1 could self-assemble into oligomeric ring-like structures *in vitro*, which was to be an important insight into the mechanism of mitochondrial fission (Smirnova *et al.*, 2001).

In yeast, Dnm1 is recruited to mitochondria by OM protein Fis1, where, using adaptor proteins Mdv1 and Caf4, it oligomerises into a ring structure that constricts and severs the organelle upon GTP hydrolysis (Bleazard *et al.*, 1999, Mozdy *et al.*, 2000, Tieu and Nunnari, 2000, Griffin *et al.*, 2005). The 'constricting belt' model of fission is also favoured in mammalian cell mitochondria (Suen *et al.*, 2008), although recruitment of

DRP1 is still poorly understood in this context. Human orthologues of Mdv1 and Caf4 have not been identified, but a human Fis1 orthologue (hFis1) has been characterised. There are conflicting reports on the role it plays in the fission process however; its knock-down results in elongation of mitochondria in COS-7 cells and in HeLa cells, but doesn't have any effect on DRP1 recruitment to the organelles (Lee *et al.*, 2004, Stojanovski *et al.*, 2004). Interestingly, Lee *et al.* actually found that Fis1 silencing attenuated apoptosis more strongly than DRP1 silencing, suggesting a potential evolutionary divergence in function between these cells. Otera *et al.* (2010) found that the same shRNA (short hairpin ribonucleic acid) used to knock down hFis1 in HeLa cells in the studies of Lee *et al.* did not effectively reduce the levels of the protein in colorectal carcinoma HCT116 cells, but still induced an elongated mitochondrial morphology. They ascribed this morphological observation to the increased cell volume induced by this particular shRNA. They then tested a commercially available, validated shRNA that did significantly decrease hFis1 levels, but observed no change in mitochondrial morphology. The current consensus seems to be that, while hFis1 may be involved in mammalian mitochondrial fission, it may not be an essential component and may even be dispensable in some cell types (Otera and Mihara, 2011).

The most promising candidate for DRP1 recruitment in mammalian cells is mitochondrial fission factor (Mff). First reported by Gandre-Babbe and van der Bliek (2008), it is localised to the mitochondrial OM and its knock-down replicates the elongated phenotype of DRP1 knock down cells. Crucially, Otera *et al.* (2010) found that Mff knock-down disrupts DRP1 recruitment, precipitating the elongated morphology previously reported. Finally, they showed direct *in vivo* interaction between the two proteins, as Mff directed DRP1 to the plasma membrane when genetically engineered to contain a targeting sequence to this destination.

It is not yet known if OM and IM scission are separate events. It is conceivable that constriction of the DRP1 oligomeric ring upon GTP hydrolysis is sufficient to sever both membranes, but this has yet to be established (Westermann, 2010). Although proteolytic cleavage of OPA1 has been reported to promote fission (Ishihara *et al.*, 2006, Guillery *et al.*, 2008), its major role appears to be in mediating mitochondrial IM fusion. To date, there has been just one other IM protein reported to have a role in mitochondrial fission, called MTP18 (mitochondrial protein 18kDa) (Tondera *et al.*, 2004,

Tondera *et al.*, 2005). Overexpression of this protein produced excessive fragmentation of mitochondria, whilst its knock-down resulted in hyperfusion. It is interesting that overexpression of DRP1 does not result in increased fragmentation (Smirnova *et al.*, 1998, Pitts *et al.*, 1999); this indicates that an increased presence cytoplasmic DRP1 may not necessarily change mitochondrial recruitment rates, whilst increased levels of an intra-mitochondrial pro-fission protein, such as MTP18, results in excessive fragmentation. It remains to be seen if any other adaptor proteins exist for the execution of mammalian mitochondrial fission.

1.3.1.1 Regulation of Mitochondrial Fission

Control of mitochondrial fission is complex and poorly understood. Regulatory mechanisms of fission have been described at two levels; post-translational modification (PTM) of DRP1 and interaction of DRP1 with a number of potential regulatory proteins. Examples of PTM of DRP1 include phosphorylation, sumoylation and ubiquitination (Chang and Blackstone, 2010). Phosphorylation plays an important role in releasing DRP1 from its cytoskeletal location. Most studies focus on the phosphorylation of Ser637, which lies within the GED domain of the enzyme. It has been demonstrated that DRP1 is phosphorylated at this site by cyclic adenosine monophosphate (cAMP)-dependent protein kinase A (PKA), which inhibits GTPase activity. Indeed, expression of a phosphomimetic DRP1 mutant increases mitochondrial elongation, much like DRP1 knock-out experiments (Chang and Blackstone, 2007). It has also been shown that dephosphorylation of this site by calcineurin occurs in a calcium-dependent fashion and leads to the translocation of DRP1 to mitochondria (Cribbs and Strack, 2007, Cereghetti *et al.*, 2008). Most recently, a novel protein inhibitor (called PPD1) of calcineurin-mediated DRP1 dephosphorylation was shown to inhibit DRP1 translocation to mitochondria and attenuate DRP1-mediated signalling (Cereghetti *et al.*, 2010). Interestingly, another study described the promotion of DRP1 recruitment to mitochondria following phosphorylation at a different position, Ser600, by Ca^{2+}/calmodulin-dependent protein kinase Iα (CaMKIα) in neurons and HeLa cells (Han *et al.*, 2008). These results indicate that phosphorylation of DRP1 can have opposite effects depending on the site at which it occurs and also highlight an important role for intracellular calcium signalling in mitochondrial dynamics (Jeyaraju *et al.*, 2009).

Another form of PTM reported in DRP1 is sumoylation. Small ubiquitin-like modifier (sumo) addition to proteins often spares them from proteasomal degradation following ubiquitination (Chang and Blackstone, 2010). Sumo1 is reported to sumolylate DRP1 in COS-7 cells and its overexpression increases mitochondrial fission, which the authors attribute to an increased pool of DRP1 that is protected from degradation (Harder *et al.*, 2004). Despite this, others report that cells expressing DRP1 mutants lacking the capacity for sumoylation exhibit no changes in recruitment of the protein to mitochondria, nor in fission rates (Figueroa-Romero *et al.*, 2009). Dynamin related protein-1 can also be ubiquitinated, which generally targets proteins for degradation. The E3 ubiquitin ligase MARCH-V is a mitochondrial OM protein for which DRP1 is a substrate, as reported by Nakamura *et al.* (2006). Its role in mitochondrial dynamics is not clear, however, as this group reported that overexpression of MARCH-V reproduced DRP1 knock-out phenotype, whereas other studies show the exact opposite effect; RNA interference of MARCH V reproduced the elongated phenotype, inhibited DRP1 translocation and promoted cellular senescence (Karbowski *et al.*, 2007, Park *et al.*, 2010). Interestingly, the more recent studies by Park and colleagues (2010), found Mfn1 to be a major substrate for MARCH V and ectopic expression of mutant Mfn1 lacking GTPase function in MARCH-V knock-out cells abolished excessive mitochondrial elongation and senescence. These conflicting data may indicate that although MARCH-V can ubiquitinate DRP1, perhaps it has a more significant role in DRP1 stabilisation at the OM than selecting it for degradation. Furthermore, its affinity for Mfn1 as a ubiquitination target appears to be higher, such that loss of MARCH V function leads to an accumulation of Mfn1 in the cell and aberrant mitochondrial morphology.

There are several proteins implicated as direct DRP1 interactors, including MiD49 and MiD51, and endophilin B1 (Karbowski *et al.*, 2004b, Palmer *et al.*, 2011, Zhao *et al.*, 2011). MiD49 and MiD51 are two recently reported novel parts of the fission regulatory machinery (Palmer *et al.*, 2011). MiD49/51 assemble into foci on the mitochondrial OM, like DRP1, and their knock-down adversely affects mitochondrial DRP1 recruitment. Interestingly, their overexpression appeared to sequester DRP1 at mitochondria but prevented fission. This was also found by another group, who independently identified MiD51 as mitochondrial elongation factor 1 (Mief1) (Zhao *et al.*, 2011). They report that Mief1/MiD51 negatively regulates DRP1 activity, by recruiting it to mitochondria and reducing its GTPase activity, thereby inhibiting fission. Endophilin B1 is a fatty acyl

transferase, from a group of Bin-Amphiphysin-Rvs (BAR)-domain containing proteins with important roles in dynamin-mediated endocytotic vesicle scission. Only one study has been published on its effects on mitochondrial dynamics, which showed down-regulation of endophilin B in HeLa cells to produce extremely unusual mitochondrial morphology, with hyperfused OM containing vesicles of dissociated IM (Karbowski *et al.*, 2004b). Endophilin B1 translocated to mitochondria after the initiation of apoptosis, but the investigators did not examine DRP1/endophilin co-localisation. Double knock-down of endophilin B1 and DRP1 replicated DRP1 single knock down phenotype, indicating that DRP1 acts upstream of endophilin B1. No further work on this line of investigation appears to have been published by the group, thus the role of this protein in mitochondrial fission/fusion remains intriguingly obscure.

The B-cell lymphoma 2 (Bcl-2) family of proteins also seems to have an important regulatory role in mitochondrial dynamics. This large family of proteins exerts powerful control over apoptosis and cell survival and is particularly relevant in cancer biology. Anti-apoptotic members include Bcl-xL, Bcl-2, KSHV-Bcl-2 and Bcl-w, whilst pro-apoptotic members include Bax, Bak, Bim and Bid (Petros *et al.*, 2004). Anti-apoptotic members act by inhibiting the activity of the pro-apoptotic members Bax and Bak, while the pro-apoptotic members promote apoptosis by inducing freeing Bax/Bak from inhibition, allowing them to induce mitochondrial OM permeabilisation (MOMP). This involves the formation of pore-like oligomers on the OM, which facilitates the release of important apoptotic signalling molecules, most notably cytochrome c (Autret and Martin, 2010). While mitochondrial fragmentation is a very early event in apoptosis (discussed in section 1.4.2), studies have indicated an important regulatory role for both anti- and pro-apoptotic Bcl-2 proteins in mitochondrial morphology in healthy cells.

Anti-apoptotic Bcl-2 proteins appear particularly important in neuronal mitochondrial fission. Bcl-w has been shown to promote fission in cerebellar Purkinje cells (Liu and Shio, 2008), as cells lacking Bcl-w show longer mitochondria than controls and exhibit defective dendrites and synapses. Another anti-apoptotic Bcl-2 family member, Bcl-xL, has been shown to increase mitochondrial fission 1.8-fold upon overexpression in neurons, in a DRP1-dependent manner (Berman *et al.*, 2009) and has also been shown to induce Drp1-dependent synapse formation in cultured hippocampal neurons (Li *et al.*, 2008). These results highlight the importance of tight regulation of mitochondrial fission

at distinct developmental stages of the central nervous system, and also in post-developmental maintenance of neuronal function. A schematic depiction of mitochondrial fission is shown in fig 1.3.

1.3.2 Mitochondrial Fusion

The first mitochondrial fusion-mediating protein was described in *Drosophila melongaster* (Hales and Fuller, 1997). Named fzo (fuzzy onion), it was shown to be essential for the fusion of mitochondria during spermatogenesis in this organism. While fzo expression is restricted to the male germ line, *Drosophila* also ubiquitously express another mitofusin (dmfn) (Hwa *et al.*, 2002). The mammalian homologues, Mfn1 and 2, were first reported by Santel and Fuller (2001), who described their OM-anchored location, GTPase-dependent activity and the elongation of mitochondrial tubules upon their overexpression. Since then, Mfn1 and 2 have been found to have overlapping but not completely redundant roles in the fusion process, with slight structural dissimilarities. Both Mfn 1 and 2 have N-terminal GTPase domains, two hydrophobic heptad repeat regions, (HR 1 and 2), and two transmembrane domains (Rojo *et al.*, 2002). The N- and C-termini face the cytosolic side of the OM, with the central part of the protein forming a U-shaped, transmembrane anchor (de Brito and Scorrano, 2008b). Mitofusin 2 has an additional Ras-binding domain that is lacking in Mfn1 and displays a surprising level of functional pleitropy (de Brito and Scorrano, 2008b, 2009).

The mechanism of fusion is still under intense investigation. Fusion of synaptic vesicles occurs in three stages – 'tethering', where two membranes are anchored together yet still separate, 'docking', where the membranes are brought into closer apposition by soluble N-ethymaleimide-sensitive factor attachment protein receptor (SNARE) proteins and finally, fusion, a result of the close proximity of the two membranes (Koshiba *et al.*, 2004). The work of Koshiba *et al.* (2004) shed much light on the mechanism of mitochondrial tethering by the mitofusins. They demonstrated that Mfn1/2 form homo- and hetero-oligomeric complexes in *trans* and mediate mitochondrial fusion by tethering of apposing membranes, with a distance of approximately 95Å between both membranes. The HR2 regions, when isolated from Mfn1/2, form homo- and heterotypic complexes (mirroring the behaviour of the full length proteins) and are considered to mediate the 'tethering' stage of mitochondrial fusion. They have also

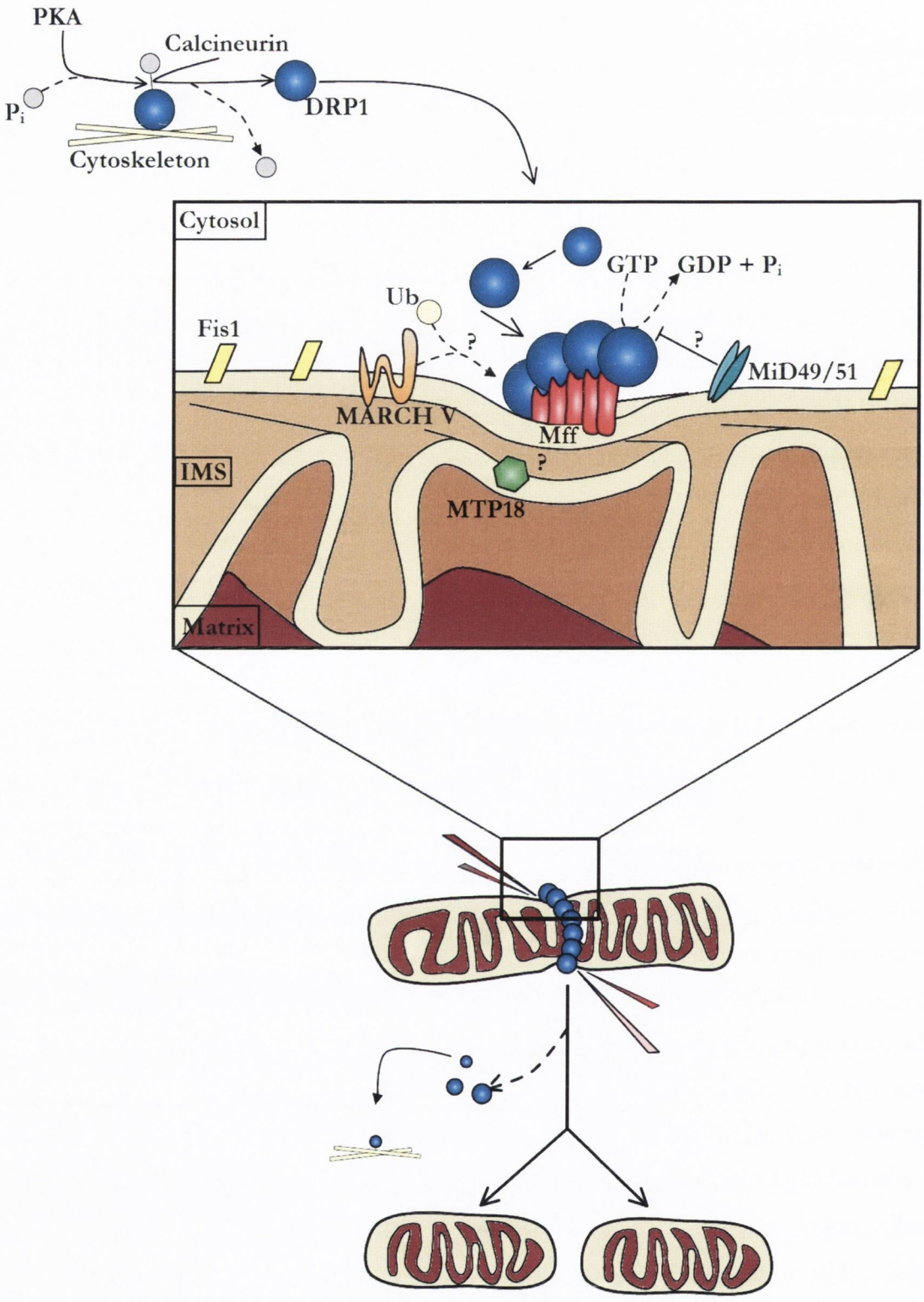

Figure 1.3: Putative mechanism of mitochondrial fission. Selected proteins with potential roles in fission are shown. Dynamin related protein 1 (DRP1) is retained at the cytoskeleton by protein kinase A (PKA)-mediated phosphorylation (P_i). Calcineurin dephoshporylates DRP1 to release it from the cytoskeleton and allow recruitment to the mitochondrial outer membrane. Here it assembles into an oligomeric ring structure around the outer membrane, which constricts upon GTP hydrolysis, causing membrane scission and organellar fission. Numerous accessory proteins have been reported to be involved but their roles are not clear. Mitochondrial fission factor (Mff) is a strong candidate as a DRP1 recruitment and assembly factor, while MiD49/51 are reputed to be negative regulators. Fis1 functions in yeast as the main DRP1 recruitment protein but its role in mammalian mitochondrial fission is less well defined. MARCHV is postulated as a stabiliser of DRP1 through ubiquitination (Ub). The only inner membrane protein described to have potential involvement is MTP18, but its mechanism of action is unknown. After mitochondrial fission, DRP1 returns to the cytoskeleton.

shown that Mfn1 is particularly important following this 'tethering' stage of fusion – in cells expressing a mutant Mfn1 without GTPase activity, the mitochondria are aggregated and trapped in a 'tethered' state. Indeed, Mfn1 shows ~eightfold higher GTPase activity compared to Mfn2 (Ishihara *et al.*, 2004). Moreover, exogenous expression of wild-type Mfn1 can rescue cells expressing Mfn2 disease mutants, whereas wild-type Mfn2 cannot (Detmer and Chan, 2007). Interestingly, it has recently been demonstrated that heterotypic Mfn1-Mfn2 *trans* complexes have greater efficacy than homotypic complexes of Mfn1 or Mfn2 (Hoppins *et al.*, 2011). New results from Huang *et al.* (2011) suggest that HR1 and 2 regions of Mfn2 bind to one another, and this interaction is actually fusion-inhibitory. The mechanistic details of fusion following GTP hydrolysis, however, remain unresolved.

Inner membrane fusion requires OPA1. This inner-mitochondrial mitodynamin is so named for the optic neuropathy, autosomal dominant optic atrophy (ADOA), caused by the mutation of the *Opa1* gene (Alexander *et al.*, 2000, Delettre *et al.*, 2000). It was through the study of this neuropathy that the importance of OPA1 in mitochondrial fusion became clear, as monocytic mitochondria from ADOA patients were abnormally condensed (Delettre *et al.*, 2000). Optic atrophy 1 is now known to be targeted to mitochondria, *via* a basic-rich N-terminal targeting sequence, where it resides in the IM, in type I topology, facing the IMS (Olichon *et al.*, 2002). It has eight mRNA isoforms as a result of the alternative splicing of exons 4, 4b and 5b (Delettre *et al.*, 2001) and even a single splice variant is found as several processed forms (Ishihara *et al.*, 2006) (fig. 1.4). Upon import into the IM, the mitochondrial targeting sequence is cleaved by mitochondrial protein peptidase (MPP), yielding the long isoform (L-OPA1)(Ishihara *et al.*, 2006). This is further processed at cleavage sites S1 and/or S2, by a number of proteases (Ishihara *et al.*, 2006, Song *et al.*, 2007), yielding at least one other long isoform and at least three short isoforms (S-OPA1) (Guillery *et al.*, 2008). Short isoforms are more loosely bound to the IM than long forms that retain a hydrophobic domain (Ishihara *et al.*, 2006, Suen *et al.*, 2008).

Consistent with a role in fusion promotion, overexpression of OPA1 leads to mitochondrial tubulation in a number of cell types, in a GTPase-domain-dependent fashion (Olichon *et al.*, 2002, Cipolat *et al.*, 2004). However, the variation in OPA1 splice variants and cleavage products has marked functional significance. Significant knock-

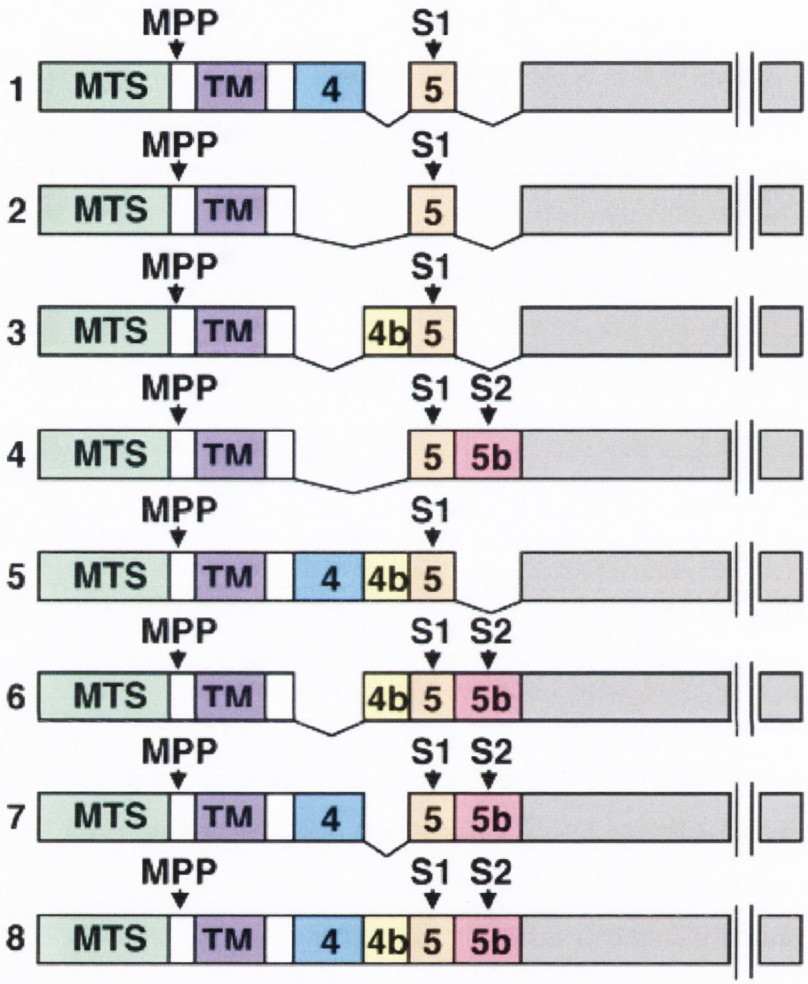

Figure 1.4: OPA1 mRNA splice variants and cleavage sites. All variants have mitochondrial targeting sequences (MTS), transmembrane domains (TM) and exon 5, but differ in the presence or absence of exons 4, 4b and 5b. The MTS is cleaved from the nascent protein following integration into the mitochondrial inner membrane, yielding one of two characterised long isoforms. Cleavage at S1 and 2 sites by various proteases yields one of three characterised short isoforms. Taken from Song *et al.*, 2007.

down of OPA1 leads to mitochondrial fragmentation, dissipation of $\Delta\Psi_m$ and pronounced cristae disorganisation (Olichon *et al.*, 2003) but this effect is only reversed by exogenous expression of full-length OPA1, not truncated OPA1 yielding only S-OPA1 (Ishihara *et al.*, 2006). Intriguingly, not all full-length splice variants can rescue OPA1-null mouse embryonic fibroblasts (MEFs) from their punctiform mitochondrial phenotype; those containing the 4b exon are fully processed to S-OPA1 and barely increase tubularity in the reticulum or increase fusion, while those lacking this exon favour the L-OPA1 isoforms and restore mitochondrial fusion (Song *et al.*, 2007). Indeed, treatment of mammalian cells with uncoupler CCCP produces rapid (yet reversible) mitochondrial fragmentation concomitant with complete cleavage of L-OPA1 to S-OPA1 (Guillery *et al.*, 2008). Thus it would appear that L-OPA1 promotes fusion, whereas S-OPA1 promotes fission. The reality may be rather more complex, however, as studies show that L/S-OPA1 isoforms work in concert and that the presence of L- and S-OPA1 isoforms has a synergistic effect on fusion (Song *et al.*, 2007).

The co-ordination of IM and OM fusion is an enigmatic process, as it is not clear if they occur simultaneously or sequentially. Yeast mitochondria undergo neither OM nor IM fusion in the absence of the OPA1 orthologue Mgm1 (Sesaki *et al.*, 2003). In mammalian cells, however, the two processes can occur independently (Malka *et al.*, 2005). Song *et al.* (2009) have reported that OPA1-null MEFs exhibit OM fusion in the absence of IM fusion, as evidenced by the presence multiple matrix compartments bounded by a single OM in polyethylene glycol (PEG)-generated cell cybrids (polykaryons). The authors also found that in stark contrast to the mitofusins, OPA1 is not required on adjacent mitochondria for fusion to proceed; OPA1-null/wildtype cell cybrids exhibited full or partial mitochondrial fusion (mostly the latter). Interestingly, IM fusion has been shown to be Mfn1-dependent. While co-immunoprecipitation studies show physical interaction between both Mfns (Guillery *et al.*, 2008), overexpression of OPA1 produces mitochondrial elongation in wild type and Mfn2-null cells, but not in Mfn1-null cells (Cipolat *et al.*, 2004). Thus, while OM fusion can proceed independently of IM fusion, the latter specifically requires Mfn1, for reasons that are not yet determined.

Interestingly, Liu *et al.* (2009) report a novel 'kiss and run' mechanism of transient fusion, whereby mitochondria can come into close apposition obliquely or laterally, partially exchange matrix components, then separate. This preserves the original morphology of

the mitochondria and occurs between mitochondria in rapid transit on separate microtubules. In contrast, complete fusions occurred from longitudinal interactions between mitochondria on the same microtubule and promoted mitochondrial stasis. These transient fusions preserved mitochondrial motility and bioenergetic integrity.

1.3.2.1 Regulation of Mitochondrial Fusion

Mitofusins are known to be regulated by a number of protein interactors and to be responsive cellular calcium levels. Unlike DRP1, however, there are few studies describing the regulation of fusion *via* PTM of the mitofusins. To date, ubiquitination is the only form of PTM described in the regulation of mitofusins, and thus, OM fusion. Several groups have identified the PTEN-induced putative kinase 1 (PINK1)/parkin pathway as an important one in the regulation of mitochondrial fusion in *Drosophila* (Deng *et al.*, 2008, Poole *et al.*, 2008, 2010, Ziviani *et al.*, 2010). Mutations in PINK1, a serine/threonine kinase, or parkin, an E3 ligase involved in the proteasomal protein degradation pathway, result in an-early onset form of Parkinson's disease (PD), called Autosomal Recessive Juvenile Parkinson's Disease (ARJPD) (Gasser, 2007, Lesage and Brice, 2009). *Drosophila* PD models can be created by genetic manipulation of either of these proteins. The studies presented by these groups strongly indicate that PINK1 phosphorylates parkin, which goes on to ubiquitinate dmfn, rendering it unable to mediate fusion.

Ubiquitination of human Mfn 1 and 2 has also been reported (Twig *et al.*, 2008a, Gegg *et al.*, 2010). In the neuroblastoma cell line SH-SY5Y, this PTM occurred in a PINK/parkin-dependent fashion, within three hours of CCCP-mediated mitochondrial damage (Gegg *et al.*, 2010). It has been suggested that this could be a mechanism by which damaged mitochondria are 'singled-out' from the healthy mitochondrial pool and targeted for mitochondria-specific autophagy (mitophagy) by degradation of the pro-fusion enzymes on the OM. In support of this, Twig *et al.* (2008a) propose a co-ordination of mitochondrial fission and fusion-prevention as a means of segregating depolarised mitochondria from the healthy majority in a pancreatic cell line. They observed an uneven fission of mitochondria, in which one daughter organelle exhibited increased membrane potential, with high probability of subsequent fusion, and an almost depolarised daughter organelle, with high probability of mitophagy. These damaged mitochondria also showed decreased immunoreactivity for OPA1. Furthermore,

inhibition of fission resulted in decreased mitophagy, increased protein oxidation and, a higher number of depolarised mitochondria and impaired insulin secretion.

As previously mentioned, Bcl-2 proteins have important roles in regulating mitochondrial morphology in health and apoptosis. Several recent studies have indicated intriguing roles for pro-apoptotic Bax and Bak proteins in mitochondrial fusion regulation in healthy cells. Karbowski *et al.* (2006) have reported that Bax/Bak double knock-out mouse cell lines exhibit fragmented mitochondria that were determined to be discontinuous separate units via fluorescence recovery after photobleaching (FRAP) studies. As well as severe fusion deficits, the cells show disrupted Mfn2 distribution along the mitochondrial OM – appearing to be distributed equally across the surface, rather than at discrete foci, as in wild-type cells. Hoppins *et al.* (2011) have also reported that a soluble form of Bax stimulated fusion in a dose-dependent manner, by specifically interacting with Mfn2 homotypic complexes. Thus, Bax and/or Bak appear to interact directly with Mfn2 and are required for Mfn2-mediated fusion.

Eura *et al.* (2006) have identified a ubiquitously expressed protein of the medium-chain dehydrogenase/reductase protein superfamily as a negative regulator of Mfn1-mediated mitochondrial fusion. Called Mfn-binding protein (MIB), it is primarily cytoplasmic, with a small fraction localised to mitochondria and its knock down results in mitochondrial elongation and cell cycle arrest, without any effects on cell death. Conversely, its over expression resulted in mitochondrial fragmentation, in a Mfn1-dependent manner. Mfn2 has been proposed to act as an anti-proliferative regulator (Chen *et al.* (2004), see section 1.4.3) and these results implicate that MIB regulates Mfn1 function in a similar role.

A recent study described by Zhang *et al.* (2010) indicates a novel role for guanine nucleotide binding protein-β subunit 2 (Gβ2) in mitochondrial fusion regulation. It is a member of the β-subunits of the heterotrimeric G-proteins, a group of GTPases classically involved in cellular signal transduction through G-protein coupled receptors (GPCR). Gβ2 is enriched at the mitochondrial membrane and co-immunoprecipitates with Mfn1. Depletion of Gβ2 with shRNA interference led to mitochondrial fragmentation and fusion cessation, which was rescued upon reintroduction of the of the protein. Moreover, Gβ2 was found to specifically interact with Mfn1, as mitochondrial

fragmentation could not be reversed by exogenous expression of Gβ2 in Gβ2/Mfn1 double knockdown cells. It is interesting to note that Gβ2, Mdv1 and Caf4 are all WD40-repeat proteins, the latter two being essential Dnm1 adaptors in yeast mitochondrial fission. These results hint at a common motif amongst some mitodynamin-regulating proteins, albeit with potentially different or opposing regulatory roles.

While no PTMs such as phosphorylation/ubiquitination of OPA1 have been reported, the sheer number of splice and cleavage variants signifies huge potential for tissue-, cell- and even mitochondrion-specific regulation of fusion. Two main proteases have been put forward as OPA-1 regulatory proteins. Ishihara *et al.* (2006) first demonstrated the proteolytic processing of OPA1 by the metalloprotease paraplegin. Paraplegin is an ATP-dependent mitochondrial matrix-facing AAA-protease (m-AAA-protease) whose mutation is responsible for hereditary spastic paraplegia (HSP) (Casari *et al.*, 1998). It is localised to the mitochondrial IM, with the protease site facing the matrix. Overexpression of paraplegin in HeLa cells leads to OPA1 cleavage to S-isoforms and mitochondrial fragmentation, whereas its knock-down resulted in mitochondrial elongation. Strangely, Guillery *et al.* (2008) did not find any difference in OPA1 cleavage patterns in HSP patient lymphoblast mitochondria compared to healthy control samples, nor did they find any difference in CCCP-induced cleavage patterns. This led to the identification of an alternative metalloprotease involved in OPA1 processing; the IMS-facing AAA-protease (i-AAA-protease) complex. They investigators knocked down the main component of the i-AAA-protease, yme1-like protein (YME1L) and found that CCCP-induced cleavage of OPA-1 was significantly reduced.

Finally, a regulatory role for the mitochondrial prohibitin PHB2 in OPA1 processing has been described. Prohibitins are a family of ubiquitously expressed membrane proteins with wide-ranging but poorly defined functions related to the regulation of gene expression, cell cycle and apoptosis (Sievers *et al.*, 2010, Semenzato *et al.*, 2011). Merkwirth *et al.* (2008) showed that PHB2, and its homologue PHB1, assemble in large ring-shaped complexes at the mitochondrial IM (as in yeast (Tatsuta *et al.*, 2005)), and influence OPA1 cleavage. Knock-down of PHB2 in MEFs led to a drastic increase in L-OPA1 processing to S-OPA1 isoforms and fragmented mitochondria with aberrant balloon-like cristae. Exogenous expression of PHB2 fully restored mitochondrial

tubularity and cristae, while expression of cleavage resistant L-OPA did so in over 50% of cells. Interestingly, a very recent study by (Sato *et al.*, 2011) cites the regulatory power of PHB proteins on OPA1 cleavage as the root of cytotoxicity observed in mammalian cells exposed to natural marine product aurilide. A schematic depiction of mitochondrial fusion is shown in fig 1.5.

Mitochondrial dynamics involves complex co-ordination of balanced fission and fusion, with multiple levels of regulation that are still not completely understood. Dysregulation of this balance has serious consequences for mitochondrial morphology, but what is the functional significance of this? Furthermore, what are the actual functions of mitochondrial dynamics in healthy cells? This topic has been touched upon in the description of ubiquitination of mitofusins being a 'quality control' mechanism for mitochondria, and in the maintenance of synaptic plasticity regarding DRP1 regulation. There are many other significant functions of mitochondrial dynamics which will now be discussed.

1.4 Functions of Mitochondrial Dynamics

As mitochondria cannot be created *de novo*, fission represents the only way for mitochondrial distribution amongst dividing cells (Palmer *et al.*, 2011). This has obvious implications for the importance of DRP1 in embryonic development; indeed, mice lacking DRP1 show developmental abnormalities and die after embryonic day 12.5, whilst neuron-specific DRP1 knock-down mice die after birth, with brain hypoplasia (Ishihara *et al.*, 2009). In 2007, Leonard's group presented the first report of DRP1 mutation in a human patient, who died 37 days after birth, with 'microcephaly, abnormal brain development, optic atrophy and hypoplasia, persistent lactic acidemia, and a mildly elevated plasma concentration of very-long-chain fatty acids' (Waterham *et al.*, 2007).

Like DRP1, Mfn1 and 2 and OPA1 also have essential roles in development. Heterozygous mouse mutants for either Mfn1 or Mfn2 demonstrate full viability and fertility, but homozygous mutants die mid-gestation (Chen *et al.*, 2003). Mouse embryonic fibroblasts (MEFs) lacking the mitofusin proteins or OPA1 show many cellular defects, including mitochondrial fragmentation and reduced fusion, poor cell growth, heterogeneity of mitochondrial membrane potential, and decreased cellular

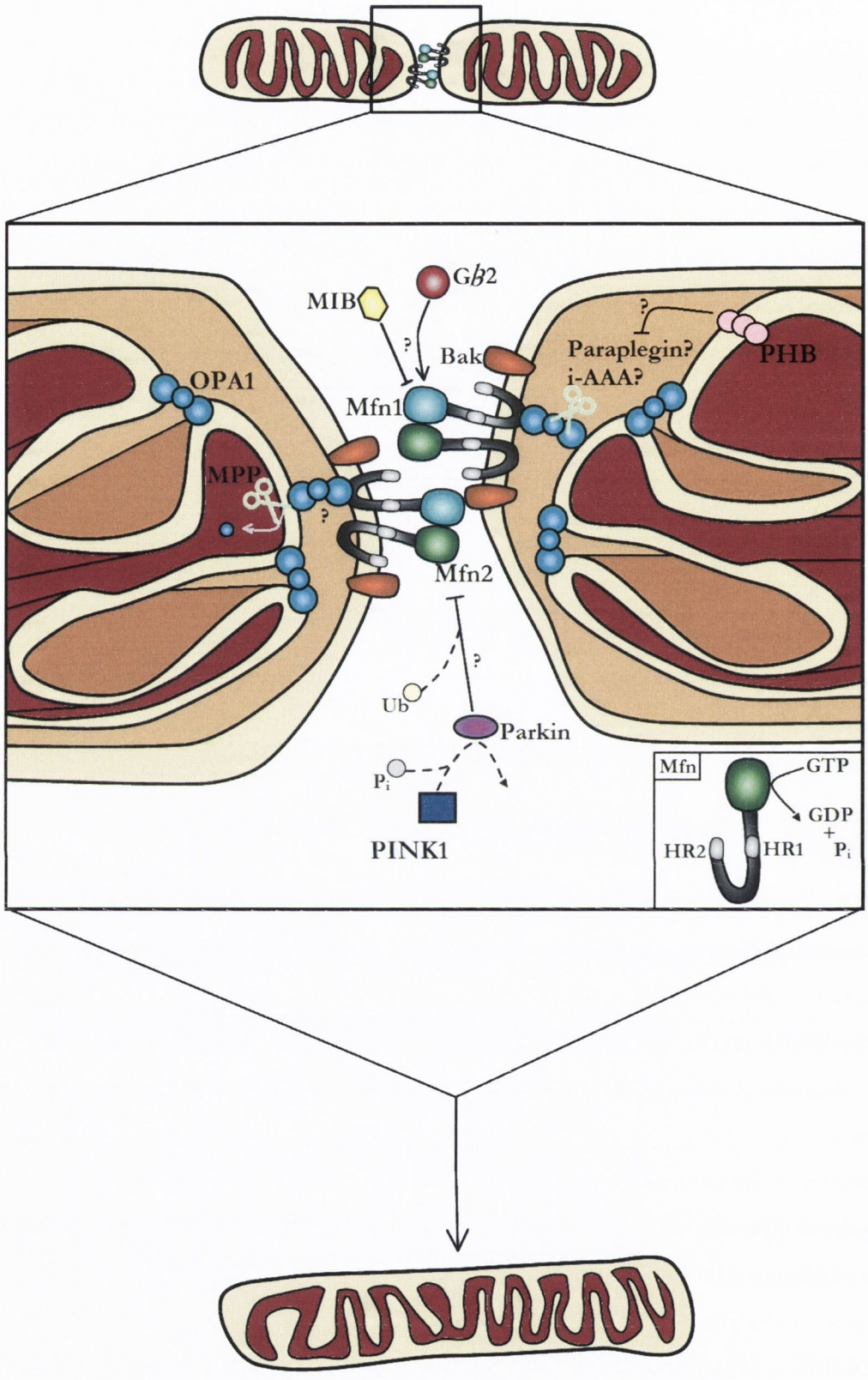

Figure 1.5: Putative mechanism of mitochondrial fusion. Selected proteins with potential roles in fusion are shown. Mitofusins 1 and 2 (Mfn) assemble in homo- and hetero oligomers and mediate fusion via apposition of mitochondria in *trans*. The exact mechanism remains elusive, but it is GTP-dependent and involves tethering of apposing membranes *via* interactions of the two heptad repeat (HR) domains of Mfn 1/2 (inset). Bak (and possibly Bax) and G-protein β2 subunit (Gβ2) are reputed to have a fusion-promotion role, while Mfn binding protein (MIB) and ubiquitination *via* the PTEN-induced putative kinase 1 (PINK1)/parkin pathway are said to be fusion inhibitory. Inner membrane fusion is mediated by OPA1, which may interact physically with Mfn1 in this process. OPA1 is also cleaved by a number of proteases (MPP, paraplegin, i-AAA protease) to yield short and long isoforms, both of which are required for fusion by a number of. Prohibitins (PHB) assemble on the IM and may inhibit proteolytic cleavage of OPA1.

respiration (Chen *et al.*, 2005). Excessive cleavage of OPA1 has also been indicated in the pathophysiology of MERRF patients (Duvezin-Caubet *et al.*, 2006). Mutations in genes encoding two fusion mediators lead to neurological disorders; Mfn2 mutation is responsible for the hereditary peripheral neuropathy Charcot Marie Tooth Disease, type IIa (CMTIIa) (Zuchner *et al.*, 2004) and OPA1 is so named for the autosomal dominant optic neuropathy caused by the mutation of the *Opa1* gene (Delettre *et al.*, 2000). This IM fusion mediator was also recently shown to be essential for embryogenesis in mice (Moore *et al.*, 2010).

The importance of mitochondrial dynamics extends far beyond development. Fission and fusion are essential in the maintenance and sharing of mitochondrial DNA (mtDNA) and the regulation of apoptosis. Both OPA1 and Mfn2 are particularly interesting as they exhibit roles outside of fusion; they represent attractive candidates as integral mitochondrial proteins that mediate the interplay between dynamics and other important functions, particularly bioenergetics.

1.4.1 Maintenance and Sharing of mtDNA

The vast majority of the sizeable number of mitochondrial proteins - predicted to be in the region of 700 in humans (Heazlewood *et al.*, 2003) - are encoded by nuclear DNA. However, mitochondria also contain small circular double-stranded DNA molecules of ~16.6kb in size, each encoding a total of 37 genes; 13 encode core catalytic subunits of ETC enzymes (ND1, ND2, ND3, ND4, ND4L, ND5, and ND6 of, complex I, cytochrome b of complex III, COI, COII, and COIII of complex IV, and subunits A6 and A8 of the ATP synthase complex), 22 encode transfer RNA (tRNA) and two encode ribosomal RNA (rRNA) of the small and large ribosomal subunits (de Moura *et al.*, 2010). Mitochondrial DNA resides in the matrix and is packaged into a discrete number of nucleoprotein complexes, called 'nucleoids', each containing 2 – 8 DNA molecules and closely associated with Tfam (mitochondrial transcription factor A) (Legros *et al.*, 2004). In stark contrast to the dipoloid nature of nuclear DNA, a single cell can contain thousands of copies of mtDNA and several nucleoids within individual organelles. This means that mitochondrial genotype–phenotype relationships arise from population genetics rather than by Mendelian relationships (Schon and Gilkerson, 2010). The large number of copies of mtDNA per cell has two consequences: (1) cells are often heteroplasmic i.e. contain both wild type and mutated forms of mtDNA (point

mutations and/or deletions) and (2) there exists a threshold effect in relation to mtDNA mutations; disease phenotypes are not observed until 80-90% of the total mtDNA load carries the pathogenic mutation (Rossignol *et al.*, 2003).

Several elegant studies conducted over the last decade have demonstrated an important relationship between mitochondrial dynamics and mtDNA maintenance. In 2002, Capaldi *et al.,* observed punctate staining of fluorescently labelled nucleoids in tubular mitochondria of osteosarcoma cells 143B, leading them to propose a 'repli-unit' model of mitochondrial functional organisation. According to this model, certain elements, such as pyruvate dehydrogenase and nucleoids, are anchored to matrix components in repeating units, while other mitochondrial elements, such as OXPHOS enzymes, can move units fluidly throughout the organelle. This model was supported somewhat by the work of Margineantu *et al.* (2002) which describes the presence of at least one nucleoid per mitochondrion following cell cycle-dependent organellar fission. Thus, fission sites must be co-ordinated with the internal distribution of mtDNA by some unknown mechanism. Furthermore, it has been demonstrated that cell cybrids generated from two homoplasmic cell lines harbouring different, non-overlapping mtDNA mutations can restore mitochondrial function through functional complementation (Gilkerson *et al.*, 2008). Polykaryons showed tubular and functional mitochondria, whereas both cell lines from which the cybrids were generated exhibited mitochondrial dysfunction and extensive fragmentation. Although the polykaryon mitochondria exhibited no recombination of mtDNA, single organelles contained both types of mtDNA in separate nucleoids, indicating the free transmission of RNA transcripts and polypeptides between fusing organelles. These results indicate important roles in both fission and fusion in mtDNA distribution and complementation.

Inhibition of mitochondrial fission causes a decrease in mtDNA, concomitant with decreased respiration and ATP levels and increased reactive oxygen species (ROS) production (Parone *et al.*, 2008). HeLa cells subjected to DRP1 knock down showed that hyperfused mitochondria lacked punctate fluorescent staining for mtDNA across long sections of the reticulum, while other areas exhibited nucleoid aggregates. Overall, quantification of total mtDNA showed a ~50% reduction compared to controls. Interestingly, inhibition of fusion is associated with nucleoid loss; Chen *et al.*, 2007 showed Mfn1-null, Mfn2-null, Mfn1/2-null and OPA1-null cells contained many

fragmented mitochondria devoid of nucleoids. In the context of their earlier findings, that fusion deficient cells show $\Delta\Psi_m$ heterogeneity and reduced respiration (Chen *et al.*, 2005), it seems to highly plausible that these heterogeneous deficiencies arise, at least partially, from populations of mitochondria devoid of essential mtDNA. This, in turn could lead to mitochondrial proteome heterogeneity (Chen *et al.*, 2010).

Finally, Chan's group have recently demonstrated a role for mitochondrial dynamics in the tolerance of mtDNA mutations and thus, the mitochondrial threshold effect (Chen *et al.*, 2010). Using mice lacking Mfn1 and 2 (double mutant) specifically in skeletal muscle, the investigators observed aberrant, punctate mitochondria within markedly smaller muscles compared to controls. Amazingly, double mutant muscle cells contained just ~250 copies of mtDNA per nuclear genome, compared to ~3500 copies of mtDNA per nuclear genome in controls. Yet more compelling was the observation than ~7-week-old double mutant mice harboured a 5-fold increase in mtDNA point mutations and a 14-fold increase in deletions. Furthermore, mice genetically engineered to accumulate mtDNA mutations at a higher rate (mice carried homozygous alleles of the $PolgA^{D257A}$ knock-in allele, which encoded a mitochondrial DNA polymerase with a deficient proofreading domain) suffered synthetic neonatal lethality only when this mutation was combined with Mfn1 knock-down (single mutants survived well into adulthood). Thus inhibition of fusion seriously impacts mtDNA mutation accumulation and mitochondrial threshold effects.

1.4.2 A Role in Apoptosis?

The subject of apoptosis has already been touched upon several times throughout this review. This is because apoptosis, and the regulation thereof, are vitally important across multiple biological processes, from development, to adult tissue turnover, homeostasis and immune defence (Suen *et al.*, 2008, Sheridan and Martin, 2010). Indeed, dysregulation of apoptosis has serious and often fatal consequences. Under healthy conditions, it is a form of programmed cell death that allows for the destruction of non-viable or superfluous cells with minimal disruption to surrounding tissues and minimal inflammation. Apoptosis occurs through two main pathways that both converge on the activation of cytoplasmic caspases-3 and -7. These cysteine proteases go on to execute apoptosis through the cleavage of specific cytosolic and nuclear substrates, leading to the classic apoptotic cellular morphology that includes nuclear membrane breakdown,

chromatin condensation and fragmentation, cell membrane blebbing, and formation of apoptotic bodies (Zou *et al.*, 1999).

The first pathway, called the extrinsic pathway, is commonly initiated in immune cells through cell surface receptors and leads to the activation of initiator caspase-8, followed by activation of executioner caspases. The second, called the intrinsic pathway, is activated in response cytotoxic drugs, heat shock, ionizing radiation, and other cellular stresses (Creagh and Martin, 2003). It leads to MOMP by Bcl-2 family proteins and the release of pro-apoptotic mediators, including cytochrome c. Cytochrome c release is a critical step in apoptosis; it goes on to form part of a caspase-activation assembly with apoptosis protease-activating factor-1 (Apaf-1) and caspase-9, called the apoptosome. Mitochondrial apoptosis is also associated with organellar swelling due to the formation of the permeability transition pore (PTP), a high-conductance megachannel created through apposition of certain contact points on the IM (adenine nucleotide translocase, ANT) and OM (voltage dependent anion channel, VDAC) with several other accessory proteins, including matrix protein cyclophilin D, and IMS protein creatine kinase. The PTP is permeable to any molecules with a mass of 1.5kDa or smaller and is formed in response to a number of stimuli, including Ca^{2+} overload and oxidative stress (Jeyaraju *et al.*, 2009). Its opening is associated with the efflux of apoptogenic matrix components, dissipation of $\Delta\Psi_m$ and release of ROS (Abou-Sleiman *et al.*, 2006).

The Bcl-2 family of proteins has already been partially described here. To expand; the Bcl-2 family is subdivided into three groups based on their anti- or pro- apoptotic function and Bcl-2 homology (BH) domains. Anti-apoptotic Bcl-2-like proteins (such as Bcl-2, Bcl-xL and Bcl-w) and pro-apoptotic Bax-like proteins (such as Bax and Bak) contain four BH domains, while pro-apoptotic BH3-only proteins (such as Bid, Bim/Bod, Bad, Bmf and Puma), as evidenced by their name, contain just one BH3 domain (Martinou and Youle, 2011). BH3-only members integrate and transmit cell death signals to mitochondria as they are activated and/or upregulated in response to cell stress and go on to promote MOMP by Bax and Bak. These latter two Bcl-2 family members execute MOMP through mechanism that is not fully understood. While Bax is mainly cytosolic under healthy conditions, Bak is a constitutive OM protein (Martinou and Youle, 2011). Upon induction of apoptosis, Bax joins Bak at mitochondrial OM where they assemble into homo- and hetero-oligomeric pores that cause

permeabilisation. In healthy cells, anti-apoptotic Bcl-2 proteins inhibit Bax and Bak through binding and sequestration, whereas cell stress induces the binding of BH3-only proteins to anti-apoptotic members, releasing Bax and Bak and allowing MOMP. Some BH3-only proteins e.g. Bid and Bad, can interact directly with Bax and Bak to promote a change to active state. Thus Bcl-2 proteins represent a dynamic group of regulators and effectors of the intrinsic apoptotic pathway.

1.4.2.1 OPA1 in Apoptosis

Although mitochondrial fragmentation is an early event in apoptosis, and indeed, observed across species, there is controversy over the role of mitochondrial dynamics in the regulation/execution of programmed cell death (Sheridan and Martin, 2010). Lee *et al.* (2004) demonstrated that OPA1-deficient HeLa cells were highly susceptible to apoptosis, particularly of a spontaneous nature, while Fis1-deficient cells were highly resistant, moreso than DRP1-deficient cells. However, there is also evidence to suggest the involvement of fusion and fission mediators in apoptosis is not connected to their well-established roles in dynamics. The Bcl-2 family proteins have been implicated in the regulation of mitochondrial dynamics in healthy cells, as previously discussed, but they have also been described to interact with mitodynamins during apoptosis. It is tempting to assign a role for mitochondrial dynamics in apoptosis regulation, given the apparent functional interplay between enzymes of both processes, but scientists have not yet been able to determine if this is truly the case. This is an area of intense research interest; what follows is a review of the information currently available on the role of mitochondrial dynamics in apoptosis, with particular reference to the potential roles of OPA1 and DRP1.

The majority of cytochrome c (~85%) resides within the intracristal space of mitochondria, possibly anchored to complexes of the ETC and phospholipids such as cardiolipin (Landes and Martinou, 2011). Its release during apoptosis requires cristae remodelling and it is in this respect that OPA1 implicated. During apoptosis, individual cristae become fused and the intercristal junctions enlarge, thus releasing the sequestered cytochrome c into to IMS (Scorrano *et al.*, 2002), which then translocates to the matrix following MOMP. It has been experimentally determined that this remodelling occurs within 2 - 5 minutes of apoptosis induction by BH3-only protein tBid in isolated mouse liver mitochondria, in a Bak/Bax-independent manner (Scorrano *et al.*, 2002). The

investigators designated mitochondria as 'type I' and 'type II' before and after cristae remodelling, respectively. A fascinating study by Frezza *et al.* (2006) found that OPA1 is enriched at intercristal junctions and exists as oligomers of the long and short isoforms, which are disrupted by tBid, leading to intercristal junction widening and cytochrome c mobilisation. Strikingly, another study has demonstrated the co-release of OPA1 with cytochrome c in apoptotic HeLa cells (Arnoult *et al.*, 2005). Thus OPA1 appears to maintain type I cristae morphology and is released during apoptosis.

The interaction between BH3-proteins and OPA1 oligomer disassembly has been further supported by later studies, but the involvement of Bak/Bax is not clear. Yamaguchi *et al.* (2008) demonstrated that Bid disassembled OPA1 oligomers in mitochondria isolated from wild type cells but not in those from Bak/Bak double knock-out cells. Addition of oligomerised recombinant Bax restored wild type OPA1 disassembly. However, somewhat counter-intuitively, MOMP-inhibiting drugs did not inhibit OPA1 disassembly, which the authors interpreted as an indication that Bid does not affect OPA1 oligomers *via* access gained through Bak/Bax oligomeric pores. Thus there could be a regulatory role for Bak/Bax in cristae remodelling outside of MOMP activities. Interestingly, they also showed that disassembly-resistant mutant OPA1 self-oligomerised in a GTP-dependent manner and that expression of this mutant in HEK293 cells potently prevented Bim-induced apoptosis, despite the fact that Bak activation still occurred. Recently, (Landes *et al.*, 2010) have implicated another BH3-only protein, Bnip3, in OPA1 oligomer disassembly, cristae remodelling and fusion dynamics. Interestingly, Bnip3 integrates into the mitochondrial OM through its C-terminal transmembrane domain (TMD), exposing its last 10 residues to the IMS. Abolition of this IMS residue also abolished OPA1 interaction, but the same result was not obtained upon abolition of the cytosolic residues. Furthermore, polykaryons overexpressing Bnip3 replicated the mitochondrial fragmentation and fusion deficit observed in OPA1 knock-out cells, while cells expressing Bnip3 with a mutated BH3 domain (Bnip*mut*BH3) induced fragmentation while failing to trigger apoptosis. Later experiments showed that Bnip3*mut*BH3 failed to disassemble OPA1 oligomers, while the wild-type protein did so successfully, in a Bax/Bak dependent manner.

The proteolytic processing of OPA1 has already been discussed in the context of fusion regulation, but it has been suggested as a substrate of another protease in relation to this

cristae remodelling. Cipolat *et al.* (2006) have described a rhomboid protease of the mitochondrial IM called presenilin-associated rhomboid-like (PARL) that influences cytochrome c release through OPA1 cleavage. In this study, PARL-null mice developed muscular, splenic and neurological degeneration, dying within eight weeks of birth, with general cachexia. These symptoms were found to be from increased apoptosis in these tissues, most severely affecting muscle and immune tissue. PARL-null MEFs displayed normal mitochondrial morphology, respiration and $\Delta\Psi_m$, but prematurely released cytochrome c and displayed condensed cristae morphology significantly faster than wild type cells after induction of apoptosis with tBid. Bax/Bak oligomerisation was not significantly different between cell types, nor were OPA1 levels, nor mitochondrial fusion rates. Finally, the authors showed that PARL-null mitochondria lacked soluble S-OPA1 found in the IMS of wild type cells. Exogenous expression of OPA1 protected wild type cells but not PARL-null cells from apoptosis and expression of PARL in PARL-null cells restored S-OPA1 cleavage products. Thus cleavage of OPA1 seems to regulate cristae remodelling, possibly by providing short isoforms for assembly of OPA1 oligomers at cristae junctions.

It must be acknowledged that some investigators dispute the degree of cristae remodelling required for cytochrome c release. As an example, Sun *et al.* (2007) found that cytochrome c release occurred in HeLa cells before mitochondria assumed 'type II' cristae conformation and in cells incubated with the pan-caspase z-VAD inhibitor, cytochrome c was released without any cristae remodelling observed during experimentation. This does not necessarily disprove the admittedly strong argument for the involvement of OPA1-regulated cytochrome c release, but indicates that there may be other routes to cytochrome c release that are more pronounced in certain cell types.

1.4.2.2 DRP1 in Apoptosis

As previously mentioned, mitochondrial fragmentation usually accompanies the progression of apoptosis. Again, there is controversy surrounding the subject – it is not known if fragmentation is part of the execution of apoptosis or merely a consequence of it. There is a general consensus that DRP1 may be involved in apoptosis, but that it is a dispensable factor (Sheridan *et al.*, 2008, Sheridan and Martin, 2010, Landes and Martinou, 2011). Indeed, reconsidering the study mentioned earlier by Lee *et al.* (2004), DRP1 silencing attenuated apoptosis is HeLa cells but did not fully block it. Moreover,

fragmentation and cytochrome c release are not interdependent processes (Arnoult *et al.*, 2005); overexpression of Mfn1/2 does not prevent cytochrome c release from apoptotic HeLa cell mitochondria (Sheridan *et al.*, 2008) and wild type HeLa cell mitochondria fragment a full ten minutes after cytochrome c release during UV radiation-induced apoptosis (Gao *et al.*, 2001). Despite these findings, several groups have convincingly demonstrated the recruitment of DRP1 to mitochondria during apoptosis in multiple cell types (Frank *et al.*, 2001, Karbowski *et al.*, 2002, Neuspiel *et al.*, 2005).

Numerous groups have also confirmed that Bcl-2 family proteins do not only interact with OPA1 during apoptosis. Karbowski *et al.* (2002) elegantly demonstrated an interaction between Bax, DRP1 and Mfn2 in HeLa and COS-7 cells. Following induction of apoptosis, Bax was observed to accumulate at foci on mitochondria which frequently became scission sites. Expression of mutant DRP1 did not affect this Bax assembly, but fission was prevented. Interestingly, mitochondria in wild type cells often remained anchored to one another following fission *via* complexes that were found to contain Mfn2 in addition to Bax. The authors speculate, in their 2006 paper on Bax/Bak regulation of mitochondrial fusion, that apoptotic activation of Bax/Bak could cause a conformational change that specifically ends their fusion promoting activities and allows increased fission (Karbowski *et al.*, 2006). Germain *et al.* (2005) have shown that DRP1 is involved in Bik-mediated cristae remodelling and cytochrome c release, though the authors did not examine OPA1 cleavage/oligomers in this study. Finally, a fascinating study by Wasiak *et al.* (2007) used fluorescence recovery after photobleaching (FRAP) to examine yellow fluorescent protein (YFP)-tagged DRP1 recruitment to mitochondria in healthy and apoptotic cells. They found that DRP1 in healthy cells rapidly cycles between the cytosol and mitochondria with a half time of 50 seconds. Upon induction of apoptosis, Bax/Bak assembly on the mitochondrial OM causes this cycling to cease as DRP1 is stably recruited. Furthermore, the mechanism of this stable recruitment involves Bax/Bak-dependent sumoylation of DRP1. These studies support the findings of Karbowski *et al.* (2002) and also provide another example of fission regulation through PTM of DRP1.

Finally, an unusual state between fission and fusion, termed 'hemifusion', induced in liposomes by DRP1, has been described in the context of apoptosis. Montessuit *et al.* (2010) used liposomes containing phosphatidylcholine, phoshpatidylethanolamine and

cardiolipin to examine tBid-dependent Bax oligomerisation. Having tested a number of cell and tissue lysates that stimulated tBid-mediated Bax oligomerisation in liposomes, they determined that DRP1 was a key stimulant. This effect was dose-dependent, GTP-independent but, unexpectedly, ATP-dependent, although DRP1 was found not to hydrolyse ATP. The group found that liposomes aggregated following DRP1 addition and further investigation revealed that liposomes had undergone hemifusion, in which the outer leaflets of opposing membranes had mixed but the contents of each vesicle had not. Promotion of hemifusion in the absence of DRP1 (using cytochrome c at pH 6) also promoted Bax oligomerisation, suggesting the key factor was not DRP1 *per se*, but its ability to facilitate hemifusion. This may go some way towards explaining why knock down of DRP1 in cells does not completely abolish apoptosis – the presence of other hemifusion facilitators could offset the decrease in this protein (Landes and Martinou, 2011).

1.4.2.3 Mitofusins in Apoptosis

It should be clear at this point that depletion of DRP1 causes mitochondrial hyperfusion and is somewhat protective against apoptosis. It is difficult to deduce from these experiments whether the hyperfusion itself plays a part in the protection against apoptosis, or if it is merely an unrelated variable. Neuspiel *et al.* (2005) examined the significance of the distinctly lower affinity of Mfn2 for GTP (relative to Mfn1) in the context of apoptosis through the overexpression of an 'activated' mutant Mfn2 in COS-7 cells. This 'activated' mutant has an increased nucleotide binding affinity but reduced hydrolysis rate and as such, utilises GTP rather more like a Ras protein; tight binding of GTP activates Ras proteins in signal transduction and the low rate of hydrolysis prolongs the activation phase. Overexpression of 'activated' Mfn2 was protective against apoptosis, but this was not due to hyperfusion. Rather, 'activated' Mfn2 was shown to localise to mitochondria diffusely rather than at punctae and interfere with Bax activation and MOMP; indeed, less than 20% of 'activated' Mfn2-cells analysed exhibited activated Bax and cytochrome c release after three hour treatment with staurosporine. These results suggest a bidirectional regulatory crosstalk between Bax/Bak and Mfn2 in apoptosis regulation.

Other studies suggest a role for mitochondrial fusion itself in delaying the progression of apoptosis. A phenomenon called 'stress induced hyperfusion' (SIHF) has been described

by Tondera *et al.* (2009) in several cell types, including MEFs, HeLa cells, mouse primary fibroblasts and astrocytes. Cells exposed to a number of stressors, e.g. UV radiation, serum deprivation and treatment with actinomycin D (transcription inhibitor), exhibited hyperfused mitochondria within 2-3 hours, peaking after 6-9 hours. This increase in fusion resulted in increased ATP levels, specifically through OXPHOS, and resistance to further stress and apoptosis. Interestingly, this process was dependent on a mitochondrial protein of ill-defined function called stomatin-like protein 2 (SLP2). Previously reported as a putative Mfn2 interactor (Hajek *et al.*, 2007), it was found to stabilise OPA1 in the long isoform, which allowed hyperfusion to proceed in a Mfn1 (but not Mfn2) dependent manner. Mitochondrial hyperfusion has also been described during cellular starvation (Gomes *et al.*, 2011) but this will be described in section 1.4.4.3.

A schematic summarising our current knowledge of mitochondrial dynamics in apoptosis is provided in fig. 1.6. Given the rich array of interactions documented between apoptosis effectors and mitodynamins, it is quite difficult to conceive that these two essential functions of mitochondria are not connected in some way. One must concede that because fragmentation can occur several minutes after the release of cytochrome c, it is possible that this morphological change during apoptosis merely functions to 'prime' the organelles for degradation as part of systematic programmed cell death (Sheridan and Martin, 2010). However, in light of the fact that not only one, but *all* of the mitodynamins function as control points in apoptosis, or interact with other regulatory proteins at some level during the process, it seems very likely that mitochondrial dynamics are influential during the progression of programmed cell death.

1.4.3 Mfn2 - Roles Outside of Fusion

The pleitropic roles of mitodynamins have become obvious during the course of this review. As the mitofusins are only 60% structurally identical (Santel and Fuller, 2001), it seems logical that one, or both of these mitodynamins should have roles outside of fusion. There is strong evidence to suggest that, indeed, this is the case, especially for Mfn2. In the rat brain, Mfn2 is expressed predominantly, and Mfn1 only marginally (Eura *et al.*, 2003). Curiously, though, Berman *et al.* (2009) report that in rat cortical neurons, only 1-2% apparent encounters between mitochondria result in fusion. This could be explained by the recent discovery by Hoppins *et al.* (2011) that Mfn homotypic complexes are less fusogenic than are heterotypic complexes; if there is significantly

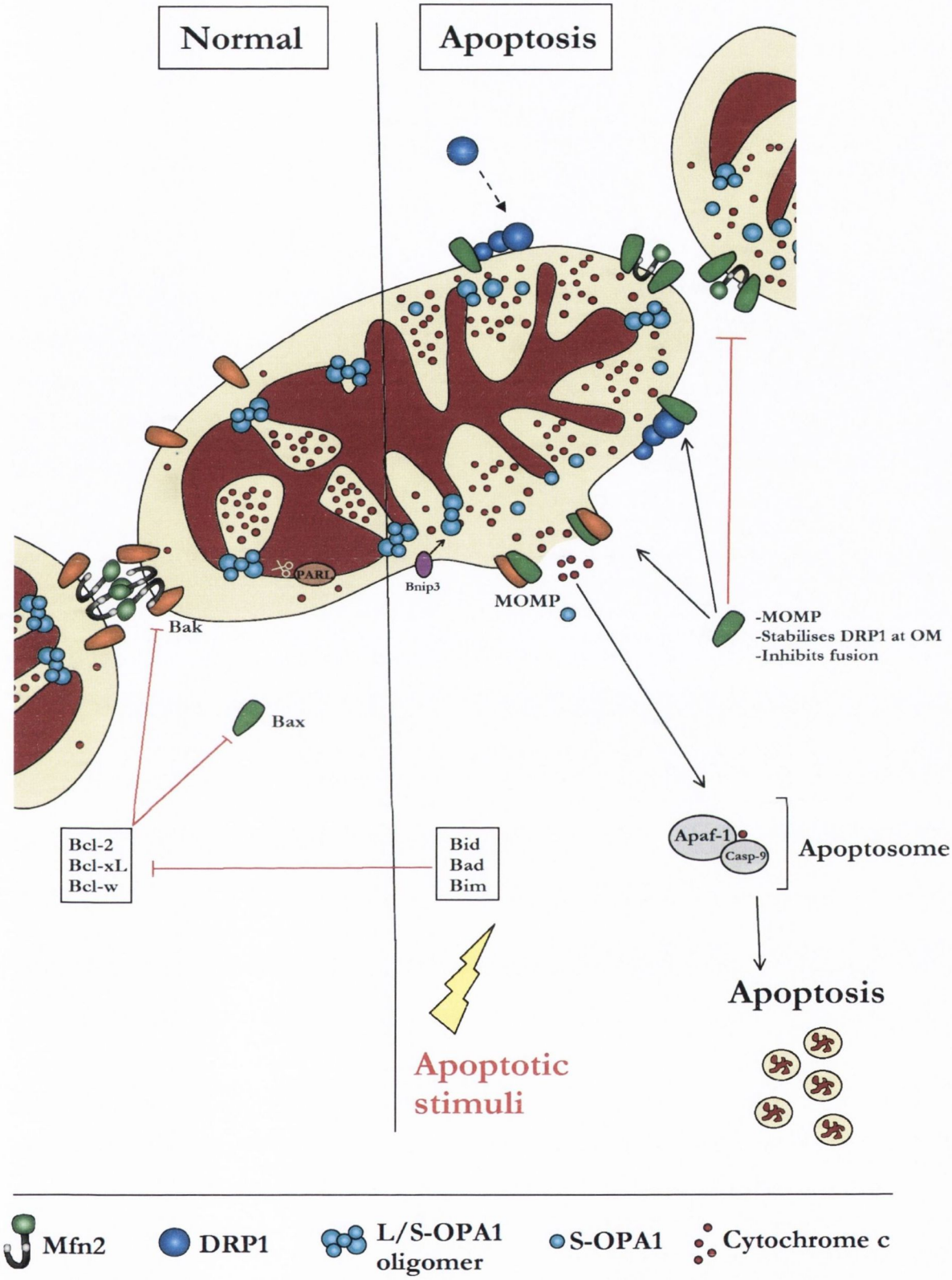

Figure 1.6: The role of mitodynamins in apoptosis. Under normal conditions, anti-apoptotic Bcl-2 family proteins (e.g. Bcl-2, Bcl-xL, Bcl-w) inhibit apoptotic effector Bcl-2 family proteins Bak (located on the mitochondrial outer membrane, OM) and Bax (mostly cytosolic). Bak colocalises with Mfn1/2 on the OM and positively regulates fusion. Cytochrome c is enriched within inter-cristal junctions, which are 'gated' by OPA1 oligomers composed of both S- and L- isoforms. The inner membrane (IM) protease PARL cleaves OPA1 into short isoforms which aids oligomer formation. In response to apoptotic stimuli, pro-apoptotic BH3-only Bcl-2 proteins (e.g. Bid, Bad, Bim) inhibit anti-apoptotic Bcl-2 proteins, liberating Bak and Bax from inhibition. During cristae remodelling, OPA1 oligomers are disrupted, possibly by BH3-only Bcl-2 protein Bnip3, unleashing cytochrome c into the IM space (IMS). Bax is recruited to the OM, where Bax/Bak hetero- and homo-oligomers form, permeabilising the OM (MOMP). Cytochrome c is released through the Bax/Bak OM pore, where it binds Apaf-1 and caspase-9 (casp-9), forming the apoptosome and committing the cell to apoptosis. The S isoform of OPA1 is also released and potentiates apoptosis through an unknown mechanism. In addition, Bax colocalises with DRP1 at future scission sites and stabilises DRP1 at the OM, while fusion is inhibited through interactions with Mfn2. This leads to eventual fragmentation of the mitochondrial reticulum as apoptosis progresses.

implicated as an anti-proliferative protein. Indeed, its increased expression in post-mitotic neurons may relate to this particular function.

In addition, Mfn2 appears to have an important role in endoplasmic reticulum (ER) regulation and calcium buffering. It has been shown by de Brito and Scorrano (2008a) that Mfn2 not only regulates ER morphology, but also tethers mitochondria to the ER thereby improving calcium buffering capacity. Interestingly, in a follow-up study (de Brito and Scorrano, 2009), the authors elucidated a potential role for Ras in this process. The investigators found that expression of Mfn2 lacking its Ras binding domain in $Mfn2^{-/-}$ MEFs could fully rescue the typically fragmented mitochondrial phenotype, but could restore neither ER/mitochondrial apposition nor errant ER morphology, though the exact mechanism underlying this remains elusive. Thus Mfn2, and its Ras binding domain, are essential for ER morphology, calcium buffering and cell proliferation. Mitofusin 2 also has an important bioenergetic regulatory role but this will be discussed in the context of bioenergetics and mitochondrial dynamics, which follows.

1.4.4 Mitochondrial Dynamics and Bioenergetics

The first indication of an interaction between mitochondrial morphology and bioenergetics came from the pioneering works of Hackenbrock, who elegantly demonstrated a rapid morphological change in isolated mouse liver and intact ascites tumour cell mitochondria upon OXPHOS stimulation (Hackenbrock, 1966, 1968, Hackenbrock *et al.*, 1971). When mitochondria were in respiratory state 4, they assumed an 'orthodox' conformation, typical of that observed in tissue following fixation i.e. filamentous cristae within a matrix of intermediate electron density and relatively small IMS. However, a dramatic change occurred upon induction of state 3 respiration, in which mitochondria assumed a 'condensed' conformation, featuring a highly condensed, electron-dense matrix, with enlarged IMS but apparently unchanged total mitochondrial volume. Several decades later, this work has been further confirmed in living cells, as mitochondria change to a more condensed and reticular form upon alternating cellular energy substrates from glycolytic to more oxidative forms (Rossignol *et al.*, 2004, Benard *et al.*, 2007). However, the relationship between mitochondrial dynamics and bioenergetics is not quite as simplistic as these data would suggest. A crucial issue is the hierarchical organisation of this relationship – does mitochondrial bioenergetic state dictate morphological behaviour, or vice versa? There is mounting evidence to suggest

both are true, that the relationship is a bi-directional crosstalk (Benard *et al.*, 2011). Understanding this relationship fully has major implications in health and disease, as myriad disease states, such as cancer, neurodegeneration and, of course, mitochondrial diseases, exhibit both bioenergetic dysfunction and concomitant alterations in mitochondrial dynamics. What follows is a discussion of the evidence demonstrating the influence of mitochondrial morphology on bioenergetics, followed by the evidence demonstrating the opposite effect – bioenergetics influencing mitochondrial dynamics.

1.4.4.1 The influence of Mitochondrial Dynamics on Bioenergetics

It is quite compelling that neurons, which derive upwards of 90% of their ATP from mitochondria (Cai and Sheng, 2009) appear to be among the most severely affected by aberrations of mitochondrial fission, fusion and transport. To some extent, this fact alone asserts the importance of mitochondrial dynamics in energy metabolism. Other circumstantial evidence of how mitochondrial dynamics influence bioenergetics can be extracted from the studies of complementation of mtDNA expression through mitochondrial fusion, discussed in section 1.4.1. To reiterate; cells homoplasmic for non-overlapping mtDNA mutations exhibited mitochondrial dysfunction and mitochondrial fragmentation but, upon PEG-induced cell fusion, exhibited restoration of mitochondrial function (including functional OXPHOS machinery and respiration rates comparative to control cells) assembled into a tubular reticulum (Gilkerson *et al.*, 2008). Thus, the fusion-competent, yet OXPHOS-dysfunctional mitochondria saw a restoration of function following fusion, through functional complementation. The literature provides examples of more direct influences of DRP1, OPA1 and Mfn2 on bioenergetics, with an emphasis on the latter, fusogenic mitodynamins.

Benard *et al.* (2007) report that DRP1-deficient cells not only exhibit the typical elongated mitochondrial phenotype, but also significantly lower respiratory rates, RCRs and decreased ATP production. Furthermore, they found decreases in mitochondrial membrane fluidity of DRP1-deficient cells, which resulted in decreased *in situ* complex IV activity (but not *ex situ*, demonstrating the membrane-dependent effect). This is remarkable in light of the demonstrated ability of DRP1 oligomers to influence lipid dynamics in liposomal hemifusion (Montessuit *et al.*, 2010) and cristae remodelling (Germain *et al.*, 2005). Thus DRP1 may influence OXPHOS through alteration of membrane properties.

Optic atrophy 1-mediated mitochondrial fusion has been revealed by many investigators to be important in bioenergetics. This is not surprising given its dual roles in fusion and cristae remodelling. It was first implicated in this context by Olichon *et al.* (2003), who showed OPA1-deficient HeLa cells had reduced $\Delta\Psi_m$. Chen *et al.* (2005) went on to demonstrate that OPA1 depletion in MEFs decreased their growth rate almost seven-fold. This was accompanied by a remarkably decreased respiration rate that could not be increased even in the presence of mitochondrial uncouplers, reduced substrate-driven respiration through complexes I, III and IV and heterogeneous $\Delta\Psi_m$. Strikingly, these effects were all reversible through exogenous expression of OPA1 in OPA1-null cells, indicating that the respiratory defects are due to decreased fusion, rather than mtDNA loss, as is seen in Mgm1-null yeast. Since this study, Zanna *et al.* (2008) have highlighted some important energetic defects in fibroblasts from ADOA patients carrying truncated OPA1-producing mutations. Cells were capable of growth under conditions of forced OXPHOS (glucose-free, galactose-containing medium) but exhibited balloon-like structures and significantly reduced mitochondrial fusion in these circumstances. Additionally, OXPHOS through complex I substrates was significantly hindered, although expression of a number of complex I subunits was not different from controls. Interestingly, OPA1 co-immunoprecipitated with apoptosis inducing factor (AIF) and with subunits of complexes I, II and III. Thus OPA1 haploinsufficiency led to perturbed fusion and OXPHOS defects in ADOA patient fibroblasts, possibly due to decreased stabilisation of ETC enzymes.

Finally, Mfn2 has been shown to have a sizeable influence on the regulation of mitochondrial bioenergetics, particularly in exercise physiology, obesity and insulin resistance in diabetes. Obesity, type 2 diabetes and even ageing are associated with insulin resistance, reduced metabolic flexibility (switching between glucose and lipid metabolism depending on substrate availability) and reduced muscle oxidation of glucose and fatty acids (Petersen *et al.*, 2003, Zorzano *et al.*, 2009). Bach *et al.* (2003) have shown an important role for Mfn2-mediated mitochondrial fusion in L6E9 myotube differentiation to myoblasts. Induction of differentiation was correlated with upregulation of Mfn2 and a significant increase of mitochondrial interconnectivity. Depletion of Mfn2 led to a decrease in mitochondrial respiration and a significant decrease in glucose oxidation. Furthermore, skeletal muscle samples from obese rats and humans showed ~40% downregulation of Mfn2 compared to controls, concomitant with

mitochondrial fragmentation. The authors suggest these data partially explain the metabolic deficiencies commonly associated with skeletal muscle from obese patients, such as reduced oxidation processes and impaired glucose-induced thermogenesis (Astrup *et al.*, 1990).

In a follow-up study, the authors found a strong negative correlation between Mfn2 mRNA expression and body mass index (BMI) in control and obese patient samples (Bach *et al.*, 2005). They also found that dramatic weight loss by surgical intervention significantly increased Mfn2 mRNA levels in skeletal muscle of formerly obese patients, which corresponded to an increase in insulin sensitivity and glucose oxidation in muscle samples. This weight-loss-induced increase in Mfn2 mRNA levels was also found by Mingrone *et al.* (2005), suggesting a role for Mfn2 in exercise physiology. Indeed, Cartoni *et al.* (2005) have reported that the nuclear transcription factor peroxisome proliferator-activated receptor γ coactivator 1α (PGC-1α), which is involved in metabolic homeostasis and mitochondrial biogenesis, positively regulates Mfn2 gene expression. Expression of PGC-1α is increased in skeletal muscle two hours after exercise, leading to a significant increase in Mfn2 mRNA expression 24 hours later, which could contribute to exercise-induced increases in mitochondrial content, size, oxidative capacity and aerobic glucose oxidation. More recently, Liesa *et al.* (2008) have demonstrated that PCG-1β directly promotes mitochondrial fusion in a Mfn2-dependent manner and suggest that PCG-1α regulates this process in response to stimulated mitochondrial activity (such as during exercise), whereas PCG-1β is a regulator at basal activity.

Interestingly, Pich *et al.* (2005) propose that some of the effects of Mfn2 on muscle cell physiology lie outside its role in fusion. Expression of loss-of-function Mfn2 in L6E9 myotubes was found to inhibit pyruvate, glucose and fatty acid oxidation and reduce $\Delta\Psi_m$, whereas expression of Mfn2 gain-of-function had the opposite effect. This Mfn2 loss-of-function led to downregulation of nuclear encoded subunits of complexes I, II, III, V, whilst over expression of functional Mfn2 causes upregulation of subunits of complexes I, IV and V. Interestingly, these effects were also observed in cells expressing a truncated form of Mfn2 lacking fusogenicity, in which mitochondria did not exhibit aberrant morphology, but adopted the 'condensed' state described by Hackenbrock to correspond to state 3 respiration (Hackenbrock, 1966). Thus, in these experiments, Mfn2 was dispensable for mitochondrial fusion but not for a functional OXPHOS

system. This does not necessarily negate the role of mitochondrial fusion in OXPHOS regulation as, presumably, the cells expressed normal levels of Mfn1 and OPA1, which would maintain healthy levels of fusion and propagate the OXPHOS-regulatory effects of Mfn2 throughout the reticulum.

Most recently, Guillet *et al.* (2011) have established a role for Mfn2 in the regulation of mitochondrial ATP-sensitive potassium channels (mK_{ATP}), macromolecular protein complexes located on the IM and proposed to comprise complex II, ATP synthase, ANT, ATP-binding cassette protein 1 (ABC1) and the phosphate carrier. Mitochondria from brains of mice expressing a CMTIIa mutant of Mfn2 exhibited reduced RCR, complex II and ATP synthase activity and dramatic reductions in ATP levels. This could be reversed with the addition of mK_{ATP} inhibitor, while an agonist of the channel reproduced the disease phenotype in healthy control samples. Thus the authors propose Mfn2 stabilises the mK_{ATP} through an unknown mechanism, and Mfn2 mutations lead to bioenergetic defects as a result of this loss of stability.

Taken as a whole, these data suggest expression of Mfn2 supports OXPHOS as the primary means of energy production. Indeed, the differentiation of embryonic stem cells into cardiomyocytes involves a switch from glycolytic metabolism to oxidative, which coincides with an upregulation of Mfn2 (de Brito and Scorrano, 2008b). This may also go some way towards explaining the disproportionately high expression of Mfn2 in neurons compared to Mfn1 (Eura *et al.*, 2003) given their high OXPHOS dependence (Cai and Sheng, 2009). These effects may or may not be related to the role of Mfn2 in fusion but in light of the information currently available in the literature, it seems likely that the effects are due to a combination and/or co-ordination of these dual roles.

1.4.4.2 The Influence of Bioenergetics on Mitochondrial Dynamics

One of the greatest hindrances to our understanding of the effects of bioenergetics on mitochondrial dynamics is the fact that OXPHOS and glycolytic capacities vary greatly between cells. For example, most cancer cells typically derive a disproportionate amount of ATP (~50% or more) from glycolysis, a process known as aerobic glycolysis or the Warburg Effect (Warburg, 1956), whereas non-transformed cells typically rely more on OXPHOS. In addition, the microscopic observation of mitochondrial dynamics is limited to the use of cultured cells as technical hurdles have yet to be overcome to repeat

such studies *in situ* or *in vivo*. Many cultured cells are known to exhibit increased glycolysis relative to those *in vivo*, to the point where inhibition of glucose phosphorylation with 2-deoxy-D-glucose (DOG) produces a 70% decrease in ATP (Sauvanet *et al.*, 2010). This issue can be overcome to some extent by culturing the cells in a glucose-free medium containing galactose, in which the inefficiency of conversion of galactose to glucose-1-phosphate *via* the Leloir pathway forces a dependence on glutaminolysis and thus, OXPHOS (Rossignol *et al.*, 2004). Nevertheless, caution should be applied when extrapolating mitochondrial dynamics data derived from *in vitro* studies. Despite these issues, studies focusing on the effects of bioenergetics on mitochondrial dynamics have yielded some important results and fall in to one of two categories; those modulating metabolism using drugs (such as those described in 1.1.2) and those observing morphological changes in cells with metabolic defects of genetic origin.

The first studies describing changes in mitochondrial dynamics following chemical inhibition of mitochondrial bioenergetics reported that uncouplers, such as FCCP and CCCP, caused extensive fragmentation in HeLa cells, with both punctate and disk-shaped organelles clearly distinguishable (Legros *et al.*, 2002, Mattenberger *et al.*, 2003). Interestingly this effect is reversible – removal of the uncoupler allows the return to tubular morphology (Duvezin-Caubet *et al.*, 2006, Guillery *et al.*, 2008). As discussed in section 1.3.2, these $\Delta\Psi_m$-dependent changes in mitochondrial morphology were later shown to correspond to specific OPA1 cleavage patterns but the reason for this response to depolarisation is unknown. It is conceivable that maintaining and/or rectifying the $\Delta\Psi_m$ is more achievable in a smaller organelle and sudden depolarisation stimulates fission to facilitate this, but this has yet to be established. Mitochondrial depolarisation is arguably one of the only forms of chemical bioenergetic modulation that reliably reproduces the fragmented mitochondrial reticulum across most mammalian cell type; ETC/OXPHOS inhibition seems to have cell type-dependent effects on mitochondrial morphology.

De Vos *et al.* (2005) report that inhibition of complex I with rotenone, complex III with antimycin A, or ATP synthase with oligomycin results in mitochondrial fragmentation in epithelial CV1 cells and MEFs. Yet, Legros *et al.* (2002) found that, of these, oligomycin was the only agent to induce fragmentation in HeLa cell mitochondria, while DOG also produced fragmentation. To obfuscate matters further, Pletjushkina *et al.* (2006) found that fragmentation occurs with complex I,III and ATP synthase inhibitors in CV1 cells,

but oligomycin was ineffective in HeLa cells, while complex I and III produced fragmentation. Benard *et al.* (2007) found that rotenone had a dose-dependent effect on mitochondrial fragmentation and cell death in MRC5 fibroblasts, while oligomycin also induced fragmentation. Insulinoma INS-1E and hepatocellular carcinoma HEP-G2 cells exhibited fragmentation upon rotenone treatment according to the work of Plecita-Hlavata *et al.* (2008). Studies of human skin fibroblasts (HSF) have been somewhat contradictory also; cells were found to exhibit mitochondrial outgrowth upon rotenone exposure, rather than fragmentation according to Koopman *et al.* (2005a), while Guillery *et al.* (2008) describe the same cells undergoing partial mitochondrial fission following chemical inhibition of complexes I, III, IV and ATP synthase. While differences in inhibitor concentrations and incubation times may account for some of the variation, it appears there are also cell-specific effects of ETC/OXPHOS inhibition on the mitochondrial fission/fusion balance, the intricacies of which are not yet clear.

Human skin fibroblasts derived from patients with mitochondrial dysfunction are commonly used to model the effects of genetic bioenergetic aberrations on organellar morphology. Koopman *et al.* (2005b) showed that genetic complex I deficiency led to morphological aberrations in the mitochondria of thirteen HSF cell lines carrying mutations in nuclear genes encoding different complex I subunits or complex I assembly proteins/chaperones. Of these cell lines, two exhibited fragmented mitochondria, three exhibited an increased number of mitochondria, three showed increased reticulation and branching of mitochondria and five exhibited shortened mitochondria with decreased branching (distinct from fragmentation). Thus there appeared to be a mutation-dependent influence of ETC defect on mitochondrial morphology. The general trend amongst the cells was that those exhibiting the greatest inhibition of complex I activity (~60%) also presented with shortened or fragmented mitochondria, while those exhibiting the lowest inhibition of complex I activity (~30%) presented with increased branching and no reduction in organelle number. Interestingly, PEG-generated polykaryons between two cell lines with mutations in two different complex I core catalytic subunits (NDUFS1 and 2) exhibited mitochondrial morphological restoration through functional complementation. Thus defective ETC function in these cells had direct effects on mitochondrial morphology. More recently, Moran *et al.* (2010) have described HSF carrying mutations to core complex I subunits different from those of (Koopman *et al.*, 2005b) These cells did not exhibit significant differences in

mitochondrial morphology compared to control, however, their mitochondria were significantly slower to recover filamentous morphology following transient exposure to the uncoupler CCCP, indicating dysfunctional OXPHOS can affect mitochondrial morphological changes in response to further organellar perturbation.

Transformed cell lines have also been used to examine genetic mitochondrial defects in the context of mitochondrial morphology. Hayashi *et al.* (1994) created a cell cybrid by fusion of HeLa cells lacking mtDNA (ρ^0 HeLa) with HSFs from a patient carrying a mutation in the $tRNA^{ARG}$ gene and presenting with mitochondrial myopathy, encephalopathy, lactic acidosis, and stroke (MELAS). They found the disease phonotype replicated in the HeLa cell cybrids, with severe OXPHOS deficiency combined with swollen and balloon-like mitochondria clustered around the nucleus. Likewise, Szczepanowska *et al.* (2004) showed that when human osteosarcoma cells carrying a mtDNA mutation associated with neurogenical muscle weakness, ataxia and retinitis pigmentosa (NARP) contained 68% mutant mtDNA (below safe heteroplasmy threshold), mitochondria were filamentous like those of controls but when cells were almost homoplasmic for the mutant mtDNA, mitochondria became disorganised and fragmented.

Taken together, it is clear that although bioenergetic modulation can demonstrably change the balance between mitochondrial fission and fusion, the effects can be cell type-specific and as yet, no clear pattern has emerged whereby cellular oxidative capacity can be deduced from observation of mitochondrial morphology.

1.4.4.3 Stress-Induced Hyperfusion – Integration of the Bidirectional Crosstalk?

Interestingly, the aforementioned phenomenon of stress-induced hyperfusion (SIHF) may represent a unique bioenergetics-dynamics feedback loop that integrates the two sides of the bidirectional crosstalk discussed so far. Gomes *et al.* (2011) have found that mitochondrial hyperfusion during starvation spares them from autophagic degradation and promotes survival through optimal ATP production. Autophagy is a survival mechanism employed by cells during periods of nutrient deprivation; recycled breakdown products, like sugars, fatty acids and amino acids, resulting from the lysosomal degradation cytoplasmic material, are metabolised to maintain cellular homeostasis (Rambold *et al.*, 2011).

Gomes and colleagues demonstrated that MEFs maintained in physiological saline (rather than culture medium) for several hours exhibited an increase in cyclic AMP, which led to the activation of PKA and subsequent inhibition of DRP1 *via* phosphorylation. This not only allowed for fusion to proceed unopposed, but actually increased fusion rates. Strikingly, hyperfusion was associated with an increase in the formation of ATP synthase oligomers, which are believed to be more efficient in the production of ATP (Strauss *et al.*, 2008). In addition, when hyperfusion was blocked, mitochondria 'cannabilised' cytosolic ATP to maintain $\Delta\Psi_m$, probably by reversal of ATP synthase, which resulted in massive cell death. Therefore, the cellular bioenergetic state initially influenced mitochondria to elongate, which in turn improved ATP production efficiency and cell survival. Assuming no irreparable damage had occurred to the cells during starvation, it is conceivable that they would resume normal mitochondrial dynamics upon return to nutrient-rich medium, but this has not yet been assessed.

1.5 Conclusion

The field of mitochondrial dynamics is a point of convergence for many cellular functions and dysfunctions, from mitochondrial maintenance and quality control, to apoptosis execution and regulation, to numerous disease states including neurodegeneration, cancer and diabetes. Despite the incredible progress made in this area in the past decade, there are significant gaps in our knowledge. The mechanism of mitochondrial membrane fusion is still very much a mystery, as is the process of DRP1 recruitment and assembly at the OM. Furthermore, it is still not known how significant fragmentation is in the process of apoptosis, but given its ubiquity across species, it seems to be a relevant aspect of programmed cell death. A better understanding of the mechanisms of all of these processes should give valuable insight into the diverse regulatory pathways relating to mitochondrial function in health and disease may provide new therapeutic targets.

Evidently, examples abound of changes in mitochondrial morphology following bioenergetic modulation. A critical aspect that has been neglected, however, is the actual fusion rates of mitochondria in cells following treatment. Mere observation of morphology does not provide information regarding the change in rates of the opposing forces governing organellar shape. If mitochondria are fragmented, it is impossible to tell if this is due to an increase in fission rate that overwhelms the fusion machinery, or if

it is due to an inhibition of fusion, while fission proceeds as normal. Thus, observation of morphology is generally not a reliable indication of mitochondrial bioenergetic state.

1.6 Aim of Thesis

Mitochondrial morphology is regulated by the balanced processes of fission and fusion. Emerging evidence indicates that the maintenance of this balance is critical in the regulation and execution of numerous mitochondrial functions. Conversely, dysregulation of this balance has far reaching implications in human health and disease, particularly in relation to conditions in which mitochondrial dysfunction is a critical element of pathogenesis. Cancer and neurodegeneration are two such illnesses and advancing our knowledge of how and why mitochondrial dysfunction develops in each case will aid in the design of treatments for both. This project focuses on the effects of bioenergetic modulation on mitochondrial fusion rates in human cervical carcinoma HeLa cells and rat primary cortical neurons. Specific aims are described in relevant chapters.

CHAPTER 2

Materials and General Methods

2.1 General Methods

2.1.1 Antibodies and Reagents

All reagents were obtained from Sigma-Aldrich Co., Poole, Dorset, UK, unless otherwise stated. Mitochondria-targeted photo-activatable green fluorescent protein (PA-GFP-mito) and pDsRed2-mito plasmids were kind gifts from Dr. Richard Youle (NIH, Bathesda, Maryland, USA) and Dr. Seamus Martin (Trinity College, Dublin), respectively. Antibodies used are as follows; mouse anti-DRP1 (BD Transduction Laboratories, Oxford, UK, Cat No. 611112); rabbit anti-Glial Fibrillary Acidic Protein (GFAP, Dako, Denmark, Cat No. Z0334); rabbit anti-Hexokinase I (Abcam, Cambridge, UK, Cat No. 65069); rabbit anti-hexokinase II (Cell Signalling, MA, USA, Cat No. 2867); rabbit anti-Mfn1 (Santa Cruz, CA, USA, Cat No. SC-50330); rabbit anti-Mfn2 (Sigma, Cat No. M6319); mouse anti-OPA1 (BD Transduction Laboratories, Cat. No. 612606); mouse anti-α-tubulin (Millipore, MA, USA, Cat No. 05-829 mouse anti-TUJ1 (Covance, NJ, USA, Cat No. MMS-435P) and rabbit anti-VDAC1 (Abcam, Cat No. 15895).

2.1.2 Preparation of Solutions and Pipetting

Reagents were weighed either on a Mettler College Model analytical balance or on a Mettler K7T top-loading balance for weights above or below 5g, respectively. All aqueous solutions were prepared using deionised water from a Millipore Direct-Q3 Water Purification System. All solutions were adjusted to the appropriate pH using a Corning pH meter, Model 240, which was calibrated daily using standard buffer solutions of pH 4.0, 7.0 and 10.0. Gilson pipettes were used to pipette volumes from 1μl to 5ml.

2.1.3 Centrifugation

A variety of centrifuges were used. For volumes of 2ml or less, an Eppendorf Benchtop Centrifuge 5415 was used. Various steps in the purification of rat brain mitochondria required the use of a Sorvall RC-5B centrifuge with an SS34 rotor. For subcellular fractionation of the rat brain, a Sorvall Discovery 100 centrifuge, fitted with an AH-629 rotor (6 x 30ml tubes), was used. All centrifuge tubes were balanced on the Mettler College Model analytical balance before centrifugation. Finally, a Thermo Scientific

Heraeus Multifuge 3SR Centrifuge was used to pellet cells suspended in volumes of 2 – 50ml.

2.1.4 Electrophoresis

An AE-6450 Dual Mini Slab Kit and a BioRad PowerPac 300 were used for all SDS-PAGE.

2.1.5 Experimental Animals

All experimental animals were obtained from the Bioresources Unit, TCD. Adult female Wistar rats, weighing approximately 250g each, and were killed by cervical dislocation. Neonatal pups were, weighing approximately 20g each, were sacrificed at postnatal day 1 and killed by swift beheading using sharp, sterile, surgical scissors.

2.1.6 Cell Culture

All cell culture work was carried out under sterile conditions in a NUAIRE laminar flow hood. All cells were maintained at 37°C, in 95% humidity and 5% CO_2. Cell growth and viability was monitored visually using a Nikon Eclipse TS100 light microscope with 10x, 20x and 40x dry objectives. Cell counts were performed using a Reichert haemocytometer and cell viability was assessed by exclusion of trypan blue dye.

2.1.7 Statistical Analysis

Statistical analyses were carried out using a combination of Microsoft Excel 2003 and GraphPad Prism 5. All data were tested for Gaussian distribution and equal variance within the GraphPad Prism 5 software. All data are presented as mean $\pm$ SEM unless otherwise stated. A P-value of 0.05 or less was deemed to be statistically significant. The particulars of statistical analyses pertaining to each experiment are described in the relevant results sections.

2.1.8 Image Processing

All images were processed using a combination of FV10-ASW Olympus Fluoview Ver. 2 software (for confocal microscopy images), Microsoft Paint 2007, Image J (NIH) and Adobe Photoshop 7. All diagrams and illustrations were created using a combination of Creative Docs .Net freeware, Version 3.3.6 (Epsitec SA, www.creativedocs.net) and Microsoft Paint 2007.

2.2 Protein Estimation

The protein concentrations were estimated as per the method of Bradford (1976), with modifications. Bovine serum albumin served as a standard and was prepared, from a stock of 0.1mg/ml, as a series of dilutions ranging from 2 - 20μg/ml with a final volume of 800μl (in triplicate). To these (and to diluted samples of unknown protein concentration), 200μl of Protein Assay Dye Reagent Concentrate (Bio-Rad, CA, USA) was added and samples were incubated for 30 minutes. Two-hundred microlitres of each sample was transferred into a well of a 96-well microtitre plate and the absorbance of each was read at 595nm in a SpectraMAX PLUS Microplate Spectrophotometer, corrected for blank. An example of the standard curve commonly generated is given in fig. 2.1.

2.3 Western Blotting

Samples were estimated for protein content and loaded onto 8% - 15% polyacrylamide gels in *Laemmli* sample buffer. Between 10 and 20μg protein were loaded into each well, using Spectra Multicolour Broad Range Protein Ladder (ThermoFisher, MA, USA) as a molecular weight marker. Gels were run at constant Amps (20mA/gel) for 90 minutes using BioRad Bio-Rad PROTEAN II xi Cell and a BioRad PowerPac 300. A semi-dry transfer technique was employed to transfer the samples onto Immobilon nitrocellulose membrane, at constant voltage (10V) for one hour. The membrane was blocked in 5% BSA in TBST overnight at 4°C and incubated in primary antibody in 5% BSA (1:500 – 1:2000 dilution) overnight at 4°C. Finally, the membrane was incubated in secondary antibody in 1% BSA (goat anti-rabbit HRP, Millipore, goat anti-mouse HRP, Sigma, both 1:10000 dilution) for 2 – 3 hours at room temperature. For visualisation of bands, the

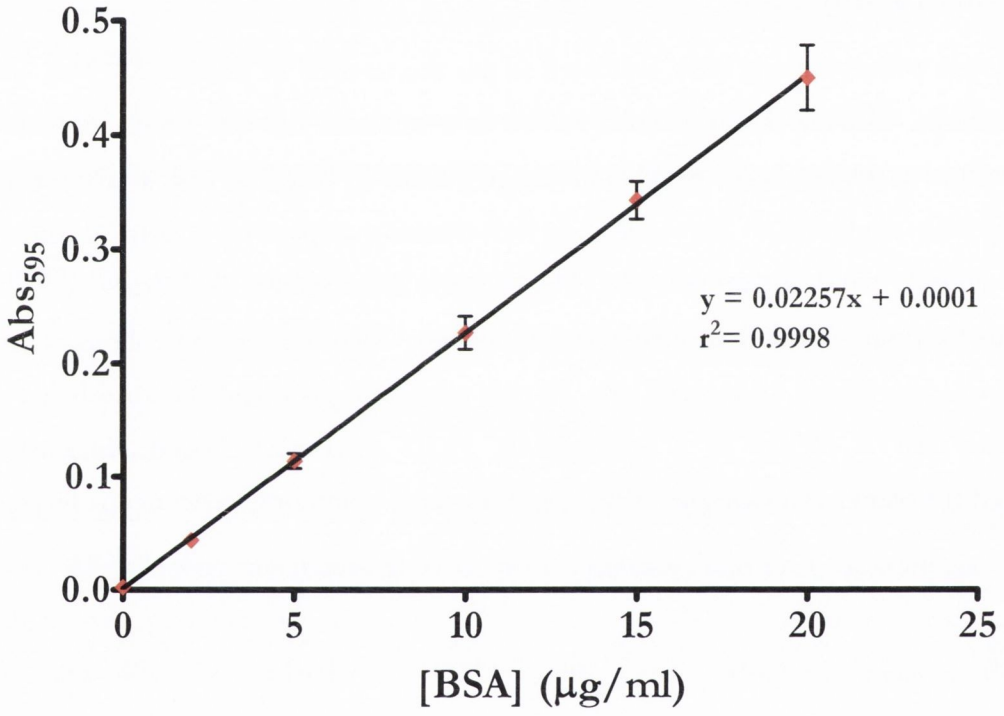

Figure 2.1: Standard curve generated in Bradford protein estimation. Representative of standard curve commonly generated in protein estimation experiment, where the slope is defined by the equation '$y = mx + c$' and the r^2 value estimates 'goodness of fit' of data to linear regression (a value of 1 indicating a perfect fit). Data presented as mean ± SD.

membrane was covered in 0.3 - 2ml chemiluminescent reagent (Santa Cruz) for 2 - 5 minutes and incubated with photographic film for the appropriate time (10 – 300s). The film was developed using a Fuji X-Ray Film Processor RG II. Densitometry measurements of bands were carried out using Image J software.

2.4 Microscopy

2.4.1. Fluorescence Microscopy

Indirect fluorescence of cells cultured on glass coverslips was viewed with a Zeiss Axiovert/Axiocam CCD system and AxioVision AxioVs40 software. The system's mercury lamp light source was used to irradiate samples, which were viewed using standard filter sets for for 4,6-diamidino-2-phenylindole (DAPI), FITC & rhodamine chromophores Blue/green/red, through 10x and 20x dry objectives and a 60x oil objective.

2.4.2 Confocal Microscopy

Direct and indirect fluorescence of fixed and live cells were viewed using an Olympus FV1000 Point Scanning Confocal Microscope, FV10-ASW Olympus Fluoview Ver. 2 software and a 60X oil immersion objective. Sequential excitation at 405nm, 488nm and 546nm were provided by near-violet laser diode, argon and helium-neon gas lasers, respectively. The imaging chamber was heated to 37°C, humidified and contained 5% CO_2 for live cell imaging. Fixed samples were imaged at a resolution of 1024 x 1024 with Kalman filter set to 6, while live cells were imaged at a resolution of 512 x 512 without Kalman filter, to avoid phototoxicity in the samples.

2.4.3 Quantification of Mitochondrial Fusion Rates

The method of quantification of mitochondrial fusion rates was based on that of Karbowski *et al.* (2004a), with modifications, and relied on the principle that mitochondria share matrix contents upon fusion. By conferring high fluorescence to a small group of mitochondria within the cellular mitochondrial matrix (photoconverting mitochondria-expressed GFP to a state of 100-fold increased fluorescence in a small

region of interest, or ROI), the rate of fusion can be monitored by measuring the rate of decrease in fluorescence intensity in the ROI as matrix contents are shared by fusing organelles. All experiments were carried out using the Olympus FV1000 Point Scanning Confocal Microscope, FV10-ASW Olympus Fluoview Ver. 2 software and a 60X oil immersion objective with 1.7x zoom applied. Cells cultured in 35mm glass bottomed μ-dishes (Ibidi, Munich, Germany) were placed in the live imaging chamber and covered with the CO2 regulator/humidifier apparatus. Sequential excitation at 488nm and 543nm allowed for visualisation of PA-GFP and DsRed protein expression in transfected cells, respectively. Using the software's Multiple Time Lapse facility, six separate fields were pre-selected per group (control and inhibitor-treated) per dish, each containing 1 – 7 cells per field. Cells were imaged, with z-stacking (5 – 8 slices of 0.8 – 1.4μm thickness), before and after photoactivation of discrete 7μm^2 regions of interest (ROIs) of the mitochondrial network, with post-activation imaging intervals set at 1, 15 and 30 minutes. Photoactivation was achieved by 5 second irradiation of ROIs using the 405nm laser set to 1 - 4% power output, depending on cell type. The photoactivated protein exhibited 85-95% increased fluorescence compared to its non-activated state. Regions exhibiting less than 85% increase in fluorescence post-activation were excluded from studies, as were cells that entered mitosis during the experimental period. Using the software's Image Analysis facility, the mean pixel intensities of the photoactivated ROIs were calculated in both the red and green channels at all time points and expressed as a percentage of pixel intensity 1 minute post-activation, deemed to be the point at which the pixel intensity was highest. Pixel intensities were also measured in three 7μm^2 ROIs in cell-free areas and subtracted from the cellular ROIs as 'background' fluorescence. Each treatment was repeated on at least three separate dishes of cells on three separate occasions (n = 3); thus each data point on graphs depicting fusion rates is representative of data from 18 – 126 cells (average ~60 cells).

2.4.4 Quantification of $\Delta\Psi m$

Mitochondrial membrane potential was measured by confocal microscopy using the $\Delta\Psi_m$ –dependent dye tetramethylrhodamine, methyl ester (TMRM, Invitrogen, CA, USA). This cationic, red-orange fluorescence-emitting dye is sequestered by mitochondria in a $\Delta\Psi_m$-dependent manner and at non-quenching concentrations (below 50nM), indicates mitochondrial depolarisation upon loss of signal (and, conversely, hyperpolarisation upon increase in signal). Cells were loaded with the dye in normal culture medium

containing 20nM TMRM for 30-60min (depending on cell type), followed by incubation with 5nM TMRM for the duration of imaging. Excitation with the 543nm laser set to 1.4% power output allowed for visualisation of red-emitting TMRM within mitochondria of cells, viewed through a 60x oil objective. The imaging settings were adjusted such that the background fluorescence was negligible and the signal from cells was below saturation level. Six randomly chosen fields were pre-selected using the software's Multiple Time Lapse facility and imaged before and after incubation with or without inhibitors. Using the software's Image Analysis facility, mean pixel intensities of each field were calculated and expressed as a percent of initial, pre-incubation values.

2.5 Immunocytochemistry

Cells cultured on 13mm glass coverslips were fixed in 4% paraformaldehyde in PBS for 15 minutes, permeabilised in 0.2% Triton in PBS for 10 minutes, rinsed in PBS and blocked in 1% BSA in PBST for 30 minutes. Cells were incubated in primary antibody in 1% BSA in PBST for one hour and in secondary antibody (anti-rabbit/mouse 488 or 546, Invitrogen) in 1% BSA in PBST for one hour. Coverslips were placed on 3ul Vectashield mounting medium containing the nuclear counterstain 4,6-diamidino-2-phenylindole (DAPI) (Vector Labs, CA, USA) on glass slides and sealed with clear nail varnish, then stored at 4°C, in darkness, until imaging.

2.6 ATP Measurement

Measurement of cellular ATP content was performed as per the method of Kilbride *et al.* (2010) and using Enliten Recombinant Luciferase/Luciferin (rL/L) Reagent (Promega, CA, USA). The assay uses the measurement of luminescence derived from the reaction below to detect ATP levels present. As ATP is the limiting factor, direct quantitation of ATP levels is possible.

$$ATP + \text{D-Luciferin} + O_2 \rightarrow \text{Oxyluciferin} + AMP + \text{Pyrophosphate} + CO_2 + Light_{560nm}$$

Cells cultured in 24-well plates and were incubated with or without inhibitors in pre-equilibrated culture medium for the required time (5 – 20 minutes), then rinsed briefly with PBS. Two-hundred microlitres of hypotonic lysis buffer (100mM Tris, 2mM

EDTA, pH 7.75) were added to each well and the plate was immediately frozen at -80°C. For measurement of ATP levels, samples were thawed on ice and 50µl of each sample was placed in a well of a white 96-well luminescence microplate. To this, 100µl of rL/L Reagent (previously brought to room temperature for one hour) was added and the plate was immediately read in a SpectraMAX GeminiXS plate fluorimeter, set to luminescence mode. No more than seven samples were read at a time owing to the speed at which the reaction occurred. The readings obtained (in relative luminescence units, RLU) were converted to pmol ATP by use of an ATP standard curve (fig. 2.2), which was repeated every time a new batch of rL/L was used. Finally, ATP measurement were normalised to protein concentration and expressed either as pmol/µg or per cent control.

2.7 Molecular Biology

While the pDsRed2-mito plasmid is commercially available from Clontech (CA, USA), the PA-GFP-mito plasmid was developed by Karbowski and colleagues (2004). Both plasmids encode a fusion fluorescent protein and mitochondrial targeting sequence from subunit VIII of human cytochrome c oxidase. Both also contain cytomegalovirus (CMV) promoters and confer neomycin resistance in eukaryotic cells and kanamycin resistance in *E.coli*. Upon receipt of PA-GFP-mito and pDsRed2 plasmids, it was necessary to prepare larger stocks of each to ensure enough was available for all planned experiments. These stocks were prepared as detailed below. All microbiological procedures were carried out using aseptic technique.

2.7.1 Transformation of Competent Bacterial Cells

Fifty nanograms of plasmid DNA were added to 100µl Top 10 Chemically Competent *E.coli* (Invitrogen) in a sterile 1.5ml minifuge tube. The bacteria were heated to 42°C for exactly 30 seconds and then placed on ice for two minutes. Five hundred microlitres of SOC media (Novagen, WI, USA) were added to the transformed cells and the tube was sealed and incubated at 37°C, with gentle agitation, for one hour. Following this incubation, 10 – 25µl of bacteria were spread on a 9cm petri dish containing 12ml sterile Lennox LB agar (Chromatrin, Dublin, Ireland) at 35g/L, containing 50µg/ml kanamycin. The plate was incubated overnight at 37°C to allow for growth of colonies of successfully transformed bacteria.

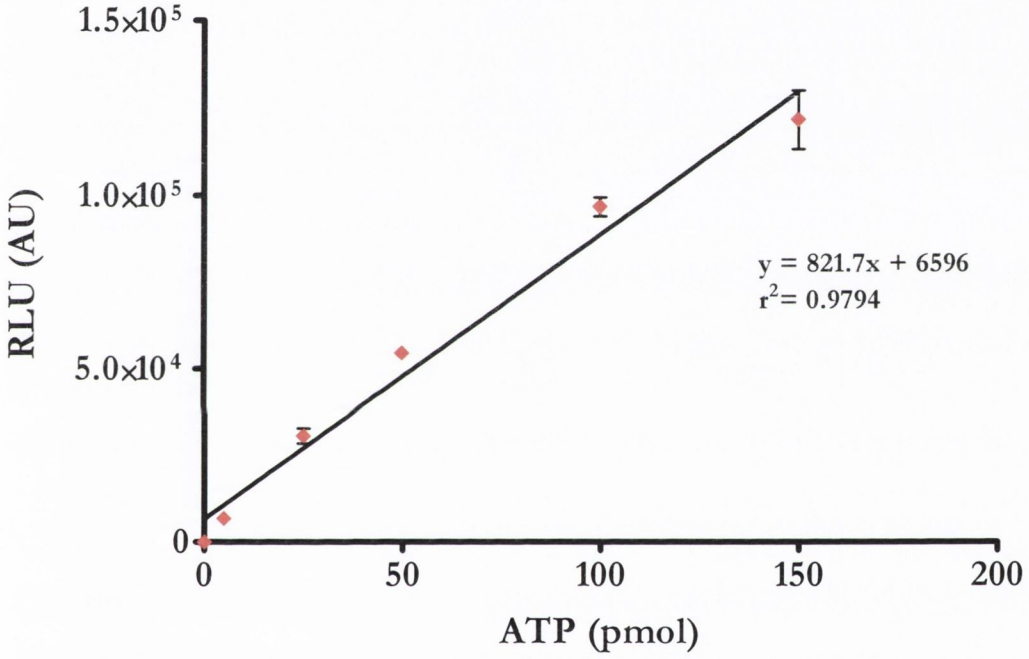

Figure 2.2: ATP standard curve for the Enliten rL/L Assay. Representative of standard curve repeated with each fresh aliquot of rL/L reagent used, where the slope is defined by the equation $y = mx + c$ and r^2 value estimates 'goodness of fit' of data to linear regression (a value of 1 indicating a perfect fit). Data presented as mean ± SD.

2.7.2 Growth of Single Colonies and Miniprep

To increase the volume of cells from an individual colony for the purposes of performing a Miniprep and making glycerol stocks, 5ml of 20g/L LB Broth (Chromatrin) (containing 50μg/ml kanamycin) in 50ml falcon tubes was inoculated with a single colony picked from agar plates using a sterile 2 – 200μl yellow tip. A total of six individual colonies were selected for amplification and incubated overnight with constant swirling (200 rpm) at 37°C. The following day, 1ml of each culture was set aside and stored at 4°C for making glycerol stocks, pending a successful Miniprep. The remaining 4ml of each was centrifuged at 16, 000 x g for one minute in batches of 1.5ml, to pack the cells from each tube into a pellet. The Miniprep was then carried out using a QiaPrep Spin Miniprep Kit (Qiagen, Hilden, Germany) as per manufacturer's instructions.

2.7.3 Restriction Digest and Agarose Gel Electrophoresis

The final plasmid isolates produced in the Miniprep were assessed by agarose gel electrophoresis. For the restriction digest, 500ng plasmid DNA was incubated with 5% (v/v) BamH1 restriction enzyme (Fermentas, Germany) in a final volume of 20μl digest buffer (Fermentas) for two hours at 37°C. To this, 5μl of 6X Sample Loading buffer (Novagen) was added and 25μl was loaded per well of a 1% (w/v) agarose gel (1g agarose in TAE buffer; 40mM Tris-HCl, 200mM sodium Acetate, 1mM EDTA, pH 8.2) containing 2μg/ml ethidium bromide. The samples were run alongside 5μl DirectLoad Wide Range DNA Marker, 50 – 10,000bp range (Sigma). The gel was run at 65V for 90 minutes and the DNA bands were visualised under UV light using a UVP Bioimaging Systems Epi Chemi II Darkroom and Labworks Image Acquisition and Analysis Software V 4.0.0.8. The results of the digests for each plasmid are shown in fig. 2.3.

2.7.4 Glycerol Stocks and Maxiprep

Glycerol stocks were prepared by adding 20% (v/v) sterile glycerol to the 1ml of culture derived from the single colonies chosen and previously set aside before the miniprep. Stocks were frozen at -80°C until required. For the maxiprep, LB agar plates containing 50μg/ml kanamycin were streaked with *E.coli* from glycerol stocks and incubated overnight at 37°C. The following day, a single colony was picked and used to inoculate

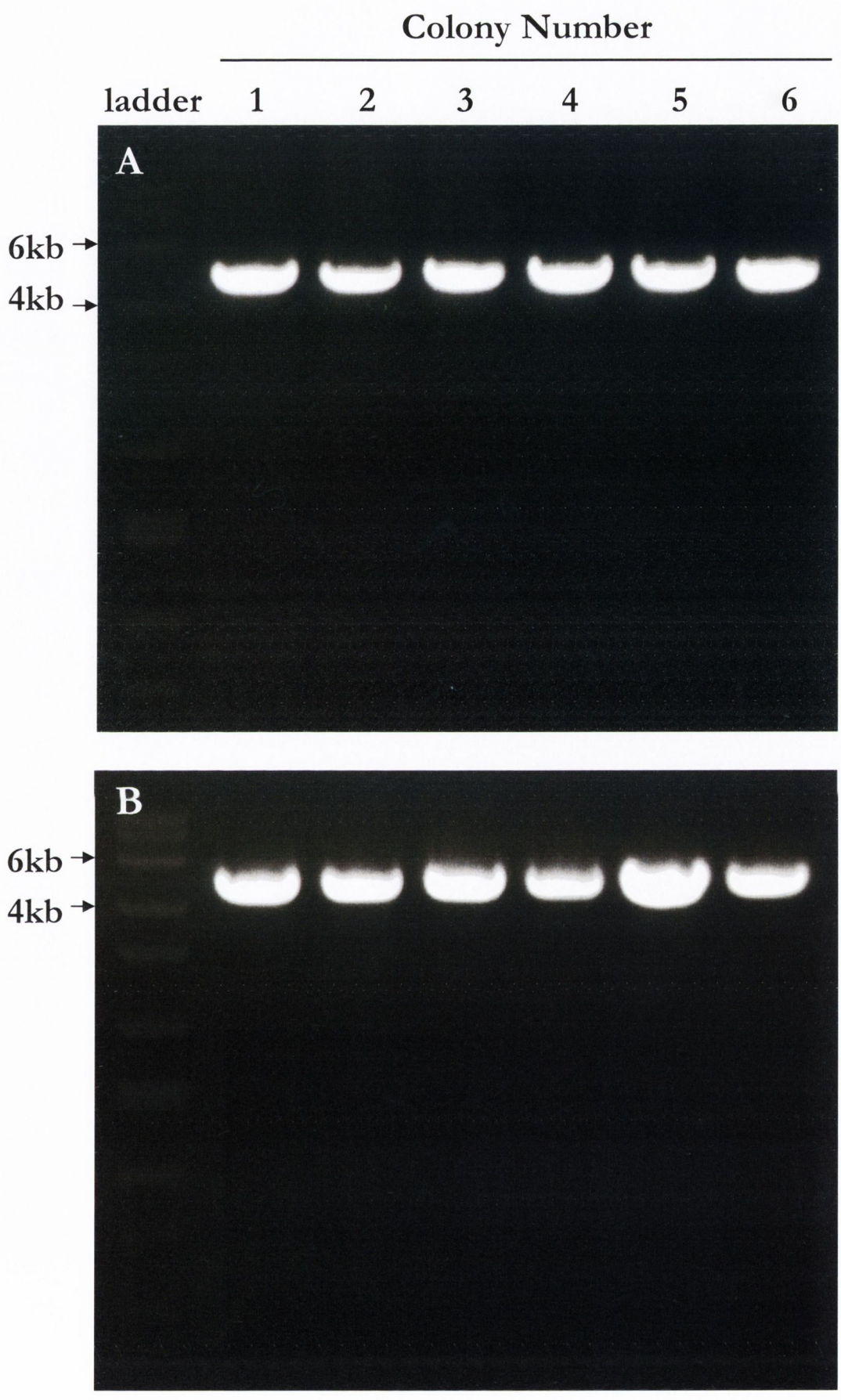

Figure 2.3: Agarose gels of digested plasmids from six colonies selected for Miniprep. Six *E.coli* colonies growing on agar plates following transformation with PAGFP-mito (A) or DsRed-mito (B) expression plasmids were selected for Miniprep. A restriction digest was carried out on the plasmid DNA purified from each colony and the digested plasmids were analysed agarose gel electrophoresis. All bands satisfactorily migrated to the portion of the gel corresponding to a plasmid size of 5kb. In both cases, colonies 1 and 6 were deemed to be the best and it was these from which glycerol stocks were prepared.

10ml of LB broth containing 50μg/ml kanamycin in a 50ml falcon tube. The tube was incubated at 37°C for eight hours, with swirling (200 rpm), then added to 145ml of LB broth/kanamycin in a 200ml Erlenmeyer flask and incubated overnight at 37°C,with swirling. The cells were then pelleted by centrifugation at 4000 rpm for 20 minutes. The pure plasmid was extracted using Invitrogen's PureLink HiPure Plasmid DNA Purification Maxiprep kit, according to manufacturer's specifications. Plasmid purity was assessed by ensuring that the ratio of Abs260/280 was less than 1.80, indicating minimal lipopolysaccharide contamination. This was perfomed using an Eppendorf Biophotometer Plus and Eppendorf UVette cuvettes.

2.8 Generation of DsRed-stable clones

For studies of mitochondrial morphology (rather than mitochondrial fusion), a HeLa cell line stably expressing the mitochondrially-targeted DsRed protein was generated.

2.8.1 Neomycin Kill Curve

As the plasmid confers neomycin resistance in eukaryotic cells, a kill curve was constructed to ascertain the optimum concentration to use to select positively transfected cells. Cells were seeded in 6 well plates at 8 x 10^4/well and were exposed to neomycin concentrations from 200 – 800μg/ml 24 hours later. Cells were visualised every 24 hours thereafter for seven days using an Olympus IX81-long focal length fluorescent microscope and phase-contrast images of ten random fields per neomycin dose were captured at 20X magnification, using a F-View II black and white camera in conjunction with *Cell P* software. Cell counts in the images collected were performed using *Image J*'s 'Cell Counter' function, the results of which are presented in fig 2.4. The appropriate neomycin concentration was deemed to be 600μg/ml.

2.8.2 Transfection of Cells and Selection

Cells were transfected using Gene Juice Transfection Reagent (Merck) as per manufacturer's instructions. Briefly, cells were seeded in two wells of a six well plate at 1.3 x 10^5/well. When 80% confluent, 100μl transfection solution containing 3μl Gene Juice and 1μg DsRed plasmid in serum-free DMEM was added to the cell culture medium of each well. The medium was removed after four hours and replaced with

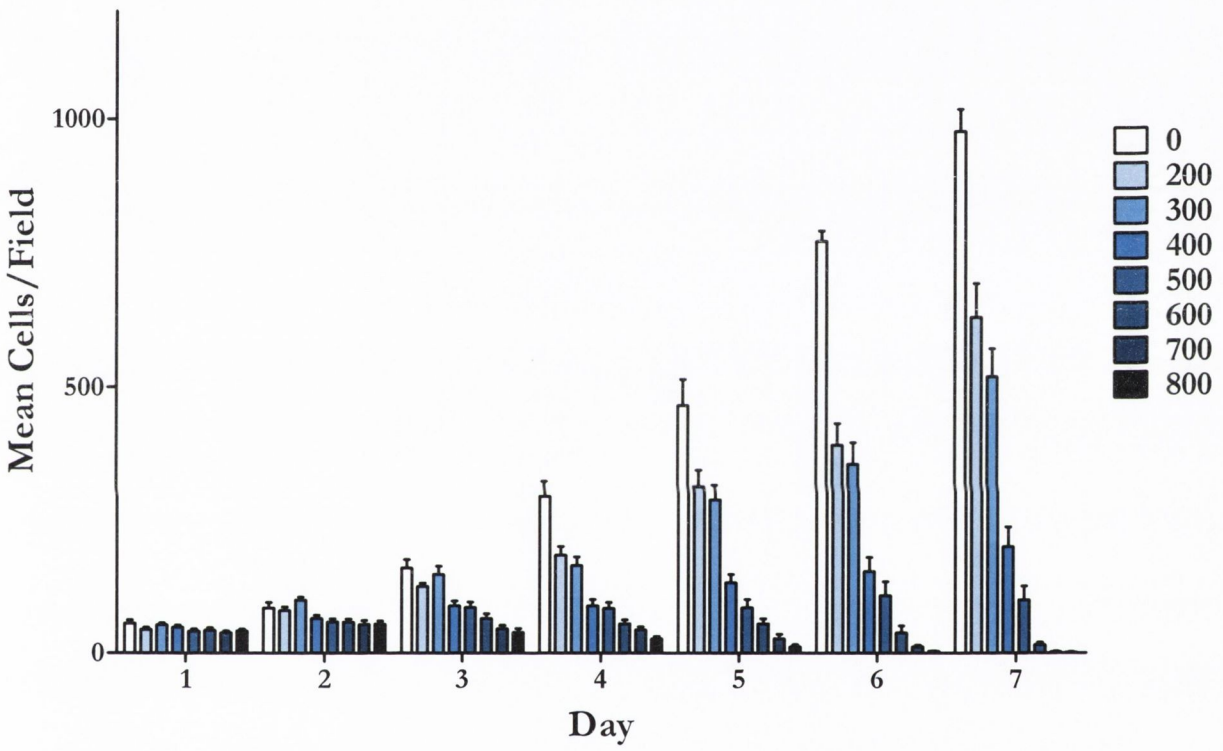

Figure 2.4: Neomycin kill curve in HeLa cells. Cells were seeded in 6-well plates, at a density of 8 x 10^4/well and exposed to neomycin 24 hours later at the concentrations indicated (μg/ml). Cells were counted daily in 10 random fields per concentration for one week. Control cells grew to complete confluence, whilst those exposed to neomycin exhibited time-and dose dependent cell death. Data presented as mean ± SEM.

fresh, pre-warmed medium. Cells were exposed to 600μg/ml neomycin 48 hours later. Surviving cells were allowed proliferate before further purification. Cells were selected and purified into 5ml sterile DMEM in a Beckman Coulter MoFlo FACS Machine, using a 150mW Coherent blue laser and a 580/30 band pass filter. The high-fluorescing cells were replated and allowed to rest for 48h before exposure to a maintenance-level dose of neomycin (120μg/ml). When sufficient stocks has been accumulated, cells were frozen in FBS containing 10% (v/v) dimethyl sulfoxide (DMSO) and stored in liquid nitrogen until required. Upon retrieval from liquid nitrogen, cells were cultured for at least a week before use in experiments.

CHAPTER 3

Bioenergetic Control of Mitochondrial Dynamics in HeLa Cells Cultured in High Glucose Medium

3.1. Introduction

Hanahan and Weinberg defined six classic hallmarks of cancer as sustaining proliferative signalling, evading growth suppressors, resisting cell death, enabling replicative immortality, inducing angiogenesis, and activating invasion and metastasis (Hanahan and Weinberg, 2000). Recently, they suggested the addition of a seventh hallmark; reprogramming of energy metabolism (Hanahan and Weinberg, 2011). Mitochondria in cancer have come into focus owing to their central roles in two of the distinguishing hallmarks of tumorigenesis; apoptosis regulation and cellular bioenergetics. Moreover, mitochondrial fission and fusion are fast being accepted as powerful regulatory mechanisms in both of these functions (Karbowski *et al.*, 2002, Suen *et al.*, 2008). Therefore, it is envisioned that a better understanding of the central attributes that distinguish mitochondria in cancer cells from their non-transformed counterparts will provide new insights into tumorigenesis and possibly reveal new therapeutic targets. What follows is a brief description of cancer bioenergetics, followed by a discussion of the potential role of mitochondrial dynamics in neoplastic transformation and progression.

3.1.1 Cancer Metabolism

At the core of the clonal selection that leads to invasive and metastatic disease is the ability of cancer cells to adapt to, and modify, their microenvironment. Key to this is altering cellular bioenergetics, as evidenced by the discovery that expression of a number of mutated oncogenes/tumour suppressor genes has direct effects on metabolism. For instance, tumour suppressor p53 has been shown regulate the balance of glycolysis and OXPHOS in the production of ATP (Matoba *et al.*, 2006). In non-transformed cells, p53 promotes OXPHOS by upregulating a number of OXPHOS promotion factors, including SCO2 (synthesis of cytochrome c oxidase 2), a complex IV subunit assembly factor. Mutation or knock down of p53 leads to a significant decrease in respiration and an increase in glycolysis (Ma *et al.*, 2007), a common feature of cancer cells (see section 3.1.1.1). The oncogene MYC encodes transcription factor c-Myc which transactivates a number of glycolytic enzyme genes, such as lactate dehydrognase A (LDHA) and hexokinase (HK) II (Dang *et al.*, 2009). Thus, mitochondrial function and oncogenesis are inextricably linked.

3.1.1.1 The Warburg Effect

German biologist Otto Warburg was the first to discover one of cancer's most common metabolic features; the derivation of a disproportionate amount of energy (~50 - 70%) from glycolysis rather than OXPHOS, and the conversion of most pyruvate to lactate, even in normoxic conditions (Warburg, 1956). Termed 'aerobic glycolysis' or the 'Warburg effect', it is now the basis of one of the most common detection systems for cancer; positron emission tomography (PET) (Mathupala *et al.*, 2009). In non-transformed cells, glucose is phosphorylated by HK to glucose-6-phosphate (G-6-P), which is then converted to pyruvate and transported to mitochondria. There, it is converted to acetyl CoA via the pyruvate dehydrogenase complex (PDHC), which enters the TCA cycle and yields reduced equivalents that donate electrons to the ETC/OXPHOS system. Of the four HK isoforms characterised in humans (HK I – IV), HKIV (also called 'glucokinase') is the smallest (50kDa) and has the lowest affinity for glucose (K_m = 5 – 8mM). Hexokinases I – III are 100kDa proteins that duplicate the basic unit of HK IV and have vastly higher affinity for glucose (K_m = 0.02 – 0.03). Hexokinase I is generally accepted as a constitutively expressed 'housekeeping' isoform, while HK II is typically regulated in response to extracellular glucose levels (Robey and Hay, 2006). Importantly, HK II is the only HK isoform in which both catalytic sites of the two 50kDa 'glucokinase units' are catalytically active. These attributes may contribute to the fact that HK II is the primary isoform that is upregulated in cancer and involved in the Warburg effect (Pedersen *et al.*, 2002, Robey and Hay, 2006).

The PI3K/Akt pathway promotes cell survival through upregulation of anabolic and proliferative pathways when nutrient availability is high. It is also instrumental in the inhibition of apoptotic pathways *via* Akt-mediated inhibition of pro-apoptotic Bcl-2 proteins (Yamaguchi and Wang, 2001). This pathway is frequently dysregulated in cancer (Elstrom *et al.*, 2004, Hennessy *et al.*, 2005). Indeed, the mutation of phosphatase and tensin homolog (PTEN), a potent negative regulator of PI3K signalling, is one of the most common in cancer genetics (Pandolfi, 2008, Azim *et al.*, 2010). Deregulation of the PI3/Akt pathway can directly affect HK II in cancer cells; rather than residing in the cytosol, HK II is phosphorylated by Akt (Majewski *et al.*, 2004), which promotes its translocation to the mitochondrial OM via interaction with the VDAC. This holds three main advantages for the enzyme; the first is that it reduces allosteric inhibition by G-6-P, the normal negative-feedback regulatory mechanism of HK, the second is that it gains

preferential access to mitochondrial ATP by exploiting the close proximity of VDAC to ANT within the ATP synthasome (a putative complex comprising ATP synthase, ANT and the inorganic phosphate carrier) and the third is that VDAC-bound HK II has 4.8-fold higher affinity for ATP compared to the cytosolic form (Bustamante and Pedersen, 1980, Mathupala *et al.*, 2009). Thus, HK II can phosphorylate glucose at a higher rate at a mitochondrial location.

It seems counterintuitive that rapidly proliferating cells would make use of a decidedly less efficient metabolic pathway to generate ATP. This may only be an important factor when the energy source is limited i.e. the cell must make efficient use of scarce substrates. However, this is generally not a problem faced by mammalian cells, as there is a constant supply of nutrients circulating in the blood. Thus energy efficiency may not be a prerequisite for survival in these conditions (Vander Heiden *et al.*, 2009). One of the main advantages of aerobic glycolysis is that cells can channel glycolytic breakdown products not towards OXPHOS, put towards anabolic pathways, generating biomass for the purpose of proliferation. For instance, G-6-P can be channelled to the PPP to generate ribose-6-phosphate and reduced NAD-phosphate (NADPH) for nucleotide synthesis, while citrate generated in the TCA cycle is excreted back to the cytosol to make lipids (Jose *et al.*, 2011) (see fig. 3.1). In addition, NADPH generated through the PPP can be used by glutathione reductase to regenerate reduced glutathione and provide ROS defence.

Thus, committing glucose to the generation of ATP is a lesser priority for proliferating cells than is the generation of anabolic building blocks. The production of amino acids, lipids and nucleotides requires more carbon intermediates and NADPH than it does ATP. Furthermore, high intracellular ATP/ADP ratio inhibits HK, which would lead to a shortage of glycolytic intermediates and the cessation of cell growth (Vander Heiden *et al.*, 2009). In addition, the relatively little amount of glucose that is converted to pyruvate can be preferentially converted to lactate rather than decarboxylated to acetyl CoA (Vander Heiden *et al.*, 2009). This is due to the oncogenic hypoxia-induced factor-1 (HIF-1)-mediated upregulation of LDH and PDH-kinase (negative regulator of PDH) and has a protective function: the release of lactic acid into surrounding tissue lowers the local pH and provides a protective acidified microenvironment that is intolerable to other cell types (Wu *et al.*, 2007, Jezek *et al.*, 2010), aiding invasion.

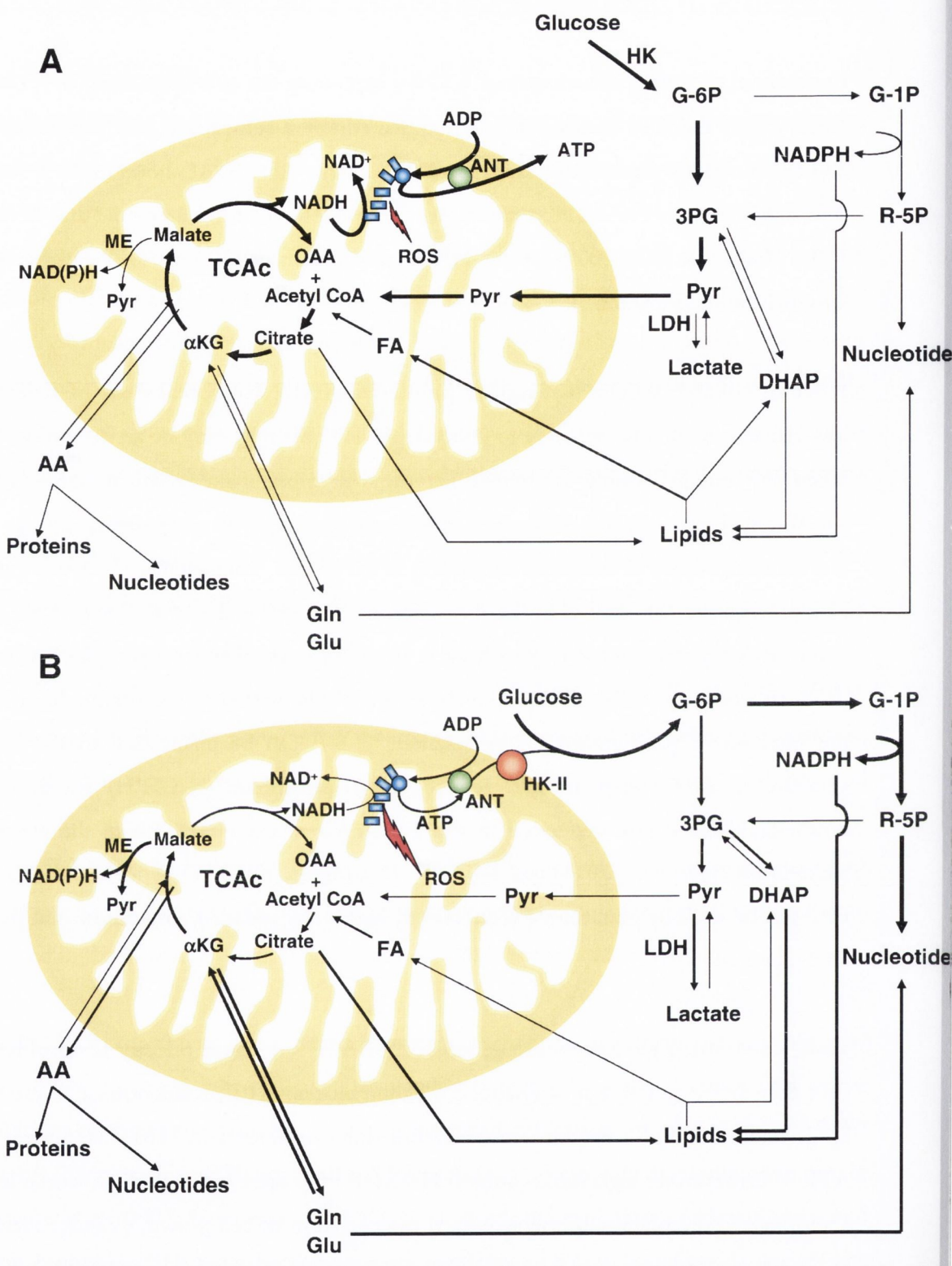

Figure 3.1: Comparison of metabolism in normal and cancer cells. (A) In normal cells glucose is phosphorylated to glucose-6-phosphate (G-6P) by hexokinase-I (HK), which is converted to pyruvate (Pyr). Upon import into the mitochondrion, it is decarboxylated and oxidized to acetyl CoA and enters the TCA cycle. This yields reduced equivalents (NADH), which donate electrons to the ETC (blue). A small amount of G-6P is shuttled to the pentose phosphate pathway to generate ribose 5-phosphate (R-5P) and NADPH, for nucleotide synthesis, while triose phosphates, NADPH and acetyl coA are used to synthesize lipids. Amino acids (aa), including glutamine (Gln) are also used in the TCA cycle and, in small amounts to synthesize the nucleotides. ATP synthase phosphorylates ADP and the resulting ATP is exchanged for ADP by the ANT. Reactive oxygen species (ROS) production is at basal levels. The emphasis is on ATP production, with lesser prority given to generation of biomass. (B) In cancer cells, anabolism is key, therefore glucose is mostly phosphorylated by HK-II (red), which is dramatically up-regulated and is localised to the mitochondrial OM where it gains easy access to mitochondrial ATP. Glucose-6-phosphate is only partially oxidized to pyruvate and this, in turn, is mostly reduced to lactate. The majority of G-6P is used to synthesize nucleotides that also require amino acids and Gln. Furthermore, citrate is diverted to the cytosol for conversion to acetyl CoA and is used, with NADPH, to make lipids. Mitochondria may become dysfunctional, giving rise to excess ROS. DHAP, dihydroxyacetone phosphate; FA, fatty acid; α-ketoglutarate; LDH, lactate dehydrogenase; ME, malic enzyme. Taken from Solaini *et al.*, 2011.

Finally, HK II is known to confer apoptosis resistance to cancer cells (Solaini *et al.*, 2011). So much so, in fact, that knock down or chemical removal of HK II (for example, using the anti-fungal imidazole derivative clotrimazole) leads to massive cell death in cultured carcinomas (Penso and Beitner, 1998). Although it is not fully understood how HK II confers apoptosis resistance, studies have shown that HK II interferes with Bak-mediated MOMP and cytochrome c release (Pastorino *et al.*, 2002), while detachment of HK II from the OM leads to PTP opening, possibly independently of VDAC (Chiara *et al.*, 2008). Hexokinase I has been shown to prevent VDAC opening (Azoulay-Zohar *et al.*, 2004), thus it is possible these two isoforms work in concert for this function.

3.1.1.2 The Role of Mitochondria in Cancer

Warburg initially proposed that aerobic glycolysis was necessary in cancer cells because their mitochondria were non-functioning. This is now known not to be the case and it is widely accepted that mitochondria are active participants in tumorigenesis. At the very least, HKII could not get preferential access to ATP at the mitochondrial OM if none was being produced by the organelle. Furthermore, several of the anabolic pathways mentioned above make use of mitochondrial TCA cycle intermediates, such as citrate and malate. In fact, cancer cells often exhibit numerous mitochondrial aberrations that are thought to contribute to cancer progression and survival, including mtDNA mutations, overproduction of ROS, and apoptosis resistance (Solaini *et al.*, 2011).

The degree to which OXPHOS continues during the Warburg effect is contentious. Some argue that respiration remains unchanged in malignant tumours despite concurrent aerobic glycolysis, generating a biogenesis-bioenergetics synergism (Mathupala *et al.*, 2010). However, larger tumours lacking adequate vascular penetration most certainly contain anoxic cells at their core, for which OXPHOS would be impossible (Semenza, 2010). Furthermore, HIF-1, the oncogenic transcription factor with glycolysis-promoting and respiration-depressing abilities, is upregulated in hypoxic conditions (Semenza, 2010), as its name suggests, and is crucial survival of cancer cells in hypoxia. In addition, many investigators have demonstrated increased respiration in cancer cells under conditions of forced OXPHOS (Rossignol *et al.*, 2004, DeBerardinis *et al.*, 2007, Vander Heiden *et al.*, 2009) suggesting a depression, to some extent, of OXPHOS during aerobic glycolysis. However it is important to note that even non-transformed mammalian cells generally switch to a more glycolytic phenotype in culture conditions

(Sauvanet *et al.*, 2010), therefore this latter observation could be somewhat misleading. Furthermore, HIF-1 is likely to have roles in oncogenesis independent of hypoxia, as it is also active in many normoxic tumours (Solaini *et al.*, 2011).

The degree of conformity to the 'Warburg' phenotype may depend on the proliferation rate of cells; fast-growing tumours can be effectively inhibited by administration of bromopyruvate, an inhibitor of glucose metabolism targeting HK, while this drug has little effect on slow-growing tumours (Jose *et al.*, 2011). Smolkova *et al.* (2011) have posited an intriguing hypothesis, whereby waves of gene regulation sequentially suppress and restore OXPHOS in accordance with specific stages of malignant transformation. Thus, early stages of hyperproliferation may promote inhibition of OXPHOS in order to satisfy biosynthetic demands, while more mature, established tumours with adequate angiogenesis may exploit the high ATP output of OXPHOS. By this mechanism, cancer cells would be alternately vulnerable to glycolysis inhibition and OXPHOS inhibition, again indicating mitochondria as attractive targets for chemotherapeutics at crucial stages of cancer progression.

As a key downstream effector of the aforementioned PI3K/Akt pathway, the mammalian target of rapamycin (mTOR) is a major regulator of cell growth and proliferation, cell survival, angiogenesis and metabolism (Azim *et al.*, 2010). Signalling *via* mTOR is extremely relevant to tumorigenesis; as part of a rapamycin-sensitive multi-protein complex (mTORC1) containing regulatory associated protein (raptor), it promotes the increase in translation of cyclin D1 (promoting a transition from G_1 phase to S-phase), vascular endothelial growth factor (VEGF, an angiogenic factor) and, significantly, HIF-1α, among others (Sun *et al.*, 2011). In addition, its activity as part of a rapamycin-insensitive complex (mTORC2), containing rapamycin-insensitive companion of mTOR (rictor), stimulates Akt and also regulates actin remodelling (and thus cell motility) (Jacinto *et al.*, 2004, Gulhati *et al.*, 2011). Interestingly, mTOR has been shown to positively regulate mitochondrial function both in cancer and in normal tissues. In skeletal muscle, its activation is associated with the activation of transcription factors PGC-1α and yin-yang-1 (YY1) and subsequent increased expression of mitochondrial proteins (Cunningham *et al.*, 2007). Studies of leukemic Jurkat cells have shown that mTOR colocalises with the mitochondrial outer membrane (Desai *et al.*, 2002, Schieke *et al.*, 2006) and interacts with VDAC and Bcl-xL (Ramanathan and Schreiber, 2009), the

latter being a specific phosphorylation substrate. Inhibition of mTOR with rapamycin in these cells abolishes this interaction and leads to the diversion of substrates away from mitochondria, increasing aerobic glycolysis and decreasing mitochondrial respiratory capacity within 25 minutes of inhibitor exposure (Schieke *et al.*, 2006, Ramanathan and Schreiber, 2009). These results indicate that mTOR has both short-term and long-term effects on mitochondrial function in transformed and non-transformed cells. The observation that mTOR signalling positively regulates mitochondrial function, yet is increased in some cancers exhibiting aerobic glycolysis is slightly jarring. It probably reflects the vast complexity of mTOR signalling and arguably asserts the role of mitochondrial biogenesis in cancer, even in highly glycolytic tumours. Indeed, the wave hypothesis states that during the aglycaemic phase of growth, brought on by rapid proliferation that exceeds vascularisation rate and thus limits glucose availability, mTOR signalling can be transiently inhibited by AMPK signalling but then reinstated by Akt signalling when cellular ATP levels have been restored (Smolkova *et al.*, 2011).

Little data exists on the role of mTOR in mitochondrial dynamics, however the studies of Gomes *et al.* (2011) examining SIHF have given some insight. Inhibition of mTOR is a classic stimulus of autophagy; in these studies, the SIHF observed during cell starvation was also stimulated by mTOR inhibition promoted mitochondrial elongation and hyperfusion, concomitant with increased phosphorylation of DRP1. Thus, inhibition of mTOR signalling increased cell survival during starvation through simultaneous promotion of autophagy and inhibition of mitophagy. Few other studies have examined the role of mitochondrial dynamics in cancer; what follows is a review of the current knowledge on this emerging field.

3.1.2.3 Mitochondrial dynamics in cancer

As described, two key hallmarks of cancer – subversion of apoptosis and metabolic reprogramming – directly involve mitochondrial function. Given the important relationship between mitochondrial dynamics and bioenergetics/apoptosis regulation, it follows that there may be a role for mitochondrial fission/fusion/transport in cancer. Despite the fact that most studies of mitochondrial dynamics are conducted on cancer cell lines, surprisingly little is known about this aspect of mitochondrial function in tumours *in vivo*.

Electron microscopy of human and rat gliomas has revealed wide heterogeneity of mitochondrial morphology, with the existence of two predominant types; swollen mitochondria with disarrangement and distortion of cristae and partial or total cristolysis, and mitochondria with increased thickness and highly electron dense cristae were seen (Arismendi-Morillo and Castellano-Ramirez, 2008, Arismendi-Morillo, 2009, 2011). The authors speculate that these phenotypes correspond to hypoxia-sensitive and hypoxia-tolerant tumours, respectively (Arismendi-Morillo and Castellano-Ramirez, 2008, Arismendi-Morillo, 2011). Incidently, although it is impossible to define the rate of mitochondrial fission and fusion from electron microscopy, tethered mitochondria, or those in a state of hemifusion were rarely observed (Arismendi-Morillo and Castellano-Ramirez, 2008).

Interestingly, the mitochondrial irregularities frequently observed in cancer hint at dysfunctional fusion, for example, mtDNA aberrations (reductions in copy number/increased point mutations) and increased ROS (Brandon *et al.*, 2006). Yu *et al.* (2007) have shown that reduced mtDNA copy number correlates with tumour progression in breast cancer patients, suggesting breast neoplastic transformation or progression and mtDNA content might be potentially used as a tool to predict prognosis. Petros *et al.* (2005) found cytochrome oxidase subunit I (COI) gene mutations in 12% of a cohort of prostate cancer patients compared to less than 2% of healthy controls. Furthermore, a tumour from one particular patient also harboured a mutation in the ATP6 gene (encoding ATP F_o subunit 6), which, when introduced to a prostate cancer cell line significantly increased ROS production and increased tumour growth seven-fold. Thus, decreased OXPHOS may have induced higher ROS production, and both of these factors could have caused aberrant mitochondrial fission, leading to the accumulation of mutations that breached the heteroplasmic tolerance threshold. Conversely, disturbed mitochondrial fusion could have led to an accumulation of mtDNA mutations, reduction in copy number and heterogeneity in the mitochondrial network, thus promoting neoplastic transformation.

In complete contrast, carcinoma cells in culture typically contain a highly interconnected mitochondrial reticulum with extremely efficient fusion rates (Legros *et al.*, 2002). HeLa cell mitochondria become condensed and highly reticulated following a switch from energy production *via* glycolysis to OXPHOS (discussed in Chapter 4) (Rossignol *et al.*,

2004), which echoes the observations of Hackenbrock (1966). Furthermore, carcinoma mitochondria have been shown to become hyperfused in response to starvation or other stressors, promoting survival and staving off apoptosis and mitophagy (Tondera *et al.*, 2009, Gomes *et al.*, 2011). Chiche *et al.* (2010) have recently provided evidence that increased mitochondrial fusion is key to cancer survival in near anoxic conditions. While prolonged hypoxia in normal tissues, for example in cardiac or cerebral ischemia, can lead to high necrosis in the affected area, followed by apoptosis after reperfusion (Fliss and Gattinger, 1996, Zhang *et al.*, 2005), transformed cells are remarkably resilient during and after hypoxic events, owing to HIF-1-mediated metabolic reprogramming. This trait is also associated with chemoresistance. Chiche and colleagues have demonstrated in colon carcinoma cells LS174 that hypoxia induces an unusual enlargement of mitochondria, distinct from swelling, and that this enlargement is induced by a HIF-1-dependent upregulation of Mfn1. Furthermore, they showed that this process was due to an atypical form of Mfn1-dependent fusion that was facilitated by Bcl-2 family members BNIP3 and BNIP3L, expressed in response to hypoxia. In addition, these cells were resistant to staurosporine-induced apoptosis following this morphological change, which could be reversed by BNIP3/3L ablation *or* exposure to staurosporine following 48h of normoxia. Interestingly, the investigators also found that Mfn2 and OPA1 were slightly downregulated concurrent with Mfn1 upregulation during hypoxia. Both Mfn2 and OPA1 are strongly implicated in positive regulation of OXPHOS (Olichon *et al.*, 2003, Pich *et al.*, 2005) but these roles could lie outside their fusogenic functions. Thus, it is possible that mitochondrial fusogenicity and oxidative capacity can be simultaneously increased and decreased, respectively, through the manipulation of mitodynamin expression.

It is tempting to consider that dysfunctional mitochondrial dynamics may be involved both in the transformation process *and* the progression of cancer. There are parallels between the typical features of fusion-inhibited cells and transformed cells, such as increased ROS, mtDNA mutations and altered OXPHOS. Conversely, many of the features of neoplastic transformation suggest a downstream effect on dynamics that may perpetuate the transformative process. Furthermore, cancer cells exhibit fundamental changes to apoptosis pathways in which mitochondria are central. The results relating to altered mitochondrial dynamics in cancer also tentatively hint at a potential therapeutic target for cancer in mitochondrial morphogenesis. However, development of such a

therapy seems unlikely until we expand our knowledge of how these processes work, both in normal and transformed cells (Solaini *et al.*, 2011). Moreover, it is imperative that we understand how and why bioenergetics relates to mitochondrial dynamics as metabolic changes – and by extension, mitochondrial changes – are fundamental to the process of neoplastic transformation. Thus, while many cancer cells exhibit the Warburg effect, mitochondria have been assigned an important role in the of pathophysiology cancer and represent attractive therapeutic targets.

3.2 Aims of the Chapter

Fission and fusion are critical in the maintenance and regulation of mitochondrial function. Disturbing the balance between these opposing processes, in particular the inhibition of fusion, has been shown to significantly affect many other aspects of mitochondrial function, including bioenergetics, mtDNA maintenance, ROS production and apoptosis. Conversely, disruption of any of these latter functions has serious effects on mitochondrial dynamics, which, in turn, further perpetuates the original imbalance. This has clear implications for cancer biology, in which metabolic reprogramming and mitochondrial dysfunction are considered to be key to oncogenic transformation. While numerous studies have explored the effects of bioenergetic modulation on mitochondrial morphology in cancer cells, none have provided quantitative mitochondrial fusion data to accompany these morphological observations. This study focuses on the effects of bioenergetic inhibition on fusion rates in HeLa cells engaging in aerobic glycolysis. The objectives were as follows:

1. **Quantify mitochondrial fusion rates in HeLa cells engaged in aerobic glycolysis following mitochondrial inhibition.** Using live-cell confocal microscopy and HeLa cells expressing mitochondrially-targeted photoactivatable GFP (PA-GFPmito), fusion rates in small regions of interest throughout the mitochondrial reticulum were quantified. Rates were compared between control cells and those of cells exposed to a number of ETC/OXPHOS inhibitors.
2. **Quantify mitochondrial fusion rates in HeLa cells following inhibition of glucose metabolism.** Photo-activation studies were repeated in HeLa cells exposed to 2-deoxy-D-glucose, an inhibitor of glucose metabolism, in the presence or absence of various substrates alternative to glucose, namely L-glutamine, pyruvate and galactose, to define the influence of glycolysis inhibition on mitochondrial fusion rates.
3. **Quantify the effects of inhibition of ETC/OXPHOS and glucose metabolism on mitochondrial membrane potential.** This vital aspect of mitochondrial function was examined in the presence of each inhibitor to assess whether the observed effects on mitochondrial fusion (if any) could be correlated with changes in $\Delta\Psi_m$.

4. **Quantify the effects of inhibition of ETC/OXPHOS and glucose metabolism on cellular ATP levels.** Assessment of this parameter gave confirmation of whether the HeLa cells used derived energy from aerobic glycolysis or from OXPHOS, or both. In addition, it allowed for potential correlates to be drawn between the observed effects of each inhibitor on mitochondrial fusion.

3.3. Methods

3.3.1. Cell Culture

Human cervix epitheloid carcinoma cells (HeLa, ECACC No. 93021013) were maintained in high glucose Dulbecco's modified Eagle's medium (DMEM) with Glutamax (Invitrogen) supplemented with 10% foetal bovine serum and penicillin-streptomycin solution (100 units/ml penicillin G, 0.1 mg/ml streptomycin sulphate, Gibco). Cells were initially seeded at a density of 1.3 x $10^4/cm^2$ and split at ~80% confluence by trypsinisation (0.05% trypsin/0.53mM EDTA solution, Gibco) for 5 minutes at 37°C followed by centrifugation at 1000 x g and seeding at 1:3 – 1:10 ratio.

3.3.2. Transient Transfection

Cells were transfected using Gene Juice Transfection Reagent (Merck) as described in section 2.8.2. For live cell imaging, 1.5 x 10^5 cells were seeded in 35mm glass bottomed μ-dishes (Ibidi) two days prior to transfection and allowed to grow to ~80% confluence. A 100μl transfection solution containing 3μl Gene Juice and 1μg DNA (0.5μg each of PA-GFP and DsRed plasmids) in serum-free DMEM was added to the cell culture medium. The medium was removed after four hours and replaced with fresh, pre-warmed medium. The medium was refreshed again after 24h and cells were used for experimentation 48h after transfection. Transfection efficiencies of 57.5 ± 13.97% (mean ± SEM), with a rate of co-transfection of both plasmids of 92 ± 4.78% (mean ± SEM), were regularly achieved with this method.

3.3.3. Assessment of Mitochondrial Fusion Rates after *Transient* FCCP Exposure

Investigation of mitochondrial fusion competence in cells following transient exposure to FCCP was conducted as follows. Imaging settings pertaining to photo-activation and pixel intensity (PI) calculation were as described as in Chapter 2. Fusion rates were measured in cells before FCCP exposure and found to be normal. FCCP (5μM) was added to the medium and, after 20 min incubation, fusion was re-assessed in the same cells by photo-activation of a different ROI within each cell. Fusion rates were seriously compromised, as expected. The FCCP-containing medium was carefully removed using

a peristaltic pump with a yellow 2 – 200μl tip attached to its extraction tube and replaced with fresh pre-equilibrated medium after three washes with same. Cells were then imaged at 15 minute intervals as mitochondrial re-established their tubular structure and concurrently resumed normal fusion rates.

3.3.4. Use of Krebs Buffer

Normal DMEM was not a suitable incubation medium for studies examining the effect of glycolysis inhibition (using 2-deoxy-D-glucose, DOG) on fusion rates, cellular ATP levels or $\Delta\Psi_m$, as manipulation of supplements (L-glutamine, glucose, pyruvate, galactose) within the medium was not possible. Thus, Krebs buffer was used (3mM KCl, 140mM NaCl, 25mM Tris-HCl, 2mM $MgCl_2$, 2mM $CaCl_2$, pH 7.4), with supplements added as required. Control cells were incubated in Krebs buffer containing 25mM glucose and 2mM L-glutamine (as in DMEM). In all imaging experiments involving the use of DOG (photo-activation studies, TMRM studies),control cells were imaged in high glucose Krebs buffer, which was then was removed, and cells were rinsed three times with pre-warmed Krebs buffer of the required composition (containing any, or none, of the aforementioned supplements). Finally DOG was added to the buffer and the imaging experiment was continued as previously described.

3.4. Results

3.4.1. Mitochondrial Fusion Rates in HeLa Cells

The rate of mitochondrial fusion in HeLa cells was assessed using live cell confocal microscopy. Cells were co-transfected with two expression plasmids encoding mitochondrially-targeted fluorescent proteins. The first, DsRed-mito, conferred red fluorescence to mitochondria, allowing for visualisation of the entire mitochondrial network and its morphology. The second, photo-activatable green fluorescent protein (PA-GFP-mito), undergoes photoconversion upon irradiation with 405nm light and exhibits significantly increased fluorescence with excitation at 488nm (Patterson and Lippincott-Schwartz, 2002). This property allowed for the photo-activation of discrete regions of interest (ROI) in the mitochondrial network, the pixel intensity of which decreased as mitochondria actively fused and shared (diluted) the photo-activated protein. Thus, a decrease in mean pixel intensity (PI) in the ROI indicated active mitochondrial fusion. Conversely, the perturbation of mitochondrial fusion resulted in a PI that did not decrease to the same degree, or at all, following photo-activation.

At resting conditions, HeLa cells exhibited highly active and efficient mitochondrial fusion (fig.3.2). For quantification of fusion rates, the mean PIs of the photoactivated ROIs were calculated in both the red and green channels before and after photoactivation (1, 15 and 30 minutes post-activation) and expressed as a percentage of PI values one minute post-activation, deemed to be the point at which the PA-GFP-mito within the $7\mu m^2$ photo-activated ROI was emitting at its highest possible level (thus, PI at 1 minute post activation = 100%). At rest resting conditions, the PI of the photoactivated ROI dropped to $36.1 \pm 1.1\%$ (mean $\pm$ SEM) of its post-activation value after 15 minutes and $25.95 \pm 0.65\%$ after 30 minutes (fig. 3.3). The PI of the DsRed protein in the same ROI showed statistically insignificant fluctuations during this time period, indicating that the PI decrease observed in relation to the PA-GFP was not due to a movement *en masse* of mitochondria away from the ROI.

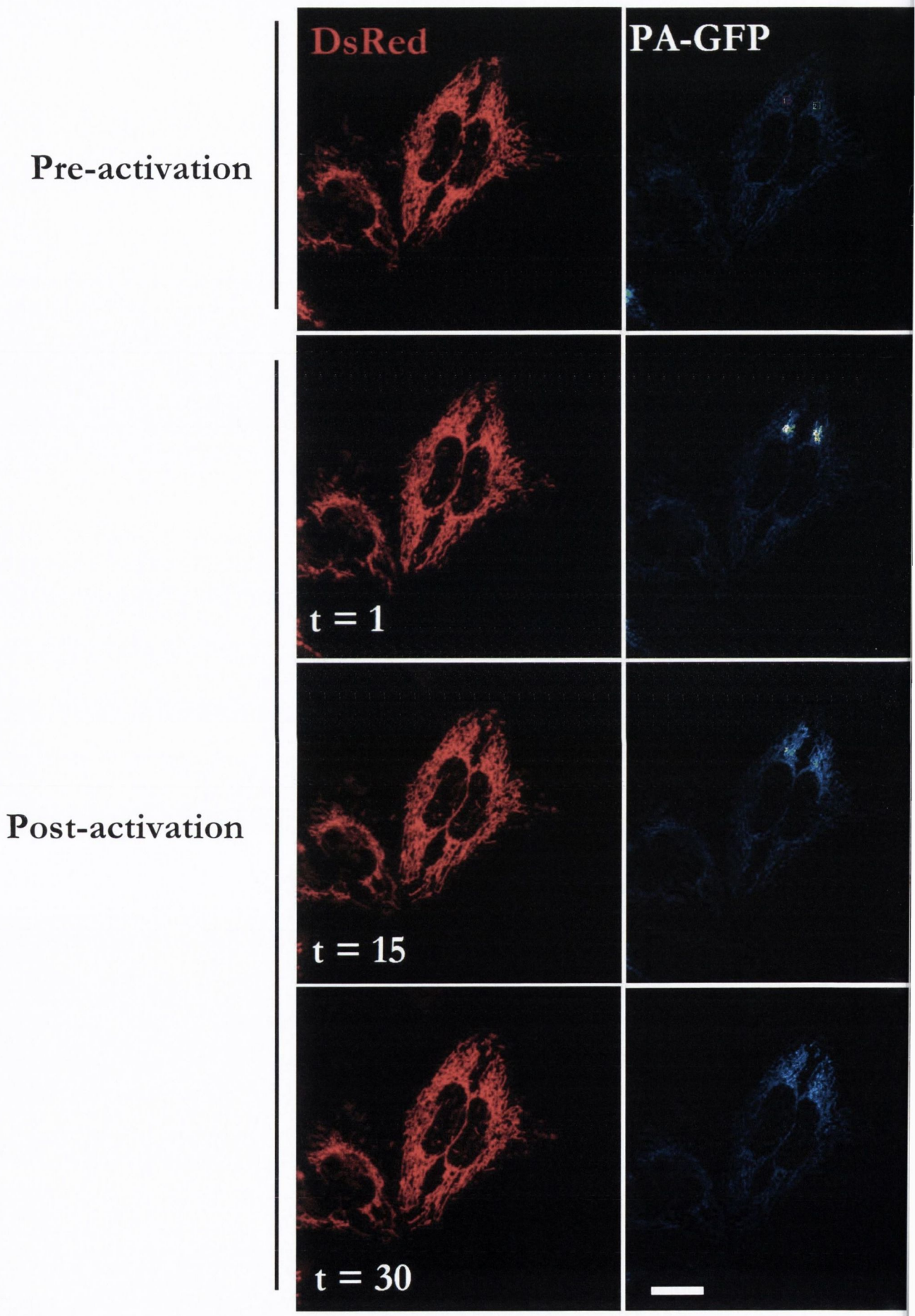

Figure 3.2: Active mitochondrial fusion in HeLa cells at resting conditions. HeLa cells co-expressing two mitochor targeted fluorescent proteins, DsRed-mito, left column, and PA-GFP-mito, right column, were imaged using live cell c microscopy. Photo-activation of discrete 7μm² ROIs of their mitochondrial networks (red and green squares, top row) ~93% increase in pixel intensity in these areas, which decreased over time as a result of mitochondrial fusion and exchange. Images were taken at 1, 15 and 30 minutes post-activation. PA-GFP channel is pseudo coloured for clarity, whe intensity is depicted as indicated in the colour chart (bottom right). Scale = 20μm

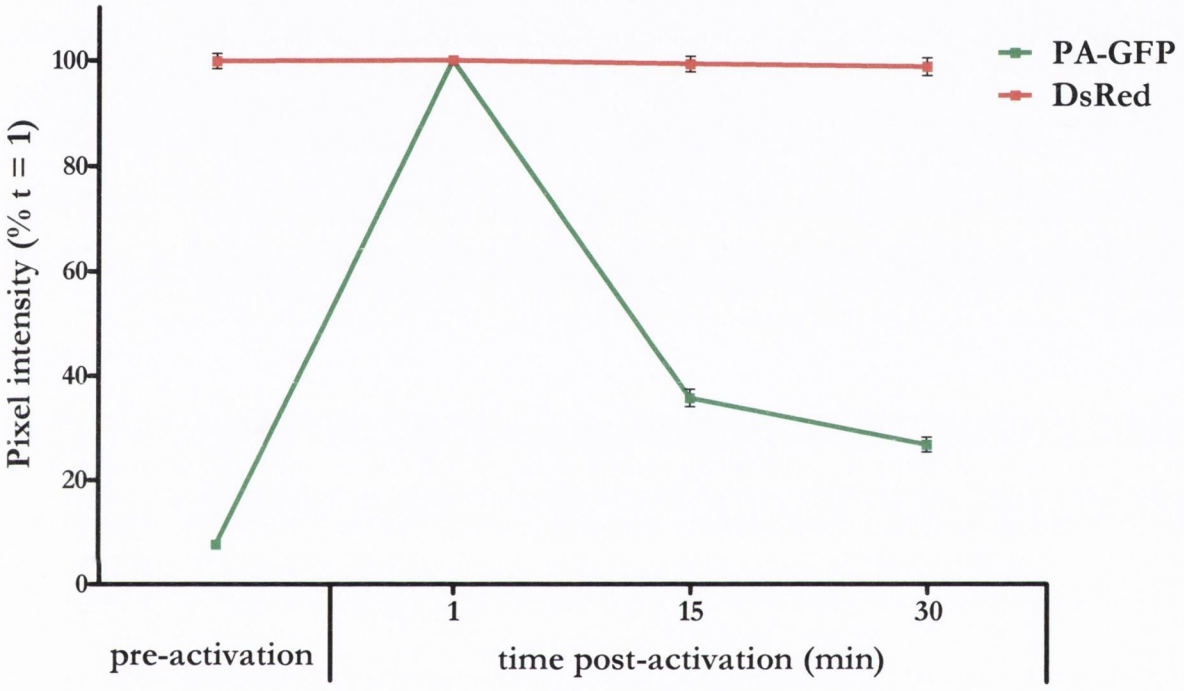

Figure 3.3: Graphical display of mean pixel intensity changes over time in photo-activated ROIs. Mean pixel intensities (PI) of photo-activated ROIs were calculated using Olympus FV10-ASW Olympus Fluoview Ver. 2 software and expressed as percentage of PI at 1 minute post-activation, deemed the point at which pixel intensities should be highest. In the PA-GFP channel (green line), there is low level fluorescence prior to activation, with a PI of 7.7 $\pm$ 0.34% that of its post-activation value. Fifteen minutes following photo-activation, the PI had dropped to 36.1 $\pm$ 1.1% of its post-activation value and 25.95 $\pm$ 0.65% after 30 minutes. The DsRed channel (red line) showed statistically insignificant fluctuations between images and indicated that the PA-GFP PI decreases observed were not due to movement of mitochondria out of the ROI or photobleaching. Data presented as mean $\pm$ SEM, n = 3, where six fields, each containing 1 – 7 cells were imaged in three separate dishes on three separate occasion. Thus, each data point is representative of 18 – 127 cells.

3.4.2. Effects of Mitochondrial Inhibition on Fusion Rates

It has previously been shown that collapse of the mitochondrial membrane potential ($\Delta\Psi_m$) using the protonophore carbonyl cyanide-*p*-trifluoromethoxyphenylhydrazone (FCCP) causes rapid and reversible fragmentation of the mitochondrial reticulum (Legros *et al.*, 2002). For this reason, FCCP treatment was used in these studies as a positive control for the blockade of fusion. Dose and time response experiments in HeLa cells stably expressing the DsRed-mito protein indicated that exposure of cells to 2, 5 and 10μM FCCP led to extensive mitochondrial fragmentation within 30, 20 and 10 minutes, respectively (fig 3.4). Incubation of cells with 5μM FCCP for 20 minutes prior to photo-activation led to severe compromise of mitochondrial fusion (fig 3.5), with PIs in photo-activated regions remaining at 84 $\pm$ 4.93% of their post-activation values after 30 minutes (fig 3.6).

Mitochondria that have undergone extensive fission in the presence of FCCP regain their tubular, reticulated morphology upon its subsequent removal (Suen *et al.*, 2008). However, a return to filamentous morphology cannot necessarily be equated with a return to normal fusion dynamics; simple observation of the former provides no quantitative information about the latter. To investigate this, the mitochondrial fusion rates of cells in a single imaging field were quantified before, during and after FCCP treatment (fig 3.7). The cells exhibited normal mitochondrial fusion rates before FCCP treatment and showed fusion perturbation following FCCP exposure, as expected. Mitochondria displayed a return to fusion competence within 30 minutes of FCCP removal, with a PI of 55 $\pm$ 26.72% (mean $\pm$ SD) of its post-activation value. At 90 minutes post-FCCP removal, all but one cell showed a decrease in pixel intensity comparable to control cells (overall average 30.66 $\pm$ 19.58%). These results show that removal of FCCP from cells not only restores tubular morphology but also leads to eventual re-establishment of normal fusion rates.

With the effects of $\Delta\Psi_m$ dissipation on mitochondrial fusion dynamics established, the effects of other forms of mitochondrial inhibition on this function were explored. Cells were incubated for 20 minutes with or without a range of inhibitors of individual enzymes of the OXPHOS system. Inhibition of complex I, with either rotenone or piericidin A had no effect on fusion rates (fig. 3.8), nor did inhibition of complex II with malonate (fig. 3.9), complex III with antimycin A or myxothiazol (fig. 3.10), nor complex

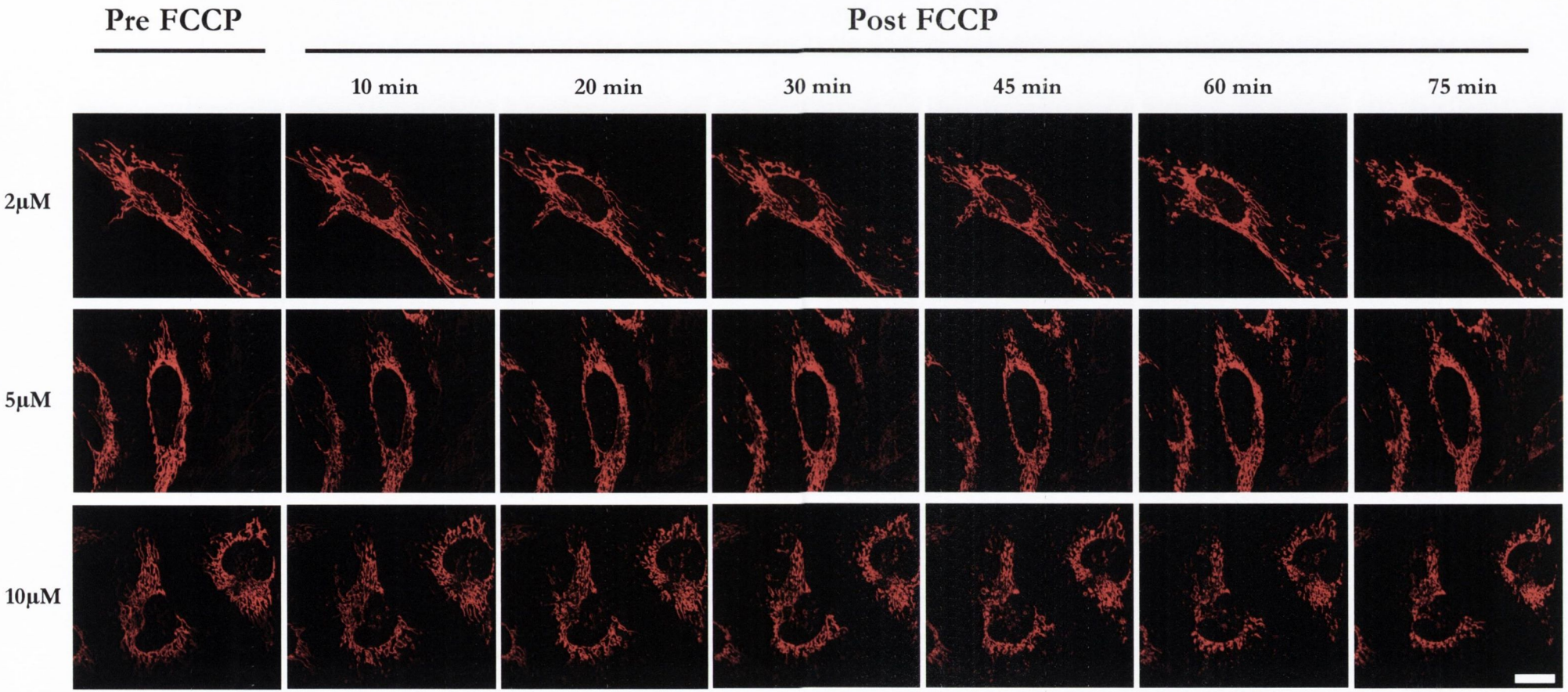

Figure 3.4: Effect of membrane depolarisation on mitochondrial morphology in HeLa cells. Cells stably expressing DsRed2-mito were exposed to protonophore and mitochondrial uncoupler carbonylcyanide *p*-trifluoromethoxyphenylhydrazone (FCCP) at the concentrations indicated and imaged, with z stacking, at the time points indicated. Cells exposed to 2μM FCCP exhibited several ring-shaped and fragmented mitochondria after approximately 30min, the number of which increased over time. This process began at earlier time points at higher FCCP concentrations (20min with 5μM FCCP, 10min with 10μM FCCP) and also led to more extensive fragmentation in both cases (compare 2μM and 10μM at 75min). Image representative of at least six fields imaged per treatment group. Scale = 20μm.

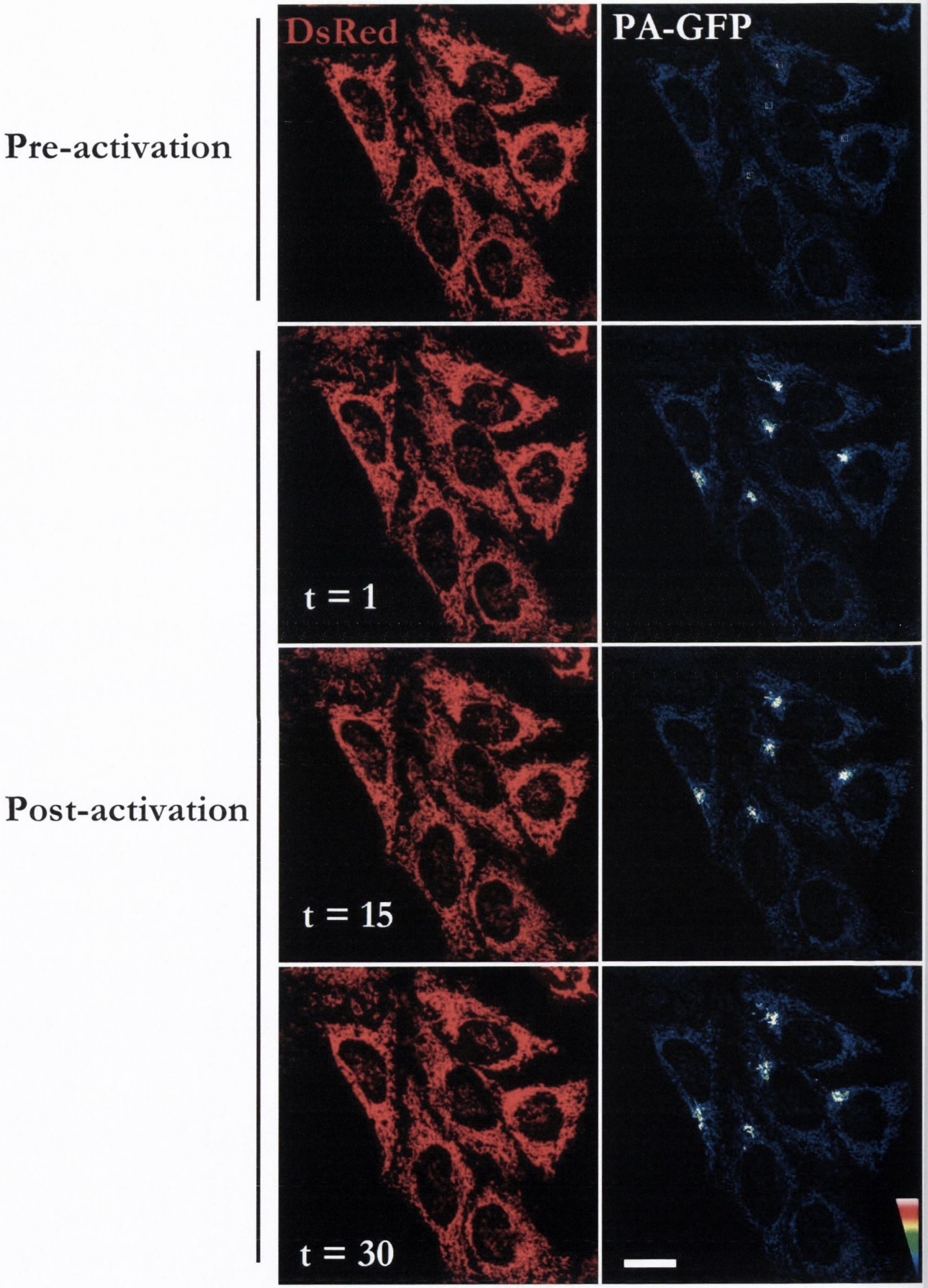

Figure 3.5: Dissipation of $\Delta\Psi_m$ compromises mitochondrial fusion in HeLa cells. Cells were pre-incubated with 5μM FCCP for 20 minutes and then had ROIs photo-activated as previously described. There is a clear cessation of fusion observed, with negligible spread or dilution of photo-activated material throughout the mitochondrial matrix, even at 30 minutes post activation. Data presented as mean ± SEM. Unpaired t-test at each time point. Scale = 20μm.

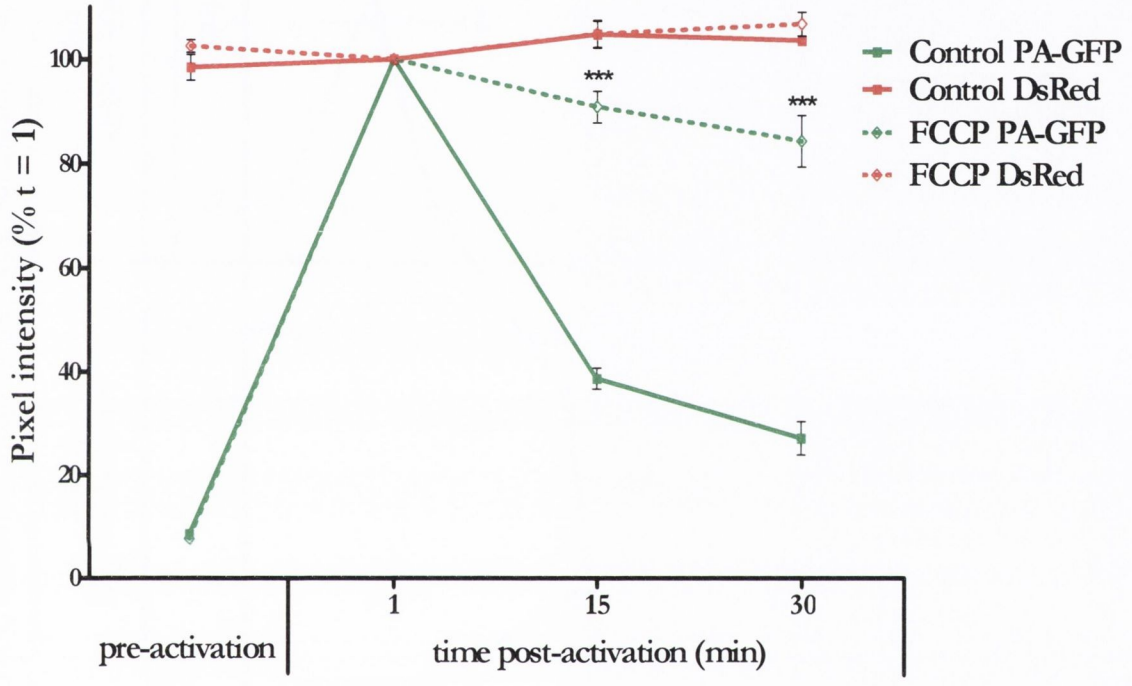

Figure 3.6: Graphical display of mean pixel intensity changes over time in photo-activated ROIs of FCCP treated cells. Cells treated with 5μM FCCP for 20 minutes showed pronounced fusion perturbation, with a mean PI of 84.29 ± 4.93% 30 minutes post-activation (dashed green line), while control cells showed normal fusion rates (PI of 27 ± 3.23% 30 minutes post-activation, solid green line). The DsRed channels (solid red line, control, dashed red line, FCCP-treated) showed statistically insignificant fluctuations between images and indicated that the PA-GFP PI decreases observed were not due to movement of mitochondria out of the ROI or photobleaching. Data presented as mean ± SEM, n = 3. Unpaired t-test at each time point. *** $P<0.001$.

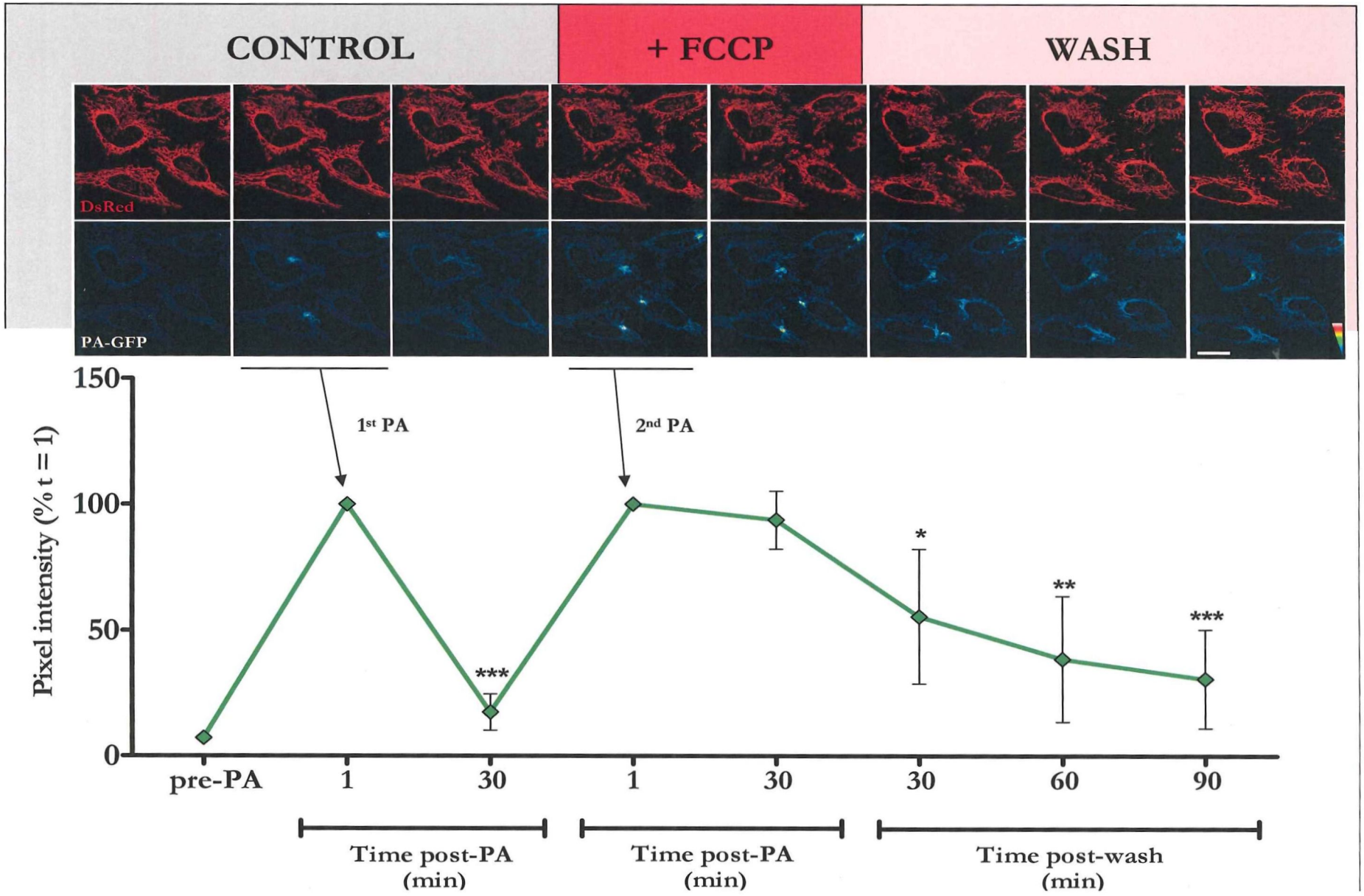

Figure 3.7: FCCP-induced fusion perturbation is reversible in HeLa cells. Mitochondrial fusion rates were first monitored in cells in normal culture medium (left panel, 'CONTROL') and were found to be in line with previously obtained rates (PI of 17.44 ± 7.22% at 30 minutes post activation). Rates were then obtained for cells after addition of 5μM FCCP and incubation for 20 minutes (centre panel '+ FCCP') and, as before, a distinct perturbation of fusion was observed (PI of 93.76 ± 11.49% at 30 minutes post-activation). Finally, FCCP was removed from medium by aspiration, followed by three washes with pre-equilibrated medium. The fusion rates were monitored in the same ROIs photo-activated after FCCP treatment to ascertain whether these mitochondria could regain fusion competence (right panel, 'WASH'). By 30 minutes post-FCCP removal, the mean PI was 55.5 ± 26.72, which fell to 30.66 ± 19.6 after a further 60 minutes (t = 90 post FCCP removal). Data presented as mean ± SD, n = 4. One way ANOVA, *P<0.05, **P<0.01, ***P<0.001. PA, photo-activation. Scale = 20μm

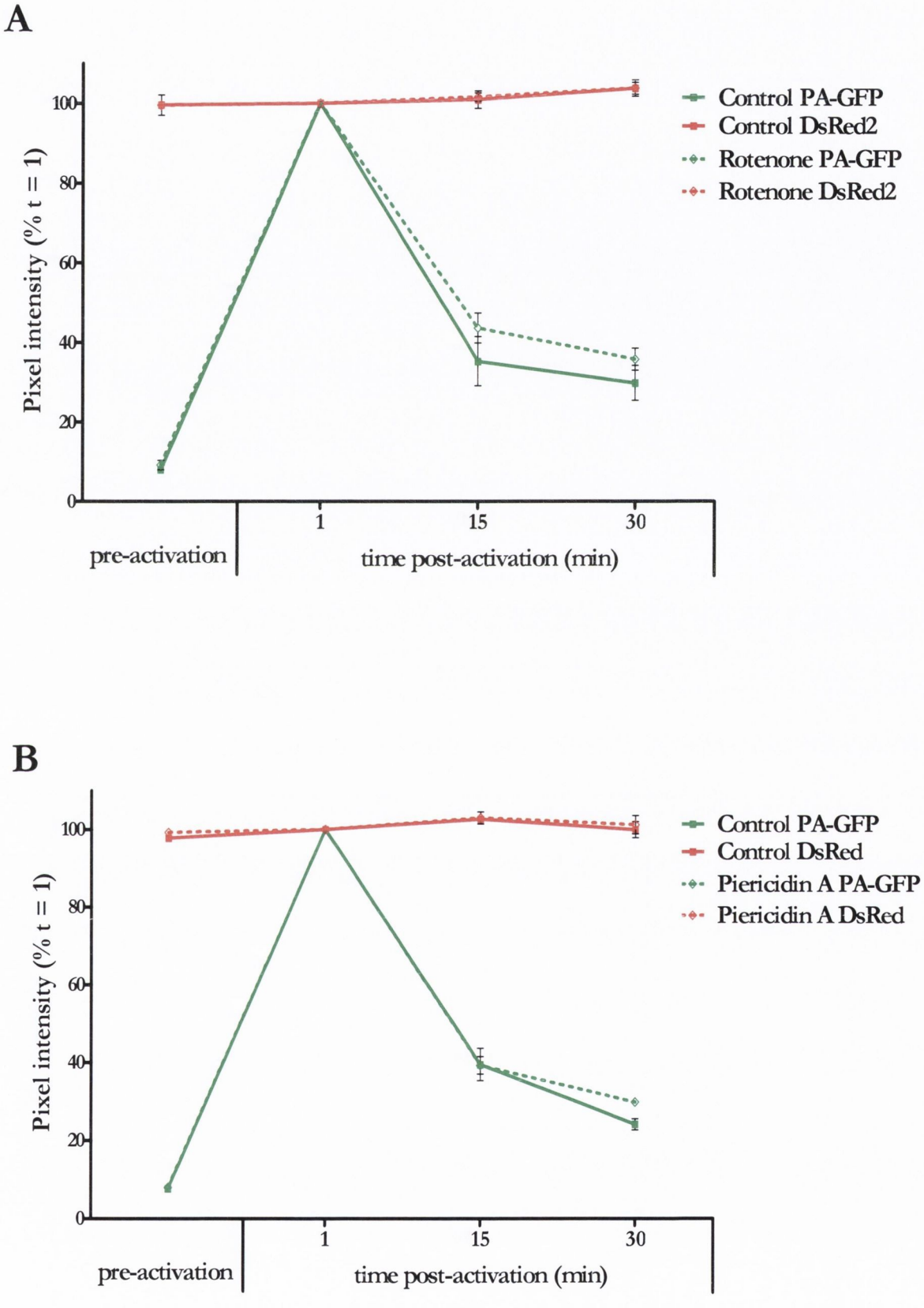

Figure 3.8: Complex I inhibition does not affect mitochondrial fusion rates in HeLa cells. Cells were incubated with either 10μM rotenone (A), or 4μM piericidin A (B) for 20 minutes prior to photo-activation of 7μm² ROIs of their mitochondrial networks, as described. No statistically significant difference in fusion rates was observed with either treatment. Data presented as mean ± SEM, n = 3. Unpaired t-test at each time point.

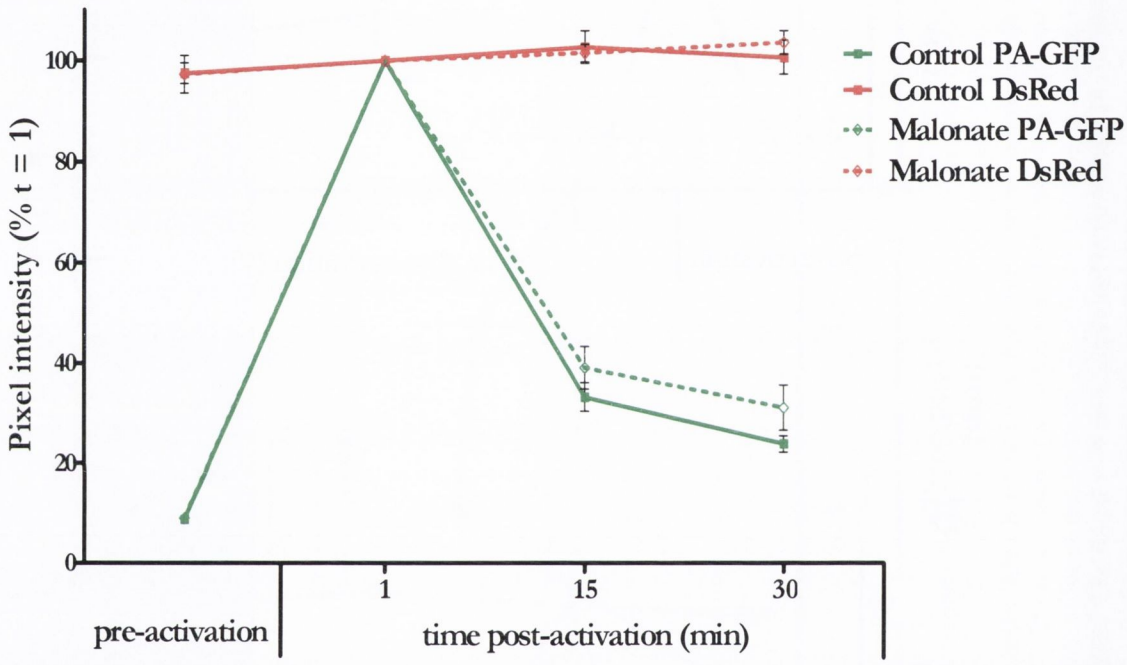

Fig 3.9. Complex II inhibition does not affect mitochondrial fusion rates in HeLa cells. Cells were incubated with 1mM malonate for 20 minutes prior to photo-activation of 7μm^2 ROIs of their mitochondrial networks, as described. No statistically significant difference in fusion rates was observed with treatment. Data presented as mean $\pm$ SEM, n = 3. Unpaired t-test at each time point.

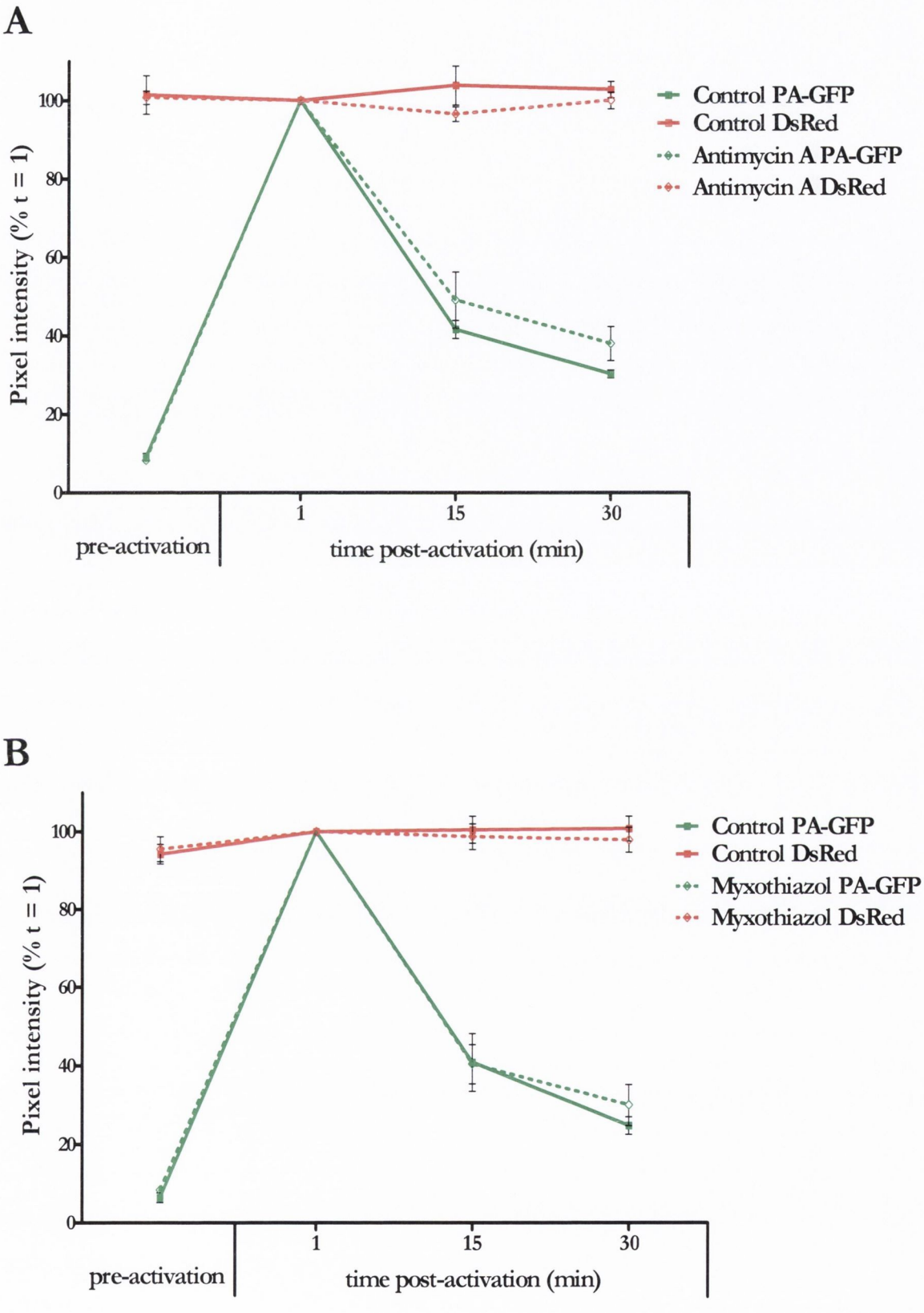

Figure 3.10. Complex III inhibition does not affect mitochondrial fusion rates in HeLa cells. Cells were incubated with either 2.4μM antimycin A (A), or 2μM myxothiazol (B) for 20 minutes prior to photo-activation of 7μm² ROIs of their mitochondrial networks, as described. No statistically significant difference in fusion rates was observed with either treatment. Data presented as mean ± SEM, n = 3. Unpaired t-test at each time point.

IV with azide (fig. 3.11). In a departure from this trend, inhibition of ATP synthase with oligomycin produced a statistically significant perturbation of mitochondrial fusion, with rates 2.6-fold slower than those of control cells (fig. 3.12). Thus, it has been shown here that inhibition of ETC enzymes in glycolytic HeLa cells had no effect on fusion rates, but that these rates were sensitive to ATP-synthase inhibition. Simultaneous inhibition of multiple mitochondrial functions also compromised fusion rates. Although dissipation of $\Delta\Psi_m$ coupled with inhibition of ATP synthase, using FCCP and oligomycin, respectively, significantly reduced fusion, the effect was not synergistic; the magnitude of perturbation replicated that of FCCP alone (fig. 3.13A). Similarly, concurrent exposure to rotenone and oligomycin compromised fusion but was not synergistic (fig 3.13B).

3.4.3. Effects of Electron Transport Chain Inhibition and Microtubule Disassembly on Mitochondrial Fusion Rates

Interestingly, inhibition of complexes I and III with rotenone and antimycin A produced a 1.7-fold slowing of fusion rates (fig. 3.14A), although neither of these agents produced an effect when applied alone, suggesting synergism (fig 3.15). However, when complexes I and III were inhibited using piericidin A and antimycin A, no fusion deficit was observed (fig. 3.14B). Thus, it appeared that the slowing of mitochondrial fusion observed with rotenone and antimycin A combined was not due to the simultaneous inhibition of complexes I and III *per se*. Rotenone is known to have effects on microtubule assembly (Choi *et al.*, 2011), thus it was hypothesised that perhaps the observed effects were due to an interaction between microtubule disruption and electron transport chain inhibition.

To confirm that rotenone was causing microtubule disassembly under the incubation conditions employed here, cells were incubated for the times indicated with either vehicle, rotenone or the anti-neoplastic agent nocodazole, fixed and stained for α-tubulin (fig. 3.16). As suspected, rotenone caused a depolymerisation of the microtubular network akin to that caused by nocodazole, albeit to a slightly lesser extent (observation, not quantified). Control cells showed distinct and filamentous microtubules characteristic of normal, healthy cells. Those treated with either nocodazole or rotenone exhibited disorganised tubules and/or diffuse staining patterns, indicating an increase in monomeric tubulin in the cytosol. The extent of microtubule depolymerisation was time-dependent in both cases. Mitochondrial fusion was then assessed in cells incubated

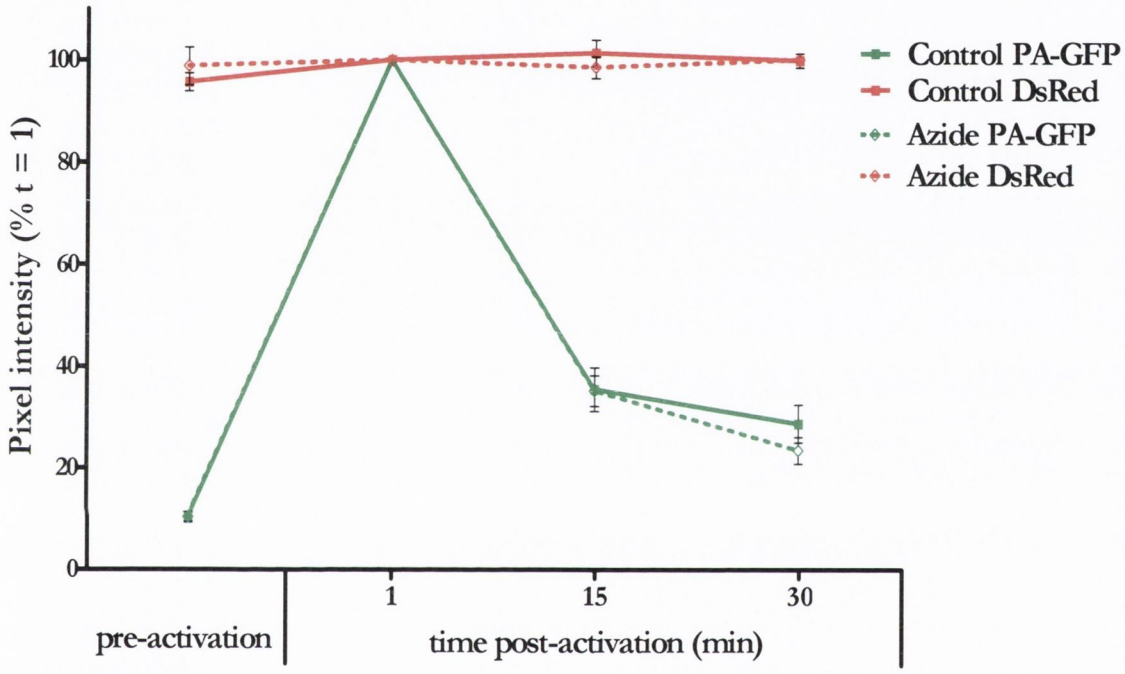

Figure 3.11: Complex IV inhibition does not affect mitochondrial fusion rates in HeLa cells. Cells were incubated with 5mM azide for 20 minutes prior to photo-activation of 7μm^2 ROIs of their mitochondrial networks, as described. No statistically significant difference in fusion rates was observed with either treatment. Data presented as mean $\pm$ SEM, n = 3. Unpaired t-test at each time point.

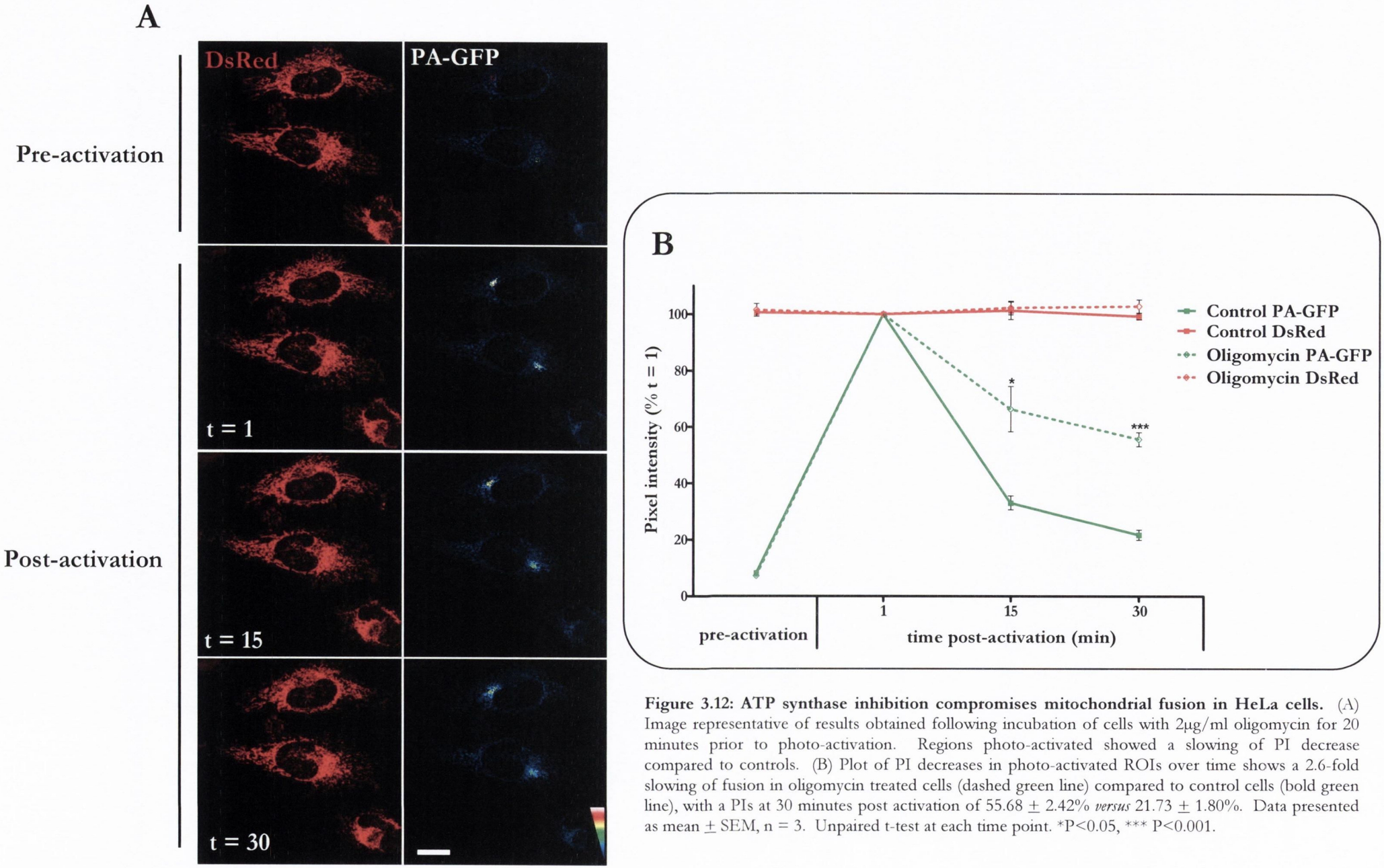

Figure 3.12: ATP synthase inhibition compromises mitochondrial fusion in HeLa cells. (A) Image representative of results obtained following incubation of cells with 2μg/ml oligomycin for 20 minutes prior to photo-activation. Regions photo-activated showed a slowing of PI decrease compared to controls. (B) Plot of PI decreases in photo-activated ROIs over time shows a 2.6-fold slowing of fusion in oligomycin treated cells (dashed green line) compared to control cells (bold green line), with a PIs at 30 minutes post activation of 55.68 ± 2.42% *versus* 21.73 ± 1.80%. Data presented as mean ± SEM, n = 3. Unpaired t-test at each time point. *P<0.05, *** P<0.001.

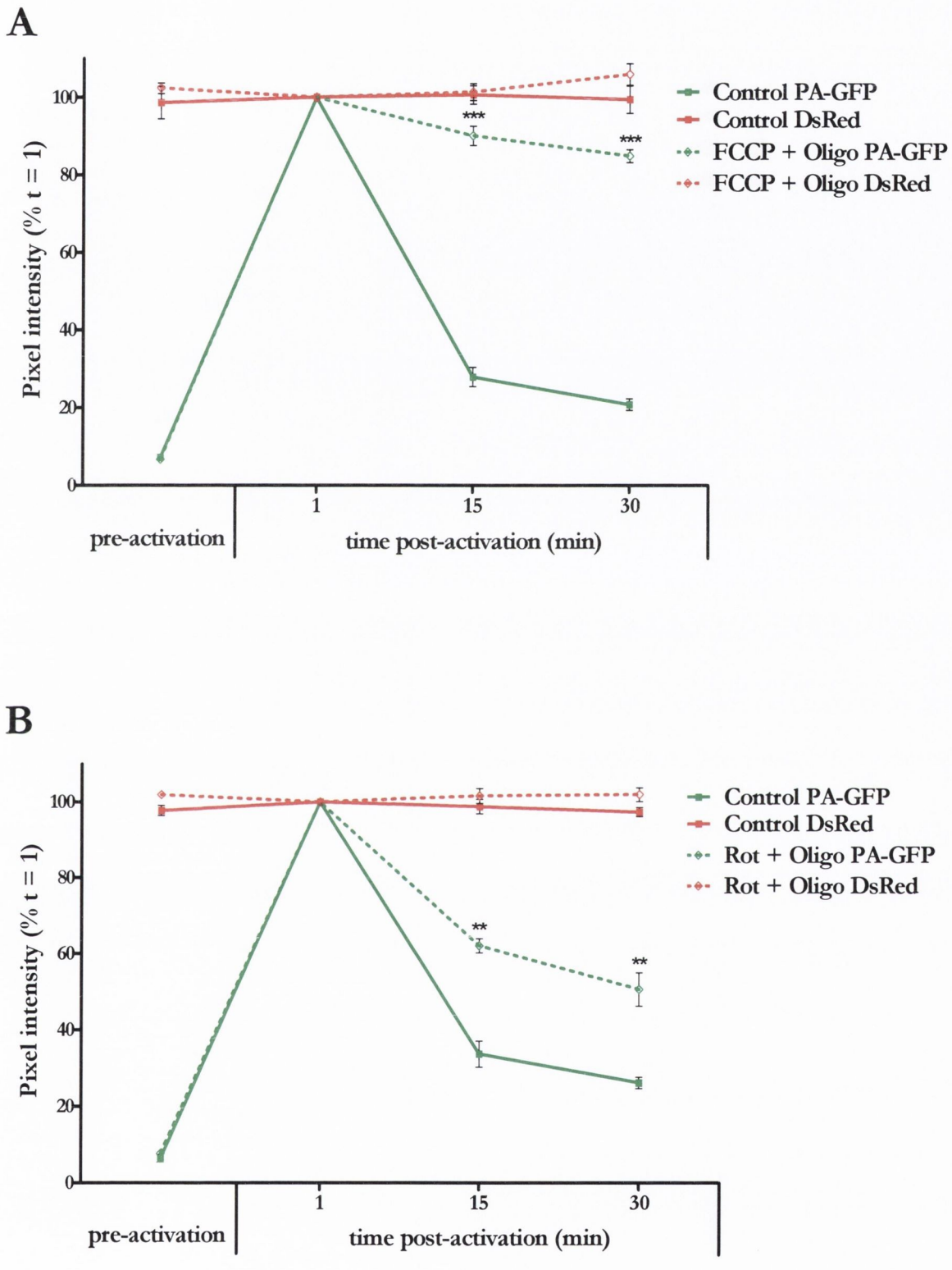

Figure 3.13: Simultaneous inhibition of multiple mitochondrial functions leads to perturbation of mitochondrial fusion in HeLa cells. (A) A 20 minute incubation combining dissipation of $\Delta\Psi_m$ with 5μM FCCP and ATP synthase inhibition with 2μg/ml oligomycin (Oligo) results in a fusion deficit, but is no greater than that which is induced by FCCP alone. (B) A 20 minute incubation combining complex I inhibition with 10μM rotenone (Rot) and ATP synthase inhibition with 2μg/ml oligomycin induces a fusion deficit which is of the same magnitude as that of oligomycin alone. Data presented as mean ± SEM, n = 3. Unpaired t-test at each time point. **P<0.01, *** P<0.001.

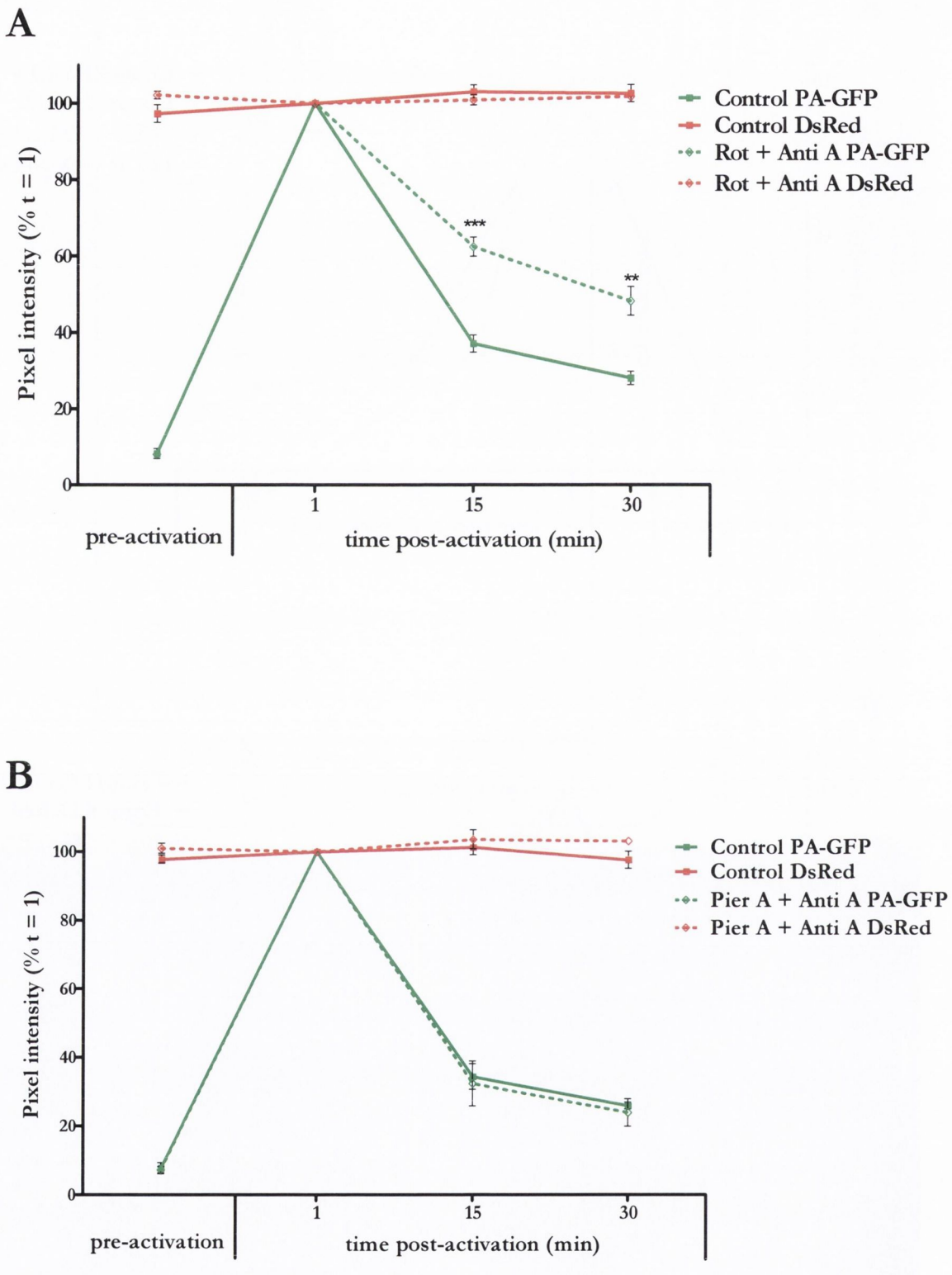

Figure 3.14: Concurrent inhibition of complexes I and III leads to mitochondrial fusion perturbation in the presence of rotenone but not piericidin A. (A) Simultaneous inhibition of complexes I and III using 10μM rotenone (Rot) and 2.4μM antimycin A (Anti A) (20 minute incubation) lead to a fusion rate that is 1.7-fold slower than control rates. (B) If the experiment is conducted with 4μM piericidin A (Pier A) in place of rotenone, there is no slowing of fusion rates observed. Data presented as mean ± SEM, n = 3. Unpaired t-test at each time point. **P<0.01, *** P<0.001.

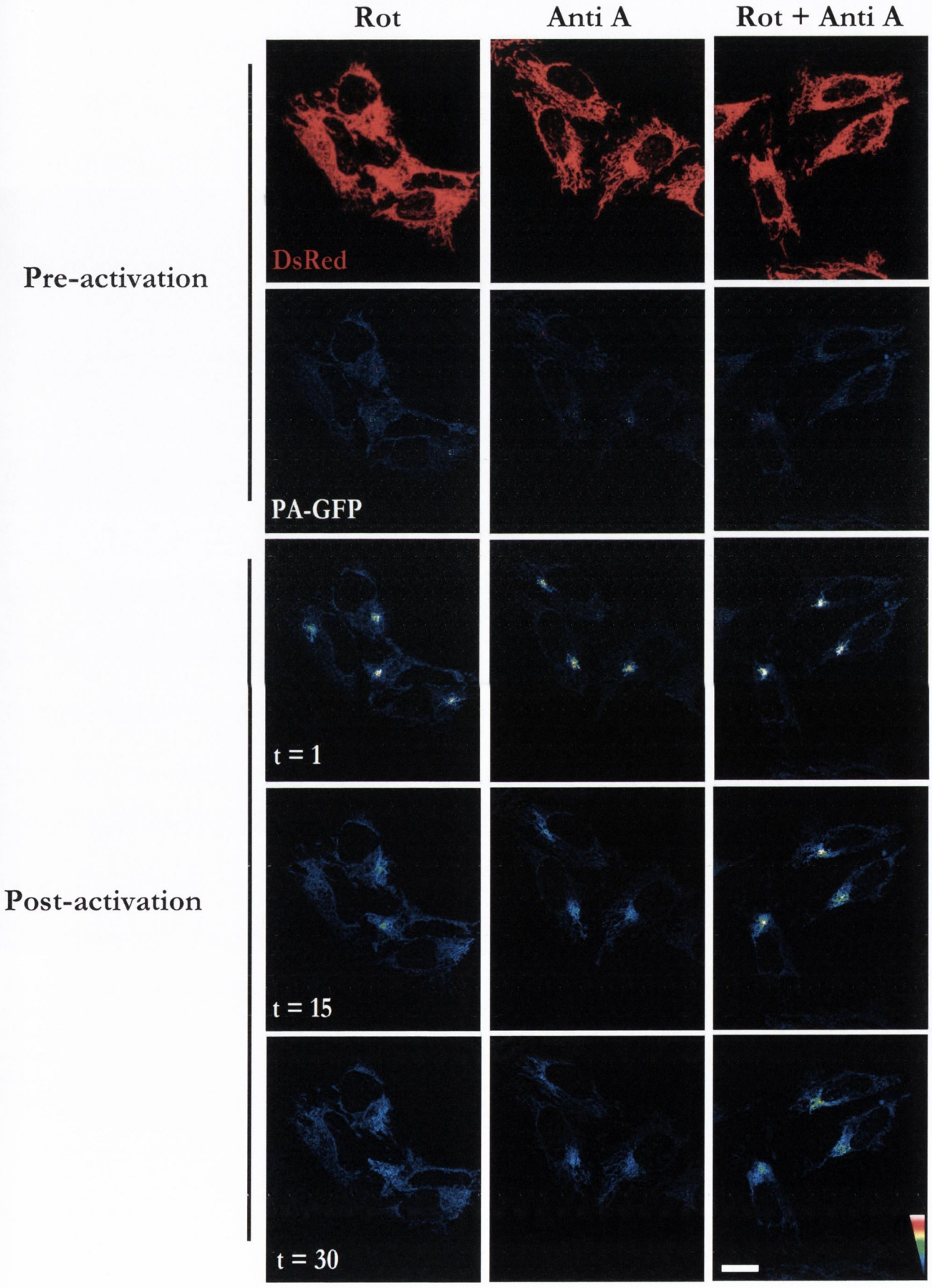

Figure 3.15: Images showing mitochondrial fusion deficit in rotenone + antimycin A treated cells. Cells treated with 10μM rotenone (Rot) or 2.4μM antimycin A (Anti A) alone (left and centre columns, respectively) displayed normal fusion rates. When both inhibitors were applied simultaneously (right column), fusion was slowed 1.7-fold compared to control cells. Scale = 20μm.

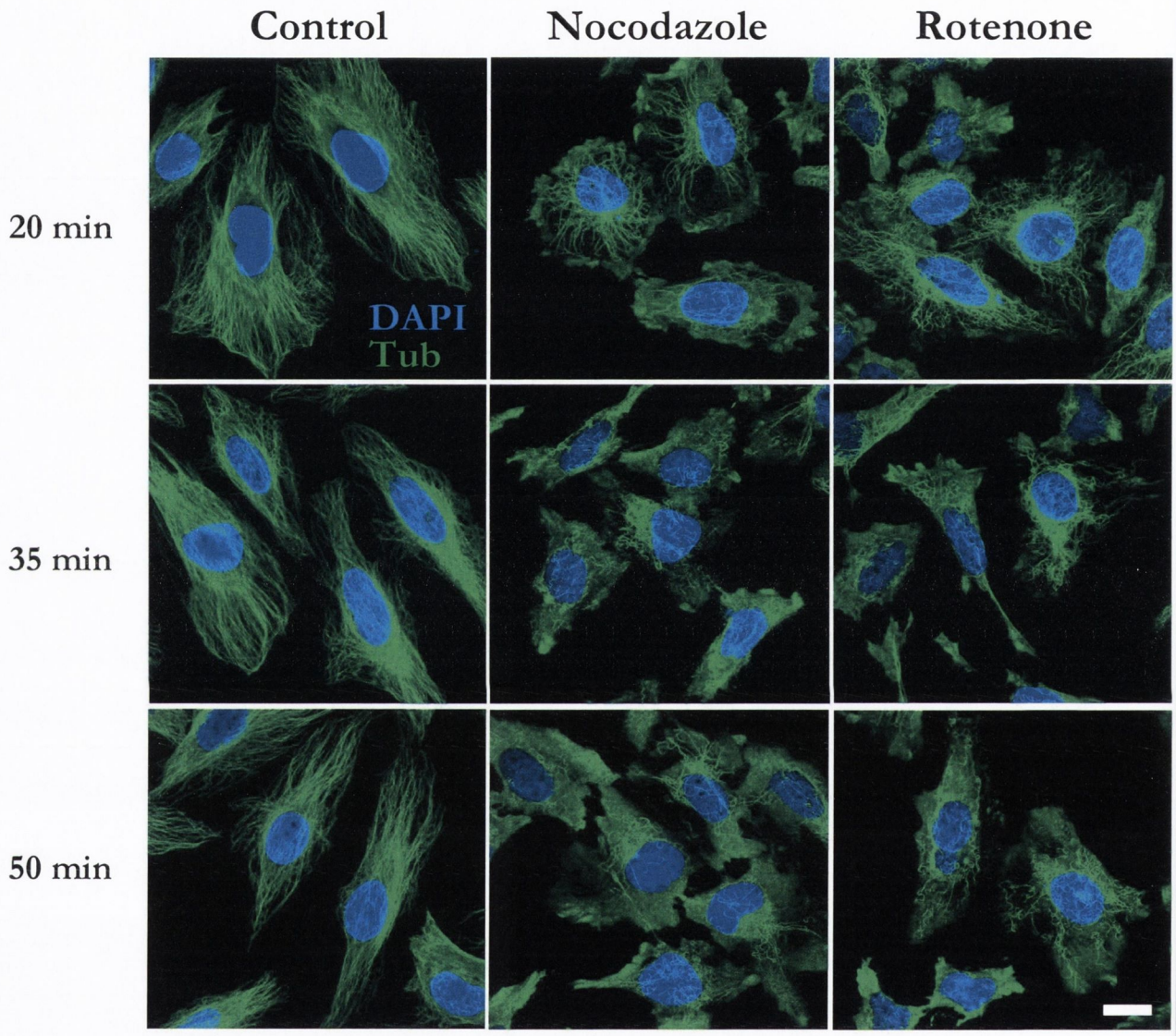

Figure 3.16: Rotenone induces microtubule depolymerisation in HeLa cells. Cells were incubated for 20, 35 and 50 minutes (in tandem with time points of photo-activation studies, i.e. photo-activation after 20 minute incubation, imaging 15 minutes later, and then a further 15 minutes later), with either vehicle (0.1% v/v DMSO), 10μM nocodazole or 10μM rotenone then fixed and immunostained for α-tubulin (tub). Control cells exhibited distinct and filamentous microtubles characteristic of normal, healthly cells. Those treated with either nocodazole or rotenone exhibited disorganised tubules and/or diffuse staining patterns, indicating in increase in monomeric tubulin in the cytosol. This effect increased over time. DAPI, 4,6-diamidino-2-phenylindole, nuclear counterstain. Scale = 20μm.

with nocodazole or nocodazole and antimycin A (fig. 3.17). Cells incubated with nocodazole alone exhibited a small but statistically significant decrease in fusion rates (PI of 37.85 ± 3.24% 30 minutes post-activation, compared to 26.49 ± 1.79% in controls, fig. 3.17A). This rate was slower still in cells incubated with both nocodazole and antimycin A (PI 51.19 ± 4.88% 30 minutes post-activation, fig 3.17B). Despite this trend, PI values of nocodazole and nocodazole + antimycin A post activation did not show statistically significant difference when analysed by one-way ANOVA (fig 3.17C). Thus the synergism of combined rotenone and antimycin A treatment was possibly not due to combined microtubule disassembly and complex III inhibition. This line of investigation was concluded at this stage.

3.4.4. Effects of Inhibition of Glucose Metabolism on Mitochondrial Fusion Rates

HeLa cells, like many cancer cells, exhibit the metabolic phenomenon of aerobic glycolysis. For this reason, the effects of inhibition of the rate limiting enzyme of the glycolytic pathway, HK, (using 10mM 2-deoxy-D-glucose (DOG)) on mitochondrial fusion rates were examined. As a glucose analogue, DOG enters the cell *via* glucose transporters and is phosphorylated by HK. DOG-6-phosphate cannot be further metabolised and upon accumulation in the cell, inhibits HK allosterically and competitively (Aft *et al.*, 2002). Thus, DOG functions as an indirect inhibitor of HK and glucose metabolism. It should be noted here that DOG is not a specific glycolysis inhibitor; the decrease in cellular glucose-6-phosphate resulting from HK inhibition may also affect the pentose phosphate pathway (PPP), with subsequent effects on cellular management of ROS, nucleotide synthesis and DNA repair (Lin *et al.*, 2003). All studies using DOG were conducted using Krebs buffer (3mM KCl, 140mM NaCl, 25mM Tris-HCl, 2mM $MgCl_2$, 2mM $CaCl_2$, pH 7.4) rather than culture medium, to allow for easy manipulation of key substrates of the incubation medium (glucose, L-glutamine, sodium pyruvate). All control cells were incubated in Krebs buffer containing 25mM glucose and 2mM L-glutamine, concentrations identical to those of DMEM culture medium. Neither short nor long incubation (30 and 90 minutes, respectively) in this buffer had any effects on mitochondrial fusion rates (fig. 3.18).

Cells incubated in glucose and L-glutamine-free Krebs containing 10mM DOG exhibited very significant perturbation of mitochondrial fusion, with PIs remaining at 77.41 ± 5%

Figure 3.17: Mitochondrial fusion is compromised by simultaneous inhibition of microtubule assembly and complex III inhibition. (A) Inhibition of microtubule assembly following 20 minute incubation with 10μM nocodazole (Noc) caused a small but statistically significant decrease in mitochondrial fusion rates. (B) Incubation of cells with nocodazole and 2.4μM antimycin A (Anti A) caused a further slowing of fusion rates. Data presented as mean ± SEM, n = 3. Unpaired t-test at each time point. (C) Analysis by one-way ANOVA and Tukey's HSD post-test reveals that fusion deficits observed at 15 and 30 minutes post-activation are not statistically different between nocodazole- and nocodazole + antimycin A-treated groups. Data presented as mean ± SEM, n = 3. *$P<0.05$, ** $P<0.01$.

A

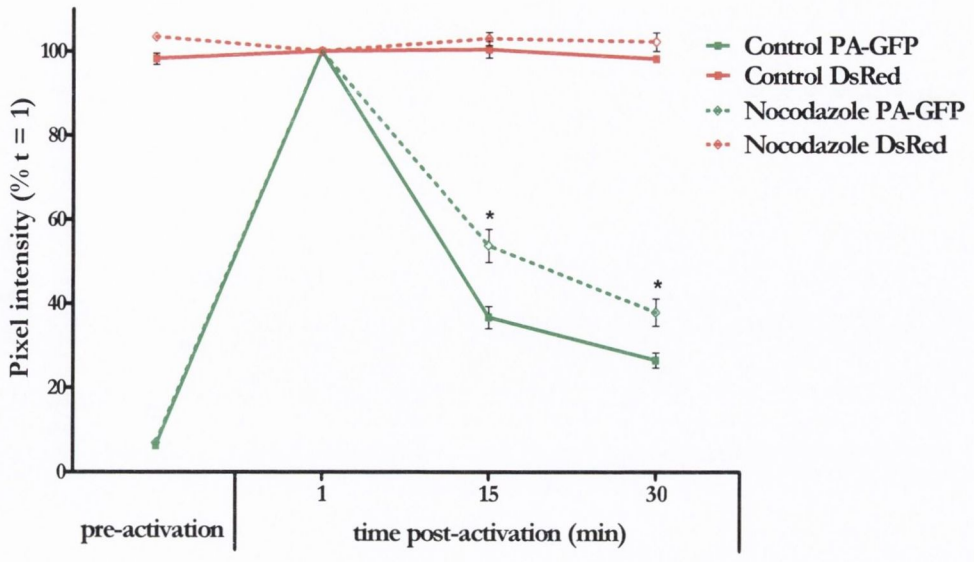
Pixel intensity (% t = 1)
100
80
60
40
20
0
1
15
30
pre-activation
time post-activation (min)
*
*
Control PA-GFP
Control DsRed
Nocodazole PA-GFP
Nocodazole DsRed

B

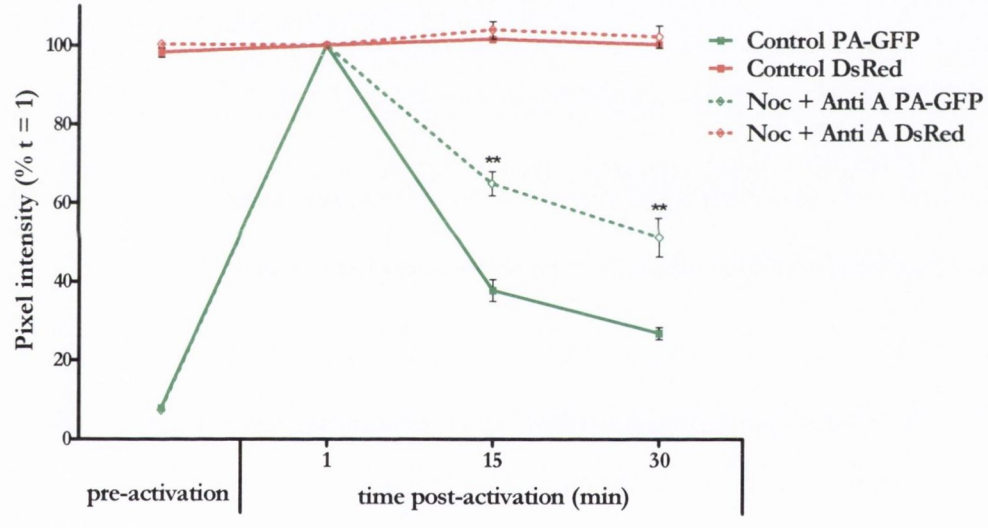
Pixel intensity (% t = 1)
100
80
60
40
20
0
1
15
30
pre-activation
time post-activation (min)
**
**
Control PA-GFP
Control DsRed
Noc + Anti A PA-GFP
Noc + Anti A DsRed

C

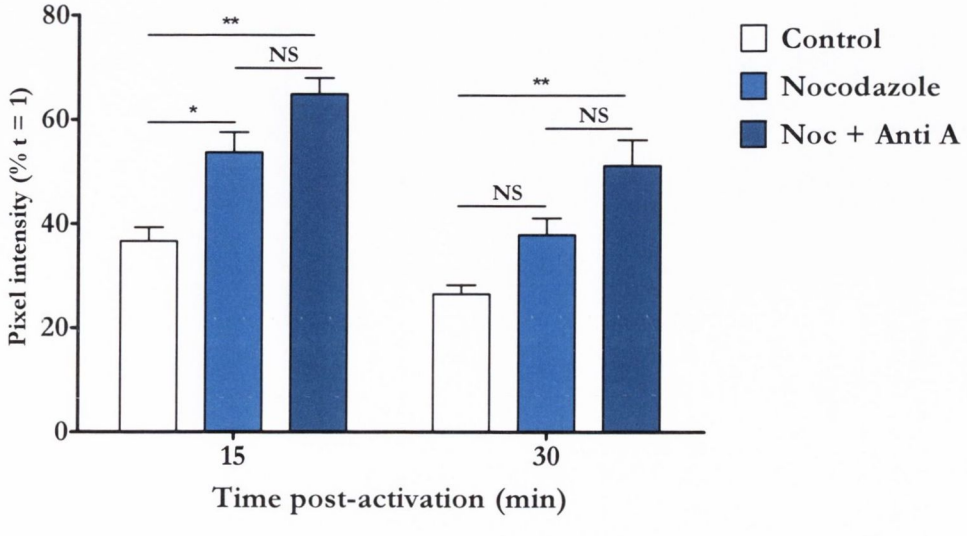
Pixel intensity (% t = 1)
80
60
40
20
0
**
NS
*
**
NS
NS
15
30
Time post-activation (min)
Control
Nocodazole
Noc + Anti A

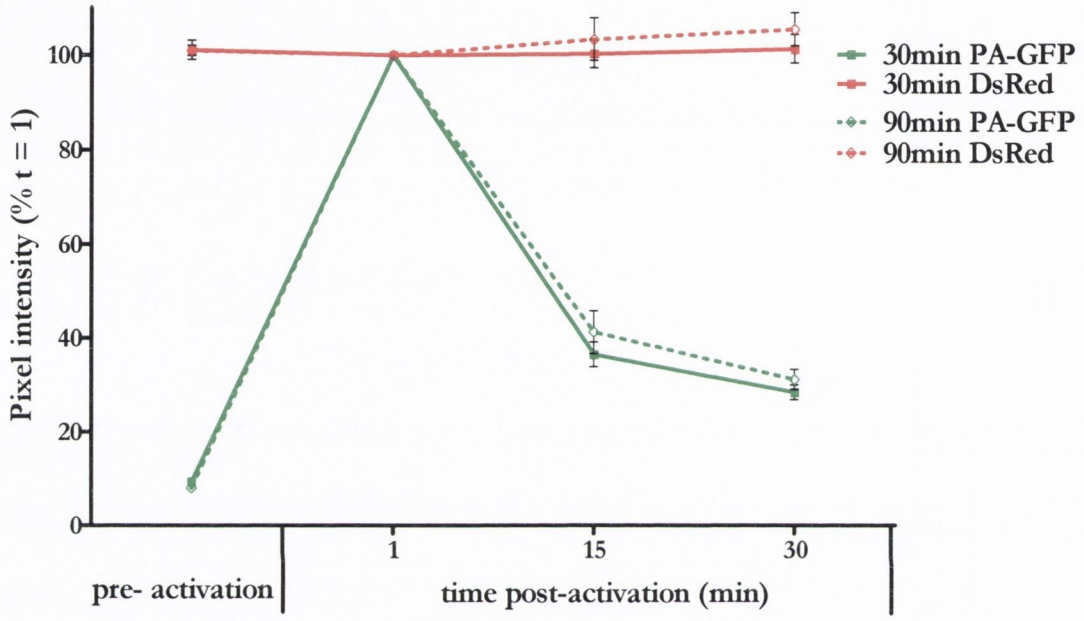

Figure 3.18: Prolonged incubation in Krebs buffer does not affect mitochondrial fusion rates in HeLa cells. Cells were incubated in Krebs buffer containing 25mM glucose and 2mM L-glutamine for 30 minutes and 90 minutes and assessed for mitochondrial fusion rates. No adverse effects on rates were observed. Data presented as mean ± SEM, n = 2. Unpaired t-test at each time point.

post activation values after 30 minutes (fig 19A). Aside from glucose, glutamine is the only other molecule catabolised to an appreciable degree in cultured cells (Vander Heiden *et al.*, 2009) and is an essential supplement in culture media. It is converted to glutamate by glutaminase, in a process called glutaminolysis, after which it can be converted to the TCA cycle intermediate α-ketoglutarate by glutamate dehydrogenase. Significantly, the DOG-induced fusion decrease was not improved by inclusion of 2mM L-glutamine in the incubation buffer (fig 3.19B). Furthermore, mitochondria in DOG-treated cells appeared to retain their tubular morphology despite being incapable of fusion (fig 3.20). This is in stark contrast to FCCP-treated cells, in which the fusion decrease is accompanied by obvious increased fission, and further emphasises that information relating to fusion cannot be deduced from simple observation of organelle morphology.

As previously described, pyruvate is an end product of glycolysis which is decarboxylated by the PDHC to form acetyl CoA, used in the citric acid cycle and thence, in the mitochondrial generation of ATP. However, in cancer cells, a significant amount of pyruvate is converted to lactate by lactate dehydrogenase (LDH). Adenosine monophosphate-activated kinase (AMPK) is an important regulator of energy homeostasis, through AMP:ATP ratio sensing, that primarily functions to increase fatty acid oxidation and glucose uptake and oxidation during cell stress or nutrient deprivation (Jorgensen *et al.*, 2006). Treatment of HeLa cells with DOG has been shown to stimulate AMPK (Hurley *et al.*, 2005), while AMPK activity in rat soleus muscle is associated with an increase in PDH activity and subsequent increase of glucose oxidation (Smith *et al.*, 2005). Thus, it was hypothesised that treatment of HeLa cells with DOG may lead to the diversion of more pyruvate to mitochondria for ATP synthesis and thus, improve fusion rates. To the contrary, it was found that 1mM pyruvate, in addition to 2mM L-glutamine, in the incubation buffer did not significantly restore the fusion rates in the presence of DOG (PI of 67.75 $\pm$ 4.74% 30 minutes post-activation, fig 3.21A). A 10-fold higher pyruvate concentration did increase fusion rates somewhat (PI of 55.5 $\pm$ 6.66% 30 min post-activation, fig. 3.21B) but this was still not comparable to control levels.

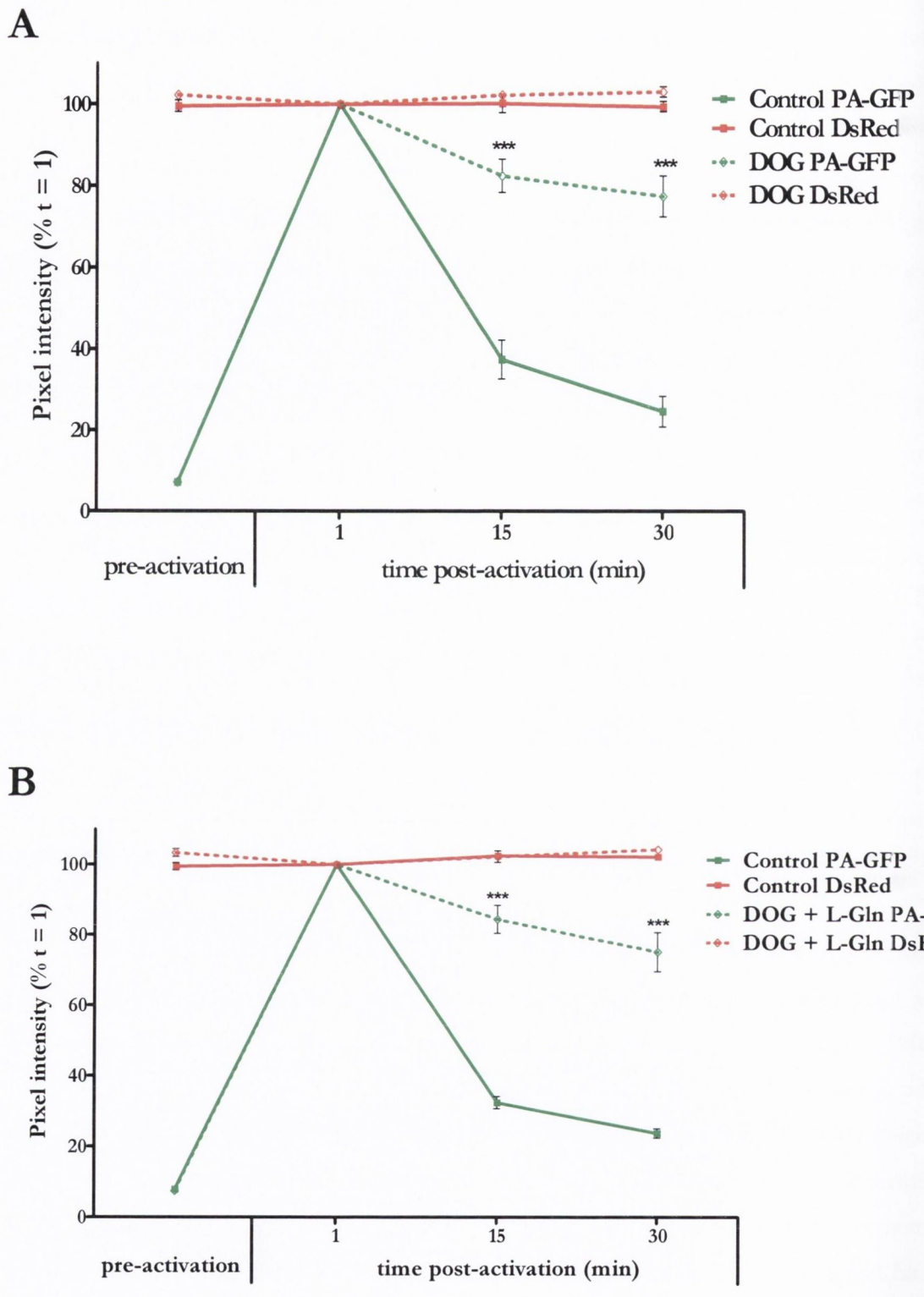

Figure 3.19: Inhibition of glycolysis severely compromises mitochondrial fusion in HeLa cells. (A) Cells were incubated in Krebs buffer free of glucose and L-glutamine (L-Gln) containing 10mM 2-Deoxy-D-glucose (DOG) for 20 minutes. Inhibition of glycolysis led to very pronounced slowing of mitochondrial fusion, with PI remaining at 77.41 $\pm$ 5% at 30 minutes post-activation. (B) Inclusion of 2mM L-Gln did not improve fusion rates during DOG treatment. Data presented as mean $\pm$ SEM, n = 3. Unpaired t-test at each time point. *** P<0.001.

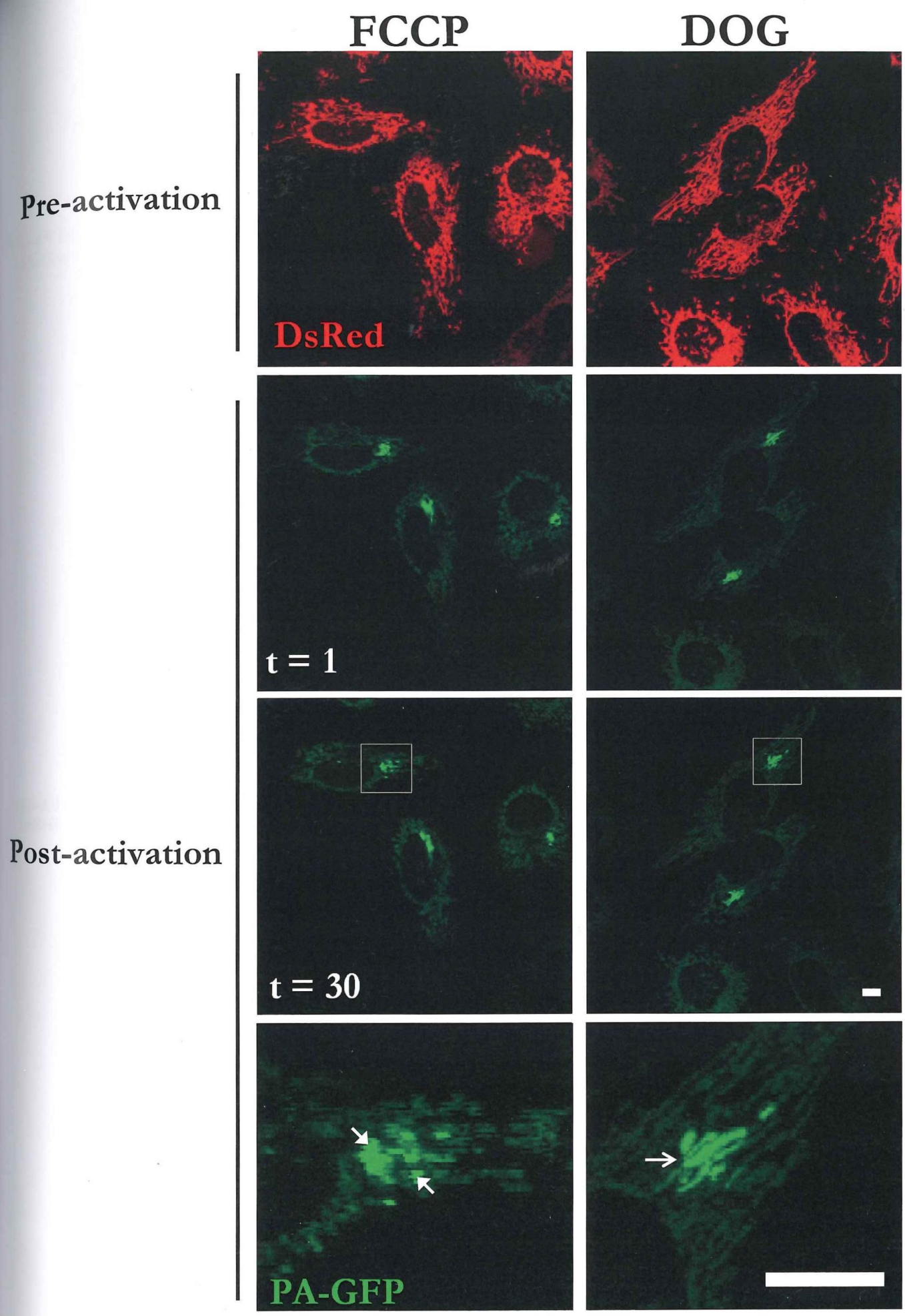

Figure 3.20: HeLa cells treated with DOG exhibit cessation of fusion in the absence of increased fission. Treatment of cells with 5μM FCCP and 10mM 2-deoxy-D-glucose (DOG) leads to a decrease in mitochondrial fusion of comparable magnitude but the mechanisms responsible for these effects may differ. FCCP-treated cells exhibit highly fragmented mitochondria (left column, closed-head arrows), whereas DOG-treated cells exhibit tubular, yet non-fusing mitochondria (right column, open-head arrow). Scale = 5μm.

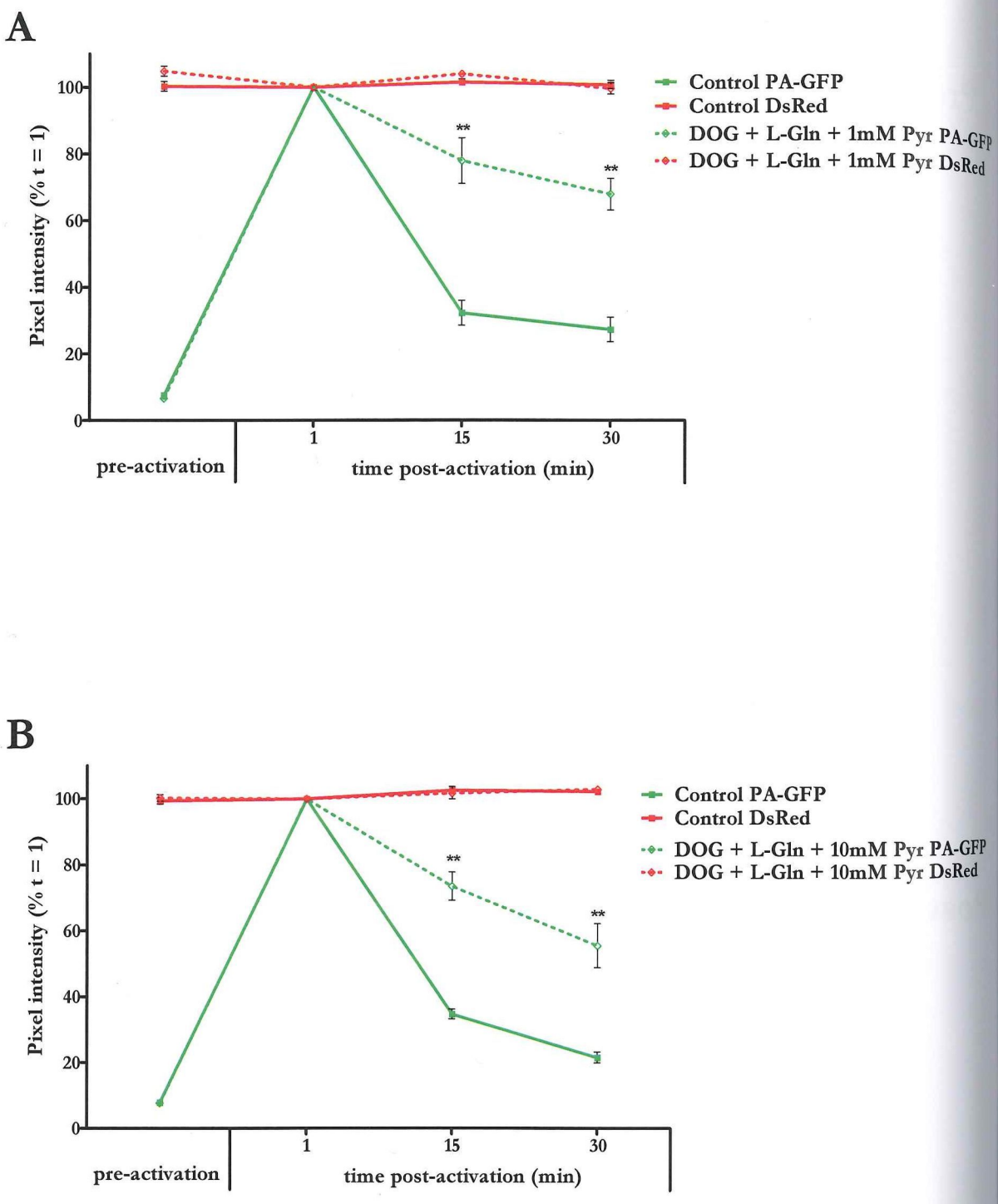

Figure 3.21: Pyruvate does not restore mitochondrial fusion rates in DOG-treated HeLa cells. Neither inclusion of 1mM (A) nor 10mM (B) sodium pyruvate (pyr) in Krebs buffer containing 2-deoxy-D-glucose (DOG) and L-glutamine (L-Gln) is sufficient to fully restore mitochondrial fusion rates in HeLa cells. Data presented as mean ± SEM, n = 3. Unpaired t-test at each time point. **P<0.01.

Galactose is a six-carbon sugar derived from dairy products and is converted in tissues to the more metabolically useful glucose-1-phosphate by a process known as the Leloir pathway (Holden *et al.*, 2003). Glucose-1-phosphate can then be fed into the glycolytic pathway by conversion to G-6-P by phosphoglucomutase. This sugar did not serve as an adequate alternative to glucose when DOG-containing Krebs buffer was supplemented with 10mM galactose and 2mM L-glutamine, as it did not improve the fusion deficit to any significant degree (PI of 71.26 $\pm$ 10.44% 30 minutes post-activation, fig. 3.22A). Finally, when DOG was administered in the presence of 2mM L-glutamine, 10mM pyruvate and 10mM galactose, mitochondrial fusion was still hindered, with PIs in photo-activated areas of cells remaining at 49.41 $\pm$ 2.81% after 30 min, more than double those of control cells (fig. 3.22B). One-way analyses of variance (ANOVA), with Tukey's honestly significant difference (HSD) post-test of PIs at 15 and 30 minutes post-activation for all DOG incubations show no statistical difference between treatments at each time point, with the exception of DOG alone *versus* DOG + L-glutamine + galactose + pyruvate at 30 minutes post-activation (fig 3.23). This illustrates that in the presence of DOG, other substrates do not sufficiently restore fusion to a statistically significant degree. These results suggest that the metabolism of glucose, at least its phosphorylation to G-6-P, is essential in the maintenance of HeLa cell mitochondrial fusion.

3.4.5. Effects of Inhibition of Oxidative Phosphorylation and Glucose Metabolism on Mitochondrial Membrane Potential

The observed decrease in mitochondrial fusion rates resulting from dissipation of the $\Delta\Psi_m$ shows a clear link between these two important aspects of mitochondrial function. Live cell confocal microscopy was used to measure $\Delta\Psi_m$ in HeLa cells before and after 20 minute incubations with all previously described inhibitors. Cells were loaded with tetramethylrhodamine methyl ester (TMRM), a cationic, red-orange fluorescence-emitting dye sequestered by mitochondria in a $\Delta\Psi_m$-dependent manner. At non-quenching concentrations, mitochondrial depolarisation is indicated by loss of signal (and, conversely, hyperpolarisation by increase in signal). Pixel intensities of imaged fields were expressed as a percentage of initial values. To confirm the sensitivity of this method in detecting $\Delta\Psi_m$ changes, time course and dose-response experiments with FCCP were conducted (fig. 3.24). Cells loaded with 20nM TMRM were imaged before and after 5, 10 and 20 minutes incubation with a range of FCCP concentrations (0.5 –

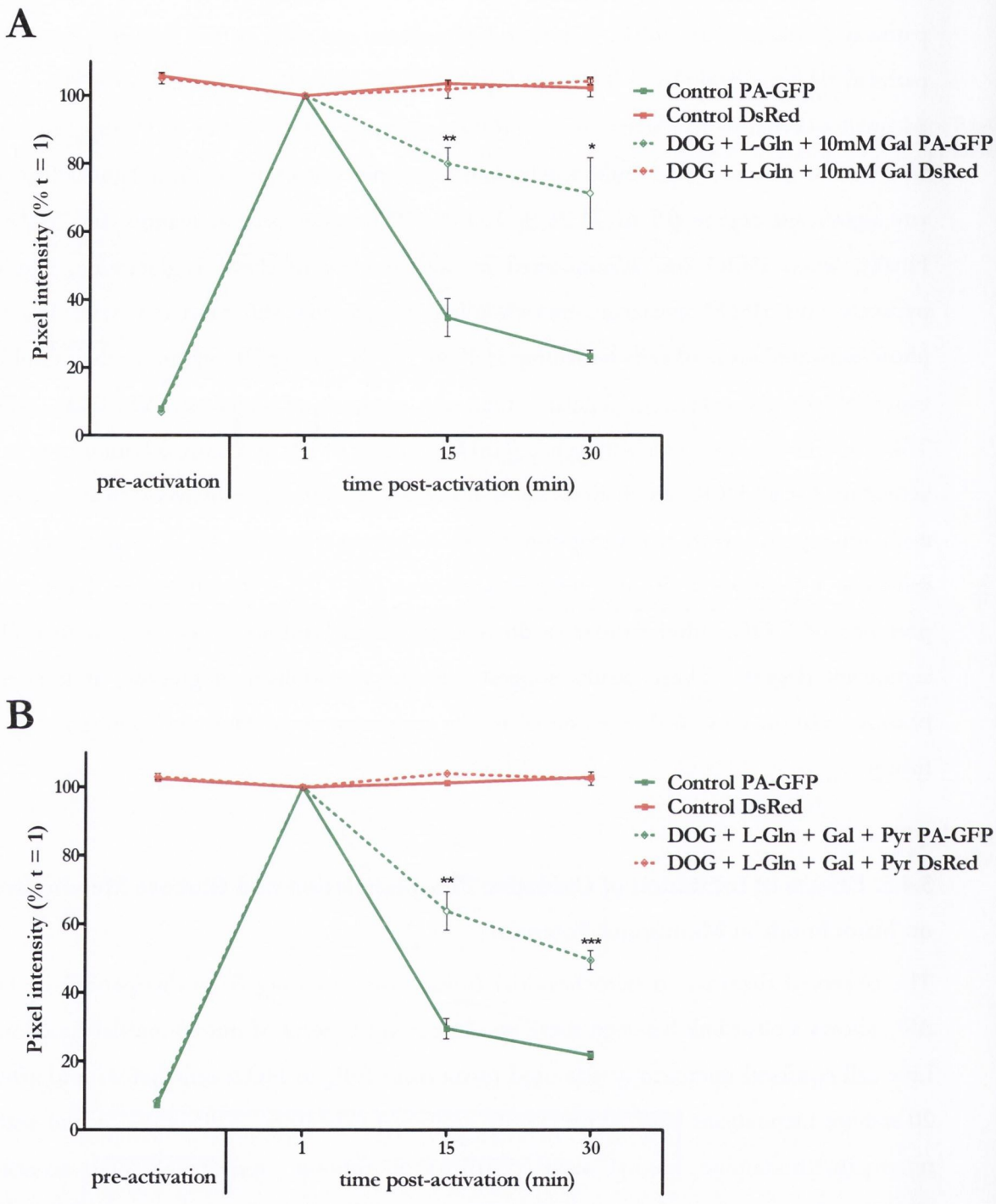

Figure 3.22: Galactose does not restore mitochondrial fusion rates in 2-deoxy-D-glucose-treated HeLa cells. Galactose (10mM), when applied with L-glutamine (A) or with L-glutamine + 10mM pyruvate (B) is not an adequate alternative energy source to restore mitochondrial fusion rates in 2-deoxy-D-glucose-treated cells. All cells were incubated in Krebs buffer with or without the supplements indicated. L-Gln, L-glutamine; Gal, galactose; Pyr, pyruvate. Data presented as mean ± SEM, n = 3. Unpaired t-test at each time point. *P<0.05, **P<0.01, *** P<0.001.

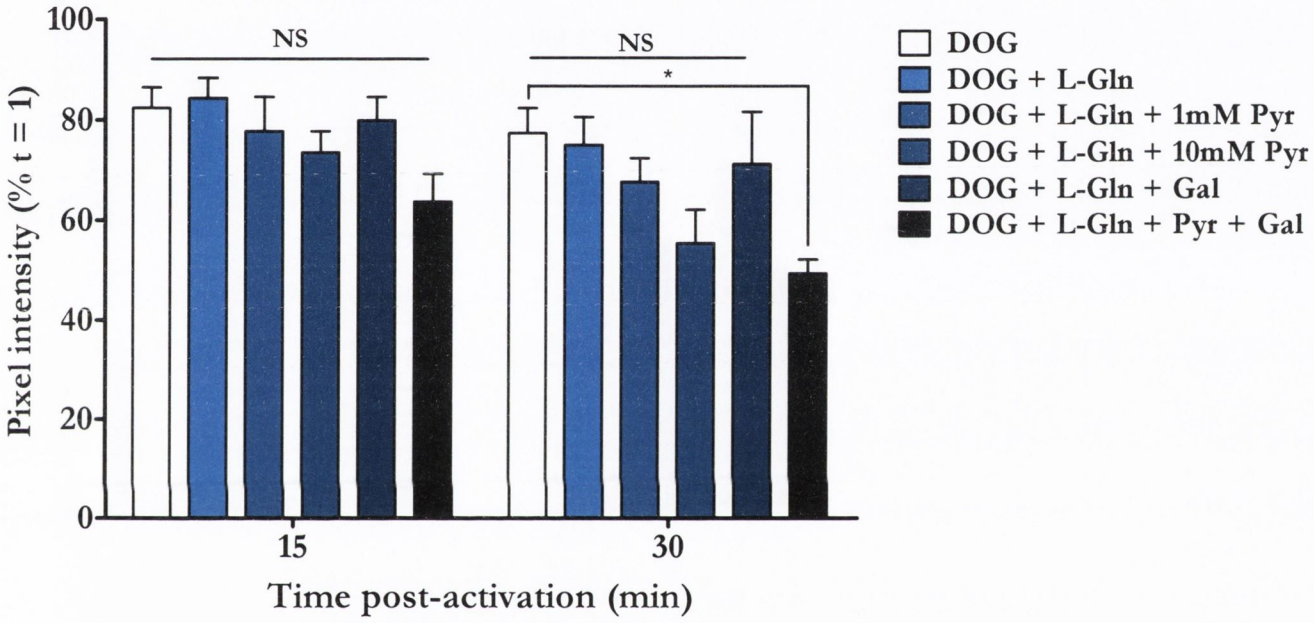

Figure 3.23: The glycolytic pathway is important in the maintenance of mitochondrial fusion rates in HeLa cells. One way ANOVAs with Tukey's HSD post test of PIs of photo-activated regions in cells across 2-deoxy-D-glucose (DOG) treatment groups at 15 and 30 minutes post-activation reveals that they do not differ to a statistically significant degree generally, emphasising the importance of glucose as a substrate in the maintenance of healthy mitochondrial fusion rates. The exception is the DOG alone group *versus* the DOG + L-glutamine (L-Gln) + galactose (Gal) + pyruvate (Pyr) group, the latter showing a statistically significantly lower PI at 30 minutes post-activation than the former. This PI, however, is still 2.7-fold higher than control values. Data presented as mean ± SEM, n = 3. *P<0.05.

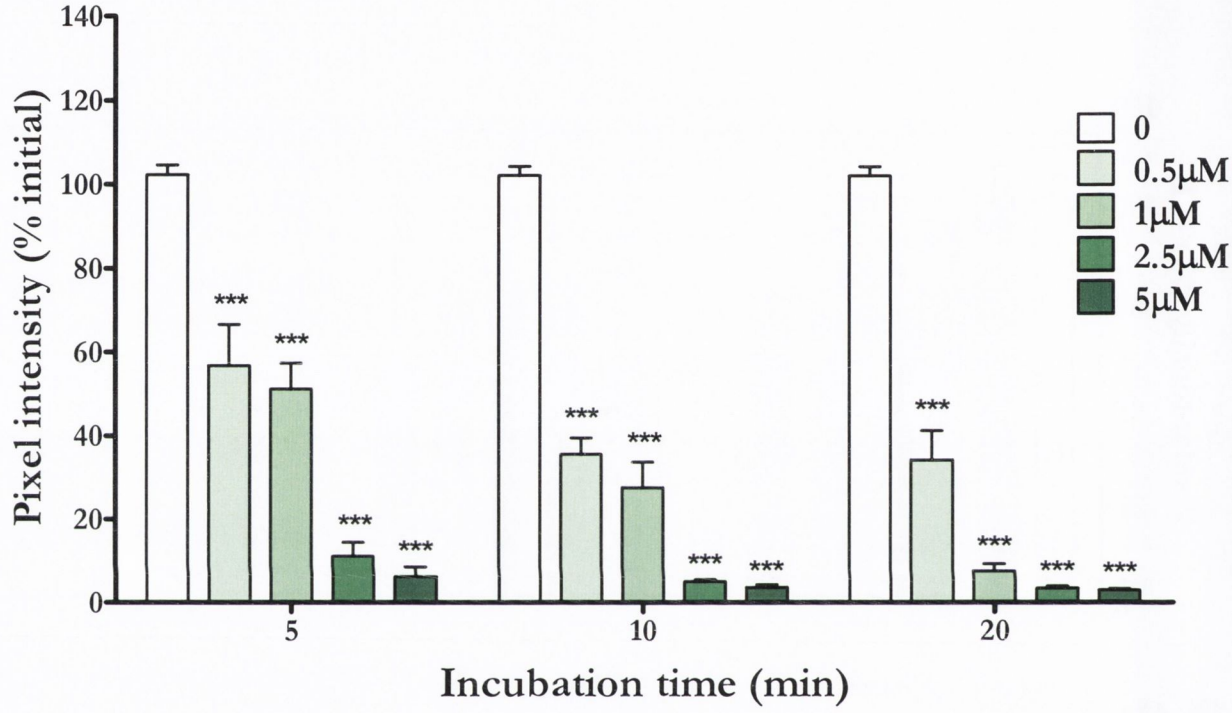

Figure 3.24: FCCP causes $\Delta\Psi_m$ depolarisation in a dose- and time-dependent manner in HeLa cells. A dose-response and time course experiment was performed to establish the sensitivity of the method used to detect $\Delta\Psi_m$ changes in HeLa cells. Cells were imaged before and at 5, 10 and 20 minutes after incubation with 0 – 5μM FCCP in 25mM glucose DMEM. Mean PI of each field imaged were expressed as percentage of their initial, pre-FCCP value. FCCP caused rapid loss of TMRM signal in a dose- and time-dependent manner, with all concentrations producing a depolarisation of at least 56.74 ± 9.86% within 5 minutes. Data presented as mean ± SEM, n = 3. Two-way ANOVA with Bonferroni post-test. ***P<0.001.

5μM). Pixel intensities were reduced within 5 minutes to at least 56.74 ± 9.86% of initial values at all concentrations, with the largest PI decreases in the 2.5-5μM FCCP range (decrease to 11.07 ± 3.34% and 6.20 ± 2.28% of initial, respectively). Gradual reductions at 10 and 20 minutes were observed in the lower concentration range (0.5 – 1μM), but further reductions were detectable even at 5μM FCCP (PI of 2.96 ± 0.34% after 20 minute incubation. These results confirmed that this method was suitable for detecting small changes in $\Delta\Psi_m$ in response to mitochondrial inhibition.

The changes in $\Delta\Psi_m$ following exposure to mitochondrial inhibitors were then assessed (fig. 3.25). Many inhibitors targeted to the ETC (rotenone and piericidin A; complex I, antimycin A; complex III and azide; complex IV) elicited a statistically significant decrease in PIs compared to controls. The exceptions were malonate (complex II) and myxothiazol (complex III), neither of which seemed to affect $\Delta\Psi_m$ significantly. ATP synthase inhibition with oligomycin caused a statistically significant increase in PI, indicating hyperpolarisation, as expected. These results suggest that HeLa cell mitochondria are capable of maintaining fusion rates despite partial depolarisation, but not with complete depolarisation. There is no evidence in the literature to suggest hypolarisation hinders fusion.

Simultaneous incubation of cells with FCCP and oligomycin led to complete depolarisation (fig. 3.26A) whilst incubation of cells with rotenone and oligomycin (fig. 3.26B) prevented oligomycin-induced hyperpolarisation (PI of 65.21 ± 5.95% of initial values). Co-incubation with either rotenone + antimycin A (fig. 3.27A), or piericidin A + antimycin A (fig. 3.27B) caused depolarisation of comparable magnitudes, with PIs of 80.66 ± 1.82% and 75.66 ± 2.75% post incubation, respectively. Finally, incubation with DOG with or without L-glutamine, pyruvate or galactose had no statistically significant effect on $\Delta\Psi_m$ (fig 3.28). These results suggest that mitochondrial fusion rates are not necessarily $\Delta\Psi_m$-dependent. In the case of ETC inhibition, cells that have undergone partial $\Delta\Psi_m$ depolarisation may still maintain normal fusion rates. Conversely, cells in which glucose metabolism is inhibited exhibit mitochondria that are unable to fuse whilst maintaining normal $\Delta\Psi_m$.

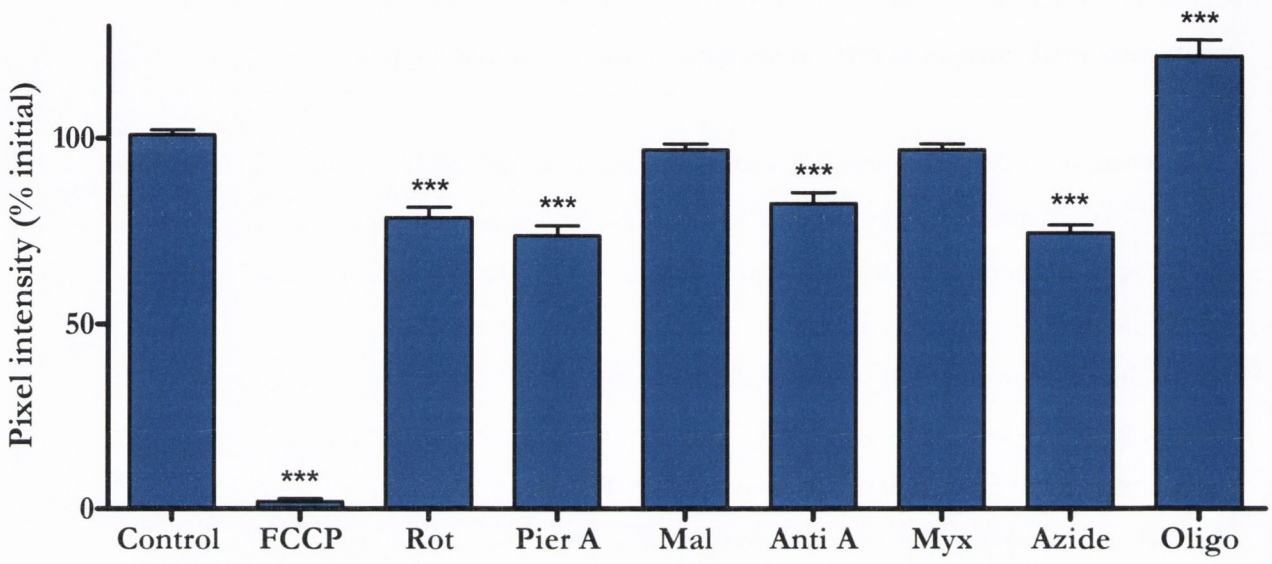

Figure 3.25: Effects of mitochondrial inhibitors on $\Delta\Psi_m$ in HeLa cells. Cells were imaged before and after 20 minute incubations with the inhibitors indicated in 25mM glucose DMEM and the pixel intensities of each field were plotted as a percentage of pre-incubation values (% initial). FCCP and oligomycin caused complete depolarisation and significant hyperpolarisation, respectively. All inhibitors targeting enzymes of the ETC caused statistically significant PI decrease of approximately 18 – 20%. The exceptions were malonate (mal) and myxothiazol (myx), neither of which appeared to impact $\Delta\Psi_m$. Anti A, antimycin A; oligo, oligomycin; pier A, piericidin A. .Data presented as mean ± SEM. One-way ANOVA with Dunnett's Multiple Comparisons post-test. ***P<0.001.

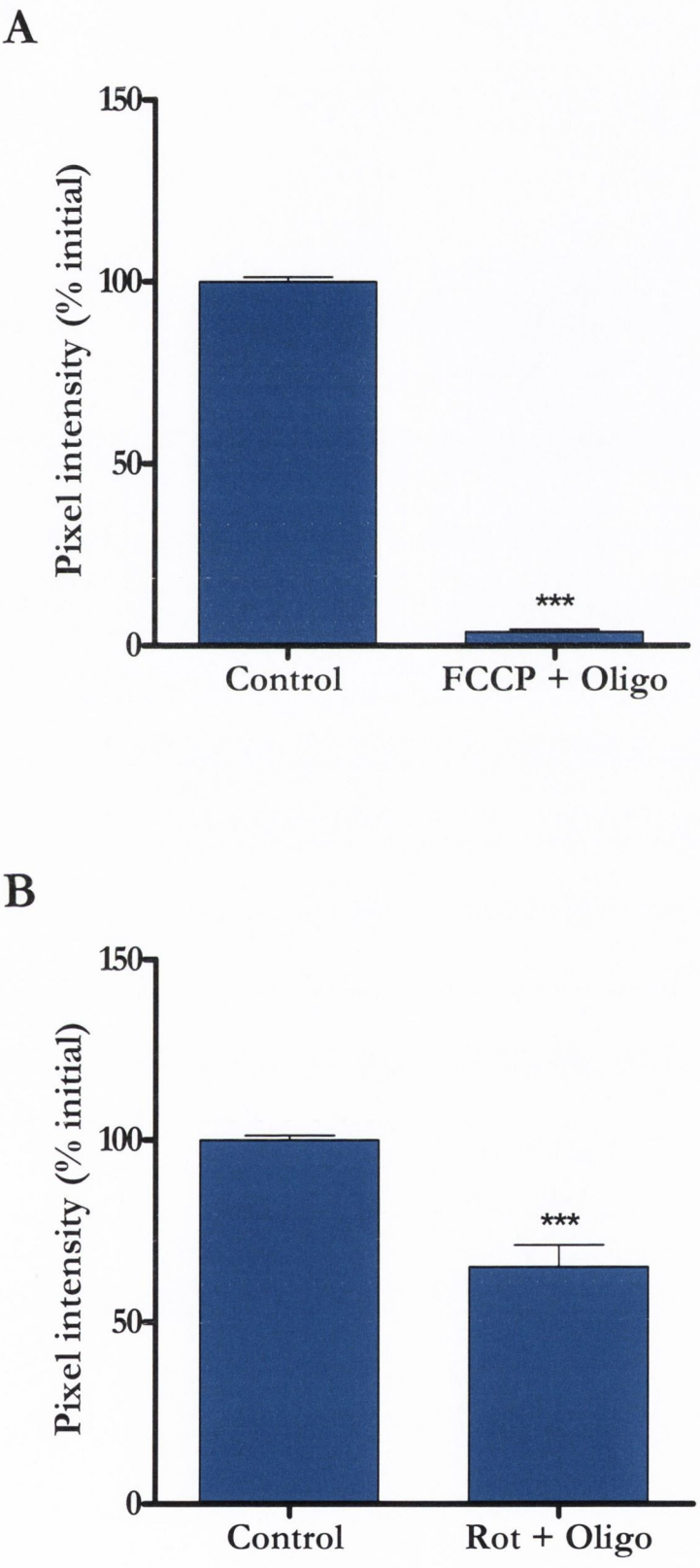

Figure 3.26: Mitochondrial depolarisation in cells incubated with multiple mitochondrial inhibitors. Cells co-incubated with FCCP and oligomycin (oligo) in 25mM glucose DMEM showed complete depolarisation (A), while cells co-incubated with rotenone and oligomycin showed a significant PI decrease of 34.79 $\pm$ 5.95% (B). Data presented as mean $\pm$ SEM. Unpaired t-test. ***P<0.001.

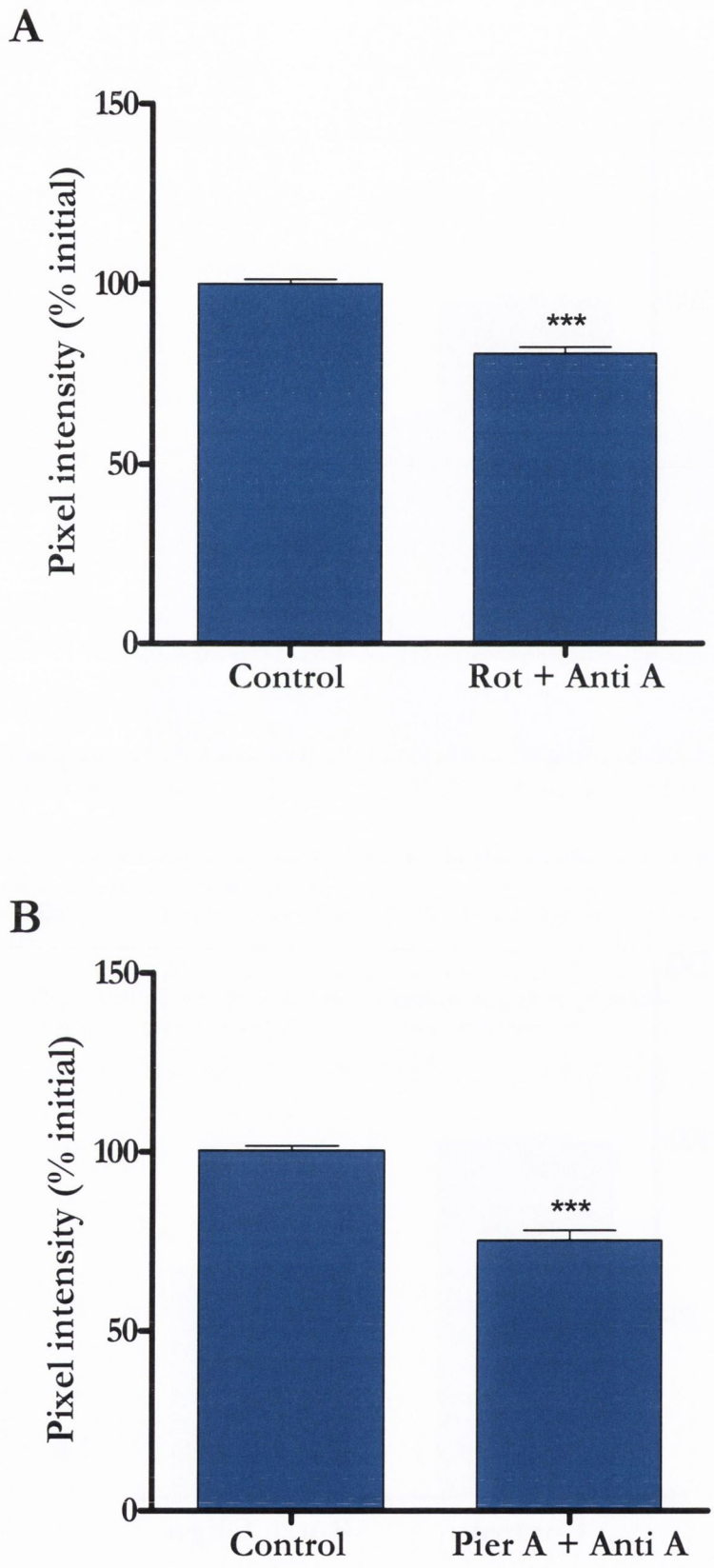

Figure 3.27: Mitochondrial depolarisation in cells simultaneously incubated with complex I and complex III inhibitors. Cells incubated with rotenone + antimycin A (A) or piericidin A + antimycin A (B) in 25mM glucose DMEM showed mitochondrial depolarisation levels of comparable magnitude and statistical significance. Anti A, antimycin A; pier A, piericidin A; rot, rotenone. Data presented as mean ± SEM. Unpaired t-test. ***P<0.001.

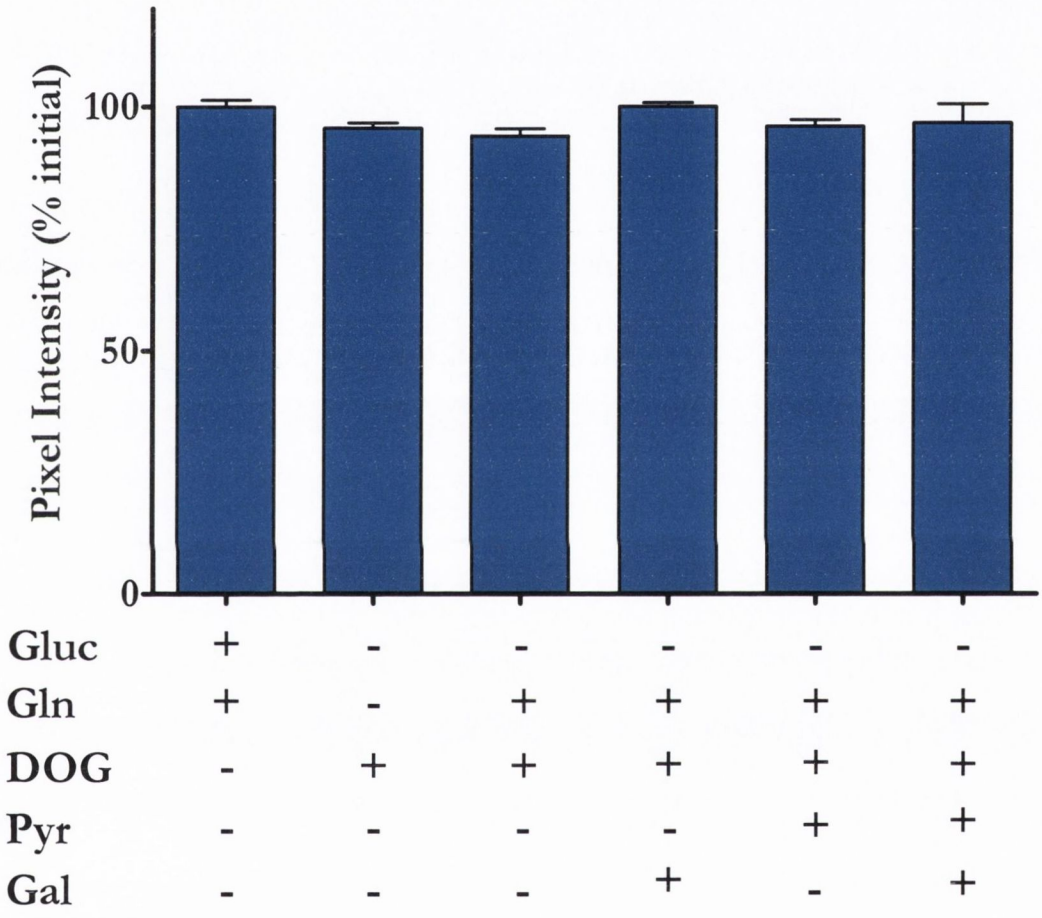

Figure 3.28: Inhibition of glycolysis does not affect $\Delta\Psi_m$ in HeLa cells. Cells incubated with 2-deoxy-D-glucose (DOG) with or without the supplements indicated (alone or in combination) do not exhibit statistically significant changes in $\Delta\Psi_m$. All cells were incubated in Krebs buffer with or without the supplements indicated. Gal, galactose (10mM); Gluc, glucose (25mM); Gln, L-glutamine (2mM); Pyr, pyruvate (10mM). Data presented as mean $\pm$ SEM. One-way ANOVA with Dunnett's Multiple Comparisons post-test.

3.4.6. Effects of Inhibition of Oxidative Phosphorylation and Glucose Metabolism on Cellular ATP levels

As previously mentioned, cancer cells often under-utilise mitochondria in the generation of ATP in favour of glycolysis. It was hypothesised that the mitochondrial inhibitors used were not affecting fusion rates because of the cells' dependence on extra-mitochondrial energy generation pathways. The fusion deficit introduced by glycolysis inhibition further supported this hypothesis. To investigate this hypothesis, cells were incubated in the absence or presence of each of the inhibitors for 20 minutes, then lysed and assayed for ATP content using a luminescence-based assay.

As expected, exposure of cells to mitochondrial inhibitors did not affect ATP levels to any statistically significant degree (fig. 3.29A), but DOG induced a very significant decrease of 84.1 $\pm$ 2.39% in ATP levels. Upon further examination of the effect of inhibition of glucose metabolism on ATP levels, it was revealed that supplementation of DOG-containing medium with L-glutamine, pyruvate or galactose, together or in combination, could not compensate for the ATP decrease induced by DOG alone (fig. 3.29B). Taken together, these data point towards a strong link between cellular ATP levels and the ability of mitochondria to fuse normally.

Figure 3.29: Effects of OXPHOS and glycolysis inhibition on HeLa cell ATP levels. (A) Cells incubated with the inhibitors indicated for 20 minutes were lysed and assayed for ATP content as described. Exposure to OXPHOS inhibitors did not lead to statistically significant changes in ATP, but incubation with 2-deoxy-D-glucose (DOG) led to a ~84% drop in cellular ATP. All cells were incubated in normal 25mM glucose DMEM, except the DOG group, which was incubated in glucose free DMEM containing L-glutamine (B) Closer examination of the effect of glycolysis inhibition on ATP levels reveals that none of the supplements indicated were sufficient to maintain normal cellular [ATP] in the presence of DOG. All cells were incubated in Krebs buffer with or without the supplements indicated. Gal, galactose (10mM); Gluc, glucose (25mM); Gln, L-glutamine (2mM); Pyr, pyruvate (10mM). Data presented as mean ± SEM. One-way ANOVA with Dunnett's Multiple Comparisons post-test. ***P<0.001.

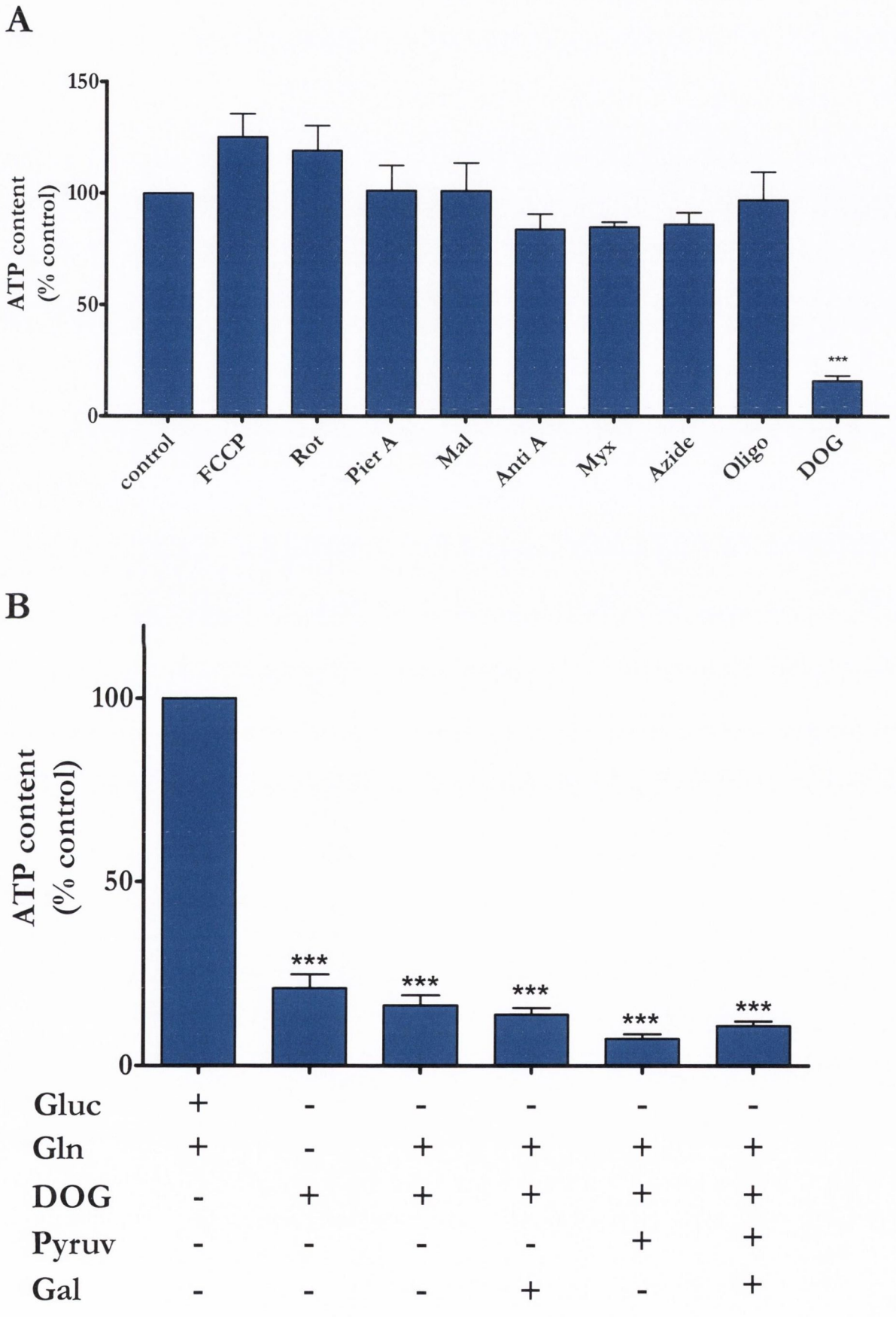
A
ATP content
(% control)
150
100
50
0
***
control
FCCP
Rot
Pier A
Mal
Anti A
Myx
Azide
Oligo
DOG
B
ATP content
(% control)
100
50
0
***
***
***
***
***
Gluc + - - - - -
Gln + - + + + +
DOG - + + + + +
Pyruv - - - - + +
Gal - - - + - +

3.5 Discussion

These studies have quantified for the first time the effects of inhibition of the ETC/OXPHOS system, microtubule assembly and glucose metabolism on mitochondrial fusion rates in HeLa cells exhibiting the Warburg effect. Complete depolarisation of the mitochondria led to extensive fragmentation and severely compromised fusion, yet did not affect cellular ATP levels. Inhibition of the ETC did not affect fusion, nor cellular ATP levels, despite inducing ~20% TMRM PI decrease. In contrast, inhibition of ATP synthase did not affect ATP levels but induced a 2.6-fold decrease in mitochondrial fusion rates and membrane hyperpolarisation. Microtubule disassembly induced a small but statistically significant decrease in mitochondrial fusion, which was not significantly affected by co-incubation with antimycin A. Finally, inhibition of glycolysis induced a severe fusion deficit close to that induced by FCCP. Supplementation of DOG-containing medium with L-glutamine, pyruvate, or galactose, alone or in combination, did not fully restore fusion rates, indicating the importance of glucose metabolism for mitochondrial fusion these cells. In addition, DOG treatment did not affect $\Delta\Psi_m$ but dramatically reduced cellular ATP levels. These results suggest a correlation between cellular ATP levels and mitochondrial fusion rates.

Fragmentation of the mitochondrial reticulum upon $\Delta\Psi_m$ depolarisation was rapid and reversible, in agreement with the literature (fig. 3.7) (Malka *et al.*, 2005, Duvezin-Caubet *et al.*, 2006). This phenomenon occurs both in neoplastic and non-neoplastic cells (Duvezin-Caubet *et al.*, 2006, Guillery *et al.*, 2008). Mitochondrial fusion was seriously inhibited until the protonophore was removed, at which point fusion was restored. It has been suggested that OM fusion can proceed in the presence of ionophores (Malka *et al.*, 2005) but this was not observed here. While the mechanism behind this response is thought to arise from $\Delta\Psi_m$-dependent cleavage of OPA1 to short isoforms (Guillery *et al.*, 2008), the reason for this phenomenon is unclear. Yeast mitochondria exhibit fragments of the mitochondrial inner compartment separated from the outer compartment called mitoplasts, which have been shown to prevent OM rupture and release of pro-apoptotic effectors during cell stress (Knorre *et al.*, 2008). Mammalian cells have been proposed to contain intramatricial lipid junctions (Benard *et al.*, 2011) but this has yet to be confirmed. The only instance in which a formation close to a 'mitoplast' has been observed in human cells is in OPA1 knock-out cells (Song *et al.*, 2009), which exhibit numerous matrix compartments bounded by a large OM. Thus,

perhaps for wild type mammalian mitochondria, the OM must also undergo scission in order to separate the inner membrane compartment into smaller units for protection. Therefore, the observed transient ionophore-induced fragmentation may be an acute protective mechanism.

This work builds on important qualitative data generated by Legros *et al.* (2002) who examined the extent of mitochondrial fusion in osteosarcoma 143B cell polykaryons lacking mtDNA or wild-type HeLa polykaryons exposed to FCCP, DOG, oligomycin or DOG + oligomycin. These polykaryons were generated by fusing two populations of cells with differently labelled mitochondria, such that mitochondrial fusion was identified as a mixing/colocalisation of these labels within single organelles. Polykaryons are generated using the PEG protocol established by Borer *et al.* (1989) and are maintained in cycloheximide to inhibit new protein synthesis. The authors found that fusion continued in the polykaryons lacking functional ETC machinery. However, it has been suggested that cycloheximide treatment stimulates mitochondrial fusion (Karbowski *et al.*, 2004a, Tondera *et al.*, 2009, Hoppins *et al.*, 2011) and thus may generate false positives. The authors of this study dispute this, as the degree of mitochondrial fusion induction could be negligible (Manuel Rojo, personal communication). Nevertheless, the results presented in this chapter robustly confirm, with quantitative evidence, that HeLa cell mitochondria can indeed undergo fusion at a normal rate with non-functional ETC (figs. 3.8 – 3.11). Interestingly, most of the ETC inhibitors used induced ~20% decrease in TMRM PI yet no effect on fusion occurred (fig 3.25). Thus, slightly depolarised mitochondria can maintain normal fusion rates in glycolytic HeLa cells. This suggests that the OPA1 cleavage induced by depolarisation must occur when depolarisation reaches a certain threshold. The extent of OPA1 cleavage in these cells in response to ETC inhibitors is explored in the next chapter.

Significantly, inhibition of ATP synthase reduced fusion levels to approximately half of control values (fig. 3.12). This effect does not appear to be related to ATP levels, as a luciferase luminescence-based assay revealed no significant changes in ATP amongst cells treated with any mitochondrial inhibitors (fig. 3.29). These data also support the study of Legros *et al.* (2002), which showed reduced fusion in polykaryons incubated with oligomycin. Interestingly, a common characteristic of human carcinomas is the downregulation of the catalytic β-F1-ATPase (Willers and Cuezva, 2011), i.e. the site at

which phosphorylation of ADP occurs in normal OXPHOS. The degree of downregulation of this subunit has been linked to colon cancer progression (Sánchez-Aragó *et al.*, 2010). In addition, many cancer cells also overexpress inhibitor factor 1 (IF_1), a protein that regulates ATP synthase activity, by preventing the enzyme working in reverse under hypoxic conditions (Campanella *et al.*, 2008). This has obvious implications for hypoxic tumours, as prevention of ATP synthase 'cannibalisation' of cellular ATP during hypoxia would promote survival. Recently, Sánchez-Cenizo *et al.* (2010) have demonstrated that IF_1 may inhibit ATP synthase function even in normoxic carcinomas, promoting a Warburg phenotype. As HeLa cells appear to be strongly glycolytic it seems likely that ATP synthase activity is constitutively lowered, although this was not directly assessed in the studies presented here. This raises the question of why inhibition of ATP synthase should impact mitochondrial fusion rates so strongly.

The effect may be structural. Compellingly, like OPA1, ATP synthase is involved in cristae formation. Strauss *et al.* (2008) have elegantly demonstrated that ATP synthase in beef heart and rat liver mitochondria is arranged in long ~1μm rows of dimeric supercomplexes, located at the apex of cristae membranes. These so-called 'dimer ribbons' produce significant local curvature on the membrane with a 17nm outer radius owing to markedly increased charge density. This dimerisation involves interactions between the oligomycin-sensitive portions of the enzymes, F_o (Hong and Pedersen, 2008, Wagner *et al.*, 2010). Indeed, Wagner *et al.* (2010) have shown that in yeast, certain dimer-promoting subunits of F_o do not assemble with F_o in the presence of oligomycin, leading to decreased dimerisation. Thus it is conceivable that in HeLa cells, oligomycin affects ATP synthase dimerisation, leading to altered cristae curvature and, possibly as a consequence, the distribution/function of OPA1.

An anomalous finding of these studies is the synergistic reduction in fusion induced by co-incubation with rotenone and antimycin A (fig 3.14). This effect was shown not to be due to simultaneous inhibition of complexes I and III *per se*, as co-incubation with piericidin A and antimycin A did not replicate the result. Furthermore, the effect was not $\Delta\Psi_m$-dependent as both treatments produced the same level of depolarisation (fig 3.27). It would be useful to examine the ATP levels in this context. It seems unlikely that rotenone and piericidin A would have significantly different effects on this parameter, as they were both present in excess in the culture medium and as such, probably inhibited

complex I maximally. As rotenone was shown to cause microtubule disassembly by immunostaining for tubulin, it was considered that perhaps the effect was due to simultaneous microtubule disruption and ETC inhibition. Thus, mitochondrial fusion rates were assessed in cells incubated with anti-neoplastic agent nocodazole or co-incubated with nocodazole and antimycin A (fig. 3.17). Unexpectedly, nocodazole alone produced a small but significant reduction in fusion rates. Microtubule disassembly has previously been shown to cause disorganisation of the mitochondrial network (Mattenberger *et al.*, 2003) which was also observed here (not shown). However, these studies show that it also impacts mitochondrial fusion rates to some degree. Microtubule targeting agents (MTAs) are regularly used in chemotherapeutic cancer treatment and mitochondria are thought to be involved in their cytotoxicity (Rovini *et al.*, 2011). These MTAs lead to apoptosis in cancer cells via the intrinsic pathway, thus involving MOMP and cytochrome c release. Given the prominent involvement of mitochondrial dynamics in this process, reduced fusion could be an early event induced by MTAs that leads to MOMP and fragmentation. Nocodazole + antimycin A treatment slightly decreased fusion further, but this was not a statistically significant difference when compared to that of nocodazole alone (fig 3.17C). Thus, the mechanism behind rotenone + antimycin A-induced fusion inhibition remains to be elucidated. There could be a synergistic effect involving simultaneous complex I, III and microtubule inhibition, which could be assessed by co-incubating cells with nocodazole, piericidin A and antimycin A and monitoring fusion. It would also be worth assessing ATP levels in cells following this treatment.

The most significant inhibition of mitochondrial fusion, apart from that elicited by FCCP, was observed upon treatment of cells with DOG (fig. 3.19 – 23). Cells were shown to be fully dependent on the metabolism of glucose for the maintenance of mitochondrial fusion rates, although the exact reason for this dependence is not clear. The supplementation of the incubation medium with L-glutamine, pyruvate or galactose could not restore fusion to control levels in the presence of DOG, possibly indicating a significant under-utilisation of OXPHOS in these cells, characteristic of the classic Warburg phenotype (Mathupala *et al.*, 2009). Indeed, ability to utilise L-glutamine for ATP varies across cancer cell types; early work by Reitzer *et al.* (1979) suggested that glutamine was the primary energy source for HeLa cells in culture, while more recent work by Rossignol *et al.* (2004) confirmed that HeLa cells could subsist primarily on

glutamine in the absence of glucose. However, the significant and rapid reduction of cellular ATP levels observed upon DOG treatment in the presence of L-glutamine is at odds with the findings of Reitzer and colleagues (1979) (fig. 3.29). In addition, high pyruvate levels did not restore fusion rates, indicating that an insufficient amount of pyruvate was undergoing decarboxylation to acetyl CoA for use in the TCA cycle (also another common trait of aerobic glycolysis). Mitochondrial membrane potential was stable under all DOG treatments, however ATP levels dropped by 80 – 90% within 20 minutes of DOG treatment, in agreement with the literature (Malka *et al.*, 2005, Guillery *et al.*, 2008, Sauvanet *et al.*, 2010). It is possible that ATP synthase consumed large amounts of ATP during DOG treatment to maintain $\Delta\Psi_m$. It would be interesting to examine ATP levels following co-incubation with DOG and oligomycin, the expectation being that oligomycin would prevent the ATP decrease induced by DOG alone.

An important effect of DOG treatment that was not examined here was the decreased flux of G-6-P through the PPP and potential subsequent oxidative stress. As previously mentioned, the PPP is a pathway that generates NADPH and pentoses from G-6-P, in two distinct phases. In the oxidative phase, two molecules of $NADP^+$ are reduced to NADPH as G-6-P is oxidised to ribulose-5-phosphate in two catalytic steps mediated by G-6-P dehydrogenase (G6PDH) and gluconolactonase. In the non-oxidative phase, ribulose-5-phosphate is converted to various pentoses, such as ribose-5-phosphate (used in nucleotide synthesis) and fructose-6-phosphate (used in glycolysis) by transketolase and transaldolase. The reducing power of the NADPH generated during the oxidative phase is essential in anti-oxidant defence, as it is used by glutathione reductase to replenish reduced glutathione (GSH) from its oxidised form (GSSG). Glutathione is the most abundant antioxidant in aerobic cells and can react directly with ROS by readily donating an electron from the thiol group of cysteine, and immediately reacting with another oxidised glutathione to form GSSG. For this reason, the low ratio of cellular GSH:GSSG can be used as a marker of oxidative stress (Owen and Butterfield, 2010). In addition, glutathione can participate in the detoxification of ROS by glutathione peroxidases and glutathione-S-transferases (Pompella *et al.*, 2003).

As previously mentioned, oxidative stress has been implicated as an inhibitor of normal mitochondrial dynamics (Pletjushkina *et al.*, 2006), while disturbing dynamics itself can lead to increased ROS (Parone *et al.*, 2008). Thus, the mitochondrial fusion data

presented here may indicate that HeLa cells in high glucose medium have access to sufficient antioxidant defence *via* the PPP to absorb ROS generated by OXPHOS inhibition but suffer oxidative stress in the face of DOG treatment, rendering mitochondrial fusion impossible. Measurement of ROS production using fluorescent probes (Amplex Red, MitoSox, 2',7'-dichlorofluorescin) and GSH:GSSG ratio in cells during or following DOG treatment would surely yield useful data. In addition, fusion could be measured in cells exposed to each inhibitor in the presence of an antioxidant, such as N-acetyl-cysteine (NAC).

In contrast to FCCP treated cells, fusion-inhibited mitochondria in DOG-treated HeLa cells retained tubular morphology despite the inability to fuse. This suggests differences in the pathways leading to fusion perturbation with both treatments. While FCCP treatment has been shown to induce OPA1 cleavage, the pathway regulating the novel fusion-inhibitory mechanism of DOG presented here is unknown. Presumably if OPA1 cleavage was involved, the mitochondria would fragment significantly, as with FCCP treatment. Therefore, although it cannot be excluded as a possibility, OPA1 cleavage may not be involved here. Potentially, mitochondria under these conditions are trapped in a form of stasis due to the dramatic drop in cellular ATP, neither fusing nor dividing. A decrease in cellular ATP could also decrease cellular GTP, especially in the immediate vicinity of the mitochondrial OM, where nucleoside diphosphate (NDP) kinases reside and convert ATP to GTP (Benard *et al.*, 2011). Thus none of the GTPase mitodynamins would have the ability to exert their effects. Potentially, the effect is related to the allosteric inhibition of HK II by DOG-6-phosphate having a structural impact on the interaction of the enzyme with VDAC and the ATP-synthasome. Indeed, oligomycin may also affect the stability of the synthasome and, in turn, disrupt HK II function, thus providing an explanation for the observed perturbation of fusion by DOG and oligomycin. Clearly, further experiments are required to identify the mechanism behind the effects of both agents.

These results further emphasise the concept that information pertaining to fusogenicity in mitochondria cannot be derived from mere observation of morphology. For instance, overexpression of OPA1 in MEFs can cause extensive fragmentation of the reticulum, yet mitochondria can still actively fuse (Chen *et al.*, 2005). The data presented here provide evidence that the opposite scenario can also occur, at least within the

experimental parameters employed. Thus, mitochondria can appear tubular yet be fusion-incompetent.

To conclude, these data show that mitochondrial fusion in glycolytic HeLa cells can proceed at a healthy rate in the presence of ETC inhibitors and while mitochondria are partially depolarised. However, fusion is seriously compromised by mitochondrial membrane depolarisation and inhibition of glucose metabolism and, to a lesser extent, by microtubule disassembly.

CHAPTER 4

Bioenergetic Control of Mitochondrial Dynamics in HeLa Cells Cultured in Galactose Medium

4.1 Introduction

In 1966, Hackenbrock published the first of a number of pioneering works describing a distinctive co-ordination of mitochondrial morphology and energetic state (Hackenbrock, 1966, 1968, Hackenbrock *et al.*, 1971). Electron microscopy revealed that during state 4 respiration, when ADP was low and OXPHOS was slowed, mitochondria assumed an 'orthodox' conformation; filamentous cristae within a matrix of intermediate electron density and relatively small IMS. Upon induction of state 3 respiration, when ADP was high and OXPHOS accelerated, mitochondria assumed a 'condensed' conformation, featuring an electron-dense matrix, with enlarged IMS but apparently unchanged total mitochondrial volume. Thus, a coupling between respiratory rate and mitochondrial structure had been established.

This coupling was observed *in vitro* some 38 years later, as described by Rossignol *et al.* (2004), who highlighted the relevance of this phenomenon in cancer biology. The authors reported that highly glycolytic HeLa cells previously cultured in standard high glucose medium (25mM) were capable of growth and proliferation in medium containing an alternative hexose, galactose, and glutamine, with corresponding changes in mitochondrial morphology. As described in the previous chapter, galactose is commonly found in dairy products and is metabolised in the body to the more metabolically useful glucose-1-phosphate via the Leloir pathway. In this pathway, galactose is initially epimerised from β-D-galactose to α-D-galactose by galactose mutarose, which then is phosphorylated to galactose-1-phosphate by galactokinase (GALK). Thence forth, it is converted to glucose-1-phosphate by galactose-1-phosphate uridylyltransferase and finally to glucose-6-phosphate by phosphoglucomutase, although this last step is strictly not part of the Leloir pathway (Frey, 1996, Holden *et al.*, 2003). While catabolism of galactose to pyruvate yields the same number of ATP molecules, it is less efficient, partially due to the lower affinity of GALK for both ATP and galactose (K_m = 2.10mM and 0.48mM, respectively) compared to that of VDAC-bound HK II for ATP and glucose (K_m = 0.25mM and 0.02mM, respectively) (Shin-Buehring *et al.*, 1979, Bustamante and Pedersen, 1980, Mathupala *et al.*, 2009). Thus, the inefficiency of converting galactose to G-6-P forced the cells to harness energy through glutaminolysis, reinstating OXPHOS as the primary energy production pathway (fig 4.1). In the studies of Rossignol *et al.*, increased OXPHOS was evident in the galactose cultured HeLa cells in numerous ways; (i) acidification of the growth medium was significantly reduced to

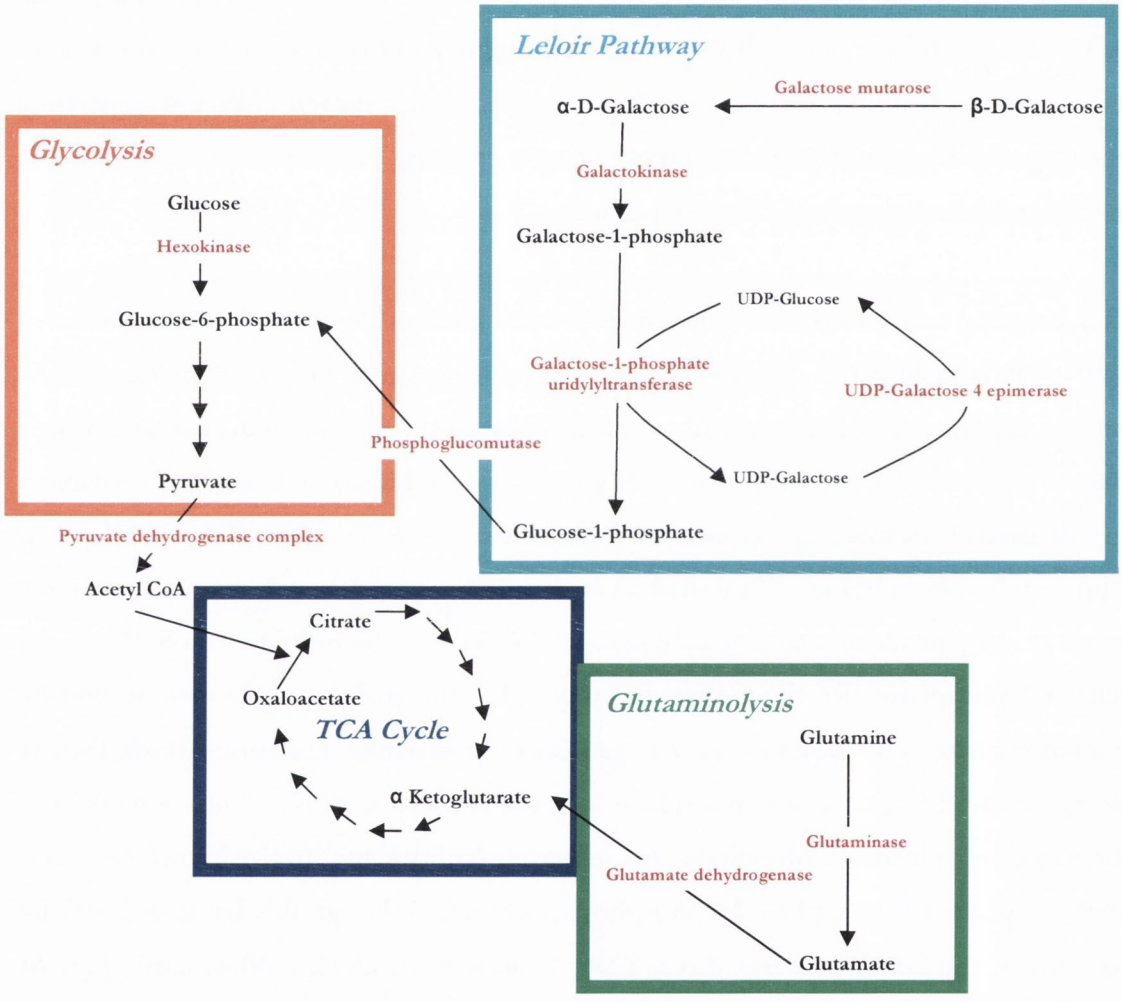

Figure 4.1: Integration of metabolic pathways. Simplified schematic of the integration of glycolysis, glutaminolysis, the Leloir pathway and the tricarboxylic acid (TCA) cyle. Successive small arrows indicate numerous catalytic reactions in glycolysis and the TCA cycle that were excluded, for clarity (not representative of the *number* of reactions that were excluded).

negligible levels, due to the reduction of lactate production, (ii) cellular respiratory rate doubled, (iii) the mitochondrial matrix was more oxidised and its steady state pH decreased, and (iv) expression of PDH and subunits of complexes I, II, and IV and ATP synthase was increased.

Compellingly, this metabolic switch was also accompanied by mitochondrial ultrastructural changes, akin to those described by Hackenbrock (1966, 1968, Hackenbrock *et al.*, 1971). Electron microscopy evidenced the change of conformation to the 'condensed' state, while fluorescence microscopy revealed the reticulum to be highly reticulated and to span the outer regions of the cytoplasm. In contrast, glucose cultured HeLa cells exhibited mitochondria that were thicker in diameter and arranged in a more perinulear fashion, and were distinctly absent from distal regions of the cytoplasm. Importantly, these data demonstrated that the diminution of mitochondrial function in cancer cells engaging in aerobic glycolysis was reversible and, furthermore, dictated by available substrates. Thus the under-utilised mitochondrial phenotype of glycolytic cancer cells was not necessarily a result of inherent mitochondrial insufficiency; organellar functionality could be restored with a simple change in substrate. This study by Rossignol *et al.* (2004) was also instrumental in shaping the recently published hypothesis of gene regulation in cancer occurring in 'waves' that sequentially depress and restore OXPHOS from transformation to steady tumour growth (Smolkova *et al.*, 2011).

These results also implicated role for mitochondrial dynamics in cancer biology and raised some important questions. The increased reticulation and spreading of the mitochondrial network suggested an increase in fusion, or a decrease in fission, or both, and possibly a change in transport. Furthermore, the increased dependence of the HeLa cells on OXPHOS for energy production may have sensitised the cells to aberrations in the regulation of mitochondrial fission, fusion or transport, or indeed energy production. These issues have not yet been addressed and thus, formed the basis of the studies described in this chapter.

4.2 Aims of Chapter

While the metabolic switch from glycolysis to oxidative phosphorylation dependence is accompanied by mitochondrial ultrastructural changes in HeLa cells, it is not known if there is a corresponding change in mitochondrial dynamics, specifically fusion rates. Furthermore, it is not known if these rates have altered sensitivity to mitochondrial inhibition and, if so, what the consequences are for cell survival. In the previous chapter, mitochondrial fusion rates were shown to be impervious to ETC inhibition in glucose cultured HeLa (Gluc-HeLa) cells. Thus, it was hypothesised that galactose cultured HeLa (Gal-HeLa) cells could acquire increased sensitivity to mitochondrial inhibition that would be reflected in mitochondrial fusion perturbation and increased cell death. To test this hypothesis, the following objectives were set:

1. **Assess if the ultrastructural changes in Gal-HeLa cell mitochondria are due to altered fusion dynamics.** Photo-activation studies were conducted on HeLa cells cultured in galactose for at least two weeks and their fusion rates compared to those of Gluc-HeLa cells. Expression of mitodynamins was compared in cells across substrates.
2. **Quantify the effects of ETC/OXPHOS inhibition and galactose starvation on Gal-HeLa cell mitochondrial fusion rates.** Gal-HeLa cell mitochondrial fusion rates were assessed in the absence or presence of the mitochondrial inhibitors or in the absence of galactose to assess the degree of cellular dependence on each metabolic pathway in the maintenance of these rates.
3. **Correlate changes in mitochondrial fusion rates with changes in $\Delta\Psi_{m}$-/ATP levels.** These parameters were examined, as before, to ascertain if they changed in response to mitochondrial inhibition/sugar starvation in a substrate-dependent manner
4. **Determine the degree of dependence on sugar metabolism across substrates.** Cell growth was quantified after three days of culture of Gluc- and Gal-HeLa cells in the absence of sugar or in the presence of one of selection of alternative sugars, namely fructose, sucrose or maltose. In addition, the HK I/II expression profiles were compared between cell types. Finally, it was determined if the presence of glucose could abrogate the fusion inhibition induced by piericidin A in Gal-HeLa cells.

5. **Assess if mitochondrial inhibition/sugar starvation had substrate-dependent effects on mitodynamins.** Western blots on mitochondria isolated from treated cells were compared across substrates to identify potential differences in PTM/proteolytic cleavage/recruitment of mitodynamins.
6. **Compare across substrates the effects of prolonged exposure to mitochondrial inhibitors/sugar starvation.** The effects of longer treatment (6 hours) on gross mitochondrial morphology were compared across substrates. In addition, cell viability was assessed after 24 hour incubation of Gluc/Gal-HeLa cells with each of the mitochondrial inhibitors.

4.3. Methods

4.3.1. Cell Culture

HeLa cells previously grown in high glucose DMEM were retrieved from liquid nitrogen stocks and cultured for two days in high glucose medium to allow for equilibration following freezing. The medium was then replaced with glucose-free DMEM containing 10mM galactose, 10% FBS, 2mM L-glutamine and penicillin-streptomycin solution (100 units/ml penicillin G, 0.1 mg/ml streptomycin sulphate). Cells showed a marked increase in doubling time as previously reported (Rossignol *et al.*, 2004) from 24h to approximately three days. Cells were grown in galactose DMEM for at least two weeks before use in experiments.

4.3.2. Transfection

Cells were transfected using Gene Juice, as described in Chapter 3. Transfection efficiency was not adversely affected by growth of the cells in galactose medium, nor was cell toxicity increased post-transfection.

4.3.3. Preparation of Whole Cell lysates

Whole cell lysates were prepared from cells grown to 90% confluence in T175 culture flasks. Culture medium was aspirated and cells were rinsed with ice-cold PBS. Cells were then scraped in the presence of 1.2ml Triton-X 100 buffer (150mM NaCl, 1% Triton-X 100, 50mM Tris, pH 8.0) containing 0.1% protease inhibitor cocktail. The cell lysate was transferred into a 1.5ml microfuge tube, which was maintained at 4°C with agitation for 30 minutes. The lysate was cleared by centrifugation at 12,000 x g for 20 minutes at 4°C. The supernatant was removed and placed in a fresh minifuge tube and stored at -80°C until required.

4.3.4. Isolation of Mitochondria from Cells

Mitochondria were isolated from cells using the Pierce Mitochondrial Isolation Kit for Cultured Cells as per manufacturer's instructions. Briefly, ~2.0 x 10^7 cells cultured in either high glucose medium or galactose medium were incubated with or without

inhibitors for 30 minutes and were rinsed with PBS. Cells were trypsinised and centrifuged at 1000 x g for five minutes. The cell pellet was washed once with PBS to remove any traces of culture medium then resuspended in 800µl Reagent A containing 0.1% protease inhibitor cocktail. The suspension was vortexed at medium speed for five seconds then incubated on ice for exactly two minutes. To this, 10µl of reagent B were added and the suspension was vortexed at maximum speed 5 seconds at 1 minute intervals for five minutes. The suspension was combined with 800µl reagent B and centrifuged at 700 x g for 10 minutes at 4°C remove nuclei and unlysed cells. The supernatant was transferred to a new tube and centrifuged at 12,000 x g for 15 minutes at 4°C. The supernatant was discarded and the mitochondria-rich pellet was resuspended in 500µl reagent C and centrifuged again at 12,000 x g for five minutes. The pellet was resuspended in 50µl STE buffer (350mM Sucrose, 10mM Tris, 1mM EDTA, pH 7.4) and stored at -80°C until required.

4.3.5. Assessment of Mitochondrial Morphology after Six-Hour Inhibitor Exposure

Cells stably expressing DsRed-mito were grown to 70% confluence on 13mm borosilicate glass coverslips in 24-well plates. The culture medium was replaced with medium containing the appropriate inhibitor and cells were incubated at 37°C for 20 minutes. The medium was aspirated and cells were briefly rinsed with PBS before fixation with 4% paraformaldehyde. Coverslips were prepared for confocal microscopy by mounting on glass slides using Vectashield mounting medium, containing DAPI counterstain. Coverslips were sealed with clear nail varnish, stored in darkness at 4°C until required and viewed within two days. Confocal settings were as described in general methods (Chapter 2).

4.3.6. Assessment of Cell Viability

Cell proliferation and viability were measured using Invitrogen's AlamarBlue redox indicator. The assay allows for quantification of cell viability by virtue of the ability of healthy, metabolically active cells to convert the dye to a colorimetric indicator. Cells were cultured in 96-well plates until confluent and following experimental treatment, were incubated in the presence of AlamarBlue for six hours (10µl reagent into 100µl medium per well). The absorbance of the wells at was measured using a SpectraMAX

PLUS Microplate Spectrophotometer. Absorbance was measured at 570nm and 600nm the readings obtained at the former wavelength were normalised to those obtained at the latter. All readings were corrected for blank and cell viability was expressed as percent control.

4.4 Results

4.4.1 Effects of Substrate Change on Mitochondrial Fusion Rates

Gluc-HeLa cells were capable of growth and proliferation in galactose DMEM, in agreement with the literature (Rossignol *et al.*, 2004). Cells also displayed the ultrastructural changes previously described (Rossignol *et al.*, 2004), such as organelle thinning and expansion to distal cytoplasmic regions (fig. 4.2). It was then investigated whether these ultrastructural changes were accompanied by changes in mitochondrial fusion rates, using the photo-activation protocol previously described. Gal-HeLa cells were found to exhibit mitochondrial fusion rates comparable to those Gluc-HeLa cells (fig. 4.3A), with PIs of 39.43 $\pm$ 2.45% at 15 minutes and 27.74 $\pm$ 1.97% at 30 minutes post-activation (fig. 4.3B). These data show that HeLa cells can adapt over time and re-establish normal fusion rates in the absence of glucose, despite their previous dependence on its metabolism for mitochondrial fusion.

This adaptation does not involve changes in expression of the mitodynamins (fig 4.4). Western blotting and densitometry analysis of whole cell lysates from Gluc- and Gal-HeLa cells show that there is no difference in expression of fission mediator DRP1, nor of OM fusion mediators Mfn1/2, nor of IM fusion mediator OPA1. An increase in VDAC1 expression in Gal-HeLas has been reported elsewhere (Rossignol *et al.*, 2004) but this was not observed in this study. Thus, the adaptation of mitochondria to a lack of glucose in the maintenance of fusion rates appears not to involve changes in expression of mitodynamins.

4.4.2 Effects of Mitochondrial Inhibition on Fusion Rates in Gal-Hela Cells

Given that Gal-HeLa cells generate energy predominantly through glutaminolysis (and thus OXPHOS), rather than glycolysis, it was hypothesised that the mitochondria of these cells may develop increased vulnerability to selective inhibition. To investigate this, mitochondrial fusion was assessed in Gal-HeLa cells following 20 minute incubations with each of the mitochondrial inhibitors used in Gluc-HeLa experiments.

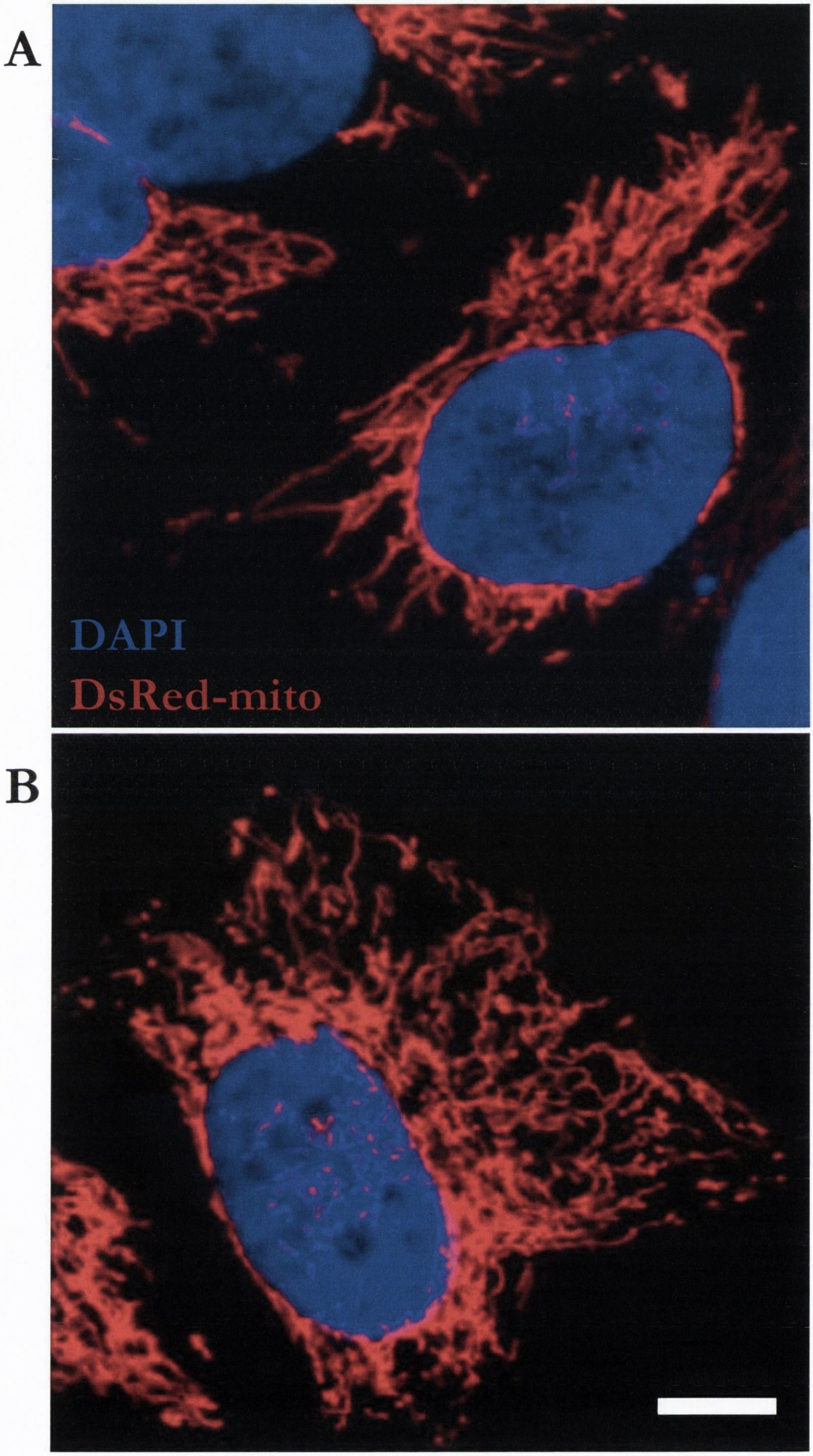

Figure 4.2: Ultrastructural changes in the mitochondrial network of HeLa cells cultured in galactose DMEM. Cells cultured in high-glucose medium (A) exhibit thick and tubular mitochondria with perinuclear clustering. Cells cultured in galactose medium (B) develop a thinner and more highly ramified reticulum which spreads to the outer reaches of the cell in addition to some perinuclear clustering. DAPI, 4,6-diamidino-2-phenylindole, nuclear counterstain. Scale = 10μm.

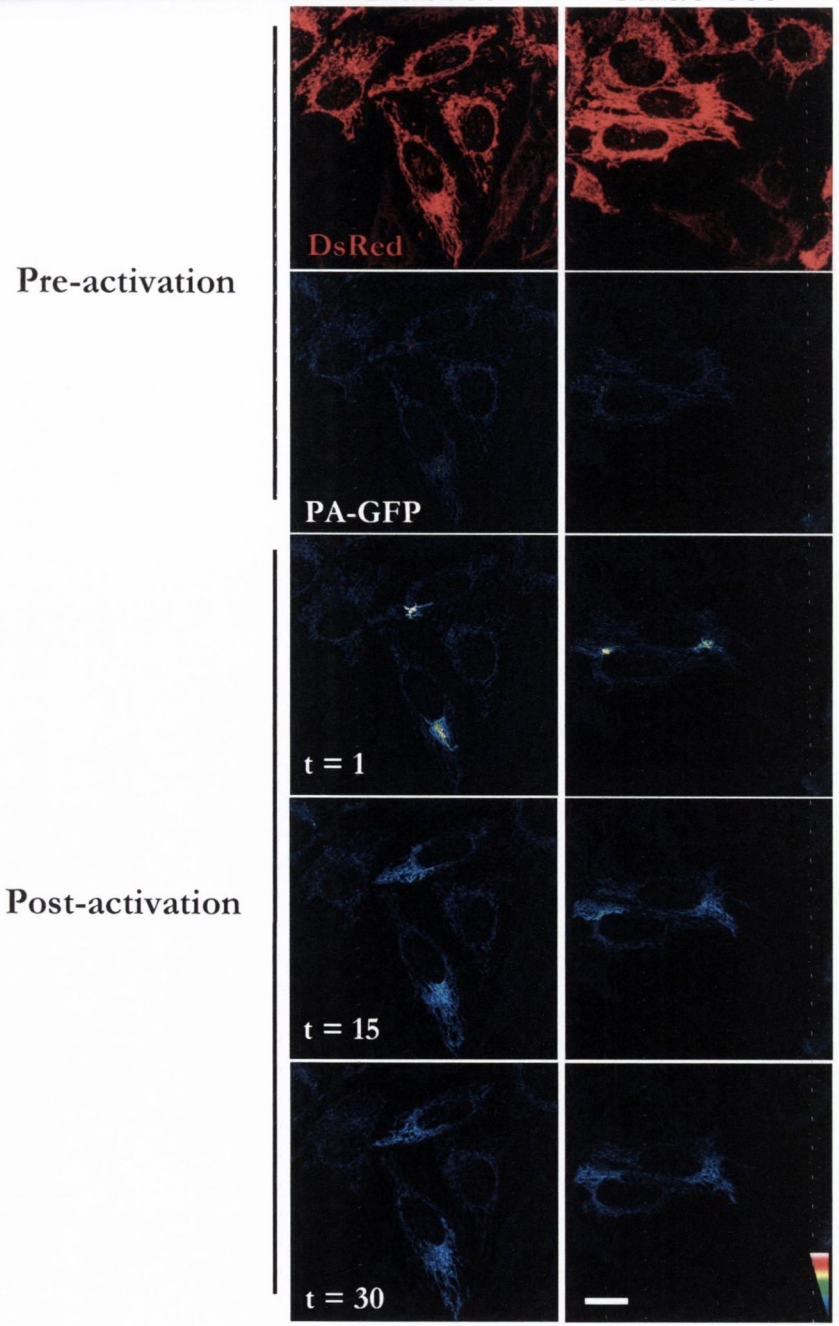

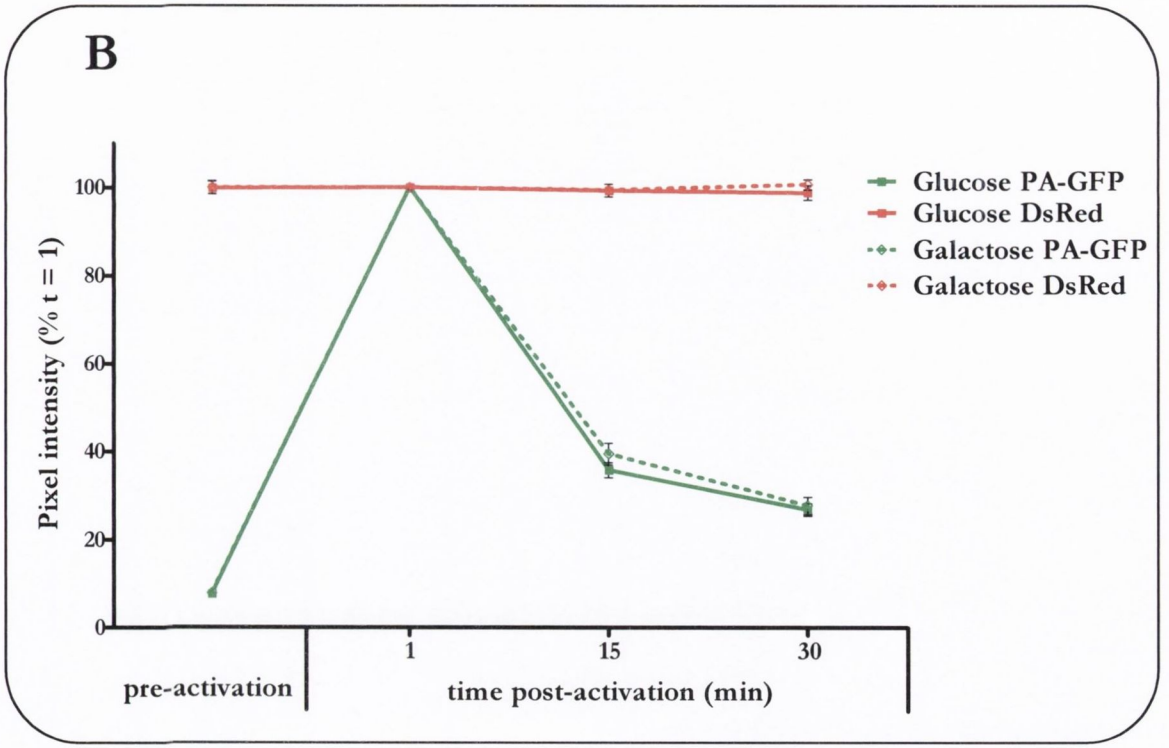

Figure 4.3: HeLa cells can adapt to absence of glucose to establish normal mitochondrial fusion rates. (A) Image showing mitochondrial fusion in Gluc-HeLa cells (left) and Gal-HeLa cells (right), which occur at comparable rates. Scale = 20μm. (B) Graphical representation of fusion data illustrating no statistically significant difference in mitochondrial fusion rates between cell types. Data presented as mean ± SEM, n = 3. Unpaired t-test at each time point.

Figure 4.4: Gal-HeLa cells do not show changes in mitodynamin expression. (A) Western blot analysis of fission mediator DRP1 and fusion mediators OPA1, mitofusins (Mfn) 1 and 2 and also mitochondrial outer membrane protein VDAC1 in cells cultured in glucose (left) or galactose (right) medium. Tubulin (tub) served as a loading control. (B) Densitometry values normalised to tubulin values reveal no statistically significant difference in expression between cell groups. Data presented as mean ± SD, n = 2.

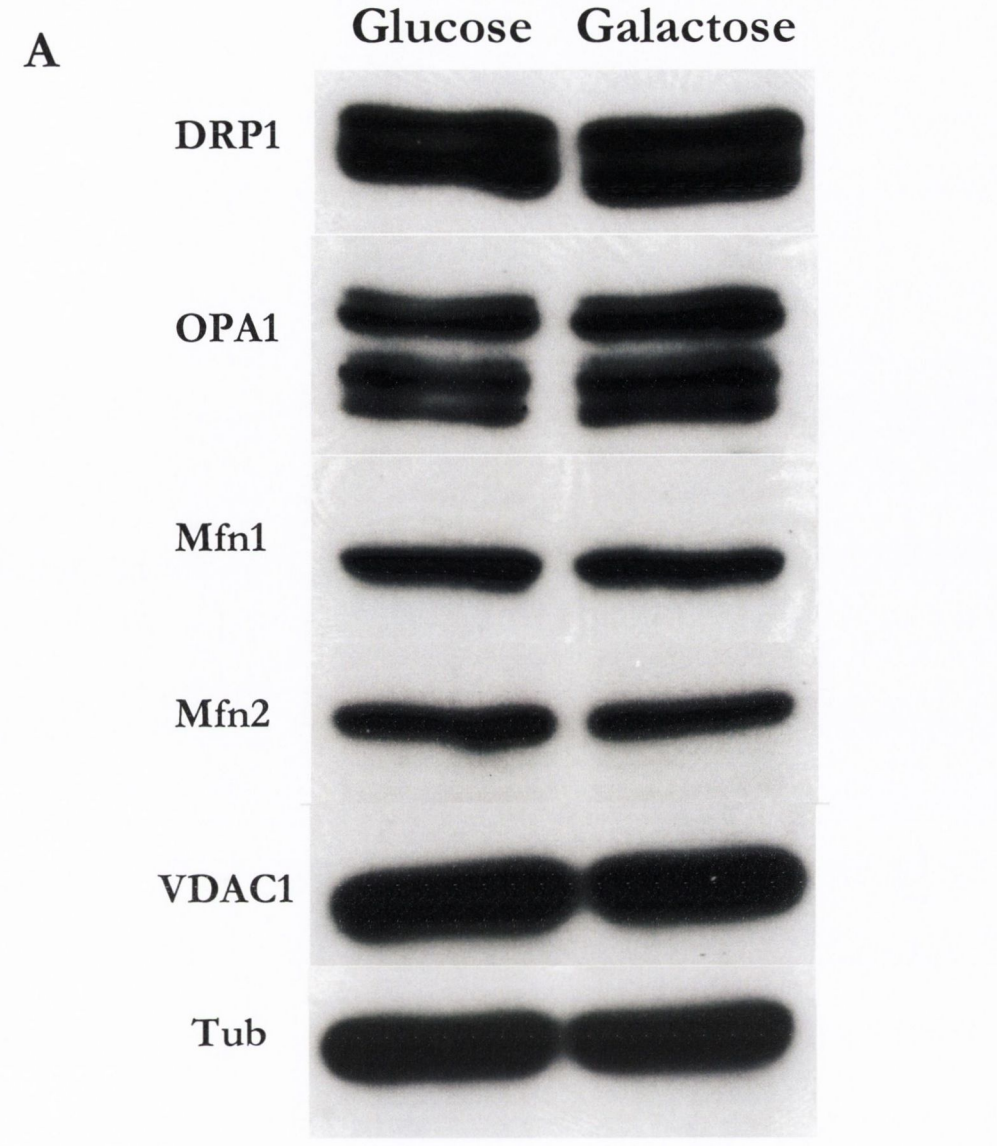
A
Glucose
Galactose
DRP1
OPA1
Mfn1
Mfn2
VDAC1
Tub
B
Glucose
Galactose
Protein quantity (AU)
2.0
1.5
1.0
0.5
0.0
DRP1
OPA1
Mfn1
Mfn2
VDAC1

Gal-HeLa cells responded in a similar way to Gluc-HeLa cells following $\Delta\Psi_m$ dissipation using 5μM FCCP. Cells exhibited a highly fragmented reticulum (not shown) and little PI decrease in photo-activated areas after 30 minutes (PI of 89.8 ± 2.55%, fig 4.5). In stark contrast to Gluc-HeLa cells, however, Gal-HeLa cells exhibited severe mitochondrial fusion deficit following incubation with almost all OXPHOS inhibitors (fig 4.6). Complex I inhibition with 10μM rotenone (fig 4.7A) or 4μM piericidin A (fig 4.7B) resulted in complete inhibition of mitochondrial fusion, with PIs remaining at 97.56 ± 2.46% and 98.75 ± 1.70%, respectively, at 30 minutes post-activation. As in Gluc-HeLa cells, complex II inhibition with 1mM malonate had no effect on fusion rates (fig 4.8) but complex III inhibition with 2.4μM antimycin A (4.9A) or 2μM myxothiazol (fig 4.9B) resulted in very significant decreases in fusion. Fusion was also inhibited with complex IV inhibition, using 5mM azide (fig 4.10). Finally, fusion was inhibited with ATP synthase inhibition using 2μg/ml oligomycin (fig 4.11) and to a much greater extent than in Gluc-HeLa cells (refer to section 3.3).

Interestingly OXPHOS inhibition is capable of halting fusion in Gal-HeLa cells after just five minutes (fig 4.12). When cells were incubated for five minutes with 4μM piericidin A (fig 4.12A) or 2μg/ml oligomycin (fig 4.12B), fusion was fully inhibited to the same degree as for the 20 minute incubation, with PI values of 92.78 ± 2.79% and 88.91 ± 2.54% at 30 minutes post-activation, respectively. Thus, fusion inhibition following OXPHOS inhibition occurs rapidly. Taken together, these results show that although HeLa cells can adapt to changing energy substrates by altering OXPHOS-dependence, they also acquire new vulnerabilities to mitochondrial inhibition. These cells show high sensitivity to inhibition of all ETC enzymes, with the exception of complex II, and appear to be particularly sensitive to complex I inhibition.

4.4.3 HeLa Cell Adaptation to Glucose-Free Environment and Independence from Sugars for Mitochondrial Fusion.

As there are no commercially available inhibitors of the Leloir pathway enzymes, it was not possible to perform studies equivalent to glycolysis inhibition in Gluc-HeLas. However, simple incubation of Gal-HeLa cells in galactose-free DMEM for 20 minutes

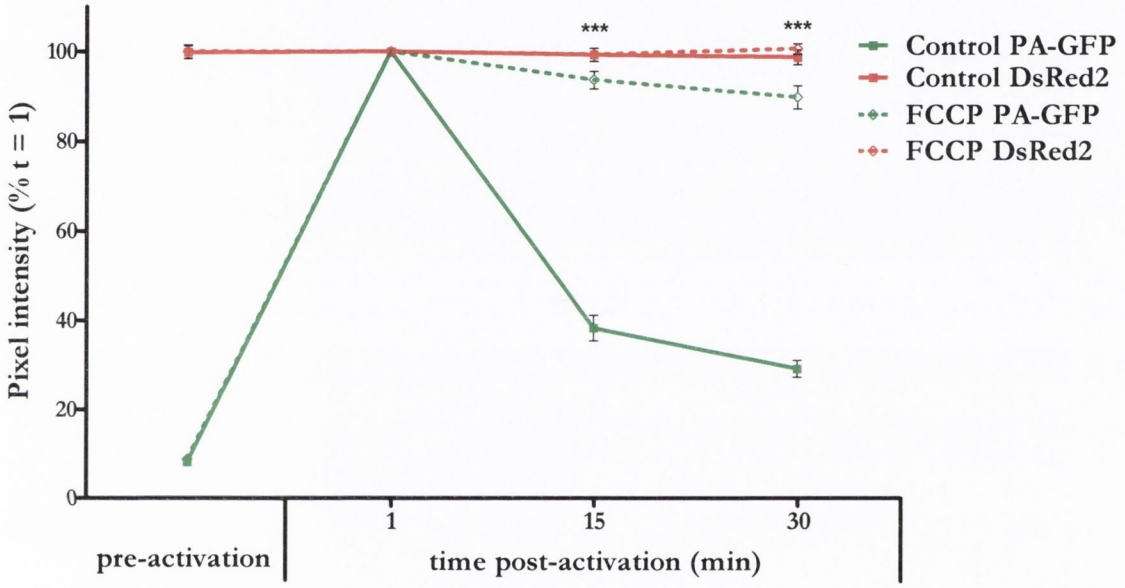

Figure 4.5: Dissipation of $\Delta\Psi_m$ compromises mitochondrial fusion in Gal-HeLa cells. Cells pre-incubated for 20 minutes with 5μM FCCP exhibited extensive inhibition of fusion, as expected (dashed green line). There was negligible change in PIs following photo-activation, indicating no exchange of photo-activated mitochondrial content through active fusion. Control cells fused normally, as evidenced by the gradual decrease in PIs following photo-activation (bold green line). The DsRed channels (solid red line, control, dashed red line, FCCP-treated) showed statistically insignificant fluctuations between images and indicated that the PA-GFP PI decreases observed were not due to movement of mitochondria out of the ROI or photobleaching. Data presented as mean ± SEM, n = 3. Unpaired t-test at each time point. ***P<0.001.

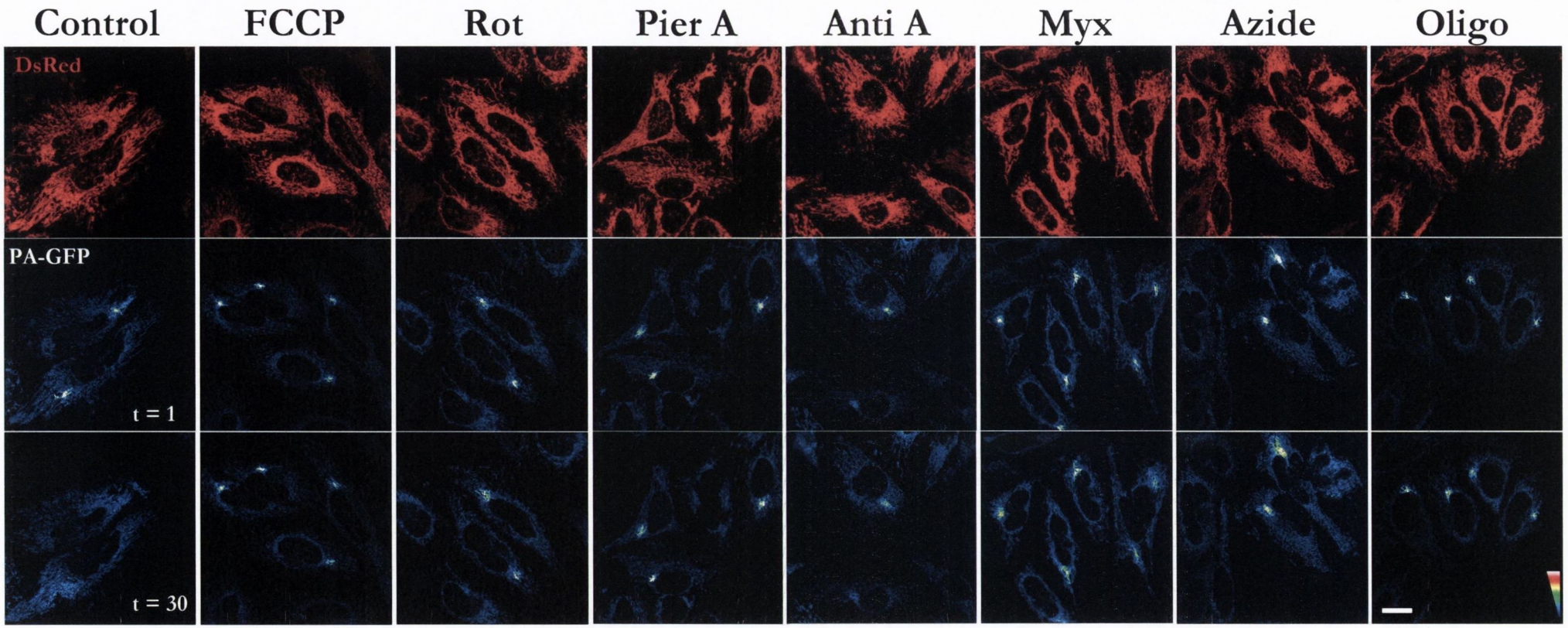

Figure 4.6: Representative images showing mitochondrial fusion inhibition in Gal-HeLa cells incubated with OXPHOS inhibitors. Decreased fusion is evident in cells exposed to complex I inhibitors rotenone (rot, 10μM) and piericidin A (pier A, 4μM), complex III inhibitors antimycin A (anti A, 2.4μM) and myxothiazol (myx, 2μM), complex IV inhibitor azide (5mM) and ATP synthase inhibitor oligomycin (oligo, 2μg/ml). Scale = 20μm.

A

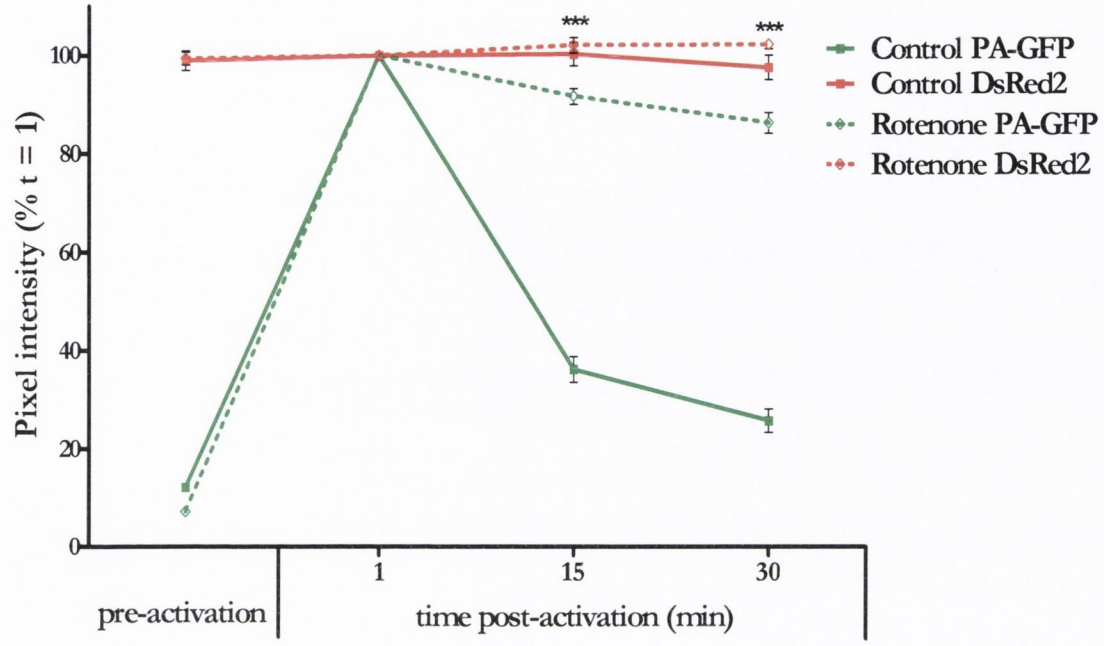

B

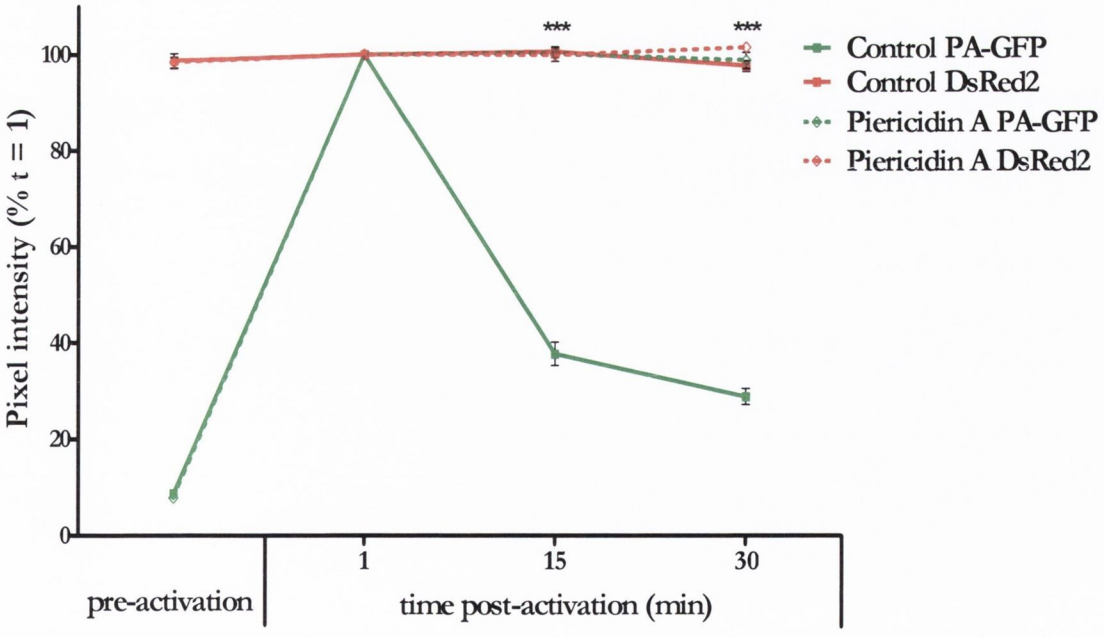

Figure 4.7: Complex I inhibition leads to perturbation of mitochondrial fusion in Gal-HeLa cells. Inhibition of complex I with 10μM rotenone (A) or 4μM piericidin A (B) for 20 minutes leads to a serious decrease in mitochondrial fusion, with negligible PI decreases in photo-activated regions after 30 minutes (dashed green lines). Data presented as mean ± SEM, n = 3. Unpaired t-test at each time point. ***P<0.001.

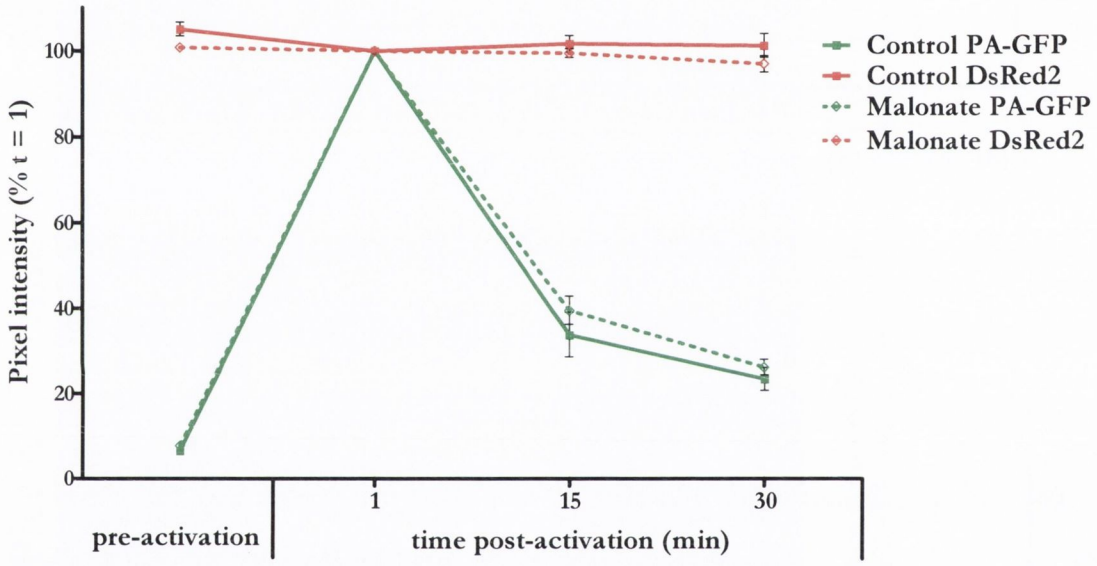

Figure 4.8: Complex II inhibition does not affect mitochondrial fusion rates in Gal-HeLa cells. Cells pre-incubated with 1mM malonate for 20 minutes (dashed green line) did not show a statistically significant change in mitochondrial fusion rates compared to controls (bold green line). Data presented as mean ± SEM, n = 3. Unpaired t-test at each time point.

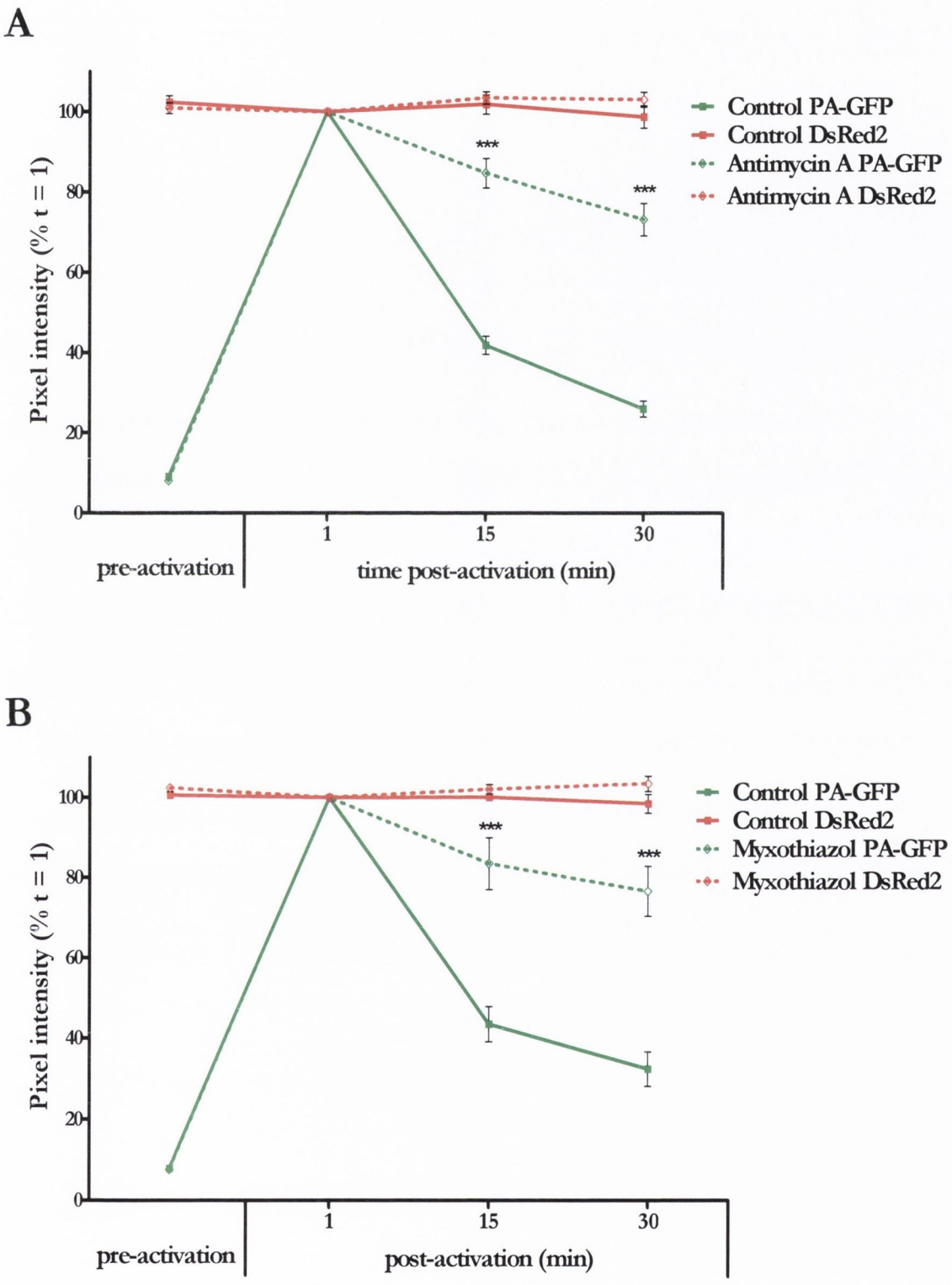

Figure 4.9: Complex III inhibition leads to perturbation of mitochondrial fusion in Gal-HeLa cells. Inhibition of complex III with 2.4μM antimycin A (A) or 2μM myxothiazol (B) for 20 minutes leads to a serious decrease in mitochondrial fusion. Pixel intensities remained at 73.15 ± 4.0% 30 minutes after photo-activation in cells treated with antimycin A, while remaining at 76.52 ± 6.24% after myxothiazol treatment (dashed green lines). Data presented as mean ± SEM, n = 3. Unpaired t-test at each time point. ***P<0.001.

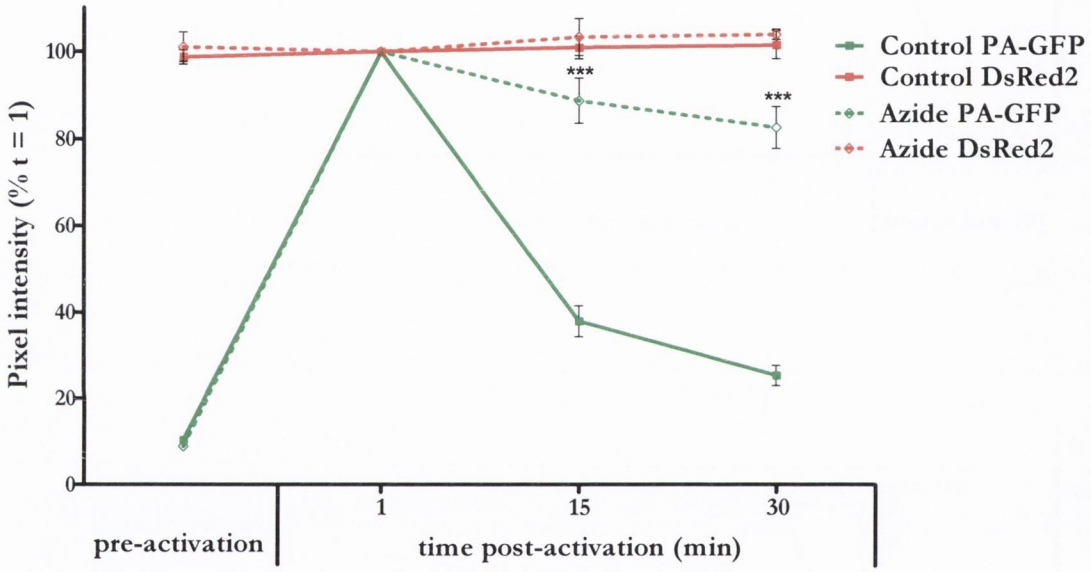

Figure 4.10: Complex IV inhibition leads to perturbation of mitochondrial fusion in Gal-HeLa cells. Inhibition of complex IV with 5mM azide for 20 minutes leads to a serious decrease in mitochondrial fusion. Pixel intensities remained at 82.59 ± 4.83% 30 minutes after photo-activation in cells treated with azide (dashed green line), while control cells exhibited the PIs in the normal range, at 25.29 ± 2.34% (bold green line). Data presented as mean ± SEM, n = 3. Unpaired t-test at each time point. ***P<0.001.

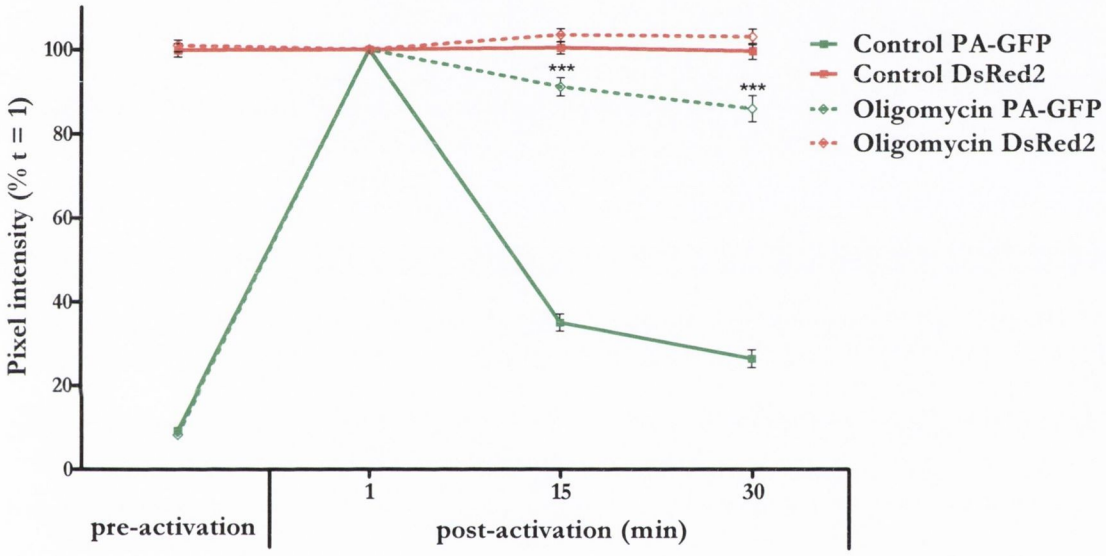

Figure 4.11: ATP synthase inhibition leads to perturbation of mitochondrial fusion in Gal-HeLa cells. Inhibition of ATP synthase with 2μg/ml oligomycin for 20 minutes leads to a significant decrease in mitochondrial fusion. Pixel intensities remained at 86.0 ± 3.09% 30 minutes after photo-activation in cells treated with azide (dashed green line). Data presented as mean ± SEM, n = 3. Unpaired t-test at each time point. ***P<0.001.

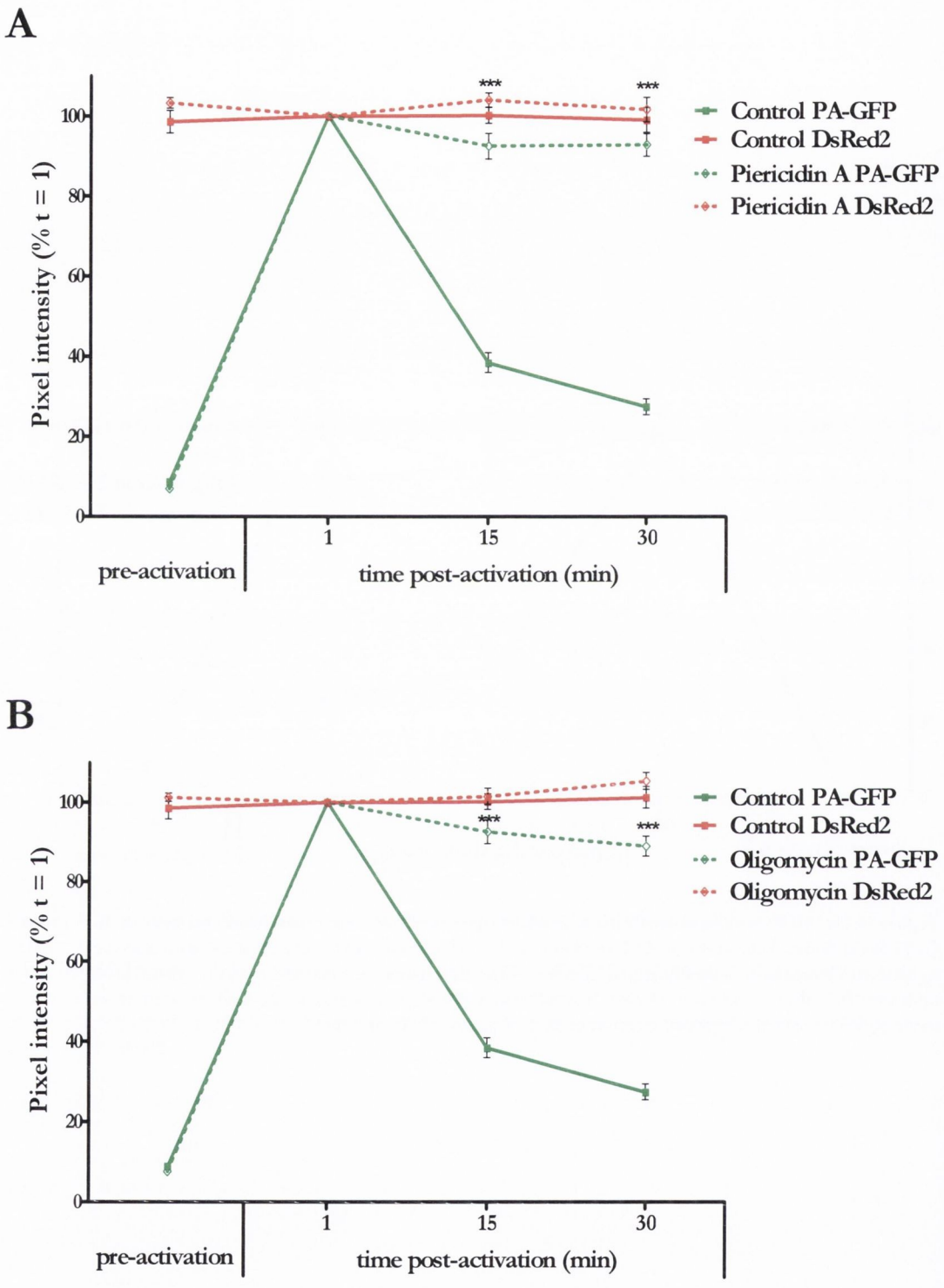

Figure 4.12: Mitochondrial fusion is inhibited in Gal-HeLa cells within five minutes OXPHOS inhibition. The effects of OXPHOS inhibition on mitochondrial fusion observed after 20 minutes pre-incubation are replicated after just five minutes pre-incubation. Inhibition of complex I with 4μM piericidin A (A), or ATP synthase with 2μg/ml oligomycin (B) leads to serious fusion deficit after just five minutes. Data presented as mean ± SEM, n = 3. Unpaired t-test at each time point. ***P<0.001.

had no effect on mitochondrial fusion rates (fig 4.13). Although it is possible that the cells retained sufficient cytosolic galactose to sustain them throughout the experiment, it was considered that perhaps they had developed reduced dependence on galactose (and, possibly sugar catabolism in general) for the maintenance of mitochondrial fusion and cell viability. To assess the dependence of Gal-HeLas on sugars for survival, both Gal- and Gluc-HeLa cells were cultured for three days in sugar-free medium, or medium containing either 10mM or 25mM of galactose, glucose, fructose, sucrose or maltose in place of their original substrate.

Using Invitrogen's AlamarBlue redox indicator, cell viability was shown to be severely compromised in Gluc-HeLa cells cultured in sugar-free medium, with viability at just 26 $\pm$ 3.09% of controls (fig 4.14). Furthermore, viability of these cells was significantly reduced in galactose, fructose, and especially in sucrose medium, at both concentrations. Gluc-HeLa cells did not appear to be capable of growth to the level seen in glucose in any other medium apart from maltose, in which cell viability remained unchanged (viability at 102.79 $\pm$ 1.87% and 104.33 $\pm$ 1.32% of controls in 10mM and 25mM maltose, respectively). Gal-HeLa cells also showed reduced viability in sugar-free and sucrose media but, significantly, this viabiltiy was more than double that of Gluc-HeLa cells in both cases. Surprisingly, Gal-HeLa cell viability actually exceeded controls in glucose and maltose media, at 10 and 25mM, by 22 – 30%.

This detection of increased reduction of the AlamarBlue indicator in Gal-HeLa cells in glucose/maltose medium indicates that either the cells' metabolic rates increased, or that their proliferation rate increased, or both, under these conditions. However, it is not possible to make this distinction using this assay. Fructose was the only sugar which affected viaiblity in both cell types in a dose-dependent manner (fig 4.14C), with viability higher at 25mM; a 10.94 $\pm$ 4.13% increase in Gluc-HeLa cells and an 18.83 $\pm$ 4.39% increase in Gal-HeLa cells. Taken together, these data suggest that, whilst Gal-HeLa cells can utilise sugars for growth, they are better adapted to survival without them and, in fact, are primed to take advantage of sudden sugar availability. It is possible that they benefit from a synergy between their increased OXPHOS capability and a latent ability to quickly utilise sugars;

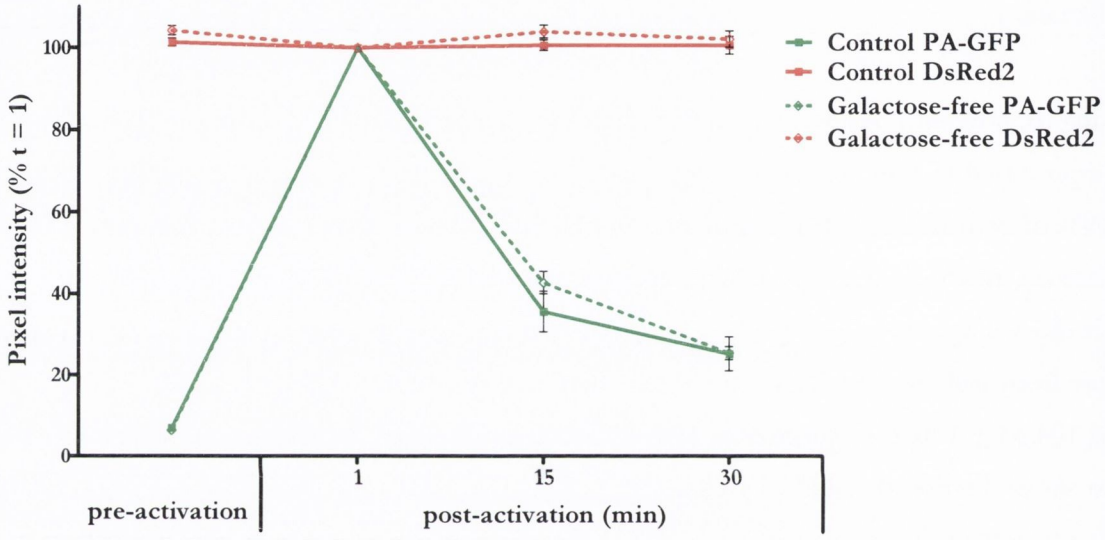

Figure 4.13: Acute galactose starvation does not affect mitochondrial fusion in Gal-HeLa cells. Cells incubated in galactose-free medium for 20 minutes did not show any differences in mitochondrial fusion rates, suggesting independence from sugar catabolism for this function. Data presented as mean ± SEM, n = 3. Unpaired t-test at each time point. ***P<0.001.

Figure 4.14: Effects of different sugars at different concentrations on cell viability in Gluc- and Gal-HeLa cells. Cells *originally* cultured in either 25mM glucose medium (blue bars) or in 10mM galactose medium (green bars) were transferred to medium containing no sugar, glucose, galactose, fructose, sucrose, or maltose at a concentration of either 10mM (A) or 25mM (B) and cell viability was measured after three days. Data was expressed as percent growth of cells in their original sugar substrate (i.e. 25mM glucose DMEM or 10mM galactose DMEM for Gluc- and Gal-HeLa cells, respectively). Glutamine was present in all media. Cell viability in Gal-HeLa cells cultured in sugar-free or sucrose-containing medium, although reduced compared to controls, was more than double that of Gluc-HeLa cells. Furthermore, Gal-HeLa cell viability was at the same level, or better than in galactose, in medium containing glucose, fructose or maltose at both concentrations, while Gluc-HeLa cell viability suffered in all but glucose or maltose media. Finally, fructose was the only sugar that exerted concentration-dependent effects on viabiltiy, with 25mM producing a statistically significantly higher level in both cell types (C). Data presented as mean $\pm$ SEM, n = 3. Two-way ANOVA with Bonferroni post-test. ***$P<0.001$.

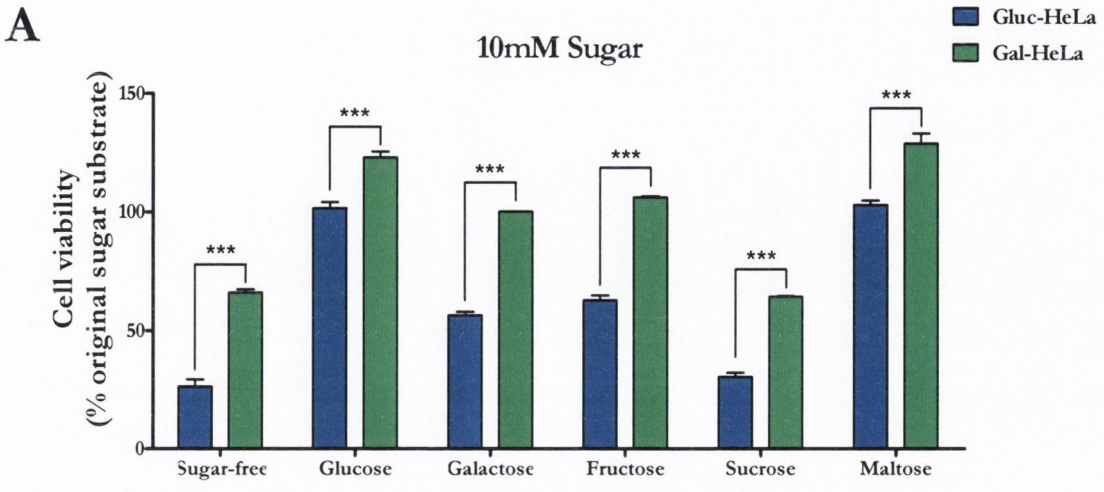
A
10mM Sugar
Gluc-HeLa
Gal-HeLa
Cell viability
(% original sugar substrate)
150
100
50
0
***
Sugar-free
Glucose
Galactose
Fructose
Sucrose
Maltose

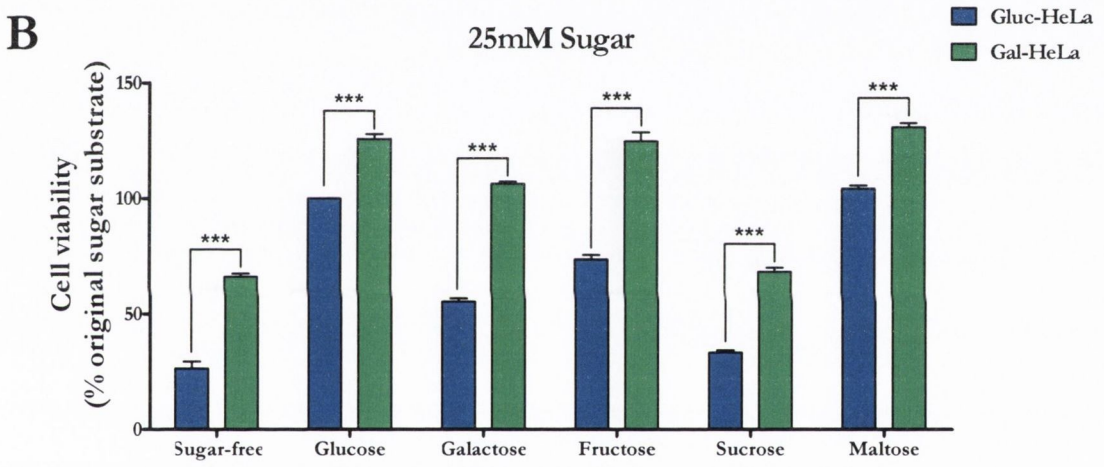
B
25mM Sugar
Gluc-HeLa
Gal-HeLa
Cell viability
(% original sugar substrate)
150
100
50
0
***
Sugar-free
Glucose
Galactose
Fructose
Sucrose
Maltose

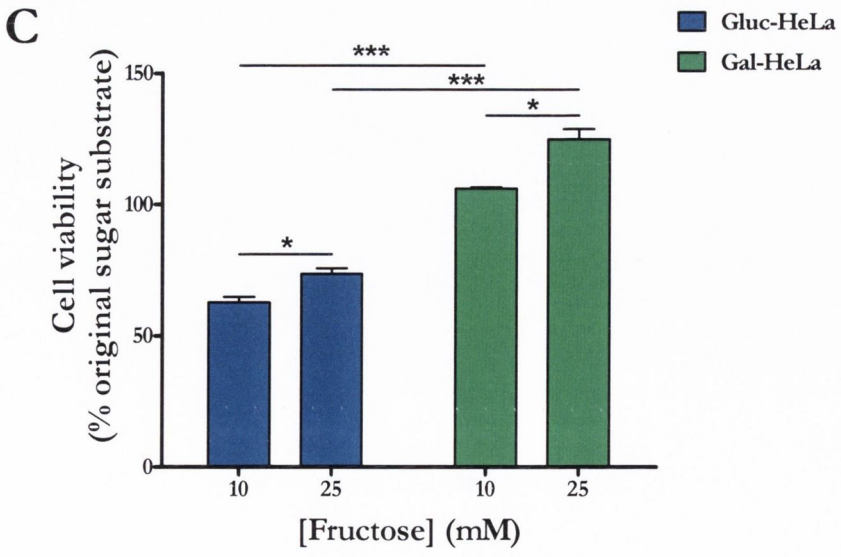
C
Gluc-HeLa
Gal-HeLa
Cell viability
(% original sugar substrate)
150
100
50
0
***
***
*
*
10
25
10
25
[Fructose] (mM)

when both energy pathways are in place, either metabolic rate, growth rate, or both exceed that which is achievable from use of either substrate alone.

In light of these results, it was hypothesised that perhaps the presence of glucose could rescue mitochondria from fusion inhibition in Gal-HeLa cells exposed to mitochondrial toxins. To investigate this, Gal-HeLa cells were incubated with 4μM piericidin A in the presence of 5mM glucose for 20 minutes and fusion rates were assessed. As expected, the presence of glucose dramatically improved fusion rates during piericidin A exposure; indeed, they returned to control levels (fig 4.15A). In an effort to elucidate how these cells were able to quickly utilise glucose so effectively, the expression levels of HK I and II were compared in whole cell lysates from Gluc and Gal-HeLa cells (fig. 4.15B(i)). Both HK isoforms were downregulated in Gal-HeLa cells when compared to Gluc-HeLa cells, with HK II showing the most pronounced decrease in expression (3.4-fold less, fig. 4.15C(i)). However, when HK levels were examined in enriched mitochondrial fractions from cell lysates (fig. 4.15B(ii)), it appeared there was more HKII localised to the mitochondria of Gal-HeLa cells (1.3-fold more, fig 4.15C(ii)). These results go some way towards explaining how Gal-HeLa cells are capable of fast adaptation to environmental changes in energy substrate; although there may be a decrease in cytosolic HKs, mitochondria-bound forms are retained, and even enriched, possibly to 'prime' cells for opportunistic glucose utilisation.

4.4.4 Effects of Galactose Starvation and Inhibition of Oxidative Phosphorylation on Mitodynamins in Gal-HeLa Cells

Despite this highly dynamic metabolic phenotype, in the absence of glucose, Gal-HeLa cell mitochondria remain extremely vulnerable to inhibition. As previously discussed, mitochondrial dynamics can be regulated through post-translational modification of mitodynamins, including phosphorylation, ubiquitination and proteolytic cleavage. To assess whether the observed decrease in fusion upon mitochondrial inhibition is due to PTM/cleavage of mitodynamins, Western blots for fusion mediators OPA1, Mfn1 and 2 and fission mediator DRP1 were performed on mitochondria isolated from Gluc- and Gal-HeLa cells following treated for 20 minutes with either 5μM FCCP, 10μM rotenone, 2.4μM

Figure 4.15: Glucose metabolism restores mitochondrial fusion in Gal-HeLa cells exposed to piericidin A. (A) Gal-HeLa cells exposed to 4μM piericidin A (pier A) in the presence of 5mM glucose can utilise this substrate to restore mitochondrial fusion rates despite their previous vulnerability to this inhibitor. (B) Western blot analysis reveals a decrease in expression of hexokinases (HK) I and II in Gal-HeLa cells compared to Gluc-HeLa cells (i) but enrichment of HK II in the mitochondria of Gal-HeLa cells (ii). (C) Densitometric analysis of Western blots shows the decreased expression of HK I and II in Gal-HeLa cells is statistically significant (normalised to tubulin (tub) levels) (i), as is the enrichment of HKII on their mitochondria (normalised to VDAC1 levels)(ii). Data presented as mean ± SEM, n = 3 (A) or ± SD, n = 2 (C). Unpaired t-test at each time point (A) or for each HK isoform (C).

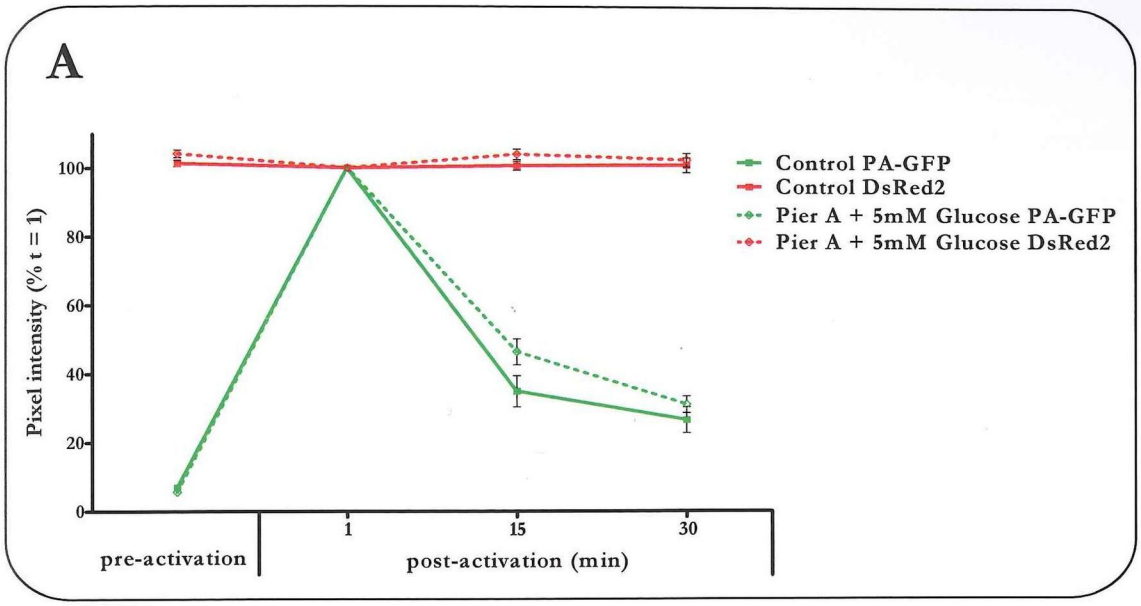
A
Pixel intensity (% t = 1)
100
80
60
40
20
0
1
15
30
pre-activation
post-activation (min)
Control PA-GFP
Control DsRed2
Pier A + 5mM Glucose PA-GFP
Pier A + 5mM Glucose DsRed2

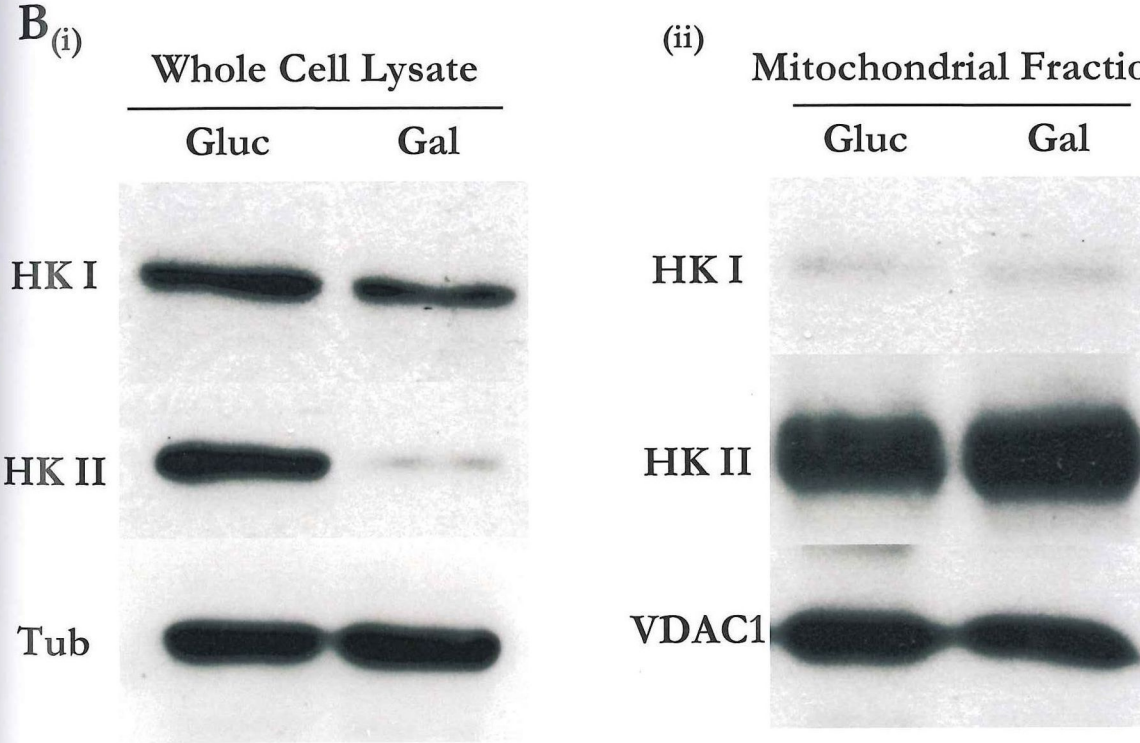
B (i)
Whole Cell Lysate
Gluc
Gal
HK I
HK II
Tub
(ii)
Mitochondrial Fraction
Gluc
Gal
HK I
HK II
VDAC1

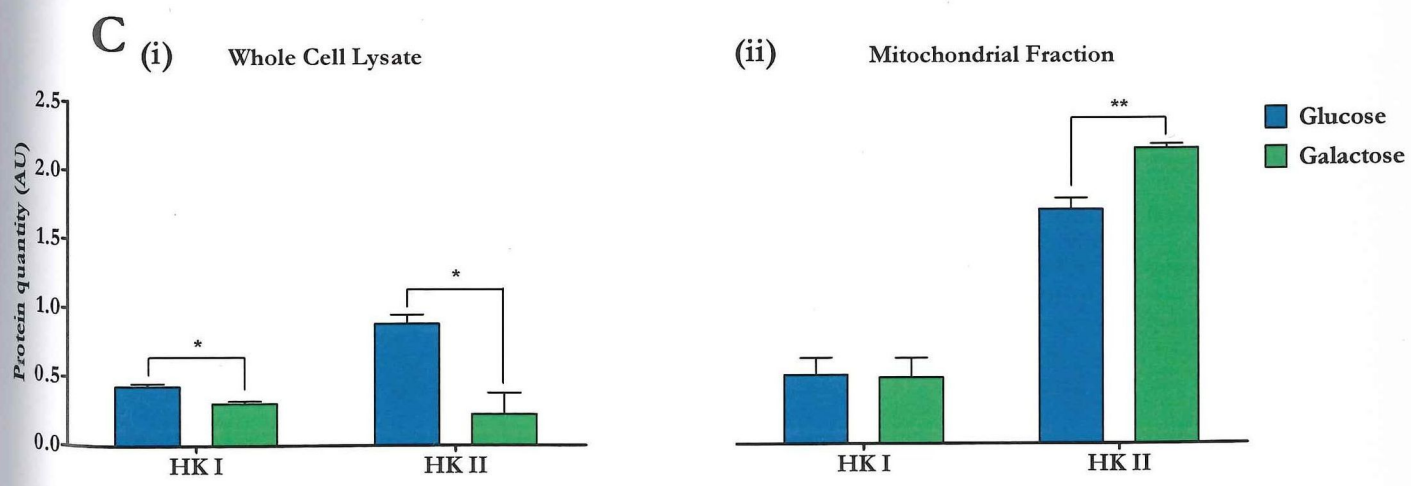
C (i)
Whole Cell Lysate
Protein quantity (AU)
2.5
2.0
1.5
1.0
0.5
0.0
*
*
HK I
HK II
(ii)
Mitochondrial Fraction
**
Glucose
Galactose
HK I
HK II

antimycin A, 5mM azide, 2μg/ml oligomycin, 10mM DOG (for Gluc-HeLa cells) or galactose-free medium (for Gal-HeLa cells) (fig.4.16). Dissipation of $\Delta\Psi_m$, as well as apoptotic stimuli, have been shown to promote the cleavage of L-OPA1 into S-OPA1 isoforms (Ishihara *et al.*, 2006, Guillery *et al.*, 2008). This study confirms that this is the case in both Gluc- and Gal-HeLa cells when treated with FCCP; both cells exhibited the disappearance of the L-OPA1 isoforms in with increased levels of S-OPA1 isoforms. OPA1 cleavage, however, does not appear to be responsible for fusion inhibition during OXPHOS inhibition, as neither cell type showed increased S-OPA1 isoforms following treatment with antimycin A, azide, or oligomycin. One possible exception is rotenone treatment, which led to slight decrease in L-OPA1 isoforms in Gal-HeLa cells, but not in Gluc-HeLa cells. The other fusion-mediating mitodynamins, Mfn1/2 did not exhibit any obvious post-translational modifications, as no extra bands arose after treatment in either cell group but this cannot be stated categorically without use of antibodies specifically targeted to post-translationally modified forms of the proteins.

Importantly, there were significant differences between cell groups in relation to DRP1 levels in mitochondrial fractions (fig. 4.17A). Densitometry analysis of Western blots revealed that Gluc-HeLa cells showed no significant changes in DRP1 levels across treatments when compared to controls but Gal-HeLa cells showed significantly increased DRP1 levels following all treatments, except galactose starvation (fig. 4.17B). These results suggest a substrate-dependent change in mitochondrial dynamics signalling pathways, which leads to recruitment of DRP1 to mitochondria following OXPHOS inhibition in Gal-HeLa cells.

4.4.5 Effects of Galactose Starvation and Inhibition of Oxidative Phosphorylation on Mitochondrial Membrane Potential in Gal-HeLa Cells.

As Gluc-HeLa cells were shown to maintain mitochondrial fusion rates following partial dissipation of $\Delta\Psi_m$ (Chapter 3), it was considered that Gal-HeLa cells mitochondria may experience more extensive depolarisation following OXPHOS treatment, leading to decreased fusion. Changes in $\Delta\Psi_m$ were measured using microscopic analysis of TMRM fluorescence, as described previously. Surprisingly, Gal-HeLa cells showed mitochondrial

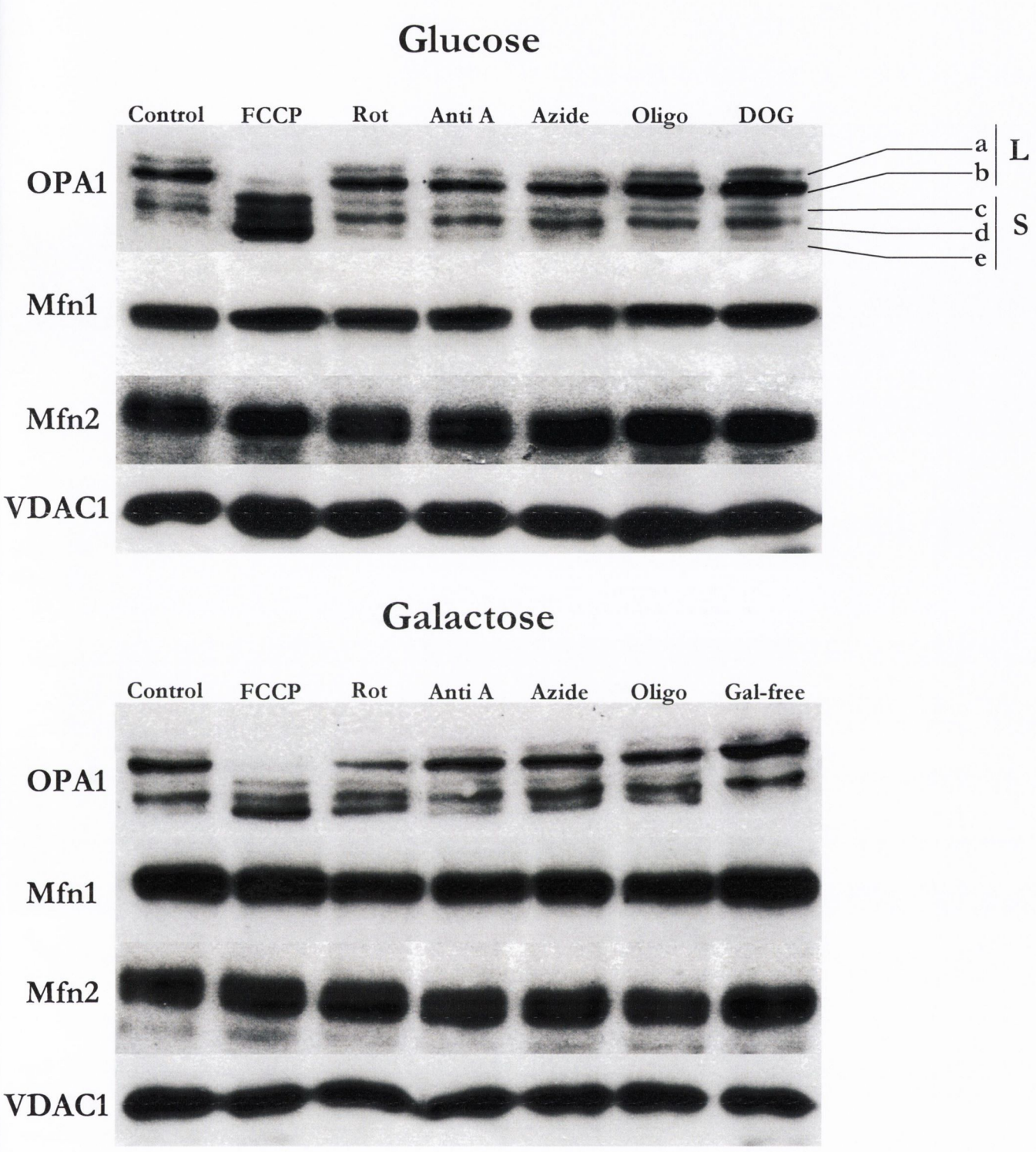

Figure 4.16: OXPHOS inhibition does not lead to alterations in the mitochondrial fusion machinery. Gluc- and Gal-HeLa cells were incubated with 5μM FCCP, 10μM rotenone (rot), 2.4μM antimycin A (anti A), 5mM azide, 2μg/ml oligomycin (oligo) or 10mM 2-deoxy-D-glucose (DOG)/galactose free (gal-free) media (as appropriate) for 20 minutes before mitochondria were isolated and analysed for fusion-mediating mitodynamins by Western blot. All five isoforms of OPA1 were resolved, the two long (L) isoforms (a, b) and the three short (S) isoforms (c, d, e) in all samples except FCCP treated cells, in which there was a disappearance of L-OPA1 isoforms and an enrichment of S-OPA1 isoforms. No other treatments led to this processing of OPA1, with the possible exception of rot-treated Gal-HeLa cells, which exhibited slightly reduced L-OPA1. No post-translational modifications were observed in mitofusins (Mfn) 1 or 2 as a result of treatment. The loading control was VDAC1.

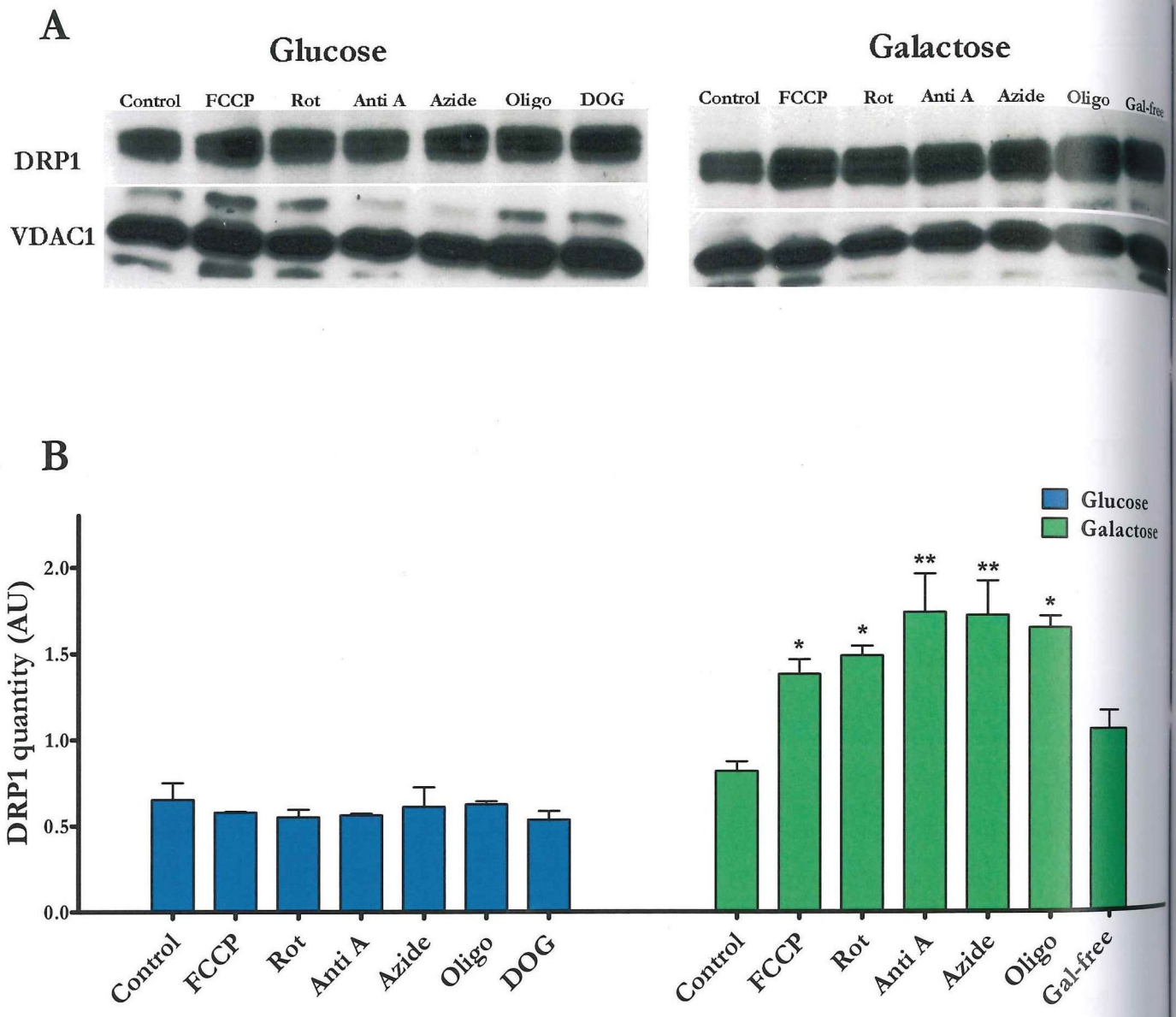

Figure 4.17: OXPHOS inhibition leads to increased recruitment of DRP1 to Gal-HeLa cell mitochondria. (A) Representative of Western blot detection of DRP1 in mitochondria isolated from Gluc- and Gal-HeLa cells treated for 20 minutes with 5μM FCCP, 10μM rotenone (rot), 2.4μM antimycin A (anti A), 5mM azide, 2μg/ml oligomycin (oligo) or 10mM 2-deoxy-D-glucose (DOG)/galactose free (gal-free) media (as appropriate). Loading control is VDAC1. (B) Densitometric analysis of Western blot data of DRP1 reveals a statistically significant increase in DRP1 localised to mitochondria of OXPHOS inhibited Gal-HeLa cells, but not of Gluc-HeLa cells. Data presented as mean ± SD, n = 2. One-way ANOVA with Dunnett's multiple comparisons post-test of each substrate group (B) or two-way ANOVA with Bonferroni post-test (C). *P<0.05, **P<0.01.

depolarisation to the same extent as Gluc-HeLa cells (fig. 4.18A). Only complex III inhibition with antimycin A/myxothiazol produced a statistically significant decrease of $\Delta\Psi_m$ in Gal-HeLa cells compared to Gluc-HeLa cells (fig. 4.18B). These results reiterate the conclusions drawn from Gluc-HeLa cell experiments; there may not be a significant role for partial $\Delta\Psi_m$ dissipation in changes in mitochondrial dynamics following inhibition in these cells.

4.4.6 Effects of Galactose Starvation and Inhibition of Oxidative Phosphorylation on ATP levels in Gal-Hela Cells

In Chapter 3, the correlation between fusion inhibition and ATP depletion was suggested in Gluc-HeLa cells treated with DOG. It was hypothesised that perhaps Gal-HeLa cells were also experiencing ATP depletion upon mitochondrial inhibition, leading to the failure of fusion. Using the same luciferase-based luminescence assay as before, Gal-HeLa cells were found to contain 1.4-fold more ATP than Gluc-HeLa cells at resting conditions (fig. 4.19A). This indicates that Gal-HeLa cells either produce more ATP (using the higher ATP-yielding OXPHOS system), consume less ATP (3-fold longer doubling time), or both. This higher basal ATP could not sufficiently compensate for mitochondrial inhibition however, as treatment with all toxins led to a severe decrease in ATP, (malonate to a lesser extent) (fig. 4.19B). Galactose starvation did not lead to a decrease in ATP, again suggesting independence from sugar catabolism for energy in these cells. The decrease in ATP in FCCP-treated cells was unexpectedly low but the reason for this is not yet clear. However, taken together, these data highlight the distinct correlation between ATP levels and mitochondrial fusion rates.

4.4.7 Effects of Longer Exposure to OXPHOS Inhibitors/Galactose Starvation on Mitochondrial Morphology and Cell Viability

Due to the pronounced effects of relatively short exposure to toxins on mitochondrial fusion in Gal-HeLa cells, the effects of longer exposure were explored. Mitochondrial morphology was examined in Gal-HeLa cells exposed to OXPHOS inhibitors/galactose starvation for six hours and compared to the of Gluc-HeLa cells following the similar

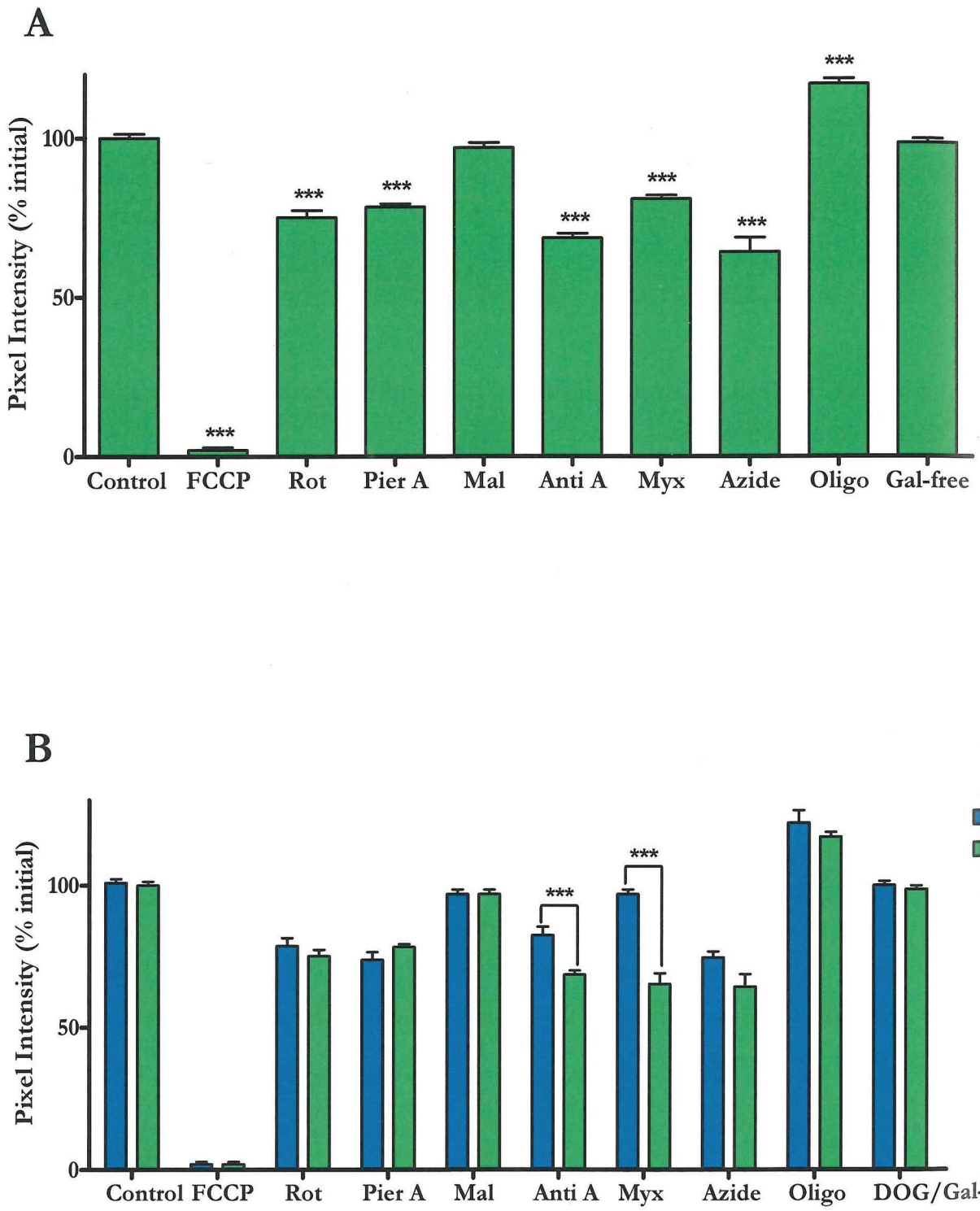

Figure 4.18: OXPHOS inhibition partially depolarises Gal-HeLa cell mitochondria but not to a greater extent than Gluc-HeLa cell mitochondria. (A) Gal-HeLa cells loaded with TMRM were imaged before and after 20 minute incubation with 5μM FCCP, 10μM rotenone (rot), 4μM piericidin A (pier A), 1mM malonate (mal), 2.4μM antimycin A (anti A), 2μM myxothiazol (myx), 5mM azide, 2μg/ml oligomycin (oligo) or 10mM 2-deoxy-D-glucose (DOG)/galactose free (gal-free) media (as appropriate) and the pixel intensities of each field were plotted as percent initial values. All treatments led to a decrease in $\Delta\Psi_m$, except malonate, which had no effect, and oligomycin, which led to hyperpolarisation. (B) When plotted alongside Gluc-HeLa data presented in Chapter 3, it is clear that the magnitude of $\Delta\Psi_m$ change in response to inhibitors does not differ significantly, except with complex III inhibition, using antimycin A/myxothiazol. Data presented as mean ± SEM. One-way ANOVA with Dunnett's multiple comparisons post-test (A) or two-way ANOVA with Bonferroni post-test (B). ***P<0.001.

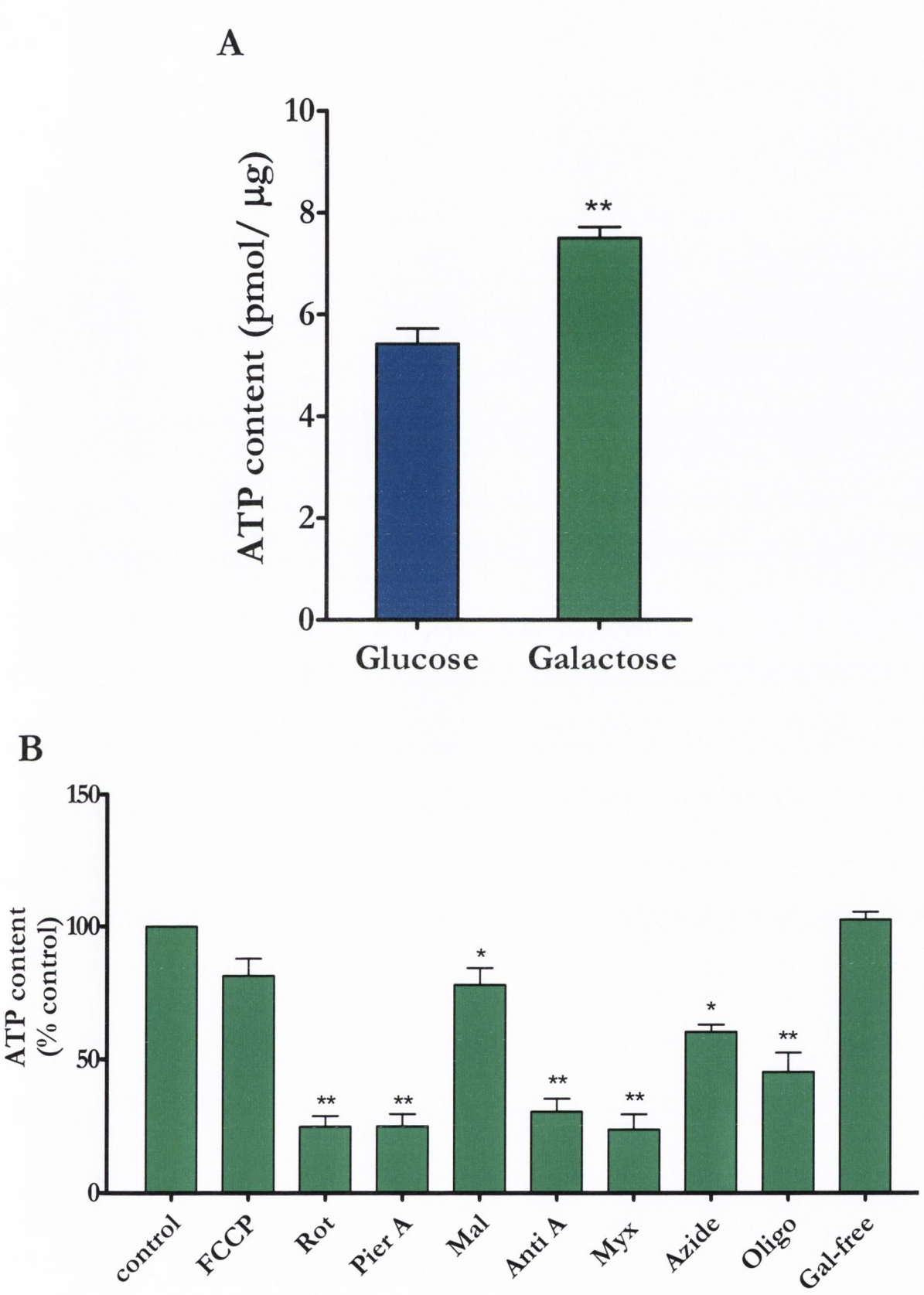

Figure 4.19: Basal ATP levels are higher in Gal-HeLa cells but are decreased by OXPHOS inhibition. Luciferase-based luminescence assays were used to measure ATP levels in both Gluc- and Gal-HeLa cells at rest and also in Gal-HeLa cells following 20 minute incubation with 5µM FCCP, 10µM rotenone (rot), 4µM piericidin A (pier A), 1mM malonate (mal), 2.4µM antimycin A (anti A), 2µM myxothiazol (myx), 5mM azide, 2µg/ml oligomycin (oligo) or galactose free (gal-free) media. (A) Gal-HeLa cells were found to contain more ATP per µg than Gluc-HeLa cells, indicating increased production, decreased consumption, or both. (B) ATP levels drop dramatically upon exposure to OXPHOS inhibitors but not galactose starvation. Data presented as mean ± SEM. Unpaired t-test (A) or one-way ANOVA with Dunnet's multiple comparisons pos-test (B). *P<0.05, **P<0.01.

treatment (fig. 4.20). Gal-HeLa cells showed complete fragmentation of mitochondrial reticula following inhibition of complexes I, III, IV and of ATP synthase, but not galactose starvation. Conversely, Gluc-HeLa cells showed no such fragmentation following inhibition of ETC enzymes, but did so after DOG treatment and ATP synthase inhibition. These results show that early fusion perturbation following inhibitor treatment is predictive of full fragmentation of the network at later stages.

Finally, the impact on cell viability of mitochondrial inhibition over a longer period was assessed. Cell viability measurements in cells after 24 hours of OXPHOS inhibition revealed significantly higher cell death in Gal-HeLa cells compared to Gluc-Hela cells (fig. 4.21A). Gal-HeLa cells showed 2.7 – 9-fold higher cell death following dissipation of $\Delta\Psi_m$ or inhibition of complexes I, III, IV and ATP synthase. Even concentrations 10-fold lower than those used in all other experiments led to 1.6-11.7-fold increases in cell death compared to Gluc-HeLa cells (fig 4.20B). Only DOG treatment led to higher cell death in Gluc-HeLa cells (61.11 $\pm$ 2.44%) compared to Gal-HeLa cells, which were unaffected by galactose starvation (fig. 4.20C). These results further illustrate how HeLa cells can adapt to utilise new substrates, such as L-glutamine, in the absence of glucose but, in doing so, acquire higher vulnerability to mitochondrial inhibition.

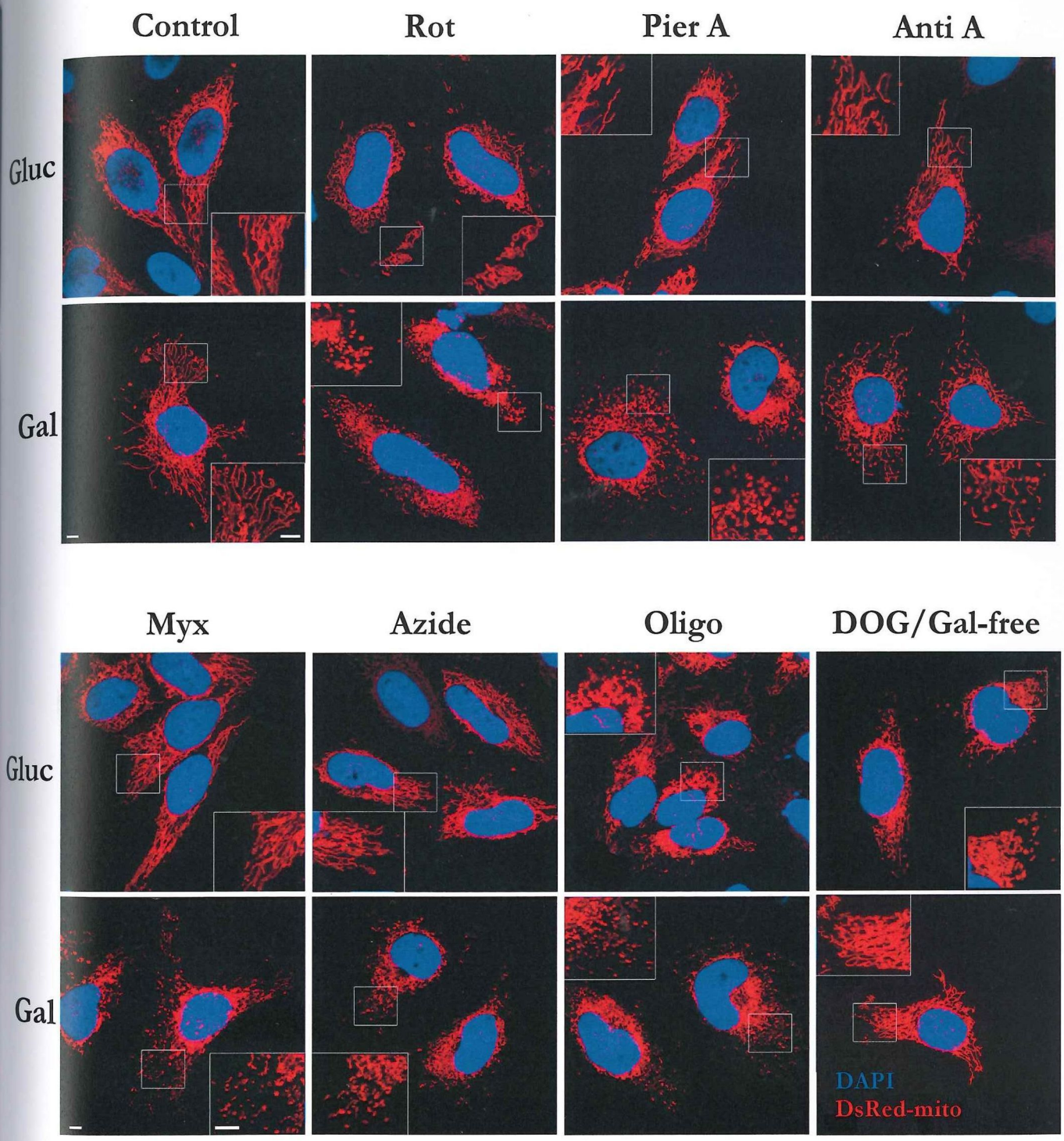

Figure 4.20: Prolonged OXPHOS inhibition leads to extensive fragmentation of the mitochondrial reticulum in Gal-HeLa cells. Gluc- and Gal-Hela cells stably expressing DsRed-mito were incubated for six hours with 10μM rotenone (rot), 4μM piericidin A (pier A), 2.4μM antimycin A (anti A), 2μM myxothiazol (myx), 5mM azide, 2μg/ml oligomycin (oligo) or 10mM 2-deoxy-D-glucose (DOG)/galactose free (gal-free) media (as appropriate), then fixed and imaged by confocal microscopy. Gal-HeLa cells exhibited complete fragmentation of mitochondrial networks following all treatments except galactose starvation. Gluc-HeLa cells exhibited no such fragmentation, except in the presence of oligomycin and DOG, while rotenone treated cells showed tubular yet disorganised morphology, probably due to microtubule disassembly. DAPI, 4,6-diamidino-2-phenylindole, nuclear counterstain. Scale = 5μm.

Figure 4.21: Prolonged OXPHOS inhibition leads to higher cell death in Gal-HeLa cells. Gluc- and Gal-HeLa cells were incubated for 24 hours in 5μM FCCP, 10μM rotenone (rot), 4μM piericidin A (pier A), 1mM malonate (mal), 2.4μM antimycin A (anti A), 2μM myxothiazol (myx), 5mM azide, 2μg/ml oligomycin (oligo) (A) or 10-fold lower doses (B) or 10mM 2-deoxy-D-glucose (DOG)/galactose free (gal-free) media (C) and cell viability was measured using AlamarBlue. Gal-HeLa cells consistently showed significantly higher cell death following OXPHOS inhibition, even at 10-fold lower doses, while viability was unaffected by galactose starvation. Data presented as mean ± SEM, n = 3. Two-way ANOVA with Bonferroni post-test (A,B) or unpaired t-test (C). *P<0.05, **P<0.01, ***P<0.001.

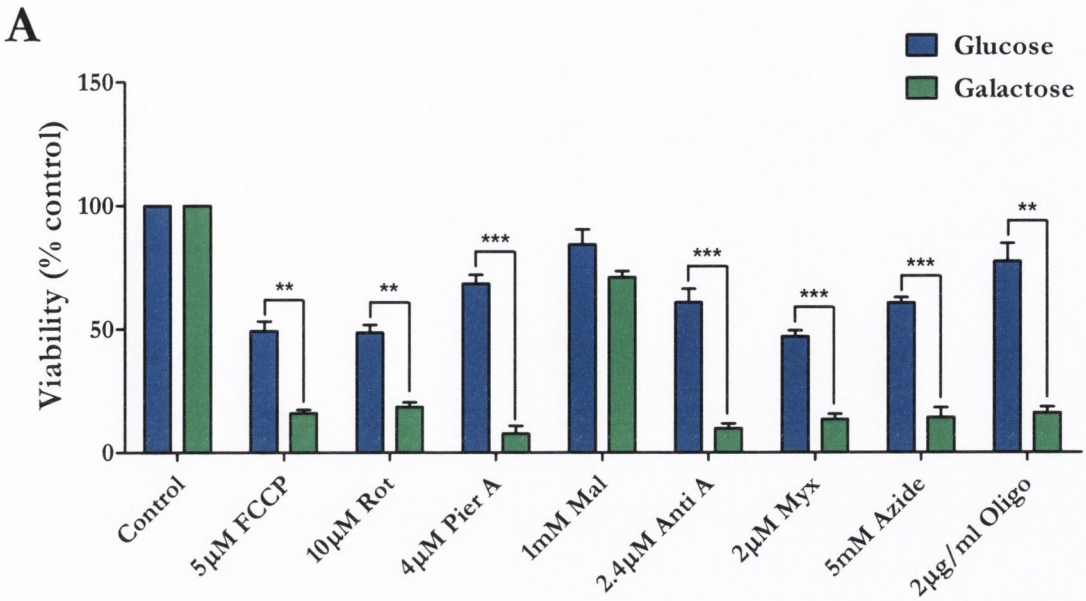
A
Glucose
Galactose
Viability (% control)
150
100
50
0
**
**
***
***
***
***
**
Control
5μM FCCP
10μM Rot
4μM Pier A
1mM Mal
2.4μM Anti A
2μM Myx
5mM Azide
2μg/ml Oligo

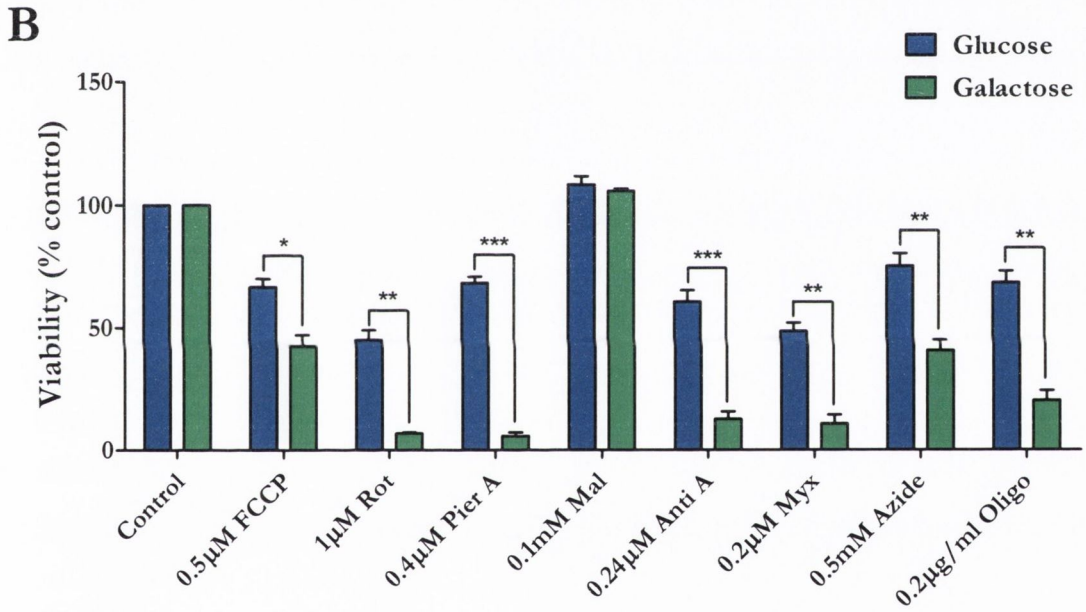
B
Glucose
Galactose
Viability (% control)
150
100
50
0
*
**
***
***
**
**
Control
0.5μM FCCP
1μM Rot
0.4μM Pier A
0.1mM Mal
0.24μM Anti A
0.2μM Myx
0.5mM Azide
0.2μg/ml Oligo

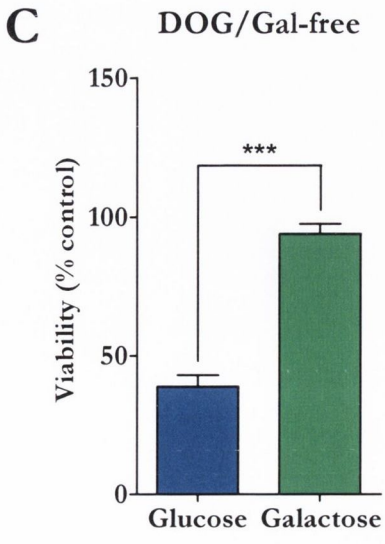
C
DOG/Gal-free
Viability (% control)
150
100
50
0
***
Glucose
Galactose

4.5 Discussion

The glycolytic needs of large tumours can outstrip glucose supply, inducing aglycemia (Eigenbrodt *et al.*, 1998, Smolkova *et al.*, 2011). This can encourage a metabolic shift from aerobic glycolysis to OXPHOS, in which glutamine is the primary energy substrate. The studies presented here reveal a substrate-dependent change in mitochondrial fusion dynamics in response to mitochondrial inhibition in HeLa cells. While ultrastructural changes modify the mitochondrial network upon adaptation to a glucose-free environment, fusion rates remain stable. However, these rates are highly sensitive to mitochondrial inhibition, and fusion is robustly blocked in the presence of ETC/OXPHOS. Thus, the sensitivity of fusion rates to mitochondrial inhibition is substrate-dependent. This sensitivity is correlated with decreased ATP levels and increased DRP1 recruitment to mitochondria of treated Gal-HeLa cells. Furthermore, early fusion inhibition is predictive of full fragmentation of the reticulum following longer (six hour) exposure to toxins, both in Gluc- and Gal-HeLa cells. Interestingly, the addition of glucose to Gal-HeLa cell medium during ETC/OXPHOS inhibition is protective and restores fusion rates to control values. Thus, glucose metabolism is a requirement for maintenance of mitochondrial fusion rates during mitochondrial inhibition. Gal-HeLa cells are also ~2-fold more viable than Gluc-HeLa cells in medium containing L-glutamine but lacking any sugars. Furthermore, Gal-HeLa cell viability in medium containing L-glutamine and glucose/fructose/maltose exceeds that observed with galactose, while Gluc-HeLa cells consistently fail to match, let alone exceed, viability levels in any substrate other than glucose. Thus, either Gal-HeLa cell metabolism, growth, or both seem to benefit from a synergistic effect of increased OXPHOS and glucose availability. Finally, Gal-HeLa cells exhibit significantly higher cell death following 24 hour exposure to mitochondrial toxins. Thus, HeLa cells can adapt to the absence of glucose, but acquire new vulnerabilities to mitochondrial inhibition, leading to perturbation of fusion and increased cell death.

Gal-HeLa cells exhibited basal mitochondrial fusion rates equal to those of Gluc-HeLa cells (fig 4.3). This is a surprising result, given the dependence of glycolytic HeLa cells on glucose metabolism for the maintenance of fusion rates, described in Chapter 3. Thus, HeLa cells are capable of adaptation to loss of this substrate to maintain normal fusion rates. The Gal-HeLa cells used in this study were cultured for at least a week in galactose DMEM before

used in experiments. It would be extremely interesting to assess how mitochondrial fusion rates are affected directly after this switch to galactose medium and in the days subsequent as it is likely that the cells would be undergoing extensive alterations in energy metabolism pathways during this time. For example, the removal of glucose would probably lead to a transient increase in the AMP:ATP ratio, leading to an activation of AMPK with subsequent inhibition of anabolic pathways. Interestingly, AMPK inhibits mTOR through phosphorylation and activation of tuberous sclerosis complex 1/2 (TSC1/2), the negative regulators of mTOR (Inoki *et al.*, 2003). As AMPK is also a stimulator of autophagy (Kim *et al.*, 2011), and given the effects of mTOR inhibition on SIHF (Gomes *et al.,* 2011), it is possible that fusion rates would transiently increase. Assessment of fusion rates during the hours and days following replacement of glucose with galactose in the culture medium could yield some interesting data.

Comparison of mitodynamin expression between Gluc- and Gal-HeLa cells revealed that the retention of normal fusion rates after adaptation to galactose medium was not due to changes in expression of fission/fusion mediators (fig 4.4), despite obvious changes in mitochondrial diameter and distribution (fig 4.2). Not only were mitochondria thinner in diameter (observation, not quantified), but the reticulum also extended to distal regions of the cytoplasm, as noted by Rossignol *et al.* (2004). This is in clear contrast to the thick tubules clustered in the perinuclear region observed in Gluc-HeLa cells. As stated in the literature, the mitodynamins are the main mediators of mitochondrial fission and fusion. However, by no means are they the only effectors of these processes. Thus, the changes in Gal-HeLa mitochondrial morphology may be related to changes in expression of mitodynamin regulators. It must be noted that while increasing expression of DRP1 does not necessarily increase fission, owing to a lack of change in DRP1 recruitment under such conditions (Smirnova *et al.*, 1998, Pitts *et al.*, 1999), an increase in phosphorylated DRP1 would indicate increased retention of DRP1 at the cytoskeleton and possibly, decreased fission. This could be investigated using antibodies raised against phosphorylated DRP1.

The decreased diameter in Gal-HeLa cell mitochondria can be explained by the 'condensed' conformation assumed by mitochondria in state 3 respiration, as noted by Hackenbrock (1966). The spreading of mitochondria into the cytoplasm may involve changes in

mitochondrial transport activity. In neurons, mitochondria are recruited to areas of high activity through interactions with cytoskeletal adaptor proteins with Ca^{2+} sensing abilities, such as Miro 1/2 (Macaskill *et al.*, 2009). Less is known about this process in other cell types but changes in mitochondrial transport mechanisms could affect their cellular distribution. Indeed, as described in Chapter 3, disassembly of the microtubule architecture in HeLa cells disorganises the mitochondrial network (Legros *et al.*, 2002), which was also observed following six hour incubation of Gluc-HeLa cells with rotenone, a proven microtubule disassembly agent.

Importantly, fusion was seriously compromised by inhibition of complexes I, III, IV of the ETC and ATP synthase (figs 4.5 – 11). Inhibition of these enzymes resulted in dramatic decreases in ATP levels (4.19), comparable to the level observed in Gluc-HeLa cells exposed to DOG, in agreement with the literature (Marroquin *et al.*, 2007). Thus, dependence on OXPHOS for maintaining ATP levels in Gal-HeLa cells is confirmed, as is the correlation between ATP levels and fusion inhibition. Although complex II inhibition caused a small but statistically significant drop in ATP levels, malonate did not affect fusion rates (fig 4.8), suggesting this enzyme is dispensable for maintenance of mitochondrial fusion within the time frame employed here. Alternatively, the concentration used may have been suboptimal for complete complex II inhibition, although this concentration (and 1 – 10-fold lower) has been used successfully in HeLa cells in other studies (Fujikawa and Yoshida, 2010, Lee *et al.*, 2011). It is possible the effects of complex II inhibition require a longer incubation period, as 3-NP has been shown to cause mitochondrial fragmentation in neurons within 3 – 6 hours (Liot *et al.*, 2009). Surprisingly, $\Delta\Psi_m$ dissipation did not differ significantly between inhibitor treated Gluc- and Gal-HeLa cells (fig 4.18). Thus, it is difficult to correlate $\Delta\Psi_m$ changes of the magnitude observed here with mitochondrial fusion inhibition. A more likely candidate is cellular ATP level. Finally, ATP synthase inhibition resulted in fusion inhibition that exceeded the level observed in Gluc-HeLa cells. Although the fusion inhibition by oligomycin in Gluc-HeLa cells seemed to occur through an as-yet undefined mechanism, the fusion deficit observed in Gal-HeLa cells with the same treatment may encompass a more general effect of mitochondrial inhibition.

Western blot analysis of mitodynamins in mitochondrial samples prepared from inhibitor-treated Gluc- and Gal cells revealed and important substrate-dependent difference. Cleavage of OPA1 was eliminated as a causative factor in the observed Gal-HeLa fusion deficits, as no changes in the relative levels of short and long isoforms were detected between groups or substrates. One possible exception could be rotenone treatment, as there was a very slight decrease in L-OPA1 levels, but this requires further verification. Proteolytic processing was readily observed in FCCP treated groups, in agreement with the literature (Duvezin-Caubet *et al.*, 2006, Guillery *et al.*, 2008). A study on isolated mitochondria has shown that azide and oligomycin cause OPA1 proteolytic cleavage in an ATP-dependent manner (high ATP being preventative of cleavage) (Baricault *et al.*, 2007) but this was not observed in the mitochondria from these treated cells. This may be related to the fundamental differences, not least structural ones, between isolated mitochondria and those in living cells. These results also suggest that the ~20% depolarisation detected in treated cells is insufficient to promote OPA1 cleavage. Therefore, it is possible this proteolysis only occurs when mitochondria fully depolarised, as with FCCP treatment. While the failure to detect higher additional bands in Western blots for Mfn1/2 in mitochondria from treated cells is indicative of no PTMs, this would have to be further verified with antibodies raised against mitodynamins with specific PTMs, or analysis by mass spectrometry.

Importantly, DRP1 levels in mitochondria isolated from inhibitor-treated cells differed significantly between substrates. While control Gluc- and Gal-HeLa cells exhibited comparable levels of DRP1 (as did Gal-HeLa cells in galactose free medium), this protein was enriched in the inhibitor treated samples from Gal-HeLa cells only. This signifies a substrate-dependent change in mitochondrial mitodynamin recruitment in HeLa cells. The mechanism of DRP1 recruitment is unclear. As it occurs with all mitochondrial inhibitors, DRP1 translocation may be a general response to ETC/OXPHOS inhibition. Potentially, ROS could play a role, as fragmentation the mitochondrial reticulum has been shown to accompany increased ROS in many cell types (Lyamzaev *et al.*, 2004, Chernyak *et al.*, 2006, Pletjushkina *et al.*, 2006, Yu *et al.*, 2006). In addition, DRP1 has been shown to become activated following S-nitrosylation by nitric oxide (NO) (Barsoum *et al.*, 2006, Cho *et al.*, 2009), promoting fission in neuronal cells. Indeed, overproduction of NO in tumour cells is associated with cytotoxicity (Dhankhar *et al.*, 2010, Muntané and De la Mata, 2010) and

improves chemotherapy efficacy. However, a low level of OXPHOS in Gluc-HeLa cells does not necessarily mean that ROS production would be any lower in response to mitochondrial inhibition. Indeed, basal ROS may be higher in Gluc-HeLa cells; slow, state 4-like respiration allows electrons to reside longer in active redox sites in ETC enzymes, increasing the probability of ROS production (Chance *et al.*, 1979, Turrens, 2003, Adam-Vizi and Chinopoulos, 2006). Conversely, it is also possible the upregulation of ETC enzymes in Gal-HeLa cells (Rossignol *et al.*, 2004) would increase the total number of redox sites within their mitochondria, providing more opportunities for ROS generation.

It is possible that Gluc-HeLa cells have a more robust anti-oxidant battery compared to Gal-HeLa cells, owing to high availability of G6P for the PPP, and thus, NADPH for the regeneration of GSH. Indeed, neurons, which are almost completely dependent on OXPHOS for ATP, have intrinsically low GSH levels and are highly sensitive to oxidative stress (Bolanos *et al.*, 2010). Interestingly, mitochondrial inhibitors have been shown to cause rapid (within ~30min) depletion of GSH in hepatocytes as a result of increased cellular efflux, rather than through increased oxidation (Mithofer *et al.*, 1992). This would presumably render cells even more vulnerable to oxidative stress during more prolonged mitochondrial inhibition. It would be interesting to compare both GSH levels and ROS production between Gluc- and Gal-HeLa cells to determine whether there is a substrate-dependent effect on this parameter in relation to fusion inhibition.

Additionally, it is possible that the energetic crisis induced in Gal-HeLa cells by mitochondrial inhibition initiates apoptosis. The role of DRP1 in apoptosis is controversial, as described in Chapter 1, however its depletion in cells has been shown to attenuate apoptosis (Lee *et al.*, 2004). The current consensus seems to be that it is involved, yet dispensable (Sheridan and Martin, 2010). Nevertheless, its translocation to the mitochondria could indicate the onset of apoptosis. Immunostaining for cytochrome c in treated cells could shed light on the matter. Interestingly, Gal-HeLa cells incubated for a longer time period of six hours showed highly fragmented reticula with all inhibitors (fig 4.20). Gluc-HeLa cells showed no such fragmentation, except when treated with oligomycin or DOG. Furthermore, Gal-HeLa cells in galactose-free medium did not exhibit fragmentation and showed no obvious signs of SIHF (Tondera *et al.*, 2009, Gomes *et al.*, 2011). Thus, early

fusion deficit was predictive of later collapse of the mitochondrial ultrastructure. It would be interesting to deplete DRP1 by RNAi in Gal-HeLa cells to assess whether this restored fusion rates and/or prevented later fragmentation.

Removal of galactose from the medium did not affect fusion (fig 4.13), DRP1 recruitment (fig 4.17), $\Delta\Psi_m$ (4.18) or ATP levels (4.19) in Gal-HeLa cells, although it is possible that the cells contained sufficient galactose to compensate for this acute galactose starvation. However, Gal-HeLa cells were remarkably resilient when cultured without sugars for three days (fig 4.14), suggesting the derivation of energy from glutamine is sufficient to sustain cell function and growth over this period. Previous studies have suggested that glutamine is the primary source of energy in HeLa cells cultured in glucose medium (Reitzer *et al.*, 1979) but the data presented here suggest that Gluc-HeLa cells primarily rely on glucose. Indeed, L-glutamine was included in all media throughout experimentation in Chapters 3 and 4, therefore the poor viability of Gluc-HeLas in sugar-free media cannot be attributed to the fact that that metabolic pathway was not available to them prior to growth without sugar.

Mammalian cells are believed to express transporters for monosaccharides only, while polysaccharides require degradation into monosaccharides before uptake (Meyer *et al.*, 2011). Cells can be cultured in polysaccharide secondary sources of glucose (sucrose, maltose) provided the appropriate hydrolytic enzymes are present in FBS supplementing the medium (Rheinwald and Green, 1974). Maltose is hydrolysed to two molecules of glucose by maltase, while sucrase hydrolyses sucrose into a glucose molecule and a fructose molecule. Quantification of Gluc- and Gal-HeLa viability in alternative sugars reiterated the reliance of Gluc-HeLa cells on glucose; their viability matched control levels in maltose, as this disaccharide liberates two glucose molecules upon hydrolysis, while viability was reduced in fructose, which requires several catalytic conversions before it is incorporated into the glycolytic pathway. Furthermore, fructokinase, which phosphorylates fructose upon entry into the cell, is not allosterically inhibited by its product and as such, continues to phosphorylate fructose indefinitely, depleting ATP levels (Johnson *et al.*, 2009). Conversely, Gal-HeLa cells seemed to benefit from access to glucose, as reduction of the AlamarBlue indicator in glucose, maltose and fructose exceeded that observed in galactose. Sucrase does not appear to be present in FBS, viability in both cell types growing in sucrose was

comparable to that in sugar-free medium. Measurement of respiration in Gal-HeLa cells after three days in these sugars would give an indication of the activity of the OXPHOS system. It would also be interesting to compare expression of Leloir pathway enzymes in across substrates to assess whether cells became more efficient in its catabolism when it was the only sugar available.

This observation inspired the assessment of mitochondrial fusion rates in Gal-HeLa cells exposed to piericidin A in the presence of glucose (fig 4.15). This led to the interesting, discovery that mitochondrial fusion rates were restored in the presence of glucose. Again, the mechanism behind this effect is not clear, as the glucose could potentially have been utilised to generate glycolytic ATP, or to generate NADPH for ROS defence. Measurement of cellular ATP and GSH after this treatment would help define how glucose metabolism prevents fusion inhibition under these circumstances. Western blotting for HK I and II revealed that although total HK II expression was dramatically decreased in Gal-HeLa cells, it was enriched at the mitochondria, and even exceeded that observed on Gluc-HeLa mitochondria (fig 4.15). It is possible that Gal-HeLa cells were able to mobilise HK II at the mitochondria to opportunistically utilise newly available glucose. Aside from the possibility that it allows for quick utilisation of glucose in the event that it becomes available, it is not clear why Gal-HeLa cells should enrich HK II at their mitochondria. Perhaps it is related to the role if HK II in apoptosis prevention at this site (Pastorino *et al.*, 2002, Solaini *et al.*, 2011). It would be extremely interesting to examine the effects of depletion of HK II in Gal-HeLa cells, both in terms of general cell viability and mitochondrial fusion rates.

These data demonstrate that Gal-HeLa cells are metabolically more adaptable than Gluc-HeLa cells, and that they can rapidly exploit glucose when available to restore mitochondrial fusion rates. Interestingly, it has been observed that astrocytic glioma cells with a primarily OXPHOS phenotype can migrate and invade Matrigel (a measure of malignancy) in the presence of sodium azide if there is adequate glucose available (Beckner *et al.*, 2005). Thus, this may be, in part, due to their ability to maintain mitochondrial viability using glycolytic ATP. In the absence of glucose, however the vulnerability of Gal-HeLa cells to mitochondrial inhibition was extremely high, as confirmed by analysis of cell viability after exposure to toxins for 24 hours (fig 4.21). Interestingly, Gal-HeLa cells were equally

vulnerable to ETC/OXPHOS inhibition using 10-fold lower doses of each inhibitor, with the exception of malonate, which did not significantly impact viability. Conversely, cell death was significantly higher in Gluc-HeLa cells treated with DOG than in galactose-starved Gal-HeLa cells. Therefore, HeLa cells display a substrate-dependent vulnerability to mitochondrial inhibition. These results also demonstrate a striking correlation between early mitochondrial fusion perturbation and later cell death, as any treatment that inhibited fusion after 20 minutes also caused extensive fragmentation of the reticulum within six hours, and significant cell death after 24 hours. It appears that inhibition of mitochondrial fusion is an early event in a biochemical cascade eventually leading to cell death, in agreement with the literature pertaining to Bak/Bax interactions with DRP1 and Mfn2 during apoptosis (Karbowski *et al.*, 2002, 2006, Wasiak *et al.,* 2007).

To conclude, these data demonstrate that when glucose is abundant, HeLa cells exhibit high dependence on its metabolism for the maintenance of mitochondrial fusion rates. However, they can adapt over time to maintain these rates in the absence of glucose, but in so doing, they acquire vulnerability to mitochondrial inhibition. Whilst respiring on glutamine, HeLa cells exhibit complete cessation of mitochondrial fusion upon exposure to mitochondrial inhibitors, concomitant with a dramatic decrease in cellular ATP. This eventually leads to the loss of mitochondrial structural integrity and fragmentation of the reticulum within six hours, and extremely high cell death within 24 hours.

CHAPTER 5

Bioenergetic Control of Mitochondrial Dynamics in Primary Cortical Neurons

5.1. Introduction

The importance of mitochondrial dynamics in neurons is compounded by their morphology, post-mitotic state, significant dependence on oxidative metabolism and frequent intracellular calcium fluctuations. Neurons are morphologically polarised; the cell soma, containing the nucleus and associated biogenesis machinery, can be located up to a meter away from the axon terminal, the site at which neurotransmission occurs (Knott *et al.*, 2008). Neurotransmission is energetically expensive, involving the production and storage of neurotransmitters, transient and rapid plasma membrane depolarisation (action potential), sudden spikes in cytosolic Ca^{2+} levels, neurotransmitter release/reuptake/catabolism and re-establishment of resting membrane potential by active ion gradient correction. The fact that neurons derive over 90% of ATP through OXPHOS places additional pressure on normal mitochondrial function (Cai and Sheng, 2009).

In addition, the polarised neuronal morphology brings the importance of mitochondrial dynamics into sharp focus, especially the active transport of these key organelles along the cytoskeletal architecture. In this way, mitochondrial bioenergetic or morphological dysfunction (or both) can have a severe impact on neuronal health and function. Indeed, metabolic disorders arising from mitochondrial dysfunction typically include severe central nervous system (CNS) or peripheral neuropathies (Rossignol *et al.*, 2003, Knott *et al.*, 2008, Chen and Chan, 2009). Furthermore, the complex interplay between mitochondrial function and dynamics has been implicated in the etiology and/or progression of several neurodegenerative disorders, such as Alzheimer's disease (AD), Huntington's disease (AD), and Parkinson's disease (AD). What follows is a description of mitochondrial dynamics in neuronal cells and how this aspect of mitochondrial function has become relevant to the field of neurodegeneration research.

5.1.1 Mitochondrial Dynamics in Neurons

Neurons can transport mitochondria (and other cargo) both anterogradely (to the synapse) and retrogradely (to the soma) using specific motor machinery; the cytoskeletal scaffold (microtubules, actin filaments), motor proteins (kinesin, dynein, myosin V) and linkers/adaptors with regulatory roles (Milton/GRIF1, Miro1/2). Microtubules are arranged

in a polar fashion in axons, with the 'plus' ends pointing towards the synapse and the 'minus' ends, towards the soma, while the polarity in dendrites can be mixed (Hirokawa and Takemura, 2004). It is on these tracts that kinesin motors transport mitochondria in the anterograde direction, while dynein motors mediate retrograde transport. Actin filaments are enriched in areas of high activity within the cell, such as presynaptic terminals and dendritic spines and are thought to mediate short-range transport of organelles, using myosin V motors (Cai and Sheng, 2009).

The transport of mitochondria is especially unique compared to that of other cargo, in that it is saltatory and bi-directional. During transport, mitochondria can start, stop and change direction several times (Hollenbeck and Saxton, 2005, Cai and Sheng, 2009), with a movement velocity that falls between that of slow moving cytoskeletal proteins and fast-moving vesicles (Blaker *et al.*, 1981). The direction and velocity of mitochondrial transport is highly sensitive to local Ca^{2+} fluctuations (Saotome *et al.*, 2008) and this is thought to be due to the presence of adaptor proteins involved in the attachment of mitochondria to molecular motors. Glater *et al.* (2006) have shown that that microtubule-dependent mitochondrial transport in both *Drosophila* neurons and in mammalian cells requires an adaptor protein called Milton (also known as GRIF1 in mammals), which recruits kinesin-1 heavy chain, KIF5 to the mitochondria. Other proteins crucial for the microtubule-based transport of mitochondria are OM mitochondrial Rho GTPases 1/2 (Miro1/2). Miro1/2 contain two EF-hand Ca^{2+} binding domains each and confer Ca^{2+} sensitivity to the transport machinery (Saotome *et al.*, 2008), ensuring the localisation of mitochondria at areas of high calcium flux (Fransson *et al.*, 2003, Wang and Schwarz, 2009). While it is not fully understood how Ca^{2+} arrests mitochondrial transport, two mechanisms have been proposed. The first, proposed by Macaskill *et al.* (2009), states that the binding of Ca^{2+} by Miro leads to its the detachment from KIF5, while GRIF1 remains bound to Miro and the mitochondrion. The second, proposed by Wang and Schwarz (2009), states that Ca^{2+} binding by Miro affects the interaction between KIF5 and microtubules, causing them to dissociate from one another.

While disruption of microtubule assembly does not heavily impact fusion in non-neuronal cells, as shown in Chapter 3 and by others (Legros *et al.*, 2002), disassembly of microtubules in neurons causes mitochondrial transport arrest and fragmentation (Ligon and Steward,

2000). Indeed, some mutations of Mfn2 do not affect fusion competence of mitochondria but abolish the protein's interaction with Miro2, thereby inhibiting mitochondrial transport and precipitating the peripheral neuropathy Charcot Marie Tooth Disease type IIa (CMTIIa) (Misko *et al.*, 2010). Furthermore, use of microtubule targeting agents in chemotherapy can induce transient neuropathy in patients (Rovini *et al.*, 2011). Chen and Chan (2009) note that mitochondrial transport and fusion are interrelated – if transport is inhibited, mitochondria become immobile and thus the chances of fusion are decreased due to spatial limitations, while fission would still be possible. Conversely, hyperfusion of mitochondria would restrict transport due to the physical hindrance of outsize cargo.

Mitochondrial fission and fusion have asserted themselves as key aspects of mitochondrial function in neuronal development and in synaptic plasticity. Li *et al.* (2004) demonstrated the importance of fission in rat hippocampal synaptogenesis. Small mitochondria were seen to redistribute to dendrites upon repeated stimulation, promoting the development of dendritic spines, projections jutting out perpendicularly from dendrites on which other cells synapse. Expression of dominant negative DRP1 decreased dendritic mitochondrial density, decreased dendritic spine formation by ~78%, and reduced synaptogenesis. Conversely, overexpression of wild-type DRP1 led to increased dendritic mitochondrial numbers and a doubling of dendritic spine formation, with increased synaptogenesis. Waterham *et al.* (2007) later described a female patient, carrying a single heterozygous dominant negative mutation for DRP1 that resulted in an Ala^{395} – Asp substitution in the conserved middle domain. The patient died 37 days after birth with an array of neurological and metabolic symptoms, namely microcephaly, optic atrophy and hypoplasia, persistent lactic acidemia, and elevated plasma long-chain fatty acids. Fibroblast samples from the patient exhibited excessive mitochondrial and peroxisomal tubularity. Ishihara *et al.* (2009) showed that mice lacking DRP1 died at embryonic day (E) 12.5, while neuron-specific (NS) DRP1 knock-down mice died postnatally with brain hypoplasia. Primary neuronal cultures from NS-$DRP1^{-/-}$ mice exhibited mitochondrial clustering at the soma and poor synapse formation. Thus mitochondrial fission is essential in neuronal development and synaptogenesis.

Mitochondrial fusion is also key in CNS development. While mice lacking Mfn1 and 2 die *in utero*, (Chen *et al.*, 2003) Mfn2-deficiency induced after E7 (to circumvent the placental

defects in Mfn2-knockout mice leading to resorption at E12.5) leads to high postnatal mortality or, for survivors, severe and progressive cerebellar degeneration with associated motor defects (Chen *et al.*, 2007). Purkinje neuron cultures from these mice have increased mitochondrial diameter due to swelling and a dearth of mitochondria in axons and dendrites, possibly due to mitochondrial aggregates (Chen and Chan, 2009). Mutation of OPA1 is known to cause autosomal dominant optic atrophy (ADOA) (Alexander *et al.*, 2000, Delettre *et al.*, 2000). Interestingly, some mutations in the GTPase domain of OPA1 produce 'ADOA-plus' phenotypes, characterized by deafness, sensory-motor neuropathy, muscle movement disorders and mtDNA instability (Amati-Bonneau *et al.*, 2008, Hudson *et al.*, 2008, Knott *et al.*, 2008). A particular mutation leading to its relocation to the cytoplasm rather than the mitochondrial IM revealed the essential role of OPA1 in mouse embryonic development; mice carrying the mutation suffered embryonic lethality with exencephaly (Moore *et al.*, 2010).

Beyond early development, and aside from neuropathies arising directly from mutations in the fusogenic mitodynamins (CMTIIa, DOA), perturbation of mitochondrial dynamics has been implicated in neurodegenerative disease. Mitochondrial dysfunction has long been associated with the pathogenesis of a number of neurodegenerative illnesses, particularly AD, PD and HD. A key factor in these illnesses is their progressive nature; both AD and PD mostly arise sporadically, while HD is autosomal dominant, but all generally emerge from middle age onwards (Swerdlow, 2009b). Thus, by the time symptoms manifest, there has been a cumulative effect of ongoing damage and a tolerance threshold has been breached. Mitochondrial dysfunction can be self-propagating; excessive ROS production, for instance, can cause mtDNA mutation, which in turn can precipitate further mitochondrial dysfunction, further ROS generation, depletion of cellular antioxidant defences, aggregation of oxidatively damaged proteins, lipids and nuclear DNA and thenceforth a vicious cycle of cellular destruction (de Moura *et al.*, 2010). The advances made in mitochondrial dynamics research in the last decade have provided the impetus to examine neurodegenerative diseases in this new context.

5.1.2 Mitochondrial Dysfunction and Dynamics in Alzheimer's Disease

Alzheimer's disease is characterised by fatal degenerative dementia and memory loss, arising from cerebral accumulation insoluble amyloid-β Aβ) protein (accumulating due to aberrant cleavage of amyloid precursor protein, APP), neurofibrillary tangles containing hyperphosphorylated tau protein, senile plaques, and progressive neuronal loss (Wang *et al.*, 2009b, de Moura *et al.*, 2010). Impaired brain metabolism is one of the best documented abnormalities of AD and post mortem brains of patients consistently exhibit marked reductions in the activities of a number of mitochondrial enzymes, including PDHC, the α-ketoglutarate dehydrogenase complex and complex IV (Blass, 2000). Indeed, Aβ selectively inhibits complex IV in a dose-dependent manner in isolated rat brain mitochondria (Canevari *et al.*, 1999). In addition, there is strong evidence of excessive ROS production in AD brains, including mtDNA alterations, with reduced copy number, lipid peroxidation, oxidative protein and nuclear DNA damage and decreased ATP production (Reddy *et al.*, 2011). Thus, mitochondrial dysfunction is likely to be an important factor in the progression of this disease.

Abnormal mitochondrial dynamics were first implicated in AD with the discovery that cell neuroblastoma cybrids, containing mtDNA from from AD patients, exhibited swollen and clustered mitochondria, often lacking visible cristae (Trimmer *et al.*, 2000). Subsequently, neurons in post-mortem AD brain tissue were found to contain fewer mitochondria per μm^2 compared to controls, and remaining mitochondria frequently exhibited broken cristae (Hirai *et al.*, 2001). Several years later, it was shown that HSFs from AD patients contained significantly reduced DRP1 levels and excessively tubular mitochondria clustered in a perinuclear fashion (Wang *et al.*, 2008a). Interestingly, they also produced three-fold higher ROS than healthy controls, and treatment of both cell types with H_2O_2 led to a decrease in cellular DRP1 levels. Furthermore, exogenous expression of APP in healthy HSFs led to a decrease in DRP1 and replicated the AD HSF mitochondrial morphological aberrations, with expression of an Aβ-generating, AD-relevant mutant (sweAPP) compounding this effect. Co-expression of DRP1 with APP attenuated the morphological effects of APP alone. Thus DRP1 dysregulation was shown to be key mediator of mitochondrial dysfunction in AD.

The same group then showed that exogenous expression of APP or sweAPP in human neuroblastoma M17 cells caused mitochondrial fragmentation and perinuclear clustering, increased ROS and decreased ATP production (Wang *et al.*, 2008b). Furthermore, neurons in AD brain slices were shown to have a dearth of mitochondria in axons and dendrites (Wang *et al.*, 2009a), while PCR analysis of AD brains by another group revealed increased DRP1 levels (Calkins *et al.*, 2011, Manczak *et al.*, 2011). Interestingly, expression of oligomeric Aβ-derived diffusible ligands (ADDLs) caused mitochondrial fragmentation and depletion in neuronal processes, leading to decreased dendritic spines and decreased synaptogenesis (Wang *et al.*, 2008b). The authors later speculated that the hyperfusion observed in AD patient fibroblasts may have been an adaptive mechanism to compensate for increase basal ROS production, that is lacking in neural cells (Wang *et al.*, 2009b). Thus it seems that the AD brain suffers from a counterintuitive combination of increased mitochondrial fission and decreased axonal transport in neurons.

Importantly, Cho *et al.* (2009) showed that DRP1 is S-nitrosylated by nitric oxide (NO) produced in response to Aβ; this PTM leads to activation of DRP1 and increases fission. Nitric oxide is a signalling molecule, particularly in the brain, but as a ROS, can have detrimental effects, such as inhibition of complex IV, if produced in excess (Moncada and Bolanos, 2006). In the study by Cho *et al.,* brains of AD patients, but not those of PD patients or non-diseased controls, contained S-nitrosylated DRP1 at Cys^{644} of the protein's GED. Moreover, primary neurons exposed to AD-relevant Aβ mutants exhibited significantly increased mitochondrial fission, concomitant with DRP1 S-nitrosylation. This was accompanied by decreased synaptogenesis and poverty of dendritic spines. Interestingly, these effects were abrogated by mutation of DRP1 Cys^{644} that blocked S-nitrosylation. Most recently, kymographic measurements of mitochondrial movement in axons of primary neurons from AD mice revealed that axonal transport of the organelles is significantly hindered (Calkins *et al.*, 2011). The authors also found that oligomeric Aβ physically interacts with DRP1 (Manczak *et al.*, 2011), further suggesting a direct impact of aberrant mitochondrial dynamics on disease progression.

Taken together, there is strong evidence that mitochondrial dynamic dysfunction is an important aspect of the AD pathophysiology, although whether or not it is causative in the

general mitochondrial dysfunction observed in the AD brain is not yet known. It is conceivable that excessive fission arising from of Aβ-mediated DRP1 hyper-activation would lead to mitochondrial heterogeneity and the accumulation of mtDNA mutations, which could then go on to induce further mitochondrial dysfunction. In addition, inhibition of mitochondrial axonal and dendritic transport would clearly impair synaptic transmission, leading to a lack of long-term potentiation (LTP, the strengthening of neural connections through repeated stimulation) and atrophy of synaptic connections.

5.1.3 Mitochondrial Dysfunction and Dynamics in Parkinson's Disease

The hallmark symptoms of bradykinesia, rigidity, shuffling gait and resting tremor, are a consequence of dramatic and progressive depletion of pigmented dopaminergic neurons in the Substantia Nigra *pars compacta* (SNpc) of the basal ganglia (Dauer and Przedborski, 2003, Van Laar and Berman, 2009). Another classic histopathological feature in the PD brain is the presence of eosinophilic, proteinaceous, intraneuronal inclusions called Lewy Bodies, which contain misfolded proteins, α-synuclein and are extensively ubiquitinated (Jin *et al.*, 2005, Fasano *et al.*, 2007). The aetiology of PD is still unknown but is thought to arise from a complex combination of genetic, environmental and inflammatory factors, with age being the most significant risk factor (Dauer and Przedborski, 2003, Onyango, 2008). An-early onset form of PD, called Autosomal Recessive Juvenile Parkinson's Disease (ARJPD), displays an aetiology more firmly rooted in inherted genetic mutations related to the proteasome protein degradation pathway (*parkin*, *DJ-1* and *PINK1* gene mutations) but such definite genetic links in sporadic PD have yet to be established (Gasser, 2007, Lesage and Brice, 2009).

Parker *et al.* (2008) have described a 40% decrease in activity of complex I that is widespread in the PD brain. Consistent with this, chronic exposure of experimental animals to complex I inhibitors, such as rotenone and 1-methyl-4-phenyl-1,2,3,6-tetrahydropyridine (MPTP) can recapitulate many of the behavioural and histopathalogical features of PD (Langston *et al.*, 1999, Fleming *et al.*, 2004). Oxidative stress also seems to play an important role; increased iron, lipid peroxidation and oxidised proteins, are common in the SNpc of PD brains (Onyango 2008). Parkinson's disease brains also display reduced levels of GSH in the

midbrain (Zeevalk *et al.*, 2008), suggesting normal antioxidant mechanisms have been overwhelmed. In addition, it has been shown by our lab, and others, that synaptic mitochondria (SM) are more vulnerable to inhibition, relative to non-synaptic mitochondria (NSM). Synaptic mitochondria have lower complex I inhibition thresholds, compared to NSM; SM require just 25% complex I inhibition before OXPHOS is affected, while NSM have a threshold of 60% (Davey and Clark, 1996, Davey *et al.*, 1997, 1998). Furthermore, 40% inhibition of Complex I activity in synaptosomes depolarised with 4-aminopyridine causes a three-fold increase in calcium-independent release of glutamate (Kilbride *et al.*, 2008), indicating a potential role for excitotoxicity in the pathogenesis of PD.

The wide acceptance of mitochondrial dysfunction as a pathophysiological feature of PD has implicated a role for mitochondrial dynamics. There is a general consensus that neuronal death in the nigrostriatal pathway begins in synaptic terminals of long, unmyelinated axons (Braak *et al.*, 2004). This predisposes cells to problems of mitochondrial transport and energy deficiency (Van Laar and Berman, 2009). Furthermore, the complex I lesion in PD is thought to arise, at least partially, from mtDNA mutations, given the over-representation of this enzyme within the mitochondrial genome (Smigrodzki *et al.*, 2004, Swerdlow, 2009a). Dysfunctional mitochondrial dynamics can lead to mtDNA abnormalities, as fusion is required for tolerance of mtDNA mutations (Chen *et al.*, 2010). Indeed, in their studies of AD cell cybrids, Trimmer *et al.* (2000) also created sporadic PD cell cybrids and reported the generation of cytoplasmic inclusions, and swollen, dysfunctional mitochondria with broken cristae. Thus, mtDNA from PD patients precipitated abnormal mitochondrial morphology. Complex I inhibition with rotenone or MPP^+ can lead to mitochondrial fragmentation in neurons (Barsoum *et al.*, 2006), but it is not known if they are still fusion competent.

Much of the insight gained into the role of mitochondrial dynamics in PD has been through the study of the rare, genetic Autosomal Recessive Juvenile Parkinson's Disease (ARJPD). This familial form of PD is thought to arise in some cases from mutations in genes encoding PINK1/parkin, which are thought to regulate mitochondrial fusion and degradation by ubiquitination of Mfn (Twig *et al.*, 2008b). Parkin is recruited to mitochondria (especially when depolarised) by unknown means, whereas PINK1 resides in the mitochondria (Burbulla *et al.*, 2010). Interestingly, PINK1 has been shown to interact with the

Miro/GRIF1 complex I mammalian cells, even when expressed without its mitochondrial targeting sequence, thus assigning it a potential role in mitochondrial trafficking (Weihofen *et al.*, 2009). Mutation of either PINK1 (proposed to activate E3 ligase parkin by phosphorylation), parkin, or both, precipitates a severe phenotype in *Drosophila*, including flight muscle degeneration, dopaminergic neuron degeneration and swollen mitochondria with disrupted cristae (Chen and Chan, 2009, Ziviani *et al.*, 2010). Despite these findings, mouse models carrying PINK1 mutations exhibit surprisingly mild phenotypes. Gispert *et al.* (2009) report that PINK1 deficient mice exhibit impairment of ETC complex activities, mitochondrial $\Delta\Psi_m$ and ATP generation in old age but in the absence of neurodegeneration. Moreover, primary neurons from these mice exhibit no morphological differences in mitochondria, except under conditions of proteasomal stress, during which PINK1-null neurons show increased mitochondrial swelling and aggregation. It is possible that this pathway is not as important for dynamic regulation of mouse mitochondria. Interference with PINK1 precipitates more pronounced phenotypes in HeLa cells (Exner *et al.*, 2007); PINK1 knock down results in fragmented mitochondria with aberrant cristae, which can be reversed by exogenous expression of wild type PINK1 but not the PD mutant. In addition, HSFs from ARJPD patients also exhibited fragmented mitochondria which could only be rescued by wild type parkin and PINK1.

Similar to PINK1 mutations, parkin mutations do not precipitate fragmented mitochondrial phenotype in mouse models. Parkin$^{-/-}$ mice show no mitochondrial morphological abnormalities, despite a significant decrease in complex I and IV subunit expression and decreased respiratory capacity (Palacino *et al.*, 2004). In contrast, parkin-null HeLa cells exhibit severely impaired mitophagy (Geisler *et al.*, 2010), while neuroblastoma cells exhibit mitochondrial fragmentation owing to increased DRP1-mediated fission (Lutz *et al.*, 2009). Strangely, HSFs from parkin-mutant PD patients exhibit *increased* branching of mitochondria, but increased fragmentation compared to controls when exposed to rotenone (Mortiboys *et al.*, 2008). This echoes the observations of Wang *et al.* (2009b), who saw hyperfusion of mitochondria from HSFs of AD patients, suggesting a common compensatory mechanism for mitochondrial dysfunction that is present in skin cells but absent in neurons.

Finally, another mutation giving rise to ARJPD is in a gene encoding DJ1, a highly conserved cytosolic protein with a number of reputed functions, including modulation of transcription, protein chaperoning, regulation of mitochondrial homeostasis and modulation of basal autophagy (Burbulla *et al.*, 2010). Krebiehl *et al.* (2010) have shown that DJ-1 knock down in MEFs leads to decreased respiratory rates, impaired $\Delta\Psi_m$, loss of mitochondrial interconnectivity, impaired lysosomal activity and reduced mitochondrial clearance by autophagy. Neuroblastoma M17 cells were also shown to have reduced resistance to oxidative stress when DJ-1 was depleted (Canet-Aviles *et al.*, 2004). This protein relocated to mitochondria when in wild type cells treated with paraquat or MPP^+ (complex I inhibitors) and promoted survival, while knock out cells exhibited significantly higher cell death.

Thus, it is clear that more research is needed if the importance of mitochondrial dynamics in PD is to be fully appreciated. In *Drosophila*, mutation of PD-relevant genes precipitates Parkinsonian phenotype with impaired mitochondrial dynamics. Studies from mammals are sometimes contradictory but a trend has emerged implicating genetic PD-relevant proteins in regulation of mitochondrial dynamics and turnover *via* mitophagy. The relevance of these results to sporadic PD, which ultimately constitutes the vast majority of PD cases, is undetermined. However, given the importance of mitochondrial dynamics in organellar regulation and quality control, it seems likely that this aspect of mitochondrial function holds clinical significance.

5.1.4 Mitochondrial Dysfunction and Dynamics in Huntington's Disease

Huntington's disease is a progressive neurodegenerative disorder arising from a cytosine, adenine, and guanine (CAG)-repeat expansion in the *htt* gene, which encodes a mutant huntingtin (mthtt) protein with a poly-glutamine tail. Its expression leads to the selective loss of γ-aminobutyric acid (GABA)-ergic medium spiny neurons in the striatum, combined with cortical degeneration, which precipitates in sufferers a number of debilitating and ultimately fatal symptoms, including progressive chorea, dementia, seizures and psychiatric disturbances (Bossy-Wetzel *et al.*, 2008). The length of the poly-glutamine repeat is directly proportional to disease severity, with a minimum of ~36 repeats necessary for emergence of symptoms (Penney *et al.*, 1997).

The exact function of wild type htt has been difficult to define, given the broad expression of the protein and its multiple cellular locations, from the cytoplasm, to mitochondria, the the nucleus and the plasma membrane. It is also not known if the mutation leads to a loss or a gain of function, though potentially both could occur (Bossy-Wetzel *et al.*, 2008). Several lines of evidence indicate that expression of mthtt induces mitochondrial dysfunction. Patients present with elevated lactate levels, and reduced glucose utilisation in affected brain areas, while mitochondria from patient samples show reduced calcium buffering capacity and reduced $\Delta\Psi_m$. Post mortem brains show decreased activity of complexes II, III and IV (Gu *et al.*, 1996), while chronic administration of complex II inhibitor 3-NP replicates HD brain lesions with striatal specificity in animal models (Borlongan *et al.*, 1997).

Hungtingtin seems to have roles both in mitochondrial fusion and in trafficking in neurons. Wild type htt has been reported to become phosphorylated at Ser^{421} by the Akt and promote anterograde vesicle trafficking through recruitment of kynesin and adaptin to microtubules (Colin *et al.*, 2008). Interestingly, constitutive phosphorylation of mthtt at Ser^{421} restores this transport function, despite retention of the poly-glutamine tail (Zala *et al.*, 2008). However, mutant htt has been shown to cause aggregate 'road-blocks' that inhibit trafficking of mitochondria and cause mitochondrial fragmentation (Chang *et al.*, 2006). Furthermore, expression of mthtt causes abnormal mitochondrial ultrastructure, impaired Ca2+ buffering, bioenergetic defects and mtDNA deletions (Bossy-Wetzel *et al.*, 2008). Two very recent studies have indicated a direct interaction of mthtt with DRP1. Song *et al.* (2011) report the mthtt abnormally interacts with DRP1 in a mutation-derived gain of function and increases its enzymatic function. They also showed that this effect was poly-glutamine length dependent; 17-glutamine long repeats had no effect, while those that were 97 repeats long caused complete fission. In addition, anterograde and retrograde transport were seriously affected. This interaction was further supported by Shirendeb *et al.* (2011) who showed an increase in the GTPase activity of DRP1 upon interaction with mthtt, leading to reduced mitochondrial biogenesis and axonal degeneration.

Overall, understanding the interaction between mitochondrial bioenergetics and dynamics is of utmost importance in neurodegeneration. The destructive cascade that follows mitochondrial dysfunction has direct effects on mitochondrial morphology, fission, fusion

and transport, which can only serve to potentiate this cascade. Importantly, correct regulation of mitochondrial dynamics can abrogate or compensate for some aspects of mitochondrial dysfunction; fission can exclude sub-optimal mitochondria from the greater network, while fusion can aid in the tolerance of mtDNA mutations and rescue ailing organelles through functional complementation. Thus, elucidating the mysteries behind these processes might provide new therapeutic targets for neurodegenerative disorders.

5.2 Aims of the Chapter

Although neurons may exhibit slower basal rates of mitochondrial fusion than other tissues (Karbowski *et al.*, 2004a), it is nonetheless an extremely important aspect of mitochondrial function in neuronal cells. Through discussion of mitochondrial dynamics in neurodegeneration, it is clear that bioenergetic dysfunction can seriously impact mitochondrial fission and fusion. Furthermore, each of the neurodegenerative illnesses described exhibit reduced activity in one particular ETC enzyme over the others but it is not known to what degree this enzyme inhibition impacts mitochondrial fusion. With particular reference to PD, complex I in brain mitochondria has been shown to tolerate a certain level of inhibition before significant impact on respiration, but it is not known if a threshold effect exists in relation to mitochondrial fusion rates. To address these issues, this study aimed to achieve the following:

1. **Quantify the effects of ETC inhibition on mitochondrial fusion rates in primary cortical neurons.** The culture and transfection of primary cortical neurons from the brains of neonatal rat pups were optimised for the quantification of mitochondrial fusion rates using the PA-GFP-based confocal assay previously described. Neurons were exposed to ETC/OXPHOS inhibitors and mitochondrial fusion rates were compared to those of controls.
2. **Attempt to find correlates between mitochondrial inhibition-induced fusion deficit and $\Delta\Psi_m$/ATP levels.** Neurons were exposed to inhibitors and assessed for changes in $\Delta\Psi_m$/ATP levels, as previously described, to assess whether the observed fusion perturbation was correlated to changes in these important indicators of mitochondrial integrity.
3. **Assess whether there exists a threshold of complex I inhibition, above which fusion is compromised.** A dose-response titration of complex I inhibitor piericidin A was conducted to attain the maximal complex I inhibition tolerable by neurons before fusion was adversely affected.

5.3 Methods

5.3.1 Primary Cortical Neuron Culture

Primary cortical neurons were isolated from the brains of one day old neonatal Wistar rats. Rats were decapitated using surgical scissors and the cortices carefully extracted using fine-tipped curved forceps. The tissue was cross-chopped and incubated for 25 min in 0.3mg/ml trypsin/PBS, at 37°C. The trypsinisation process was halted by the addition of increasingly concentrated solutions of trypsin inhibitor (PBS containing 0.03mg/ml soybean trypsin inhibitor, 0.06mg/ml DNase, and 3mM $MgSO_4$, followed by PBS containing 0.1mg/ml soybean trypsin inhibitor, 0.2mg/ml DNase, and 10mM $MgSO_4$. The cortical suspensions were passed through 40μm nylon mesh strainers and the filtrates were centrifuged at 2000 x g for 3 min, at room temperature. The resultant pellets were resuspended in 1.5ml Neurobasal medium-A (NBMA, Invitrogen), supplemented with 10% horse serum (HS, Gibco), 2mM Glutamax (Gibco), penicillin-streptomycin solution (100 units/ml penicillin G, 0.1 mg/ml streptomycin sulfate) and 2% B27 (Invitrogen) and counted, using trypan blue as a diluent. Each brain yielded approximately 3 – 5 x 10^6 cells. Immediately after isolation, cells were plated in aforementioned medium, on 13mm glass borosilicate glass coverslips in 24-well plates or in 35mm glass bottomed μ-dishes at a cell density equivalent to the total extract from one cortex per 24 well plate/per three 35mm μ-dishes. Each coverslip/dish was coated in 40ug/ml poly-l-lysine (MW 70 – 150kDa) for two hours prior to seeding of cells. After three hours, medium was replaced with NBMA supplemented with 1% HS (all other supplements identical). After 24h, cells were exposed to 20μM cytosine beta D-arabinofuranoside (Ara-C) in 1% HS NBMA to discourage the proliferation of glial cells. After a further 24h, Ara-C was removed and cells maintained in Ara-C-free 1% HS NBMA, with 50% medium changes every 3-4 days. Cells were used for experiments at DIV 8 - 11.

5.3.2 Transfection

Neurons were transfected directly after isolation from cortices using Amaxa's Rat Cortical Neuron Nucleofection system. Cells were transfected with 4μg of each plasmid (PA-GFP, DsRed) at 5 x 10^6 cells per transfection and plated on poly-l-lysine coated 35mm glass-

bottomed μ-dishes at a density of 2.5 x 10^6 cells per dish. Two to three hours post nucleofection, medium (10% HS NBMA) was refreshed to remove cell debris. After 24h, cells were exposed to 20μM cytosine β-D-arabinofuranoside (Ara-C) in 10% HS NBMA to discourage the proliferation of glial cells. After a further 24h, Ara-C was removed and cells maintained in Ara-C-free 1% HS NBMA, with 50% medium changes every 3-4 days. Cells were used for experiments at 8-11 DIV.

5.3.3 Isolation of Rat Brain Mitochondria and Synaptosomes

Non-synaptic mitochondria (NSM) and synaptosomes were prepared as per Lai and Clark (1979) , with modifications. Two female Wistar rats were killed by cervical dislocation, and the brains extracted and suspended in 40ml ice-cold STE buffer (320mM Sucrose, 10mM Tris, 1mM EDTA, pH 7.4). The brains were chopped on ice, with several changes of buffer to remove excess blood. They were then homogenized in STE using 40ml glass Kontes tissue grinder. The homogenate was centrifuged at 823 x g for 3 min in a Sorvall RC50 centrifuge fitted with SS34 rotor to remove nuclei and unwanted debris. The supernatant was centrifuged at 10,085 x g for 10 min. The crude mitochondrial pellet was then resuspended in 9ml STE buffer and layered on top of a discontinuous Ficoll gradient (fig. 5.1), which was centrifuged in a Sorvall Discovery 100 centrifuge, fitted with an AH-629 rotor, at 104,200 x g for 45 min at 4 °C. The synaptosomal layer was extracted, resuspended in 30ml STE and centrifuged at 13,173 x g for 10 minutes, while the NSM pellet was resuspended in 1ml STE, homogenised in a Wheaton 2ml homogeniser and centrifuged at 16,000 x g for five minutes. Finally both pellets were resuspended in 1ml STE and stored at -80°C until required.

5.3.4 Complex I Assay

The specific activity of Complex I in NSM and synaptosomes was determined by the method of Ragan *et al.* (1987), with modifications. The spectrophotometric assay follows the oxidation of reduced nicotinamide adenine dinucleotide (NADH) to NAD^+ by complex I (with Decyl Q as an artificial electron acceptor), which is reflected as a decrease in

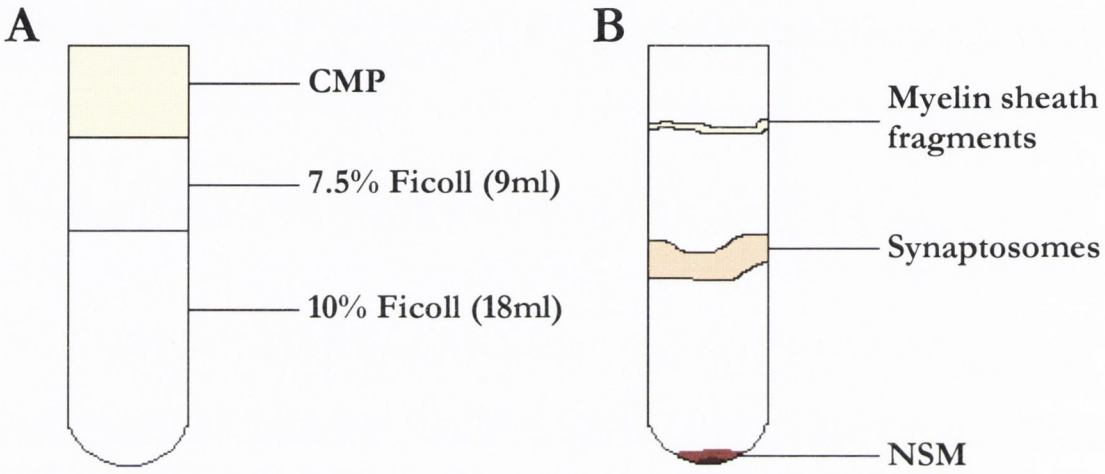

Figure 5.1: The discontinuous Ficoll gradient. The crude mitochondrial pellet (CMP) is layered on top of the Ficoll gradient (A). Centrifuging at 28,000 RPM for 45 minutes results in the fractionation of the CPM into myelin, synaptosomes and non-synaptic mitochondria (NSM), as shown in (B).

absorbance at 340nm. Samples were thrice cryolysed in liquid nitrogen before 50μg (NSM) or 100μg (synaptosomes) were added to a 1ml plastic cuvette containing, in a final volume 980μl, assay buffer (25mM Potassium Phosphate, 10mM Magnesium Chloride, pH 7.4), 1mM potassium cyanide, 150μM NADH, 25mg/ml BSA and piericidin A in concentrations ranging from 10nM to 1μM (with the exception of control samples, which contained no piericidin A).

The assay was carried out at 37°C in a Cary 300 Bio UV-Visible Spectrophotometer, using the accompanying Cary WinUV Varian Kinetics Application Software. The basal rates of ΔAbs_{340} were monitored in the samples for two minutes before the redox reaction was initiated by the addition of 50μM Decyl Q. The reaction was monitored for three minutes (NSM) or 10 minutes (synaptosomes) before 10μM rotenone was added to each sample to inhibit complex I and obtain rotenone-insensitive rates. The rotenone-insensitive rates of ΔAbs_{340} were subtracted from the rotenone-sensitive rates and specific activities expressed as μmol/min/mg.

5.3.5 Confocal Microscopy

5.3.5.1 Quantification of Mitochondrial Fusion Rates

Mitochondrial fusion rates were quantified as described in previous chapters but with modifications. Imaging conditions differed from those used for HeLa cells as follows; z-stacking was increased from 5 slices to 8, owing to the more spherical morphology of the neuronal cell body; Kalman filter of 3 was applied to images to decrease background arising from the dense meshwork of neuronal processes containing DsRed/PA-GFP-positive mitochondria surrounding the cell bodies of interest; a zoom of 2x was applied to better visualise the smaller neuronal cell bodies and finally, an extra time point of 45 minutes post-photo-activation was included to account for the previously reported slower rate of neuronal mitochondrial fusion (Karbowski *et al.*, 2004a). Photo-activation conditions differed also, requiring just 1% power output of the 405nm laser for 5 seconds.

Conditions were further modified for the piericidin A titration, as it was deemed necessary to increase the sensitivity of the assay to detect more subtle changes in fusion rates. This was achieved by increasing the zoom applied to the imaging field to 3x and by the photo-activation of a smaller ROI (2.3μm^2) with a decreased 405nm laser power output of 0.5%. This produced a faster rate of pixel intensity decrease in control cells and thus allowed for the detection of less pronounced yet significant changes in fusion rates.

5.3.5.2 Quantification of $\Delta\Psi_m$

Quantification of $\Delta\Psi_m$ was performed as described in previous chapters, with modifications. Neurons were incubated with 20nM TMRM for 40 minutes rather than an hour before a change to 5nM TMRM for imaging. Imaging conditions were as for HeLa cells, except the z-stack included 8 slices rather than 7 and the 543nm laser was set to 2% power output. Finally, pixel intensity changes owing to $\Delta\Psi_m$ changes were monitored in cell bodies of neurons rather than in averages of entire fields as with HeLa cells. This was because neuronal cultures are heterogeneous and contain glial cells which contribute to the pixel intensities in each field, thus measuring pixel intensities of entire fields would yet erroneous results.

5.4 Results

5.4.1. Optimisation of Primary Neuron Culture

Primary cortical neurons from one-day old neonatal rat pups were successfully cultured through a series of optimisation steps, summarised in fig. 5.2. Glial contamination was the first issue addressed. Cells were cultured for eight days in the absence (fig. 5.2A), or presence of 20μM cytosine β-D-arabinofuranoside (Ara-C) (fig 5.2B). A third group were exposed to Ara-C for just 24 hours one day after plating, after which time the Ara-C was removed (fig 5.2C). Cells were fixed and immunostained for neuron-specific class III β-tubulin (TuJ1) and glial acidic fibrillary protein (GFAP) to assess culture purity. Cells spared from Ara-C treatment exhibited excessive astrocytic proliferation, whereas constant exposure to Ara-C had deleterious effects on neuronal viability. Cells exposed to Ara-C for 24 hours thrived, with minimal glial contamination, indicating transient Ara-C exposure was the most appropriate treatment.

The next issue addressed was the substrate on which cells were plated. Coverslips were prepared by coating with 40μg/ml poly-L-lysine (PLL) of 15 – 30kDa molecular weight for one hour at 37°C, followed by overnight drying. However, cells cultured on these coverslips grew in poorly attached clumps (fig. 5.2D). To remedy this, coverslips were prepared using PLL of a higher molecular weight (70 – 150kDa) according to the original protocol or by coating for 2 – 3 hours at 37°C prior to cell plating (i.e. without a drying period). Cells plated on pre-dried coverslips showed reduced but still significant clumping (fig. 5.2E), while those cultured on coverslips prepared without a drying period showed no clumping and evenly dispersed cell somata (fig. 5.2F). This latter PLL coating regime was used for the following experiments.

Figure 5.2G is representative of cultures routinely prepared following these optimisation steps. Cells were plated at high density (1.6 – 2 x 10^6 cells/35mm dish) to promote high cell viability, particularly post-transfection, with an average neuronal purity of 95 $\pm$ 1.59%.

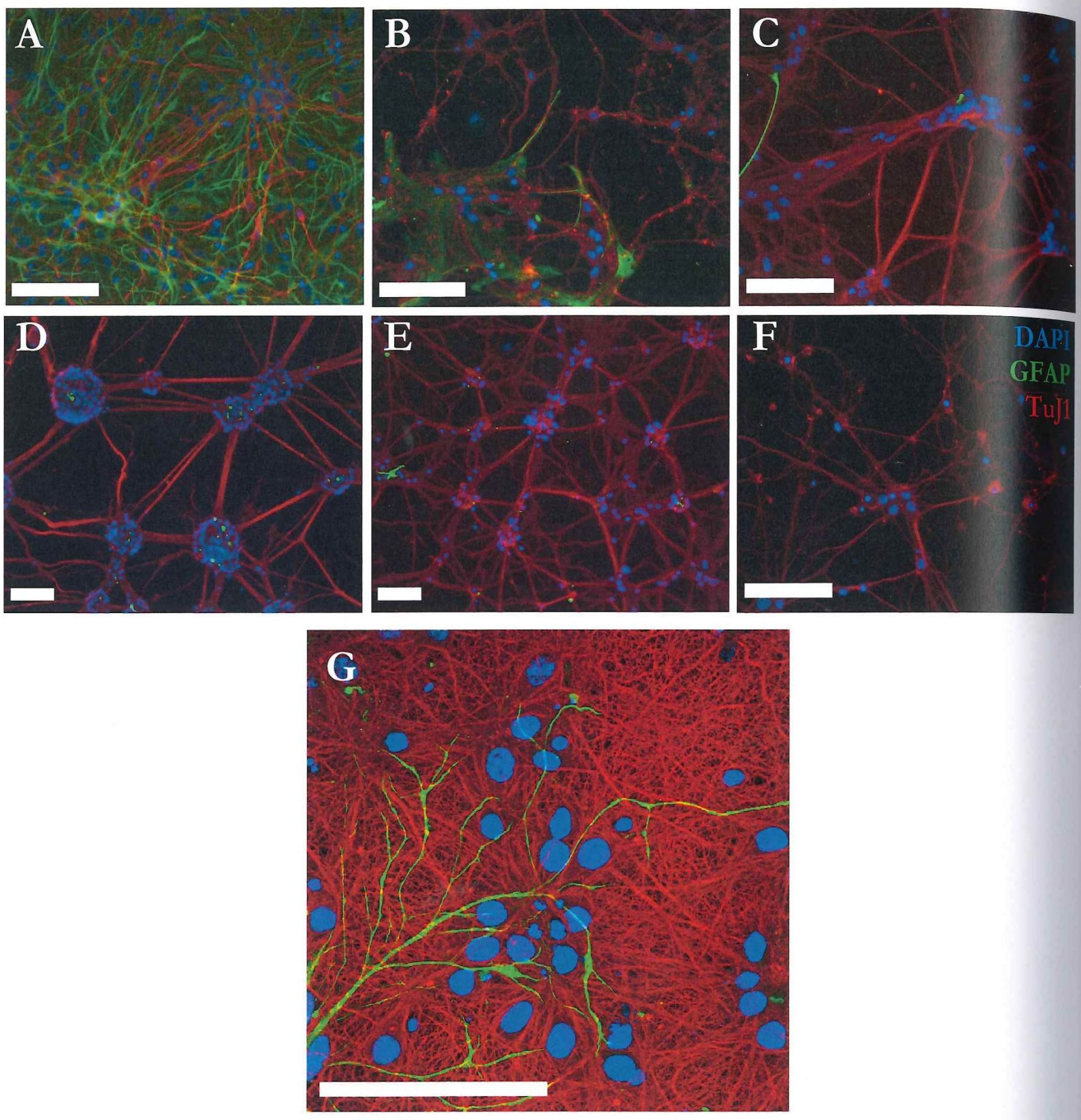

Figure 5.2: Optimisation of primary cortical neuron culture. Cells were cultured under various conditions for one week and immunostained for neurons-specific class III β-tubulin (TuJ1, red) and glial fibrillary acidic protein (GFAP, green), with nuclear counterstain 4,6-diamidino-2-phenylindole (DAPI, blue). (A) Cells cultured in absence of Ara-C showed excessive glial contamination. (B) Cells cultured in the presence of 20μM Ara-C showed reduced glial contamination but also reduced viability in neurons (C) Cells exposed to 20μM Ara-C for just 24 hours one day after plating thrived in the absence of excessive glial proliferation. (D) Cells cultured on coverslips pre-coated with low molecular weight (15 -30 kDa) poly-L-lysine (PLL), followed by an overnight drying period, grew in poorly attached clumps. (E) Cells cultured on coverslips prepared in the same way but with higher molecular weight (70 – 150kDa) PLL grew in visibly smaller clumps but still showed suboptimal attachment. (F) Cells cultured on coverslips prepared by 2 – 3 hour incubation in high molecular weight PLL, without a drying period showed excellent attachment and no clumping. (G) Image representative of cultures regularly prepared following optimisation steps. Scale 100μm.

5.4.2. Effects of Inhibition of Oxidative Phosphorylation on Mitochondrial Fusion Rates in Primary Cortical Neurons

Mitochondrial fusion rates in neuronal cell somata were assessed at resting conditions and under conditions of mitochondrial inhibition. At rest, neurons exhibited active mitochondrial fusion (fig. 5.3), although at a significantly slower rate than that of HeLa cells (fig. 5.4), in general agreement with the literature (Karbowski *et al.*, 2004a, Berman *et al.*, 2009). Pixel intensities of photo-activated areas remained at 49.7 $\pm$ 7.12% after 30 minutes, compared to 25.95 $\pm$ 0.65% in HeLa cells. For this reason, fusion was monitored for an additional 15 minutes in neurons (total 45 minutes post-activation), after which time PIs fell to 37 $\pm$ 7.02%, which was not significantly different, statistically, from PIs of HeLa cells at 30 minutes post-activation.

Mitochondrial fusion rates were then assessed in neurons exposed to mitochondrial inhibitors for 20 minutes, as with HeLa cells. Dissipation of $\Delta\Psi_m$ using 5μM FCCP led to complete fragmentation of the mitochondrial network and fusion inhibition, as expected (fig. 5.5). Mitochondrial fusion rates were extremely sensitive to OXPHOS inhibition, with inhibition of complexes I, III, IV and ATP synthase leading to rapid fragmentation of the reticulum and a complete cessation of fusion. Inhibition of complex I with 10μM rotenone (fig.5.6) or 1μM piericidin A (fig 5.7) led to fragmentation of mitochondria and cessation of fusion, but inhibition of complex II with 1mM malonate had no effect (fig 5.8). Inhibition of complex III with 2.4μM antimycin A (fig. 5.9) or 2μM myxothiazol (fig. 5.10) also caused inhibition of fusion with mitochondrial fragmentation, as did inhibition of complex IV with 5mM azide (fig. 5.11) and ATP synthase, with 2μg/ml oligomycin (fig. 5.12).

5.4.3. Effects of Inhibition of Oxidative Phosphorylation on Mitochondrial Membrane Potential in Primary Cortical Neurons

It was found that OXPHOS inhibition not only inhibited mitochondrial fusion, but also promoted dramatically increased fragmentation. Given that mitochondrial depolarisation also had this effect, it was hypothesised that inhibition of complexes I, III and IV was causing more pronounced $\Delta\Psi_m$ dissipation than that observed in HeLa cells. Mitochondrial membrane potential was measured using microscopic measurement of TMRM fluorescence,

Figure 5.3: Representative image of mitochondrial fusion in the neuronal soma at resting conditions. Photo-activated mitochondria of the neuronal soma show a gradual sharing of fluorescent contents over 45 minutes. Scale, main image = 20μm, inset = 5μm.

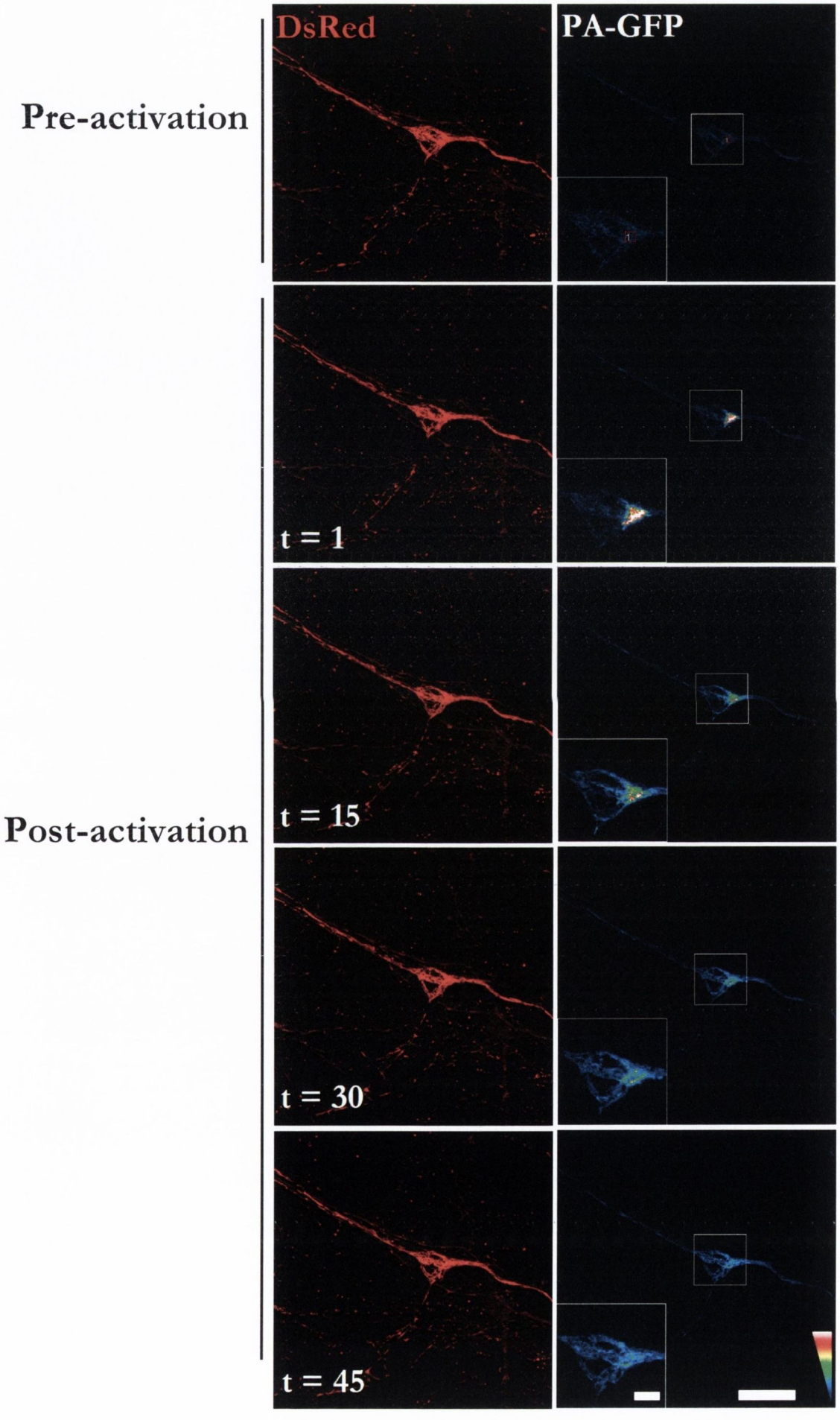
DsRed
PA-GFP
Pre-activation
t = 1
t = 15
Post-activation
t = 30
t = 45

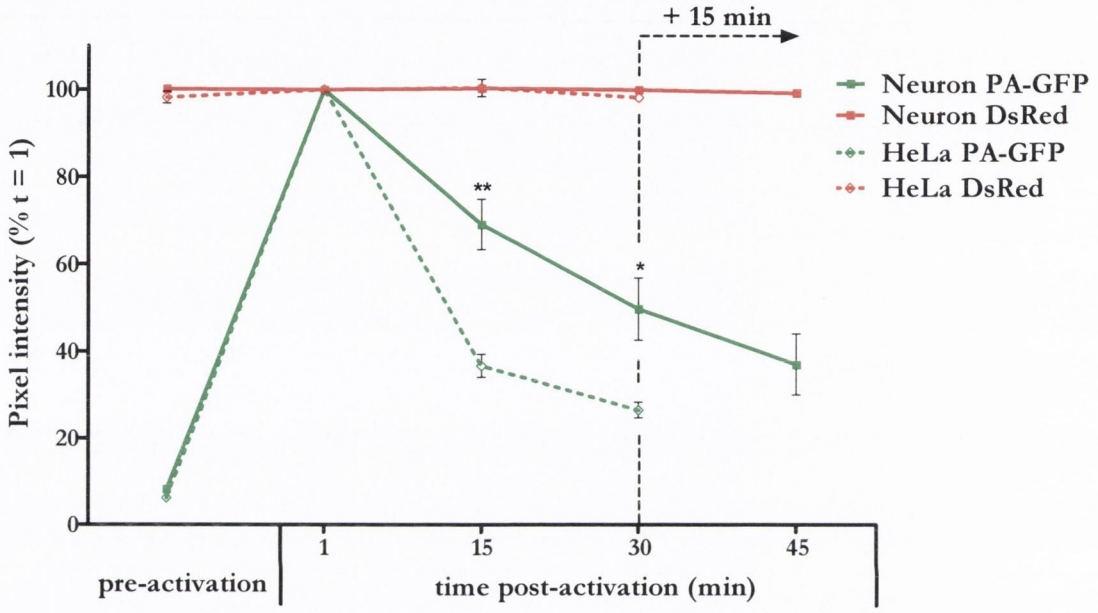

Figure 5.4: Mitochondrial fusion occurs at a slower rate in neurons than in HeLa cells. Comparison of typical quantitative fusion data from HeLa cells (dashed green line) and neurons (bold green line) emphasises the reduced efficiency of mitochondrial fusion in the latter cell type. Pixel intensities of photo-activated regions in neurons are significantly higher than in HeLa cells after 15 and 30 minutes. For this reason, fusion was monitored for an additional 15 minutes post-activation in neurons (45 minutes post-activation in total). Data presented as mean ± SEM, n = 3. Unpaired t-test at each time point. *P<0.05, **P<0.01.

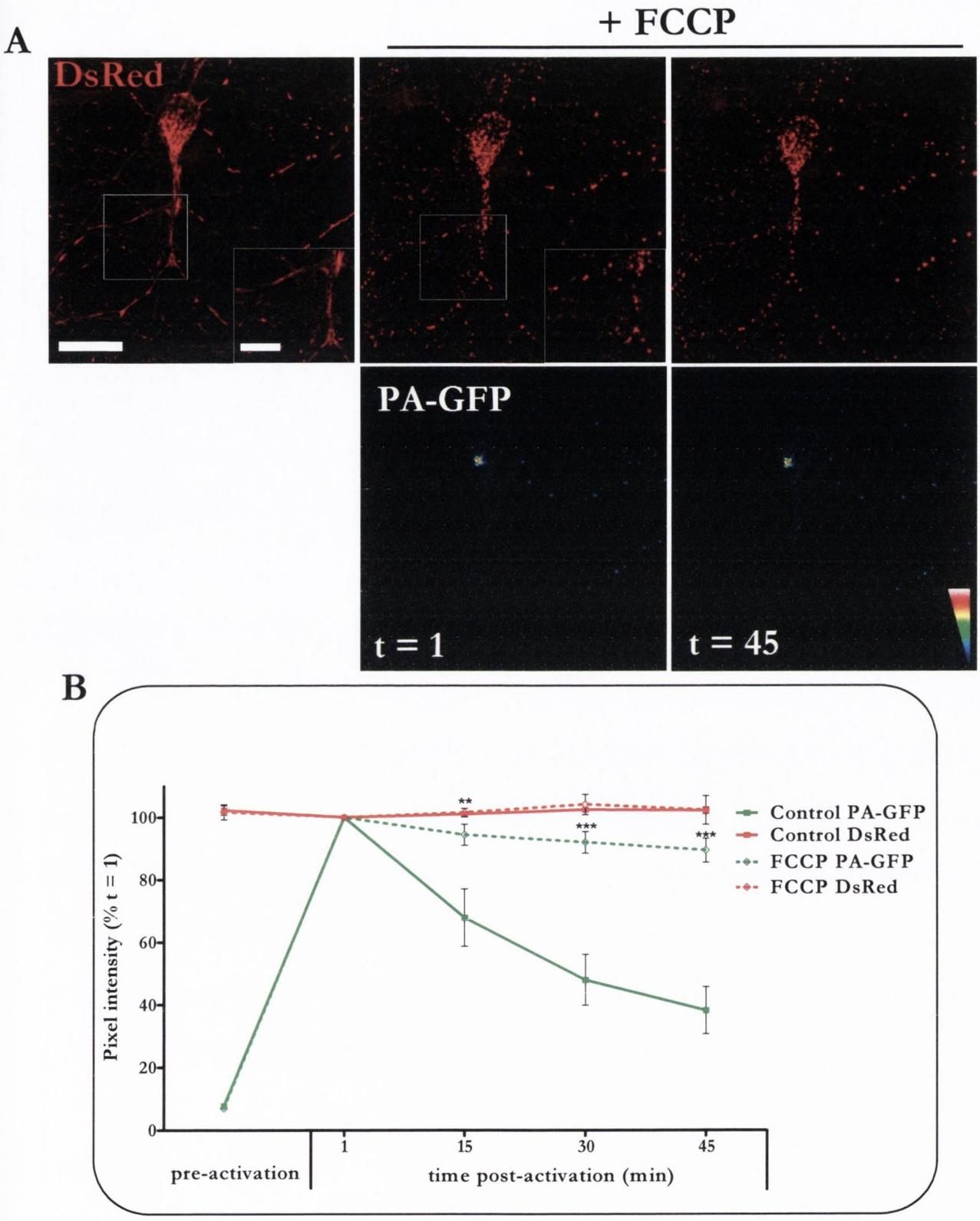

Figure 5.5: Dissipation of $\Delta\Psi_m$ causes mitochondrial fragmentation and inhibits fusion in neurons. (A) Image representative of effects of 20 minute incubation with 5μM FCCP on mitochondrial morphology and fusion in neurons. Mitochondria appear extensively fragmented after FCCP incubation (upper row) and are unable to undergo fusion (lower row). Scale, main image = 20μm, inset = 10μm. (B) Quantitative fusion data shows the inhibition of fusion in FCCP treated cells (dashed green line), compared to controls (bold green line). Data presented as mean ± SEM, n = 3. Unpaired t-test at each time point, with Welch correction for unequal variance. **P<0.01, ***P<0.001.

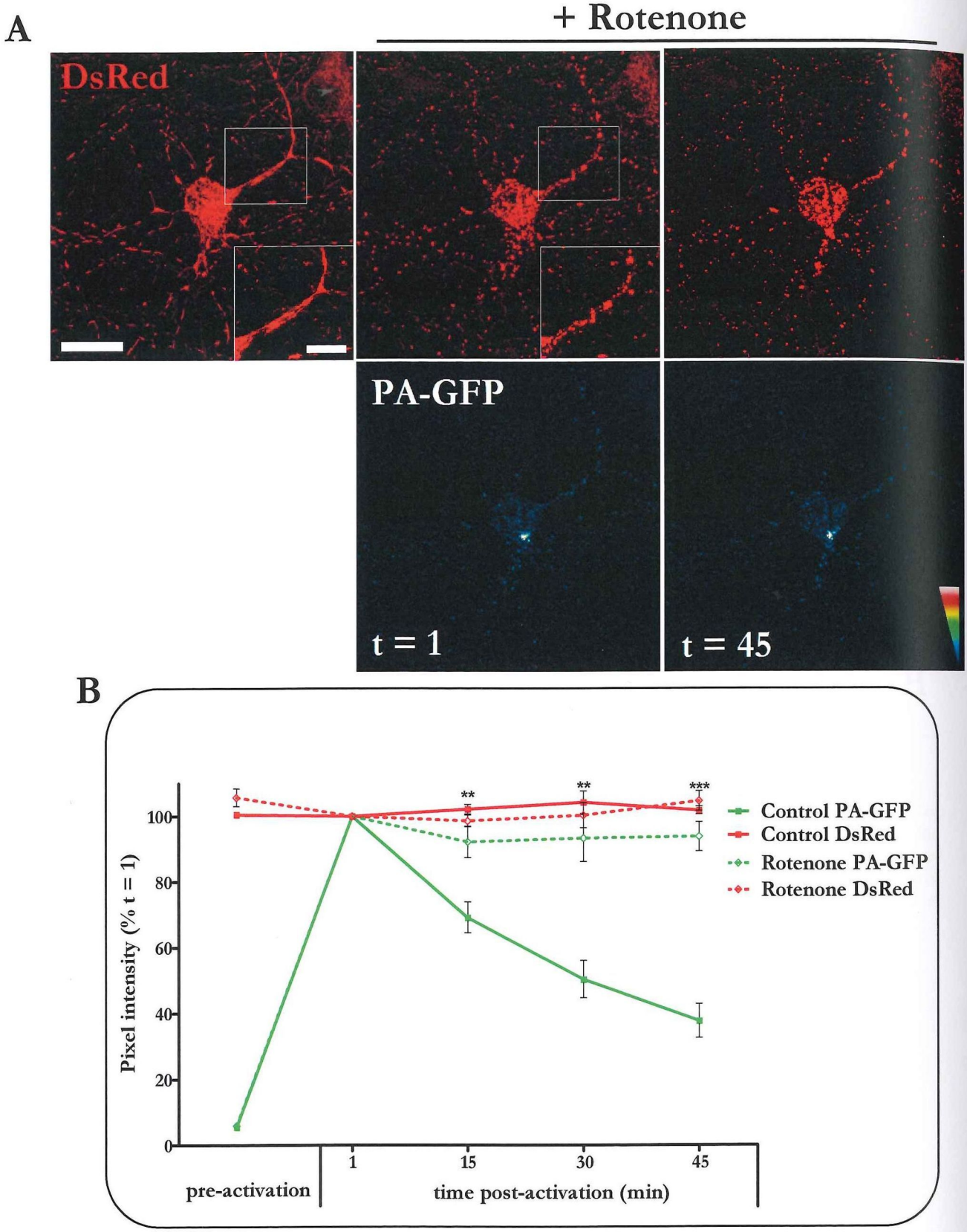

Figure 5.6: Complex I inhibition with rotenone causes mitochondrial fragmentation and inhibits fusion in neurons. (A) Image representative of effects of 20 minute incubation with 10μM rotenone on mitochondrial morphology and fusion in neurons. The mitochondrial reticulum appears fragmented after rotenone incubation (upper row) and is unable to undergo fusion (lower row). Scale, main image = 20μm, inset = 10μm. (B) Quantitative fusion data shows the inhibition of fusion in rotenone-treated cells (dashed green line), compared to controls (bold green line). Data presented as mean ± SEM, n = 3. Unpaired t-test at each time point. **P<0.01, ***P<0.001.

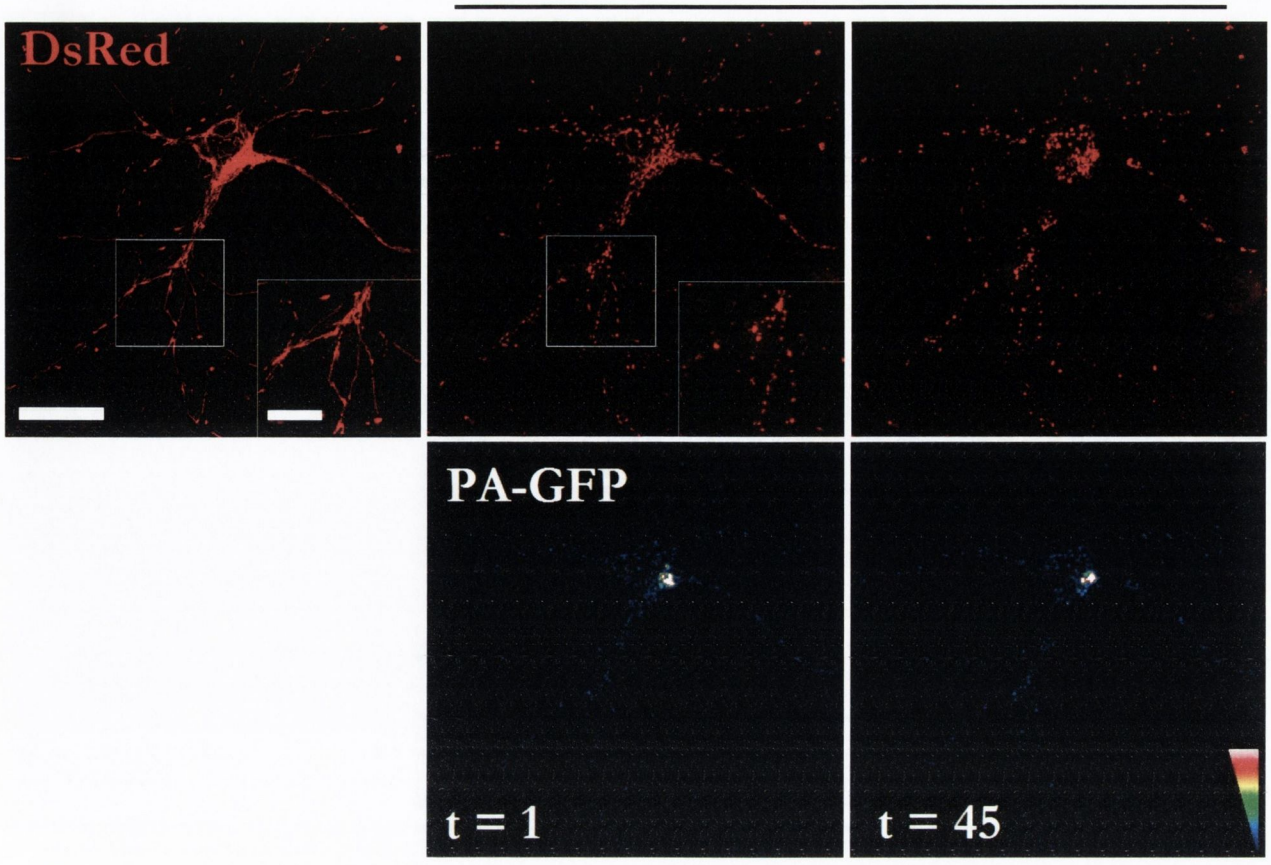

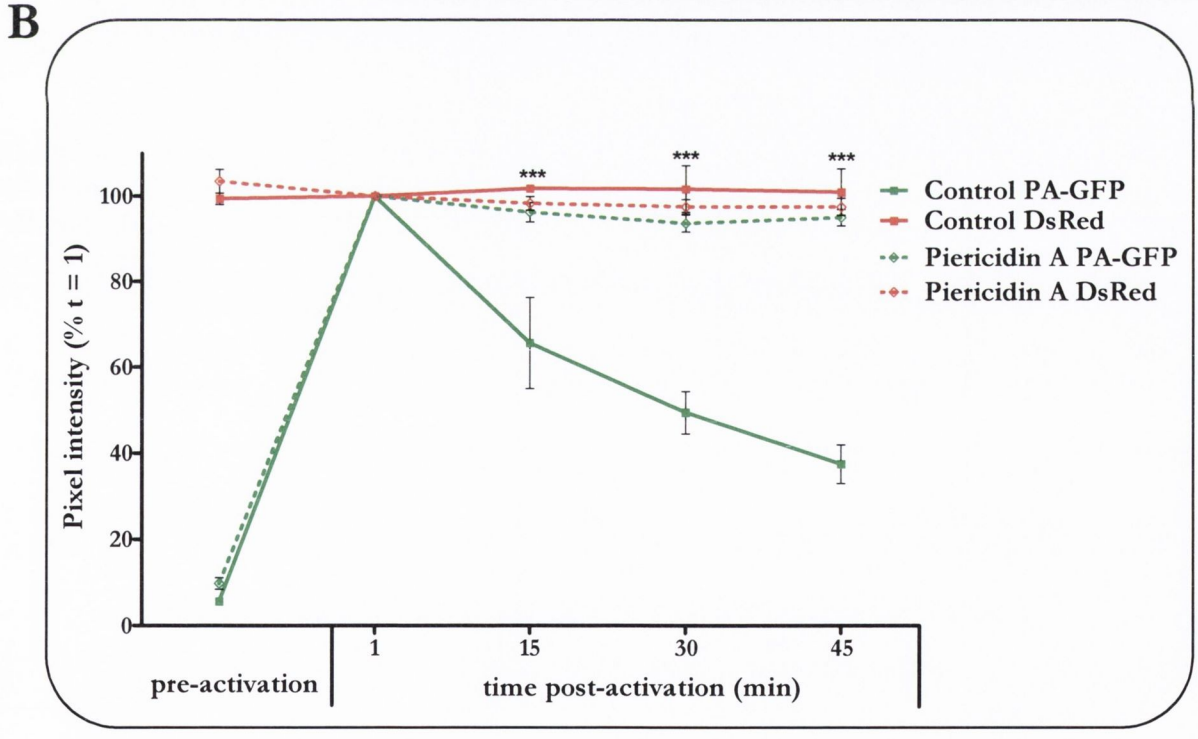

Fig 5.7: Complex I inhibition with piericidin A causes mitochondrial fragmentation and inhibits fusion in neurons. (A) Image representative of effects of 20 minute incubation with 1μM piericidin A on mitochondrial morphology and fusion in neurons. Mitochondria appear extensively fragmented after piericidin A treatment (upper row) and are unable to undergo fusion (lower row). Scale, main image = 20μm, inset = 10μm. (B) Quantitative fusion data shows the inhibition of fusion in FCCP treated cells (dashed green line), compared to controls (bold green line). Data presented as mean ± SEM, n = 3. Unpaired t-test at each time point, with Welch correction for unequal variance. ***P<0.001

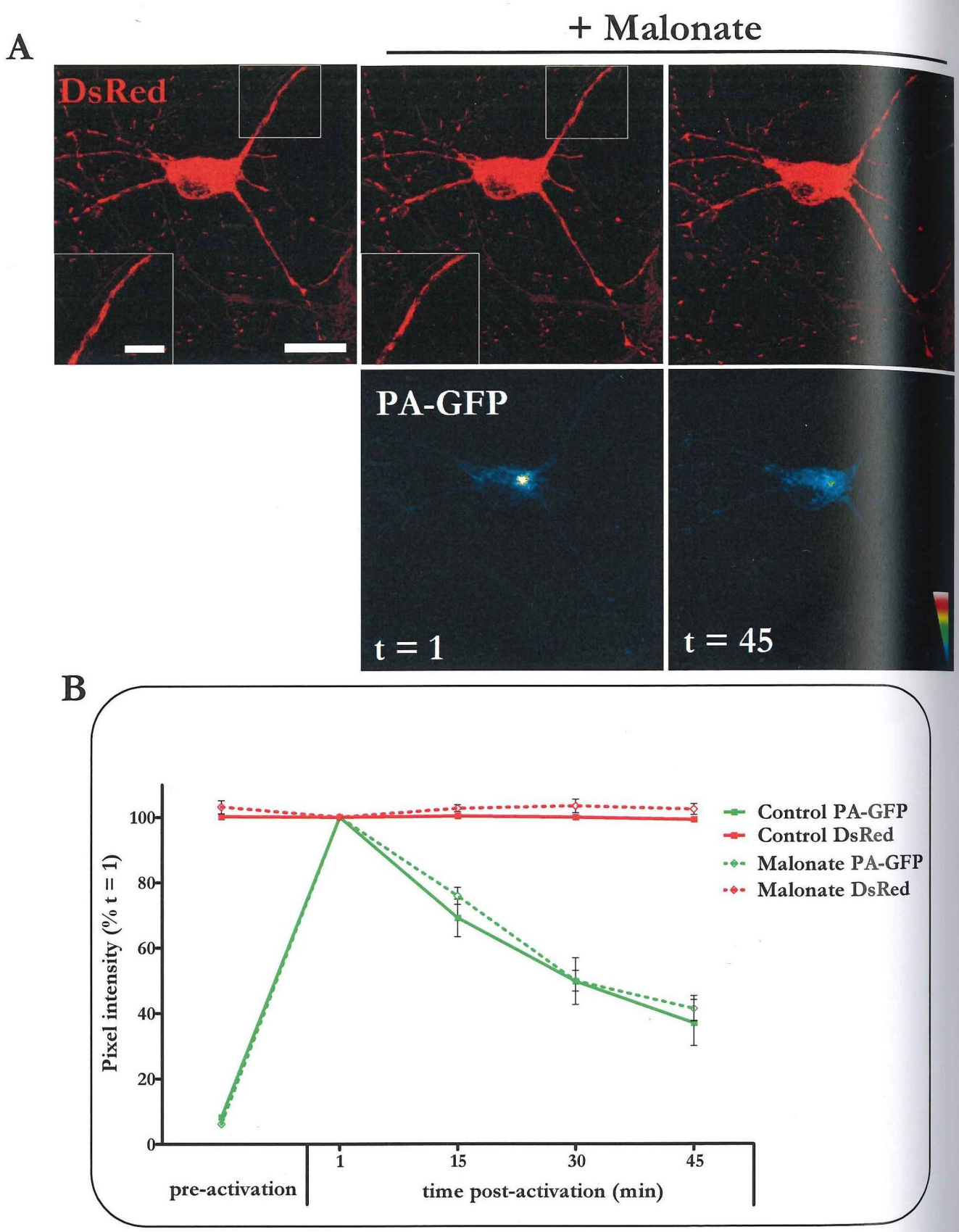

Figure 5.8: Complex II inhibition does not affect mitochondrial morphology or fusion rates in neurons. (A) Image indicates lack of effects of 20 minute incubation with 1mM malonate on mitochondrial morphology and fusion in neurons. Mitochondria remain tubular following malonate incubation (upper row) and can undergo fusion at a healthy rate (lower row). Scale, main image = 20μm, inset = 10μm. (B) Quantitative fusion data shows no inhibition of fusion in malonate treated cells (dashed green line), compared to controls (bold green line). Data presented as mean ± SEM, n = 3. Unpaired t-test at each time point, with Welch correction for unequal variance.

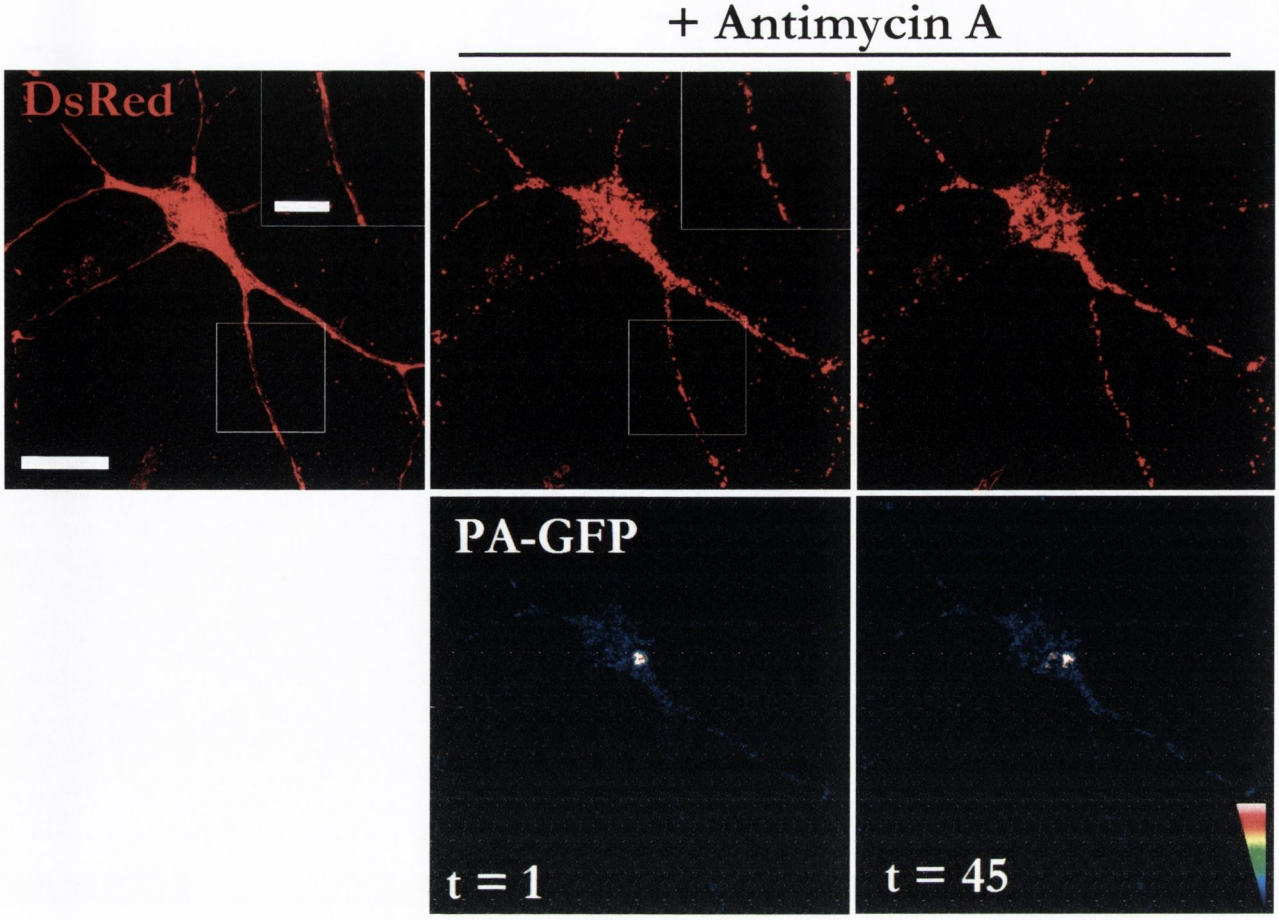

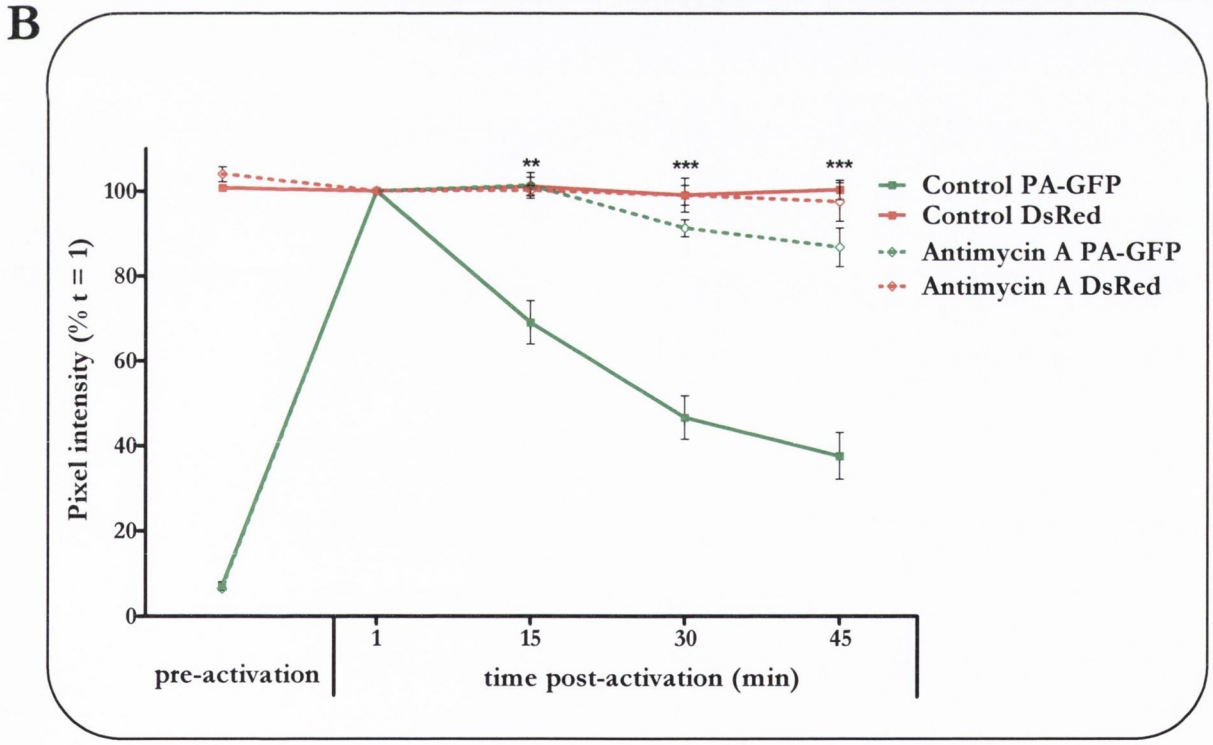

Figure 5.9: Complex III inhibition with antimycin A causes mitochondrial fragmentation and inhibits fusion in neurons. (A) Image representative of effects of 20 minute incubation with 2.4μM antimycin A on mitochondrial morphology and fusion in neurons. Mitochondria undergo extensive fission after antimycin A incubation (upper row) and are unable to undergo fusion (lower row). Scale, main image = 20μm, inset = 10μm. (B) Quantitative fusion data shows the inhibition of fusion in antimycin A treated cells (dashed green line), compared to controls (bold green line). Data presented as mean ± SEM, n = 3. Unpaired t-test at each time point, with Welch correction for unequal variance. **P<0.01, ***P<0.001.

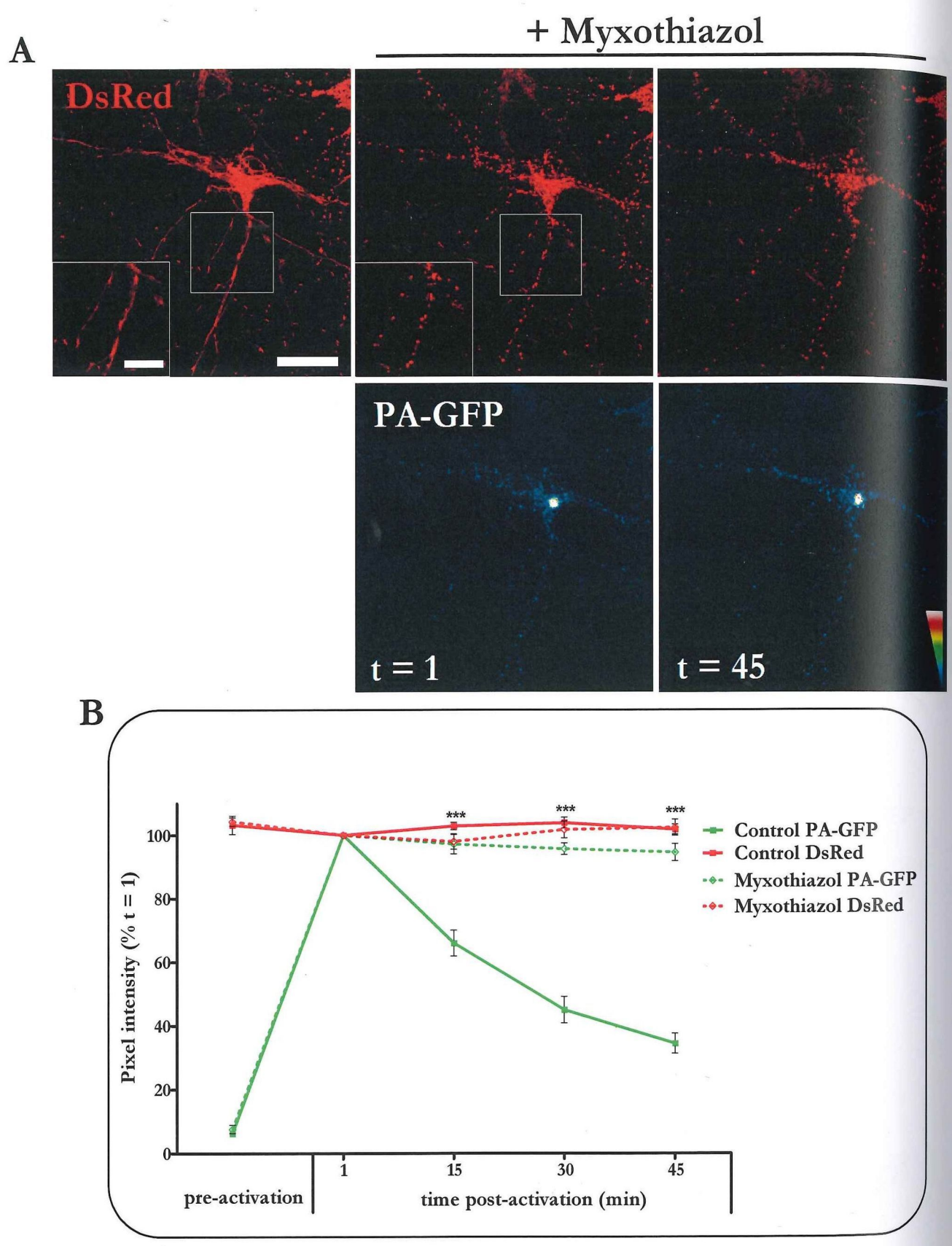

Figure 5.10: Complex III inhibition with myxothiazol causes mitochondrial fragmentation and inhibits fusion in neurons. (A) Image representative of effects of 20 minute incubation with 2μM myxothaizol on mitochondrial morphology and fusion in neurons. Mitochondria appear extensively fragmented after myxothiazol incubation (upper row) and cannot fuse (lower row). Scale, main image = 20μm, inset = 10μm. (B) Quantitative fusion data shows the inhibition of fusion in myxothiazol treated cells (dashed green line), compared to controls (bold green line). Data presented as mean ± SEM, n = 3. Unpaired t-test at each time point, with Welch correction for unequal variance. ***P<0.001

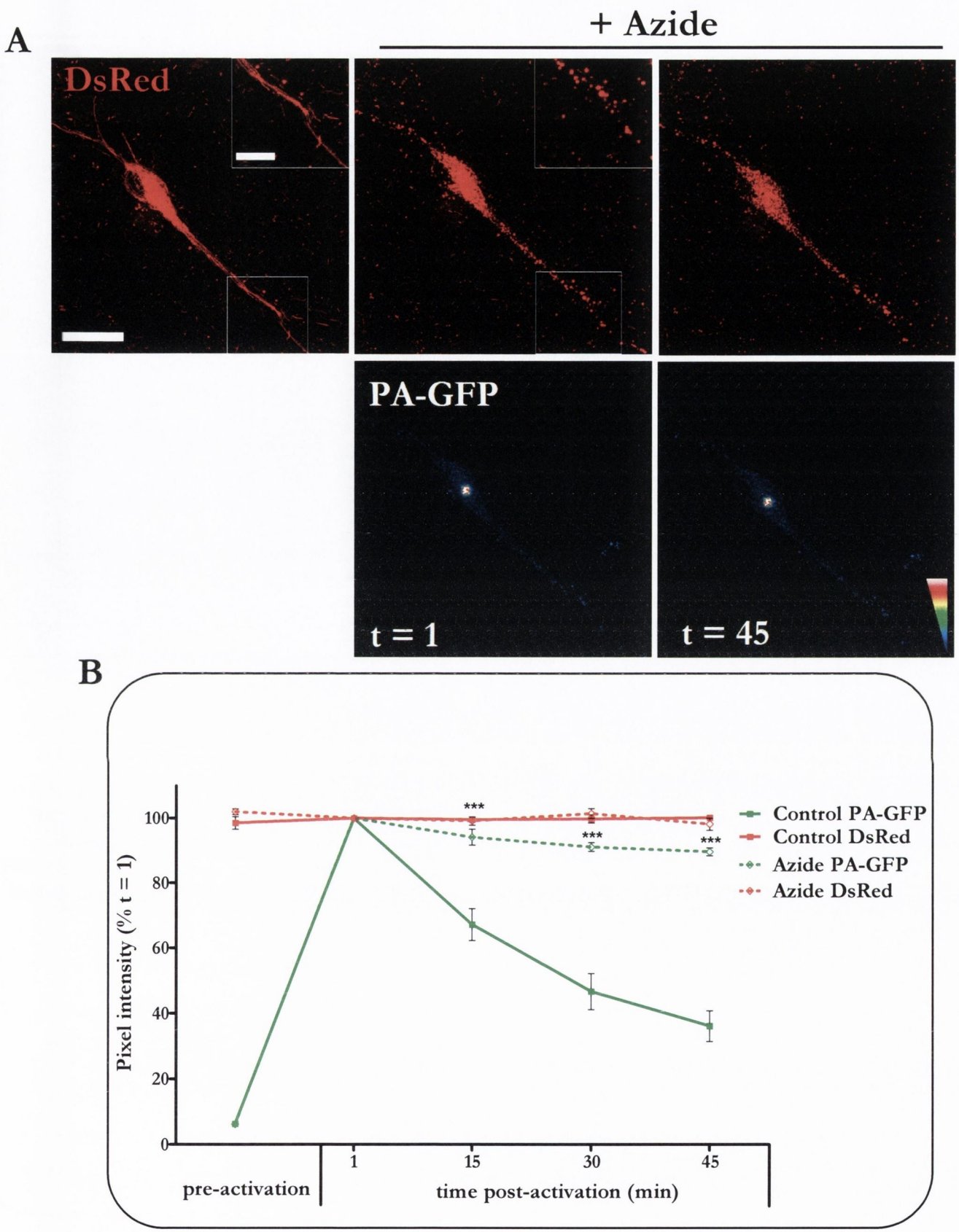

Figure 5.11: Complex IV inhibition causes mitochondrial fragmentation and inhibits fusion in neurons. (A) Image representative of effects of 20 minute incubation with 5mM azide on mitochondrial morphology and fusion in neurons. Mitochondria appear extensively fragmented after azide treatment (upper row) and are unable to undergo fusion (lower row). Scale, main image = 20μm, inset = 10μm. (B) Quantitative fusion data shows the inhibition of fusion in azide treated cells (dashed green line), compared to controls (bold green line). Data presented as mean ± SEM, n = 3. Unpaired t-test at each time point, with Welch correction for unequal variance. ***P<0.001.

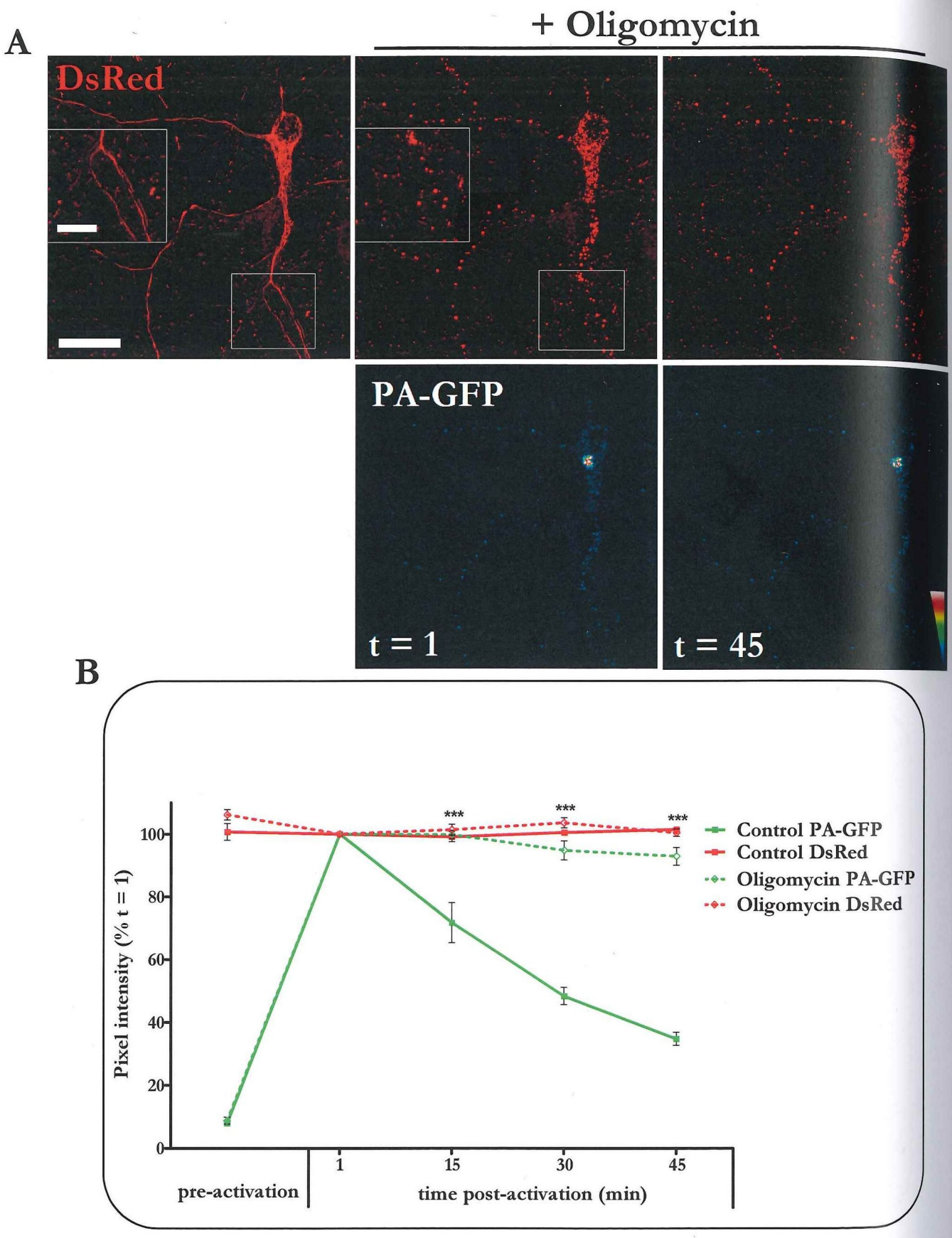

Figure 5.12: ATP synthase inhibition causes mitochondrial fragmentation and inhibits fusion in neurons. (A) Image representative of effects of 20 minute incubation with 2μg/ml oligomycin on mitochondrial morphology and fusion in neurons. Mitochondria appear extensively fragmented after oligomycin treatment (upper row) and are unable to undergo fusion (lower row). Scale, main image = 20μm, inset = 10μm. (B) Quantitative fusion data shows the inhibition of fusion in oligomycin treated cells (dashed green line), compared to controls (bold green line). Data presented as mean ± SEM, n = 3. Unpaired t-test at each time point, with Welch correction for unequal variance. ***P<0.001.

as described. Twenty minute exposure of neurons to complex I, III, and IV inhibitors led to significant PI decreases of between ~68.78 – 82.53% (fig. 5.13). ATP synthase inhibition did not lead to hyperpolarisation as expected, but did lead to a lesser PI decrease than other inhibitors (PI decrease of 35.94 ± 3.81%). These results suggest a threshold of mitochondrial depolarisation that must be reached before mitochondrial fragmentation occurs.

5.4.4 Effects of Inhibition of Oxidative Phosphorylation on ATP levels in Primary Cortical Neurons

The observation in Gal-HeLa cells that decreased fusion is correlated with decreased cellular ATP levels provided the impetus to examine this variable in neurons. Cells exposed to inhibitors of complexes I, III, IV and ATP synthase, as well as $\Delta\Psi_m$, showed very significant decreases in ATP levels (fig. 5.14). Cells treated with FCCP showed ATP levels at just 22.87 ± 2.86% of controls, while complex I-inhibited cells showed ATP levels at 20.56 ± 2.08% (rotenone) and 15.72 ± 1.05% (piericidin A). Complex III inhibition led to a drop of ATP levels to 26.6 ± 4.03% (myxothiazol) and 40.03 ± 4.43% (antimycin A) of controls, while complex IV inhibition produced a decrease to 40.28 ± 3.53%. Finally, ATP synthase inhibition caused a modest but statistically significant decrease to 80.87 ± 6.65% of controls. These results lend further support to the previously obtained results in Gal-HeLa cells, linking intracellular ATP levels and mitochondrial fusion rates.

5.4.5 Threshold Effects of Complex I Inhibition on Mitochondrial Fusion Rates in Primary cortical Neurons

Given the sensitivity of mitochondrial fusion rates to OXPHOS inhibition in neuronal cells, it was hypothesised that there may be a threshold of inhibition beyond which fusion rates were adversely affected. Complex I was selected as the target enzyme, given its important role in neuronal bioenergetics and disease; it has been shown to be the rate limiting ETC enzyme in synaptosomal oxygen consumption (Telford *et al.*, 2009) and, as discussed, has a widely accepted involvement in PD pathophysiology (Keeney *et al.*, 2006). As previously described, rotenone affects microtubule assembly; this rendered it

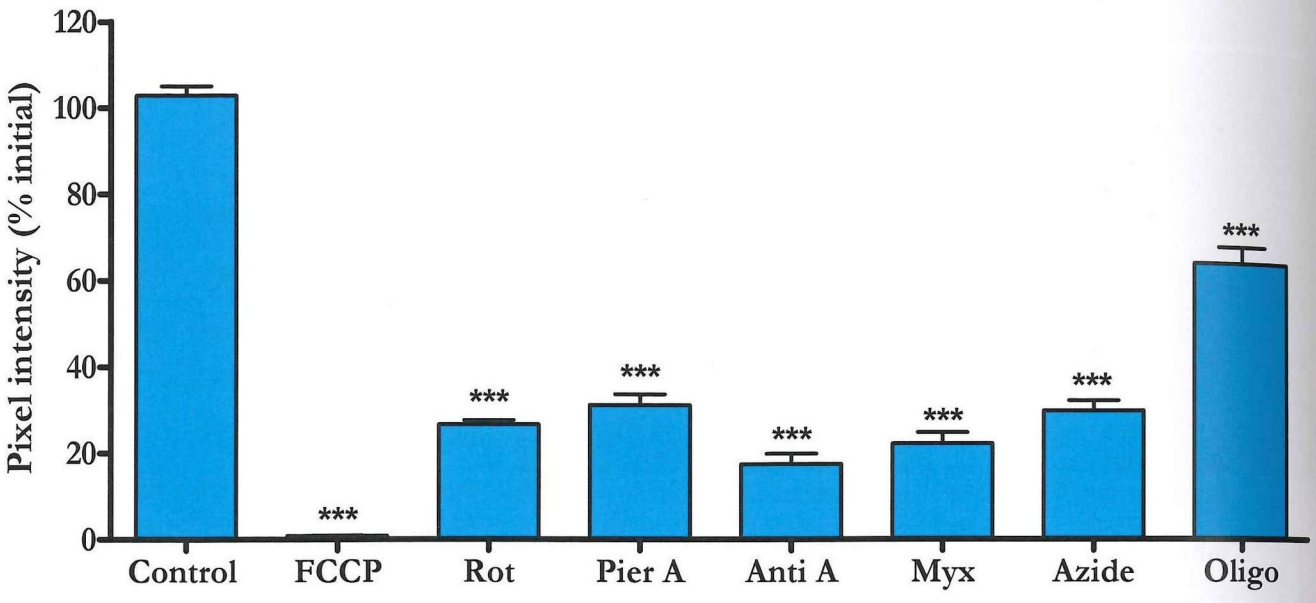

Figure 5.13: Non-fusing mitochondria in OXPHOS-inhibited neurons are significantly depolarised. Microscopic measurement of TMRM fluorescence revealed that neurons are significantly depolarised following 20 minute treatment with 5μM FCCP, 10μM rotenone (rot), 1μM piericidin A (pier A), 2.4μM antimycin A (anti A), 2μM myxothiazol (myx), 5mM azide and, to a lesser extent, 2μg/ml oligomycin (oligo). Data presented as mean ± SEM (n = 3) and expressed as % initial (pre-treatment) values. One-way ANOVA with Dunnett's post-test. ***P<0.001.

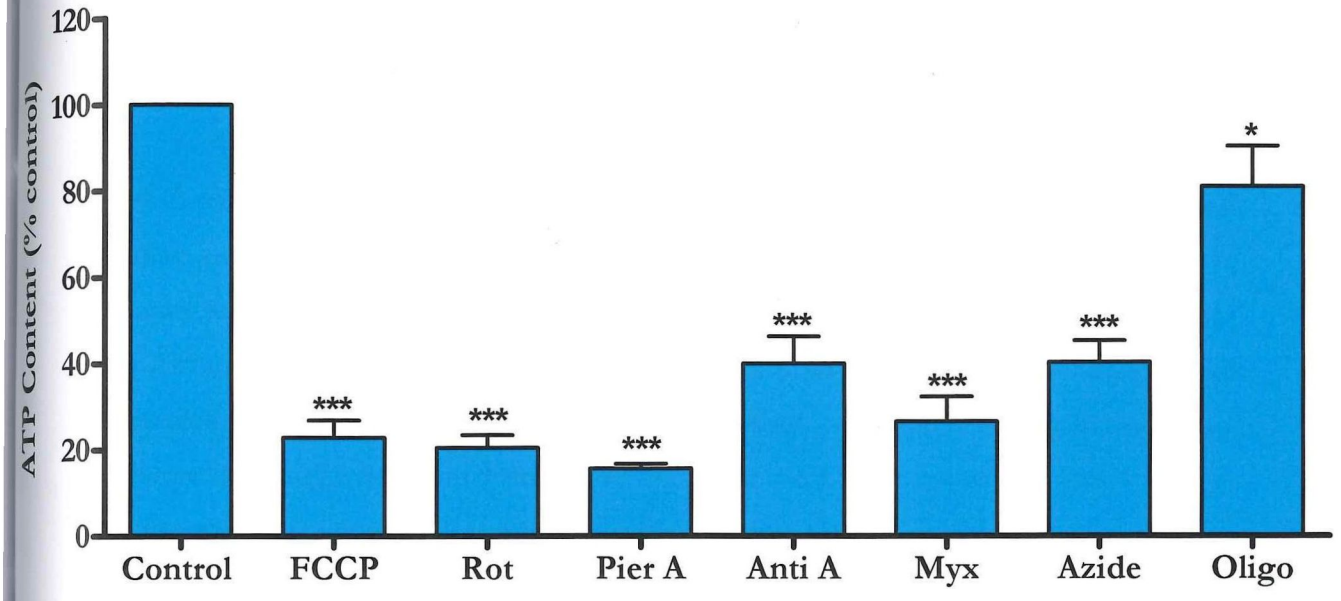

Figure 5.14: ATP is significantly reduced in OXPHOS-inhibited neurons with non-fusing mitochondria. A luciferase-based luminescence assay determined that neurons exposed for 20 minutes to 5μM FCCP, 10μM rotenone (rot), 1μM piericidin A (pier A), 2.4μM antimycin A (anti A), 2μM myxothiazol (myx), 5mM azide and 2μg/ml oligomycin (oligo) exhibit significantly reduced ATP levels. Data presented as mean ± SEM, n = 3. One-way ANOVA with Dunnett's post-test. ***P<0.001.

an unsuitable agent for complex I inhibition titration experiments, given the importance of microtubules in neuronal transport (Ligon and Steward, 2000). Thus, piericidin A was used to selectively inhibit complex I at concentrations ranging from 10nM – 1μM.The sensitivity of the fusion assay was increased through adjustment of photo-activation and imaging parameters, described in section 5.3.5.1. Among other changes, a smaller ROI ($2.3\mu m^2$) was photo-activated in cell somata, using 405nm laser set to lower power output (0.5%). These changes allowed for faster dilution of the photo-activated signal (fig. 5.15), and thus, faster PI decreases compared to those observed using the previous settings (fig. 5.16).

Earlier experiments had established that 20 minute incubation with 1μM piericidin A led to fragmentation of the mitochondrial network. Further imaging experiments using piericidin A at this concentration determined that the minimum incubation time in which this occurred was five minutes (fig. 5.17), thus, all incubations with concentrations below 1μM were of the same duration. Five-minute exposure of neurons to 500nM piericidin A led to complete cessation of fusion and, although not within five minutes, complete fragmentation of the network did occur and was obvious at 45 minutes post-activation (fig. 5.18). Piericidin A inhibited fusion at lower still concentrations of 100nM (fig. 5.19) and 50nM (fig 5.20), but had no effect at 10nM (fig 5.21). Thus it appeared neurons could withstand a certain level of complex I inhibition before mitochondrial fusion was affected.

Mitochondrial membrane potential experiments (again, using microscopic measurement of TMRM fluorescence) showed a dose-dependent decrease in $\Delta\Psi_m$ in response to five minute incubations with piericidin A (fig. 5.22). Statistically significant decreases in $\Delta\Psi_m$ were observed at all concentrations above –and including- 50nM. It is interesting to note that 50nM caused significant inhibition of fusion and a decrease of $20 \pm 3.38\%$ in $\Delta\Psi_m$. A decrease in $\Delta\Psi_m$ of this magnitude was not sufficient to cause fusion inhibition in Gluc-HeLa cells, suggesting a higher dependence of neurons on this aspect of mitochondrial function for the maintenance of healthy fusion rates.

Neuronal ATP levels were also significantly affected following five-minute exposure to piericidin A, in a dose-dependent manner (fig. 5.23). At a concentration of 100nM, piericidin A caused a $32.82 \pm 5.23\%$ decrease in cellular ATP, with a 2-fold greater

Figure 5.15: New photo-activation parameters allow for faster pixel intensity decrease in photo-activated regions. Changing photo-activation settings on the confocal microscope allowed for a faster dilution of photo-activated signal and thus a faster decrease in pixel intensity. Zoom was increased to 3x, ROI was reduced to 2.3μm, and 405nm laser power output was reduced to 0.5%. Scale = 20μm

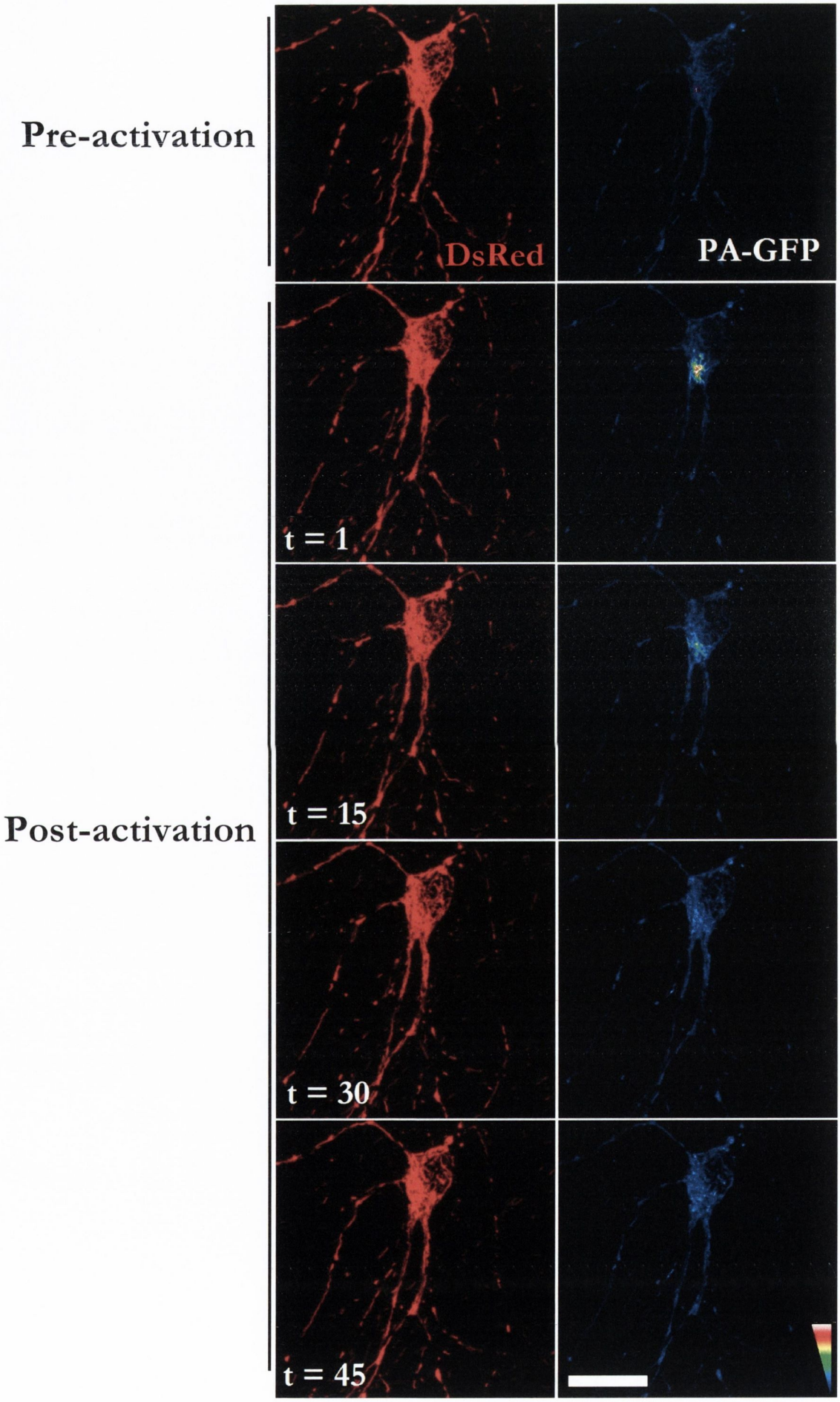
Pre-activation
DsRed
PA-GFP
t = 1
Post-activation
t = 15
t = 30
t = 45

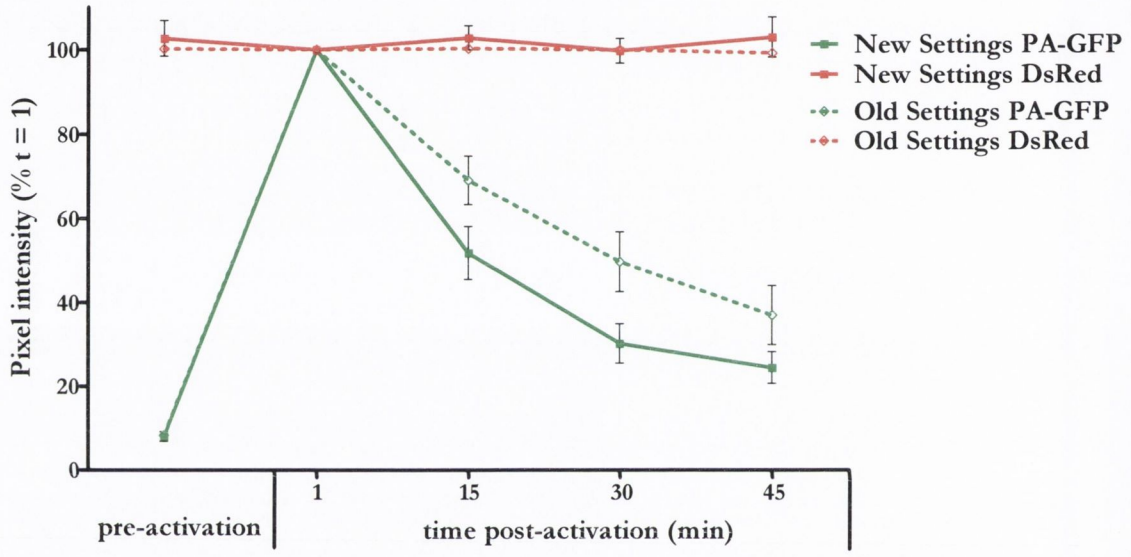

Figure 5.16: Comparison of pixel intensity decreases observed with different photoactivation settings. Photo-activating ROIs with new settings (bold green line) led to a faster dilution of photo-activated signal and thus a faster decrease in the pixel intensity, compared to those photo-activated with old settings (dashed green line). The new settings had no effect on DsRed fluorescence measurement (red lines). Data presented as mean $\pm$ SEM, n = 3.

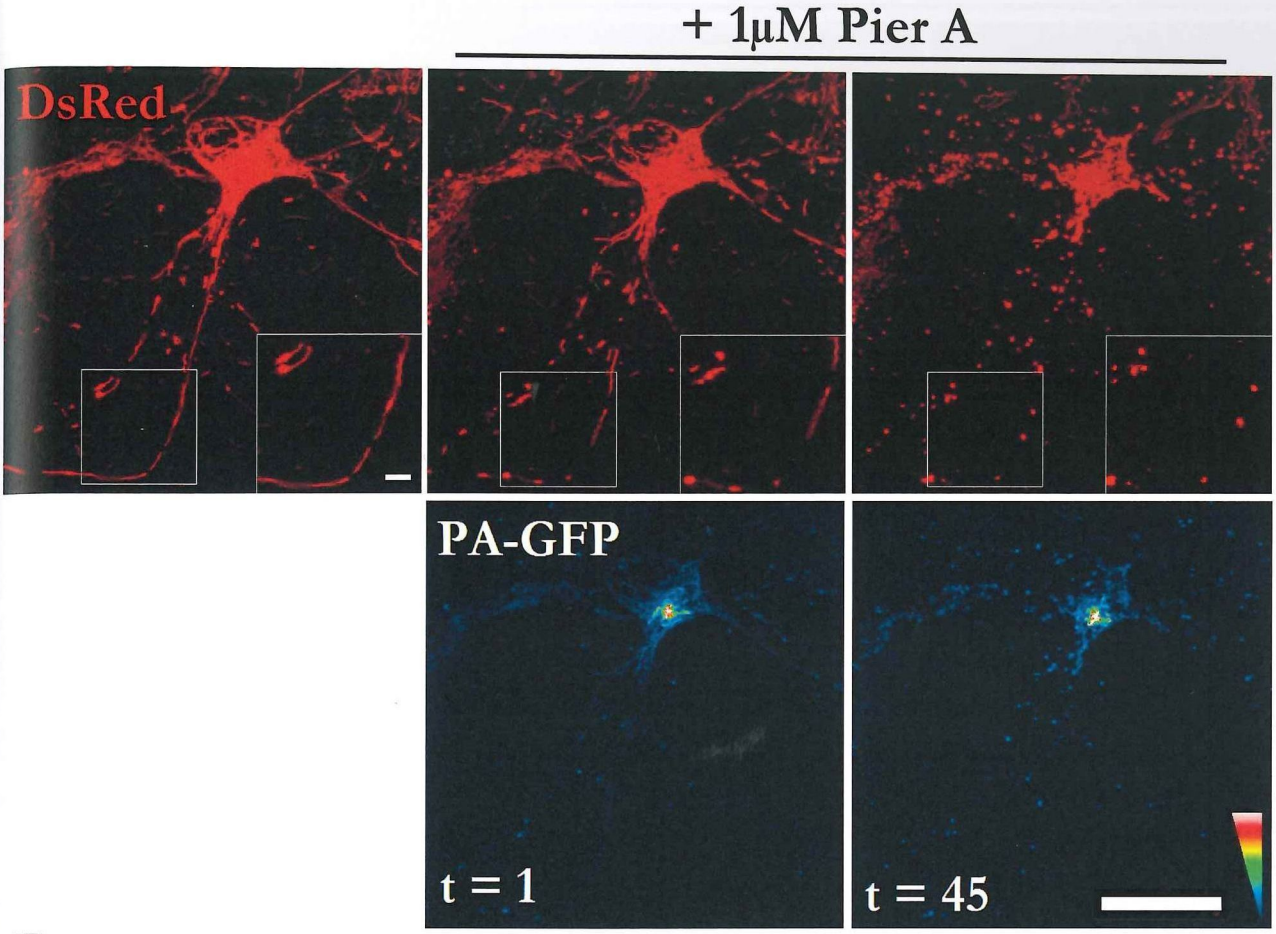

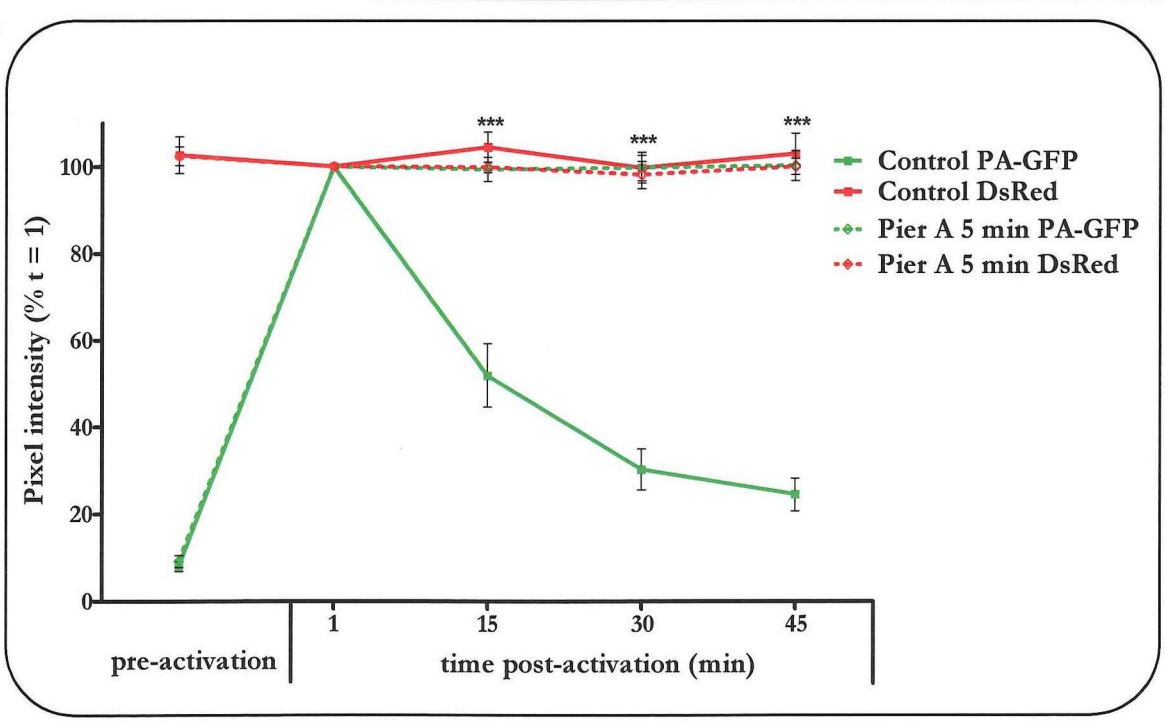

Figure 5.17: Five minute incubation with 1μM piericidin A causes inhibition of mitochondrial fusion and increased fission. (A) Neurons exposed to 1μM piericidin A for just five minutes exhibited increased mitochondrial fission (top row) and fusion cessation (bottom row). Scale, main image = 20μm, inset 5μm. (B) Quantitative fusion data shows the inhibition of fusion following five minute treatment of neurons with 1μM piericidin (dashed green line), compared to controls (bold green line). Data presented as mean ± SEM, n = 3. Unpaired t-test at each time point, with Welch correction for unequal variance. ***P<0.001.

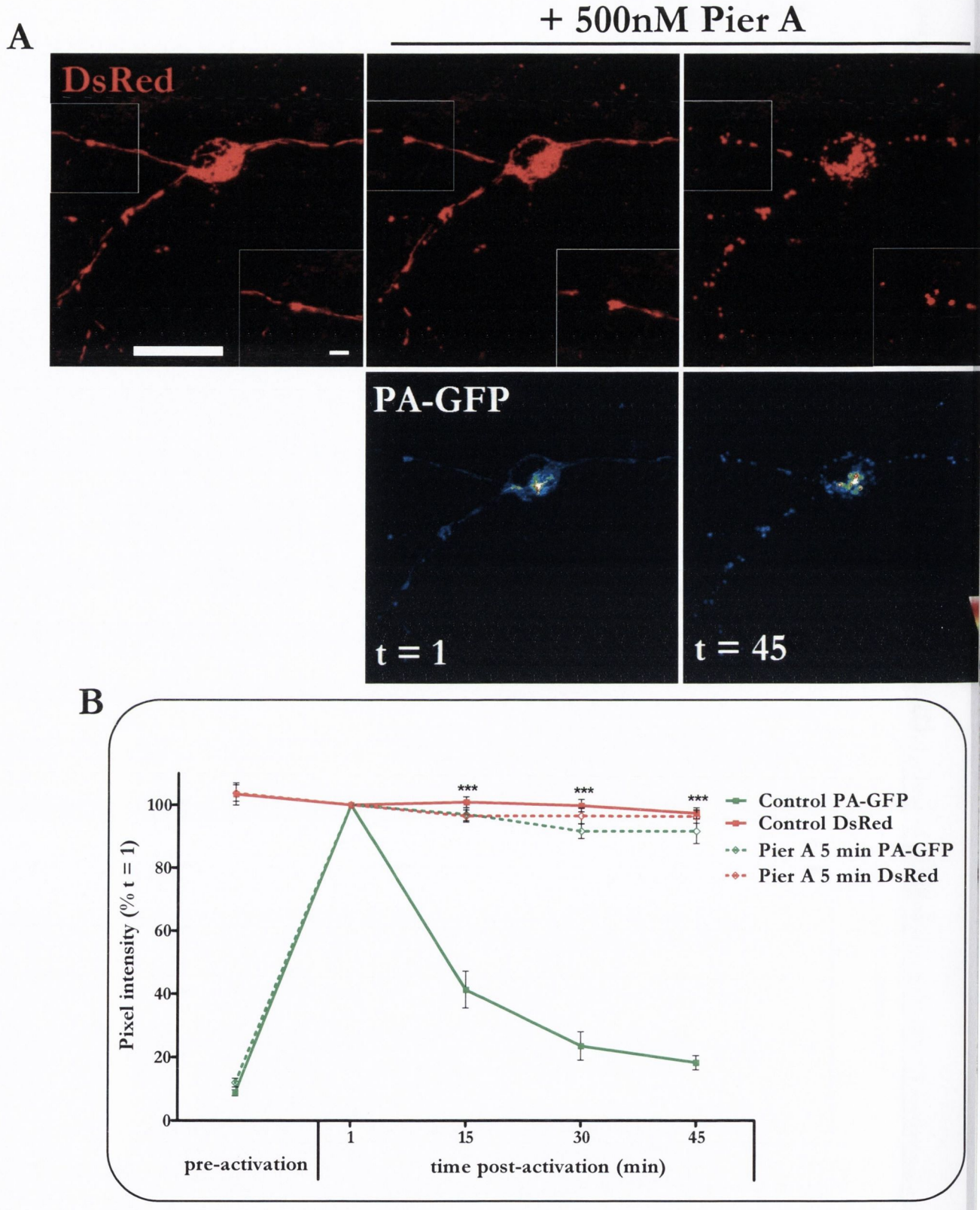

Figure 5.18: Five minute incubation with 500nM piericidin A causes inhibition of mitochondrial fusion and increased fission. (A) Neurons exposed to 500nM piericidin A for just five minutes exhibited increased mitochondrial fission (top row) and fusion cessation (bottom row). Scale, main image = 20μm, inset 5μm. (B) Quantitative fusion data shows the inhibition of fusion following five minute treatment of neurons with 500nM piericidin (dashed green line), compared to controls (bold green line). Data presented as mean ± SEM, n = 3. Unpaired t-test at each time point, with Welch correction for unequal variance. ***P<0.001.

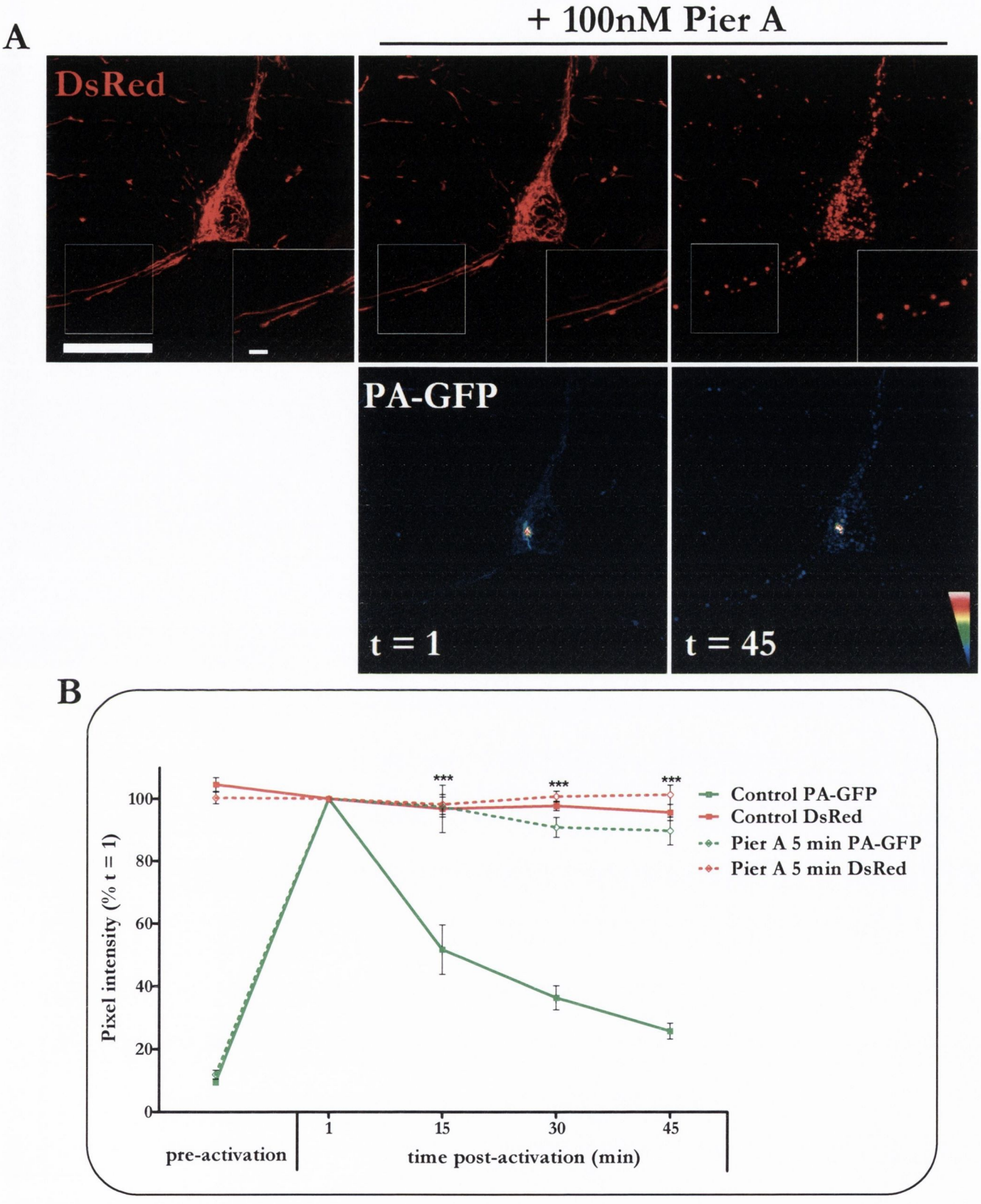

Figure 5.19: Five minute incubation with 100nM piericidin A causes inhibition of mitochondrial fusion and increased fission. (A) Neurons exposed to 100nM piericidin A for just five minutes exhibited increased mitochondrial fission (top row) and fusion cessation (bottom row). Scale, main image = 20μm, inset 5μm. (B) Quantitative fusion data shows the inhibition of fusion following five minute treatment of neurons with 100nM piericidin (dashed green line), compared to controls (bold green line). Data presented as mean ± SEM, n = 3. Unpaired t-test at each time point, with Welch correction for unequal variance. ***P<0.001.

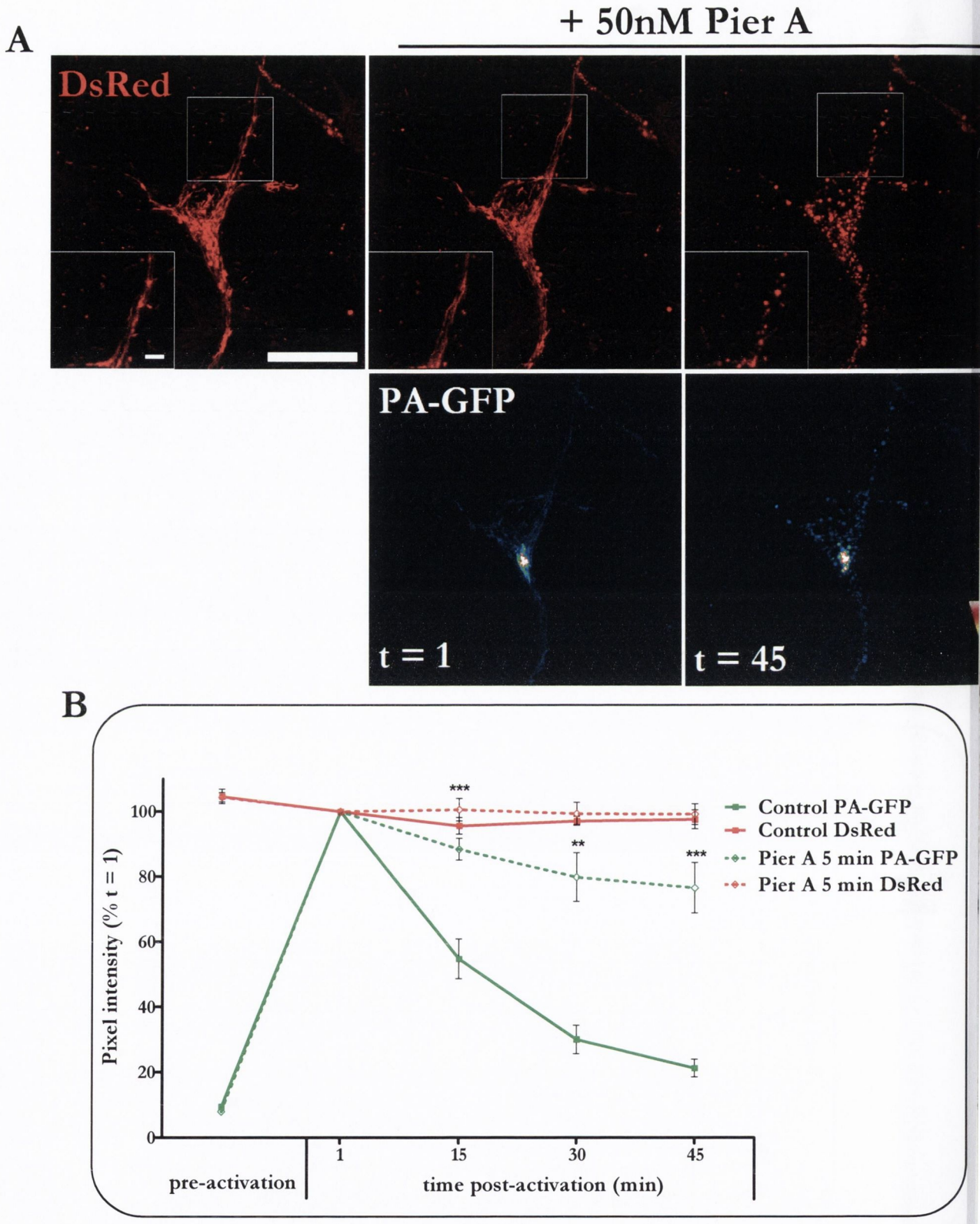

Figure 5.20: Five minute incubation with 50nM piericidin A causes inhibition of mitochondrial fusion and increased fission. (A) Neurons exposed to 50nM piericidin A for just five minutes exhibited increased mitochondrial fission (top row) and fusion cessation (bottom row). Scale, main image = 20μm, inset 5μm. (B) Quantitative fusion data shows the inhibition of fusion following five minute treatment of neurons with 50nM piericidin (dashed green line), compared to controls (bold green line). Data presented as mean ± SEM, n = 3. Unpaired t-test at each time point, with Welch correction for unequal variance. ***P<0.001.

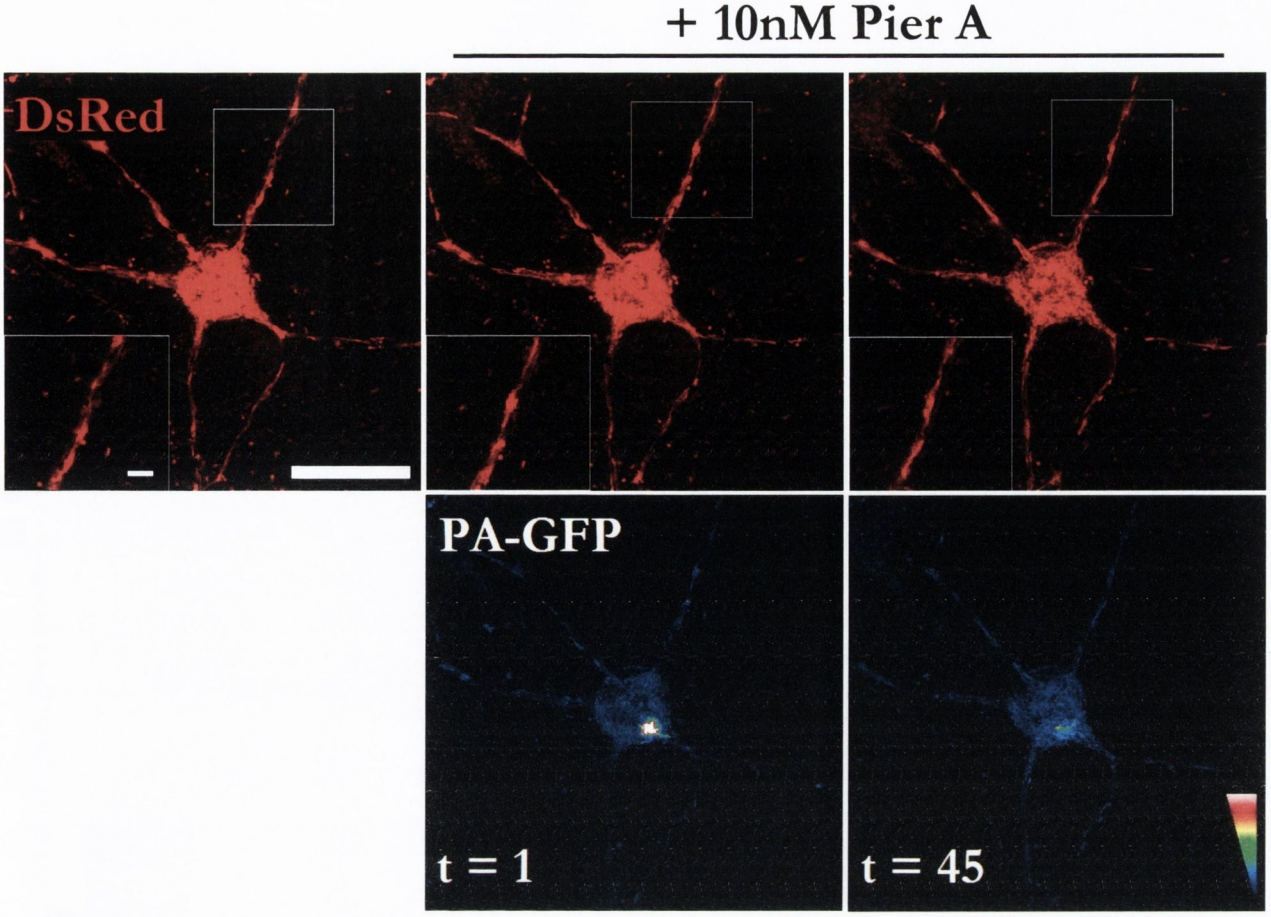

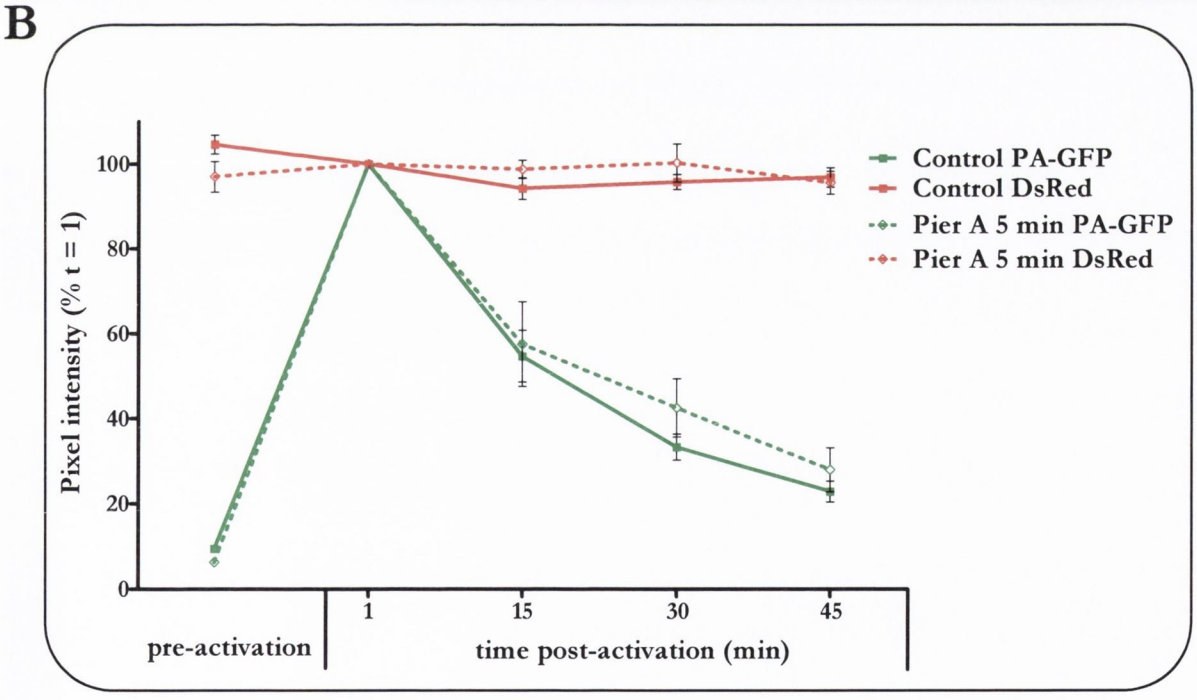

Figure 5.21: Five minute incubation with 10nM piericidin A does not affect mitochondrial fusion. (A) Mitochondria in neurons exposed to 10nM piericidin A for five minutes exhibited no morphological changes (top row) and were capable of normal fusion (bottom row). Scale, main image = 20μm, inset 5μm. (B) Quantitative fusion data shows no inhibition of fusion following five minute treatment of neurons with 10nM piericidin (dashed green line), compared to controls (bold green line). Data presented as mean ± SEM, n = 3. Unpaired t-test at each time point, with Welch correction for unequal variance. ***P<0.001.

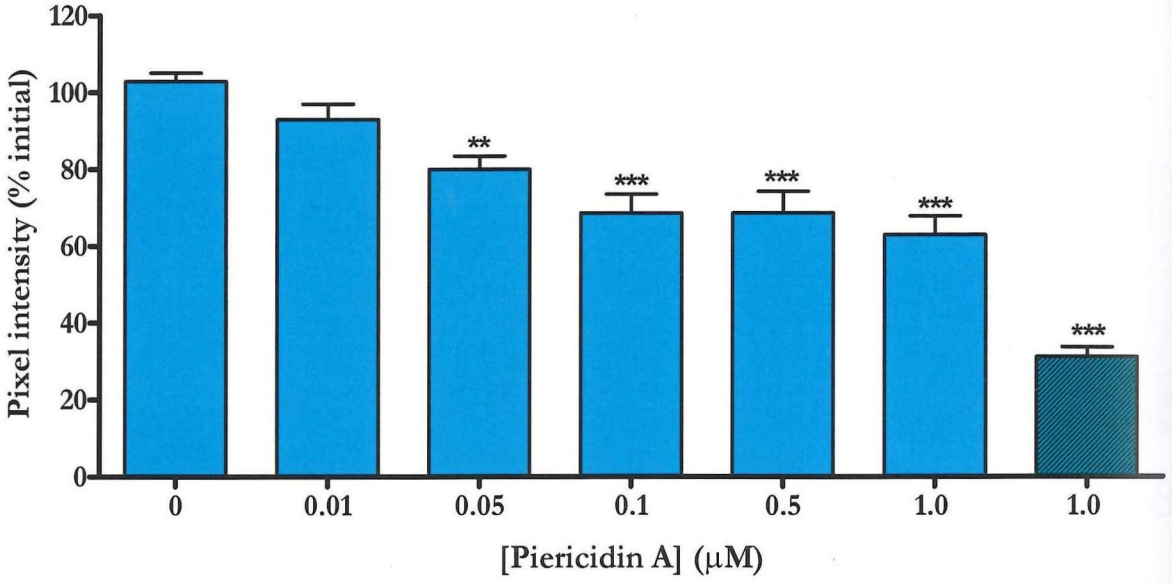

Figure 5.22: Five minute incubation with piericidin A causes partial mitochondrial depolarisation in a time and dose-dependent manner. Neurons loaded with TMRM were exposed to piericidin A at the concentrations indicated for five minutes (light blue bars) and exhibited statistically significant mitochondrial depolarisation from 50nM onwards. Incubation with 1μM for twenty minutes (striped bar) leads to an even larger depolarisation. Data presented as mean ± SEM (n = 3) and expressed as % initial (pre-treatment) values. One-way ANOVA with Dunnett's post-test. **P<0.01, ***P0.001

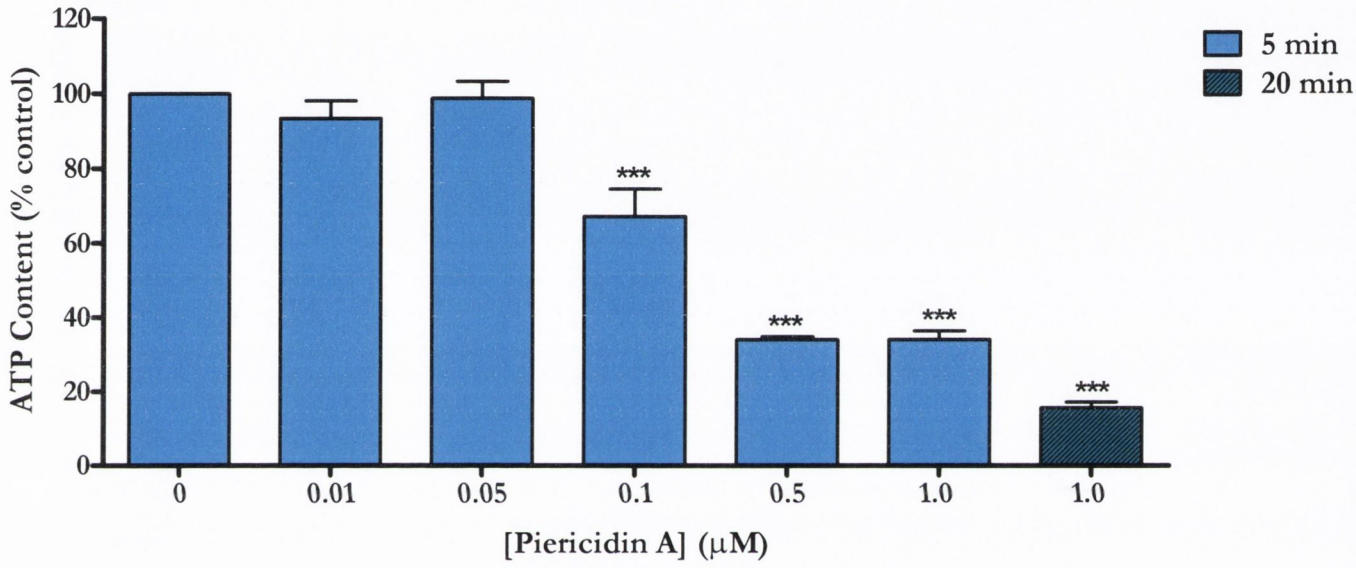

Figure 5.23: **Five minute incubation with piericidin A decreases neuronal ATP in a time and dose-dependent manner.** Neurons exposed to piericidin A for five minutes (light blue bars) at the concentrations indicated showed a dose-dependent decrease in ATP from 100nM onwards. Longer exposure to 1μM piericidin A (20 minutes, striped bar) led to a more pronounced ATP decrease. Data presented as mean ± SEM, n = 3. One-way ANOVA with Dunnett's post-test. ***P<0.001.

decrease at 500nM and 1μM. Despite the inhibition of fusion at 50nM piericidin A, there were no changes in ATP observed within five minutes. It is possible that ATP decreased significantly at a later period, given the early and significant changes in $\Delta\Psi_m$ observed at this concentration, but this cannot be stated definitively here.

Finally, to assess the degree of complex I inhibition at each piericidin A concentration, complex I assays were carried out on non-synaptic mitochondria (NSM) and synaptosomes (SYN) prepared from adult rat brains (fig. 5.24 – 25). It must be noted here that NSM contain mitochondria not only from neuronal somata but also from glia and thus are not pure preparations of neuronal mitochondria. Therefore, the results obtained were considered an *approximation* of the degree of inhibition of complex I occurring in neuronal cells exposed to piericidin A. Complex I was inhibited to approximately the same degree in NSM and SYN at each concentration, with ~33% inhibition at 10nM, increasing sharply to ~75% inhibition at 50nM, ~87% inhibition at 100nM, and ~99% inhibition at 500nM-1μM. When NSM complex I inhibition was plotted against % fusion (where a PI decrease to ~37% post-activation value after 45 minutes represented 100% fusion), it appeared that the threshold of complex I inhibition affecting mitochondrial fusion lay between ~33 – 75% (fig. 5.26). Thus, neuronal cells may withstand at least ~33% complex I inhibition before mitochondrial fusion was seriously compromised. These data indicate that the previously reported threshold effects of complex I inhibition on OXPHOS and respiration (Davey and Clark, 1996, Davey *et al.*, 1997, Davey *et al.*, 1998, Telford *et al.*, 2009) in neuronal tissue could potentially be extended to mitochondrial dynamics.

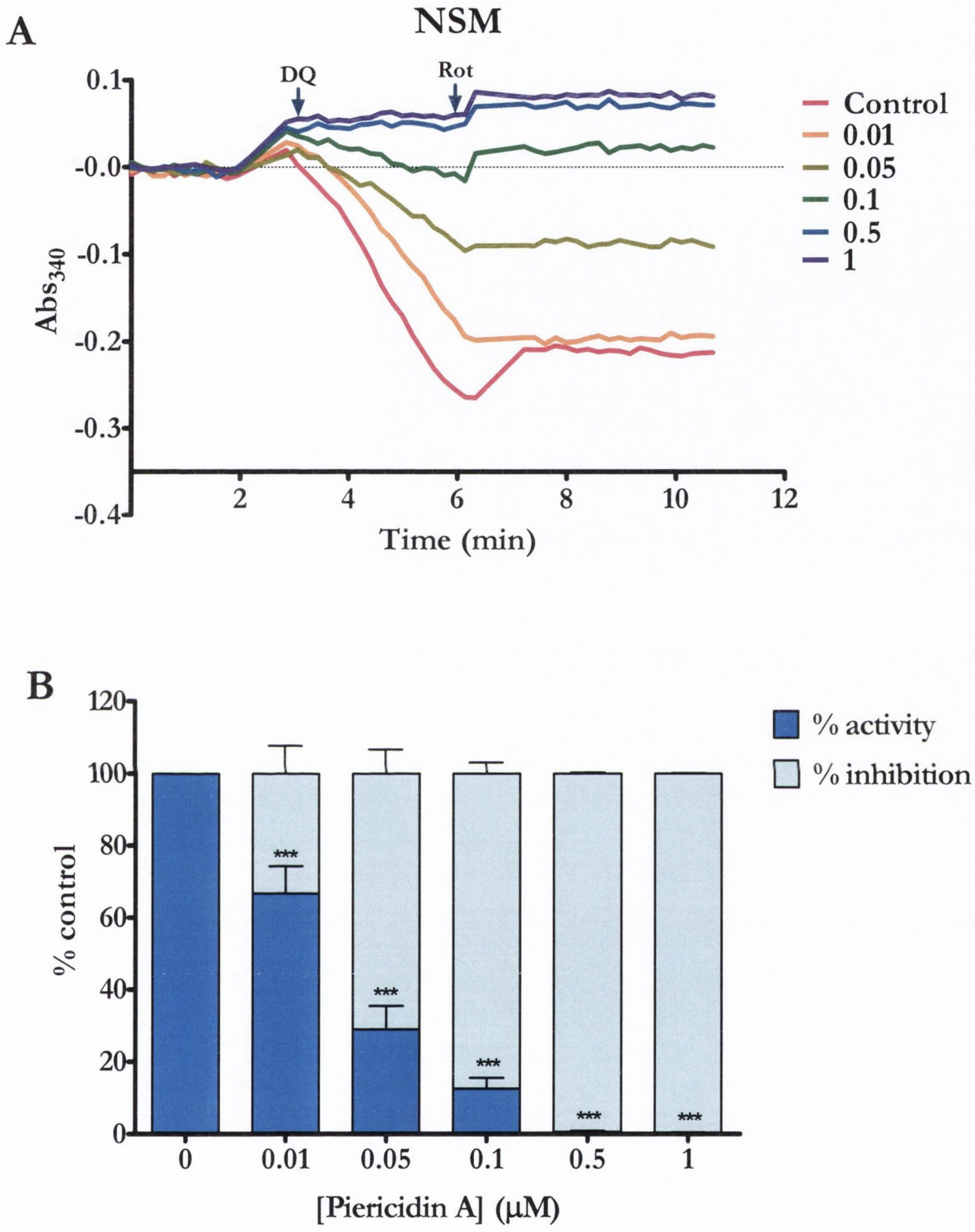

Figure 5.24: Complex I inhibition by piericidin A in non-synaptic mitochondria. (A) Typical trace obtained in spectrophotometric measurement of complex I activity in non-synaptic mitochondria (NSM), where a fast decrease in absorbance (ΔA_{340}/min) indicates rapid oxidation of NADH by complex I. Samples were assayed in the absence or presence of piericidin A at the indicated concentrations (μM) and gave ΔA_{340}/min readings of approximately 0 before the addition of artificial electron acceptor, decylubiquinone (DQ). After following the reaction for three minutes, the rotenone insensitive rates were obtained by monitoring ΔA_{340}/min after the addition of 10μM rotenone (rot). (B) Complex I activity (dark blue) and inhibition (light blue) in NSM at the piericidin A concentrations indicated. Data presented as mean ± SEM, n = 3. One-way ANOVA with Bonferroni post-test. ***P<0.001.

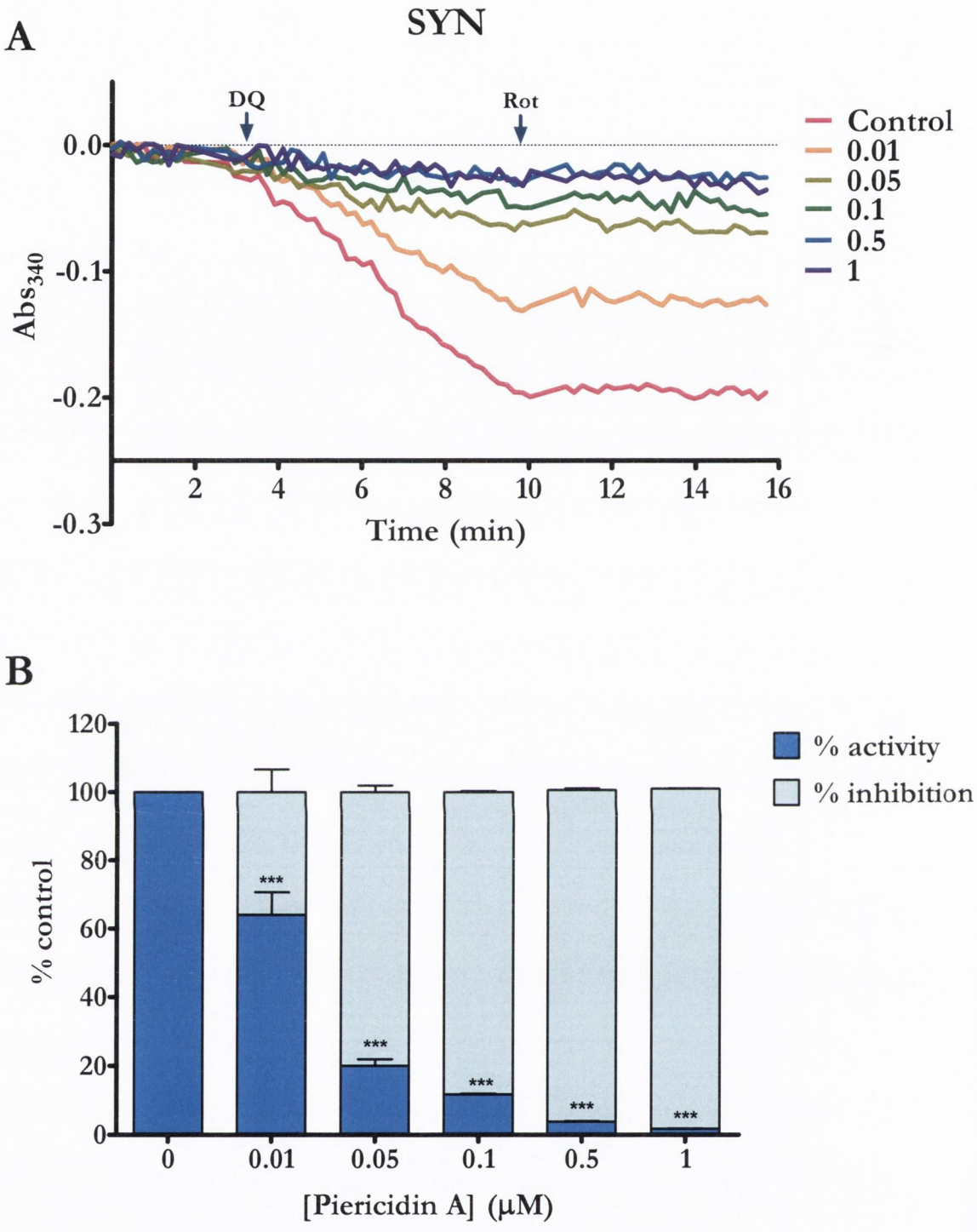

Figure 5.25: Complex I inhibition by piericidin A in synaptosomes. (A) Typical trace obtained in spectrophotometric measurement of complex I activity in synaptosomes (SYN), where a fast decrease in absorbance (ΔA_{340}/min) indicates rapid oxidation of NADH by complex I. Samples were assayed in the absence or presence of piericidin A at the indicated concentrations (μM) and gave ΔA_{340}/min readings of approximately 0 before the addition of artificial electron acceptor, decylubiquinone (DQ). After following the reaction for six minutes, the rotenone insensitive rates were obtained by monitoring ΔA_{340}/min after the addition of 10μM rotenone (rot). (B) Complex I activity (dark blue) and inhibition (light blue) in SYN at the piericidin A concentrations indicated. Data presented as mean ± SEM, n = 3. One-way ANOVA with Bonferroni post-test. ***P<0.001.

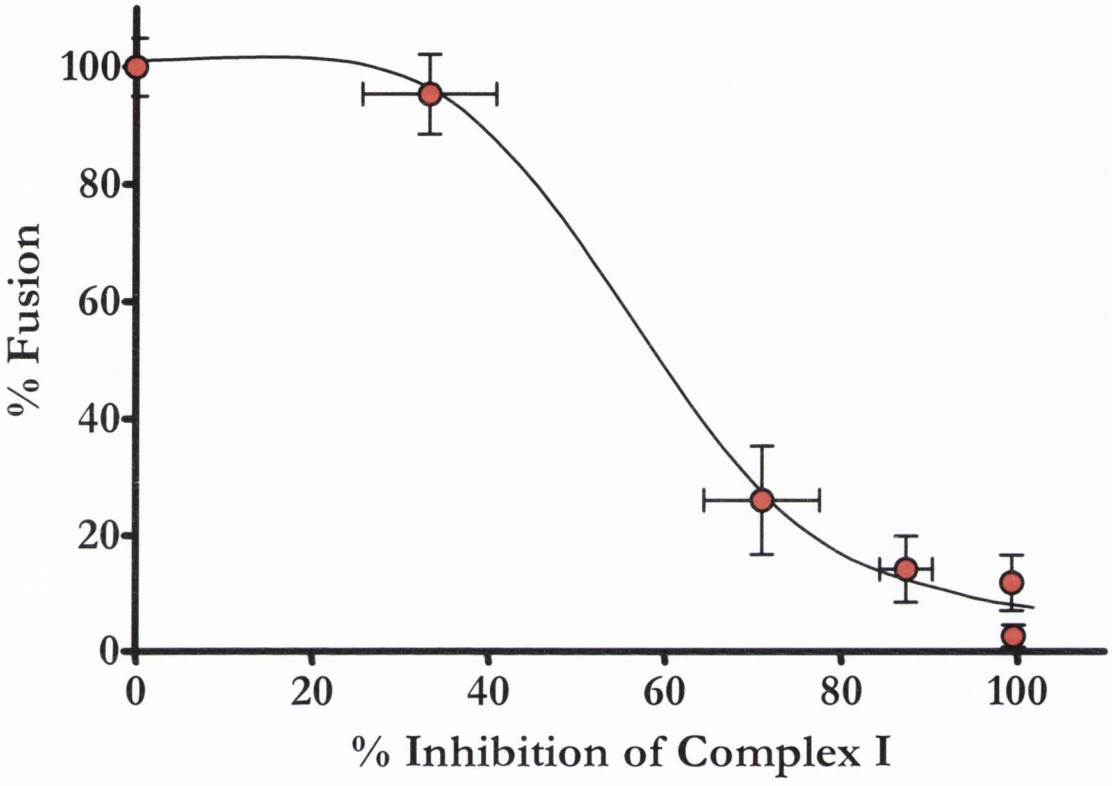

Figure 5.26: Complex I inhibition threshold and mitochondrial fusion. When % complex I inhibition (NSM) is plotted against % fusion (where a pixel intensity decreased to ~37% post-activation value after 45 minutes represented 100% fusion), it appears that complex I has an inhibition threshold between ~33 – 75% before mitochondrial fusion is seriously compromised. Data presented as mean ± SEM, n = 3.

5.5 Discussion

These studies highlight the extreme vulnerability of neurons to bioenergetic inhibition. Mitochondrial fusion was completely blocked by OXPHOS inhibition, which was concomitant with a rapid dissipation of $\Delta\Psi_m$ and significant decreases in ATP. In addition, it was shown that 5-minute inhibition of complex I had dose-dependent effects on fusion, $\Delta\Psi_m$ and ATP levels and, when plotted against complex I inhibition in NSM, neurons could withstand at least ~33% inhibition of complex I before fusion was perturbed.

Control neurons exhibited a rate of mitochondrial fusion that, although slower than that of HeLa cells, was more efficient than expected when compared to the literature (figs 5.3 – 4). Berman *et al.* (2009) observed that only 1-2% of encounters between mitochondria in primary cortical neurons from embryonic mice resulted in fusion events, while Karbowski *et al.* (2004a) report that primary neurons require an average of 1 hour to decrease PIs to the same level achieved in HeLa cells within 30 minutes. In the studies presented here, neurons required just 15 additional minutes to reach PIs comparable to those of HeLa cells. There are several possible explanations for this discrepancy. The first, of course, is that this technique is semi-quantitative and, as such, is difficult to compare across labs due to differences between activation and imaging settings. The second is that, in the studies mentioned, fusion was monitored within axons, not cell somata. Fusion is less likely to occur in axons, as extremely tubular mitochondrial would presumably overwhelm the transport machinery and potentially cause obstruction. In addition, interactions between mitochondria are spatially and temporally limited in the narrow axon, whereas those in the soma could potentially engage with others with higher frequency and in three dimensions.

However, in general, the studies presented here agree with of reports slower fusion rates in neurons. The exact reason for this inherent property of neuronal mitochondrial dynamics is not known. Neuronal mitochondria may be more dynamic during growth and development to ensure extensive branching and interconnectivity, while the maintenance of mature neurons requires less active turnover (Chang and Reynolds, 2006). As previously mentioned, Mfn2 is reputed to be expressed in preference to Mfn1 in rat brain (Eura *et al.*, 2003) and it was recently demonstrated that Mfn homotypic

complexes are less fusogenic than heterotypic ones (Hoppins *et al.*, 2011). It follows that if neuronal mitochondria more frequently present Mfn2 on their OMs, a fusion event may be less likely to occur. Interestingly, postnatal cortical mouse neurons exclusively express a truncated form of Bak, called N-Bak, that contains only the BH3-domain, thus placing it in the category of BH3-only group of the Bcl2 family (Uo *et al.*, 2005) and removing its MOMP effector function. Given the roles of Bak and Bax in mitochondrial fusion facilitation (Karbowski *et al.*, 2006), perhaps this truncated form of Bak also lacks fusogenic properties.

Exposure of neurons to ETC/OXPHOS inhibitors had marked effects on both mitochondrial morphology and fusion rates (figs 5.5 – 12). Individual inhibition of complexes I, III, IV and ATP synthase induced marked change in mitochondrial appearance in agreement with the literature. Antimycin A, azide, FCCP (Safiulina *et al.*, 2006), rotenone (Barsoum *et al.*, 2006) and oligomycin (Kaasik *et al.*, 2007) have been shown to elicit fragmentation in neuronal mitochondria. As suggested in Chapter 4, although malonate had no effect on mitochondrial form in the studies described here, complex II inhibition with 3-NP has been shown to cause fragmentation, albeit after 3 – 6 hour incubations (Liot *et al.*, 2009). Thus, it is possible that complex II inhibition with malonate may have resulted in morphological affects at a later time point. Crucially, the studies cited above neglected to assess the effects of these inhibitors on mitochondrial fusion. This is an important distinction that may not seem obvious; for instance, inhibiting mitochondrial transport would tip the balance towards fission, without inhibiting fusion *per se* (Baloh, 2008). Mitochondria would be less likely to come in contact with one another and thus the chances of fusion would decrease, but the ability to fuse would not necessarily change. Indeed, mtDNA functional complementation studies highlight this fact; polykaryons generated from cells harbouring mtDNA mutations exhibit punctate mitochondria that are nonetheless able to fuse and eventually restore mitochondrial function (Gilkerson *et al.*, 2008). Thus, this study showed for the first time that mitochondrial fragmentation induced by OXPHOS inhibition was accompanied by the complete cessation of fusion in neurons.

The reason for this effect is not clear. In contrast to HeLa cells, ETC inhibitors also dramatically decreased $\Delta\Psi_m$ in neurons (fig 5.13). Therefore, it is possible that OPA1 cleavage to short isoforms occurred in neurons is due to this more pronounced $\Delta\Psi_m$

decrease (Guillery *et al.*, 2008). This would be interesting to investigate in the future. Cellular ATP was also markedly lowered by ETC inhibitors (fig 5.14), possibly due to the 'cannabilisation' of ATP by ATP synthase working in reverse to maintain $\Delta\Psi_m$ (Nicholls and Budd, 2000). Aside from the GTP-dependence of the mitodynamins, both kinesin and dynein are ATPases (Johnson and Wall, 1983, Kuznetsov and Gelfand, 1986), while microtubule dynamic instability is GTP-dependent (Desai and Mitchison, 1997). Thus it is conceivable that energy deficiency prevented mitochondrial transport, which may have tipped the balance toward fission. ATP synthase inhibition, again, is slightly anomalous, as it induced fragmentation and fusion cessation with only modest decreases in $\Delta\Psi_m$ and ATP levels. It is surprising that oligomycin did not hyperpolarise neuronal mitochondria, as reported in the literature (Joshi and Bakowska, 2011), however, this effect is known to be transient (Kim *et al.*, 2003) and may have happened at earlier time points. The modest reduction in $\Delta\Psi_m$ observed with this treatment is probably the result of averaging across neurons in which mitochondria had either completely depolarised or slightly hyperpolarised. The modest decrease in ATP was expected, as although mitochondrial ATP production was prevented, the hydrolysis of ATP by ATP synthase was also prevented.

Interestingly, it has been demonstrated that ETC inhibition causes swelling in neuronal mitochondria which decreases their motility (Safiulina *et al.*, 2006, Kaasik *et al.*, 2007), again suggesting a potential inability of the organelles to promote physical contact with one another under these conditions. It is also possible that the mitochondria were undergoing restructuring, rather than fission. Safiulina *et al.* (2006) noted that the reduced motility of swollen neuronal mitochondrial was not accompanied by significant changes in organellar surface area. Intriguingly, although the mitochondria assumed a punctate appearance, their overall surface area did not change, indicating that fission had not occurred; fission would have induced punctate morphology and decreased surface area due to organellar scission. This has also been noted by Tan *et al.* (2011) in astrocytes exposed to high Ca^{2+}; the majority of mitochondria became punctate but did not increase in number. Mitochondrial swelling has long been associated with the formation of the PTP, which, as previously mentioned, is sensitive to Ca^{2+} overload (Jeyaraju *et al.*, 2009). Therefore, inhibition of electron transport or dissipation of $\Delta\Psi_m$ could also lead to Ca^{2+} efflux from mitochondria, as calcium buffering and OXPHOS are inextricably linked processes (Nicholls and Budd, 2000). Calcium also arrests mitochondrial movement

through interaction with Miro1/2, which in turn interacts with Mfn2. Thus it is possible that mitochondrial swelling induced by OXPHOS inhibition leads to disturbances of calcium homeostasis, with downstream effects on transport and fusion.

Increased cytosolic Ca^{2+} levels could also promote calcineurin-dependent dephosphorylation of DRP1, leading to increased fission (Cribbs and Strack, 2007). Indeed, Barsoum *et al.* (2006) note that rotenone-induced fragmentation is DRP1-dependent in neuronal mitochondria. It would be useful to examine DRP1 recruitment to neuronal mitochondria under the experimental conditions employed in this study in the future, as results from Gal-HeLa cells indicate that OXPHOS-dependence increases DRP1 recruitment in response to mitochondrial inhibition (Chapter 4). In addition, it is conceivable that the mitochondrial inhibitors were inducing apoptosis in the cells. Although the role of fragmentation in apoptosis is controversial (Sheridan and Martin, 2010), it is nonetheless a common feature of programmed cell death. Immunostaining for cytochrome c localisation would give a reliable indication of apoptosis initiation. As with Gal-HeLa cells, it would be interesting to assess whether DRP1 silencing in neurons affects inhibitor-induced fusion perturbation.

An extremely interesting aspect of these results is that glucose (25mM) was present in the neuronal culture medium during exposure to all mitochondrial inhibitors, yet provided no protection against fusion inhibition. This is in stark contrast to HeLa cells, which were protected from fusion inhibition when mitochondrial inhibitors were applied in the presence of this substrate. The highly selective permeability of the blood-brain barrier means the brain uses glucose almost exclusively for ATP production. Indeed, although the brain accounts for just 2% of total body weight, it consumes over 20% of total body glucose (Schubert, 2005). The relative utilisation of glucose between the cellular subpopulations of the brain is both poorly understood and controversial (Nehlig and Coles, 2007). A popular current hypothesis is that astrocytic uptake accounts for a large proportion of total glucose consumption (particularly following glutamate release by neurons) and that astrocytes have the ability to shuttle glucose-derived lactate to neurons, where it is converted back to pyruvate and, thence, enters the TCA cycle (Hertz, 2004). Fascinating studies in recent years have uncovered important differences in glucose metabolism between astrocytes and neurons, relating to the regulation of

phosphofructokinase 1 (PFK1), the glycolytic enzyme that irreversibly commits glucose to glycolysis, rather than entering other pathways, such as the PPP or glycogenesis.

An essential positive regulator of PFK1 is 6-phosphofructo-2-kinase/fructose-2,6-bisphosphatase 3 (PFKFB3), an enzyme that generates a potent allosteric activator of PFK1, fructose-2,6-bisphosphate (F26P) (Yalcin *et al.*, 2009). In neurons, the comparatively higher activity of the E3 ubiquitin ligase anaphase-promoting complex-Cdh1 (APC^{Cdh1}) leads to targeting of PFKFB3 for proteasomal degradation (Herrero-Mendez *et al.*, 2009), decreasing the rate of glycolysis significantly. This renders neurons unable to utilise glycolytic ATP during inhibition of OXPHOS, as seen in astrocytes (Almeida *et al.*, 2001). Furthermore, in astrocytes (Almeida *et al.*, 2004) and tissues such as the heart (Marsin *et al.*, 2000) the activation of AMPK following OXPHOS inhibition leads to the stimulation of PFK2, which in turn produces F26P, thus activating PFK1 and further stimulating glycolysis. Despite constitutive expression of AMPK, this mechanism is absent in neurons due to low expression of PFK2 (Culmsee *et al.*, 2001, Almeida *et al.*, 2004).

Interestingly, prolonged stimulation of glutamatergic N-methyl-D-aspartate receptor (NMDAR) in neurons stabilises PFKFB3 through Cdh1 inhibition, leading to increased glycolysis concomitant with decreased fluxed of glucose through the PPP (Rodriguez-Rodriguez *et al.*, 2012). This leads to oxidative stress and cell death, highlighting both the importance of glucose for ROS management and the metabolic inflexibility of neurons. It is possible that the inability of neurons to make this metabolic switch during mitochondrial inhibition has direct effects on mitochondrial dynamics. It would be interesting to investigate mitochondrial fusion in neurons exposed to OXPHOS inhibitors following prolonged NDMAR stimulation, to assess if glycolysis could be activated to maintain fusion rates. Presumably, concomitant protection from oxidative stress would be required to circumvent the diversion of glucose away from the PPP during NMDAR stimulation (e.g. by applying NMDA and an antioxidant, e.g. N-acetylcysteine, simultaneously). A recent paper by Garedew and colleagues (2012) describes how APC^{Cdh1} negatively controls cellular levels of OPA1, Mfn1 and Tfam in T cells and MEFs. The high activity of APC^{Cdh1} in neurons could partially explain the relatively low expression of Mfn1 (Eura, *et al.,* 2003) and the relatively slower rate of mitochondrial fusion. Conceivably, inhibition of Cdh1, as occurs during NMDAR

stimulation (Rodriguez-Rodriguez *et al.*, 2012) could increase mitochondrial fusion through a gradual increase in cellular levels of OPA1 and Mfn1. This is a question that warrants further investigation.

The studies presented here also suggest that neuronal mitochondria can withstand at least ~33% inhibition of complex I before fusion is seriously compromised (fig 5.26). This is in line with the reports by our lab, and others, that neuronal complex I inhibition beyond 25 - 40% has significant consequences on respiration rates and leads to synaptic dysfunction, such as aberrant glutamate release (Davey *et al.*, 1998, Kilbride *et al.*, 2008, Telford *et al.*, 2009). A limited supply of neuronal cultures, combined with well-documented low transfection efficiencies of these cultures (Zeitelhofer *et al.*, 2009) restricted the dose-response to the concentrations presented. It would be useful to expand the data at the lower piericidin A range. A concentration of 10nM inhibits complex I in NSM/SYN by ~33%, while 50nM steeply increases inhibition to 75%. Preliminary data suggest that 25nM piericidin A also inhibits mitochondrial fusion (not shown) but it is not known to what extent complex I is inhibited at this concentration. It would also be useful to examine the degree of complex I inhibition at each piericidin A concentration in primary cortical neurons rather than isolated mitochondria and synaptosomes from adult rat brains, given the limited correlations that can be drawn between the two. This would require measurement of respiration with apparatus equipped for adherent cells, such as the Seahorse XF24 Extracellular Flux Analyser, which was not yet installed in our School during the course of this project.

Finally, it is interesting to note that $\Delta\Psi_m$ was modestly but statistically significantly reduced at the lowest dose of piericidin A that inhibited fusion (50nM), whereas ATP levels were only impacted from 100nM upwards. Neither parameter was affected at 10nM, which inhibited complex I by 35% but had no effect on fusion. This suggests that $\Delta\Psi_m$ plays a more prominent role in the dynamics of neuronal mitochondria than in HeLa cell mitohcondria. It has been reported that parkin is recruited to depolarised mitochondria, where it promotes mitophagy (Narendra *et al.*, 2008, Narendra *et al.*, 2009). Furthermore, it is proposed that fragmentation of mitochondria is required for mitotophagy to take place (Tondera *et al.*, 2009, Gomes *et al.*, 2011). Thus, it is possible that fusion is somehow inhibited during mitochondrial stress to allow for the clearance of sub-optimal organelles by autophagosomes. Further experiments examining

autophagosomal localisation with mitochondria following neuronal exposure to inhibitors may yield some informative data.

To summarise, these results firmly assert the dependence of cortical neurons on OXPHOS for maintenance of mitochondrial fusion rates. The presence of glucose during mitochondrial inhibition could not prevent fusion perturbation as it could in HeLa cells, indicating that neuronal metabolic inflexibility also affects mitochondrial fusogenicity. Moreover, it has been shown complex I inhibition with a threshold between ~33 – 75% adversely affects fusion. These data have relevance to neurodegenerative diseases such as AD, PD and HD, as each of these illnesses bear the hallmark pathophysiological feature of mitochondrial dysfunction. Small changes in mitochondrial function precipitated significant alterations in mitochondrial dynamics, highlighting the sensitivity of this particular process to bioenergetic inhibition in neurons.

CHAPTER 6

General Discussion

6.1 General Discussion

Research in the last decade has revealed mammalian mitochondria to exist as part of a dynamic reticulum, which undergoes constant ultrastructural remodelling to meet the demands of the cell. Mitochondria represent a vital control point for numerous essential cellular functions, including anabolic and catabolic metabolism, Ca^{2+} homeostasis, apoptosis and the regulation of cell cycle. As a field that is still in its infancy, mitochondrial dynamics and its regulatory pathways are still poorly understood. However, there is strong evidence to suggest that mitochondrial fission and fusion are essential in the preservation of organellar integrity, mtDNA quality control, metabolite exchange and regulation of the intrinsic apoptotic pathway. Disturbing the balance between mitochondrial fission and fusion has deleterious effects, not only on mitochondria but on the cell as a whole and as such, has wide implications for human health and disease. In particular, cancer and neurodegeneration bear the hallmarks of mitochondrial dysfunction as contributory to their pathophysiology, as affected cells in each case can exhibit bioenergetic and metabolic aberrations, mtDNA mutations/copy number reductions, ROS damage and mitochondrial morphological abnormalities.

While a sizeable amount of qualitative data has been generated in relation to mitochondrial morphological changes following bioenergetic modulation, there is a dearth of quantitative data describing the effects of bioenergetic inhibition on mitochondrial fusion rates. In an effort to elucidate the consequences of metabolic dysregulation on mitochondrial dynamics, this study examined mitochondrial fusion rates in human cervical carcinoma cells and rat primary cortical neurons during bioenergetic inhibition. A semi-quantitative method was employed, using live cell confocal microscopy and cells expressing PA-GFP-mito, which allowed for the measurement of PI decrease in photo-activated areas as a function of active mitochondrial fusion.

Chapters 3 and 4 described the substrate-dependent changes in HeLa cell mitochondrial fusion rates in response to bioenergetic/metabolic inhibition. Gluc-HeLa cell mitochondrial fusion rates proved to be impervious to ETC inhibition but vulnerable to ATP synthase inhibition. Inhibition of glucose metabolism impacted mitochondrial fusion most severely in these cells and supplementation of the medium with alternative substrates failed to restore fusion rates to control levels. Gal-HeLa cell mitochondrial fusion was seriously perturbed by OXPHOS inhibition, but rescued if glucose was made

available during this inhibition. In addition, fusion inhibition by DOG or OXPHOS inhibitors was predictive of significant cell death that resulted from 24 hour incubation. Finally, Chapter 5 demonstrated that neuronal mitochondrial fusion was completely inhibited by OXPHOS inhibition, despite hyperglycaemic culture conditions, highlighting a key difference in metabolic flexibility between these cell types. Although cell death after 24 hour incubation with inhibitors was not measured in neurons, massive cell death following exposure to these toxins is well established and documented (Radad *et al.*, 2006, Yao *et al.*, 2011a). Thus, inhibition of mitochondrial fusion could be an early event in the cell death cascade resulting from bioenergetic inhibition across multiple cell types.

Taken together, Chapters 3 and 4 could be described as an examination of mitochondrial dynamics in cancer cells during an approximation of two distinct stages of the 'wave' hypothesis of gene regulation in cancer, postulated by Smolkova *et al.* (2011). The hypothesis states that in response to environmental cues and substrate availability waves of gene regulation co-ordinately diminish and restore OXPHOS in tandem with the stages of cancer progression. In the studies presented here, fusion dynamics have been shown to change in response to mitochondrial inhibition in a substrate-dependent manner. Thus, the 'waves' of gene expression regulating the metabolic flux in cancer cells could have effects on mitochondrial dynamics. Although cancer-selective delivery represents one of the greatest challenges of mitochondrial medicine ('mitocans') design (D'Souza *et al.*, 2011), it seems that therapeutically targeting mitochondria whilst also inhibiting glucose metabolism may be more efficacious than targeting either alone, especially because tumours are frequently composed of heterogeneous layers of cells that vary their metabolism in response to nutrient and oxygen availability (Jose *et al.*, 2011).

Chapter 5 examined mitochondrial dynamics in primary cortical neurons. It was demonstrated that, much like Gal-HeLa cells, mitochondrial fusion in these cells demanded a fully functioning OXPHOS system. Furthermore, the mitochondrial reticulum fragmented within minutes of application of inhibitors, indicating the most extreme sensitivity of all cells examined was by far in neurons. Thus, these studies quantified the fusion deficit in OXPHOS-inhibited neurons to be close to 100%. Significantly, neurons were unable to utilise glucose to rescue mitochondrial fusion rates when faced with OXPHOS inhibition, highlighting an important difference in metabolic flexibility between neurons and cancer cells. Intriguingly, similarities between neurons

and cancer cells and their metabolism of glucose have been described in the context of apoptosis regulation. Vaughn and Deshmukh (2008) have shown that both neurons and cancer cells utilise the glucose metabolism, *via* the PPP, to generate GSH and reduce oxidised cytochrome c when released to the cytosol, rendering it a less effective inducer of apoptosis. Thus, while cancer cells and neurons share the ability to use glucose in ROS defence, the studies presented here show that neurons are at a distinct disadvantage when required to use glucose in the maintenance of fusion rates. This is possibly due to their metabolic inflexibility arising from rapid degradation of PFKFB3 (Almeida *et al.*, 2001, 2004, Herrero-Mendez *et al.*, 2009).

It was also suggested in Chapter 5 that neurons could withstand at least 33% complex I inhibition before mitochondrial fusion rates were seriously compromised. Although ATP levels correlated well with mitochondrial fusion decreases, mitochondrial depolarisation showed stronger still correlation, potentially indicating a difference in the mechanisms behind fusion perturbation under these conditions, compared to HeLa cells. In fact, all inhibitors affected $\Delta\Psi_m$ to a much greater extent than in HeLa cells, perhaps indicating different rates of ATP hydrolysis by ATP synthase between these cells. Indeed, IF_1 has been shown to be more highly expressed in neurons compared to more glycolytic astrocytes and inhibition of complex IV in both cells leads to significant depolarisation in the former, while the latter maintains a $\Delta\Psi_m$ steady state (Almeida *et al.*, 2001, Campanella *et al.*, 2008).

Overall, the results of these studies highlight the diverse nature of the bidirectional bioenergetic-dynamic crosstalk between cell types, and even within cell types. It has been demonstrated that in HeLa cells, but not neurons, glucose metabolism is protective of fusion rates when mitochondria are under bioenergetic duress.

6.2 Future Work

There are many aspects of mitochondrial dynamics in health and disease that await further investigation. Specifically, all of the fission/fusion effectors have yet to be identified, as do the mechanisms behind the execution of fission and fusion events. The importance of mitochondrial dynamics in the regulation of apoptosis also remains poorly understood. The interaction between bioenergetics and mitochondrial dynamics is

extremely obscure, as no clear pattern emerges between cell types. Indeed, the pattern may be that the dynamic properties of mitochondrial are unique to each cell type. This fact may hinder the development of therapeutic agents targeting this aspect of mitochondrial function. Additional experimentation based on the work presented here could yield useful information.

One question that dominates studies regarding bioenergetic modulation of mitochondrial morphology is why mitochondria undergo reversible fragmentation in the presence of uncouplers. While elegant studies by Guillery *et al.* (2008) and Ishihara *et al.* (2006), among others, have answered the question of *how* this occurs, it is still not known *why* this occurs. In this thesis, it is proposed that this may be a method of segregating the inner membrane into smaller units so as to prevent the release of pro-apoptotic modulators, as a similar process is observed in yeast (Knorre *et al.*, 2008). This may become maladaptive if the depolarising agent is a chronic presence, leading to mitochondrial heterogeneity and dysfunction (Chen *et al.*, 2005). This issue clearly warrants further investigation.

With regard to the HeLa cells studies, it is imperative to elucidate the reason for mitochondrial fusion inhibition following ATP synthase inhibition. This enzyme has unique expression patterns in cancer (Willers and Cuezva, 2011) and ATP synthase inhibition was the only form of bioenergetic modulation that affected HeLa cells across both substrates. This suggests a unique vulnerability to ATP synthase inhibition across cancers of different metabolic phenotypes, i.e. is a substrate-independent effect. It is also important verify further the observation that DRP1 translocation of Gal-HeLa mitochondria is increased ETC inhibition. This could be achieved through microscopic analysis of treated cells immunostained for DRP1 and a mitochondrial marker. Furthermore, it would be pertinent to knock down DRP1 in Gal-HeLa cells to assess if fusion is still adversely affected by OXPHOS inhibition. If the fragmentation is due to the onset of apoptosis, immunostaining for cytochrome c should be possible, as fragmentation is said to occur up to ten minutes following MOMP (Gao *et al.*, 2001).

An important line of investigation pertaining to all studies is the examination of ROS production during treatments that inhibited mitochondrial fusion. Virtually all treatments that precipitated a fusion deficit across cells and substrates are likely to have

increased ROS production and/or affected ROS defence mechanisms; DOG would prevent G6P entry to the PPP and thus prevent NADPH and GSH regeneration, while inhibiting OXPHOS is a classic stimulus of ROS production. Cellular ROS could be assessed microscopically on live cells using a fluorescent indicator, such a dichlorofluorescein (DCF) or using flow cytometry, while oxidative stress could be determined by measurement of the GSH:GSSG ratio. To determine whether prevention of oxidative stress rescued fusion rates, cells could be treated with anti-oxidants (such as NAC or cell permeable GSH) concomitantly with DOG/OXPHOS inhibitors.

The results obtained using DOG in Gluc-HeLa cells are particularly captivating as they raise many questions as to the specific deficit caused by inhibition of glucose metabolism in these cells. In addition to the effects on ATP demonstrated and potential effects on ROS defence, it is possible that DOG-6-phosphate is responsible for the fusion effects through interaction with HK II. It was found that HK II was enriched at the OM of Gal-HeLa cell mitochondria, despite a marked absence in the cytosol. Treatment of Gal-HeLa cells with DOG should have no effect on cellular ATP or GSH levels, as G6P production can be maintained by the Leloir pathway. Therefore, it would be interesting to assess if there was an effect of DOG on fusion, or viability in Gal-HeLa cells. If an effect was observed, an additional role for HK in regulation of mitochondrial dynamics in cancer could be established. Indeed, this may shed light on the mechanism of cytotoxicity induced by detachment of HK II from the mitochondrial OM in cancer cells.

A number of lines of investigation are still open regarding the neuron studies. The first is the influence of glycolysis on mitochondrial fusion rates in these cells. As described in the previous chapter, it would be extremely interesting to assess whether stabilising PFKFB3 in neurons (using NMDA) whilst compensating for oxidative stress (using an anti-oxidant) could rescue fusion rates in neurons. The second is that the mechanism of the fusion inhibition, combined with complete fragmentation of the reticulum, has not been assessed. Immunocytochemical studies may shed light on the issue of DRP1 recruitment. It is also not obvious whether the mitochondria are undergoing swelling/'remodelling' or fission. If it is the former, why and how does swelling inhibit fusion or what is mediating this 'remodelling'? If it is the latter, it would be interesting to examine OPA1 proteolytic cleavage patterns in neurons following ETC inhibition.

Neurons exhibited extensive (~80%) decrease in $\Delta\Psi_m$ following treatments that reduced $\Delta\Psi_m$ by just ~20% in HeLa cells; in this way, the depolarisation of neuronal mitochondria might be closer to the threshold below which L-OPA1 is cleaved. The third important line of investigation is the expansion of the piericidin A titration in the lower concentration range. As aforementioned, preliminary data suggest that 25nM piericidin A also inhibits fusion, but this requires repetition before it can be definitively declared. In addition, a more robust method of estimating the degree of complex I inhibition induced by each piericidin A dose is required. For example, respirometry using the Seahorse XF24 Extracellular Flux Analyser system, which has very recently been installed in the School, has been used for this purpose by a number of groups (Brustovetsky *et al.*, 2011, Yao *et al.*, 2011b).

A final line of investigation pertaining to this work is the role of metabolic regulatory signalling pathways in mitochondrial dynamics. The inhibitory effects of mTOR inhibition on Jurkat cell mitochondrial function occur within 25 minutes of rapamycin treatment (Schieke *et al.*, 2006, Ramanathan and Schreiber, 2009). This time point is quite comparable to the studies presented in this thesis as most incubations were for 20 minutes. The increase in cellular AMP that is likely to have occurred during cell treatments that lowered cellular ATP could have activated AMPK, leading to inhibition of mTOR signalling, with potential effects on mitochondrial function. To this end, measurement of cellular AMPK and mTOR activity following inhibitor treatment (using antibodies raised against phosphorylated forms of each in conjunction with Western blotting or flow cytometry) would be useful. In addition, fusion could be measured during chemical stimulation or inhibition of AMPK (using 5-aminoimidazole-4-carboxamide-1-β-D-ribofuranoside (AICAR) and Compound C, respectively) and inhibition of mTOR (rapamycin) signalling. If a positive result emerged, substantial further investigation would be required to define the probably complex mechanism around this AMPK/mTOR signalling control of mitochondrial dynamics. A sensible starting point would be to assess the PTM status of the mitodynamins by a combination of Western blotting, immunoprecipitation and mass spectrometry.

To conclude, these studies have yielded some important results relating to the influence of bioenergetic modulation on mitochondrial fusion rates in cancer cells of differing metabolic phenotypes and in neurons, thus contributing to our understanding of

potential routes to pathogenesis *via* mitochondrial dynamics. However, questions surrounding the mechanisms behind these effects remain to be resolved. It is anticipated that further studies will address these issues and hopefully contribute significantly to mitochondrial research in the context of cell biology, cancer and neurodegeneration.

6.3 Conclusions of the Thesis

These studies have quantified for the first time the effects of bioenergetic modulation on mitochondrial fusion rates in cancer cells and neurons. The most significant conclusions that can be drawn from this work are:

1. Mitochondrial fusion is inextricably linked to the bioenergetic status of the cell but the intricacies of this dynamic relationship differ between cell types.
2. Perturbation of fusion is an early event in cell death resulting from prolonged bioenergetic inhibition, during which time the mitochondrial reticulum loses structural integrity and fragments completely.
3. Glucose metabolism is protective of mitochondrial fusion rates during inhibition of OXPHOS in cancer cells, but not in neurons.

BIBLIOGRAPHY

ABOU-SLEIMAN, P. M., MUQIT, M. M. K. & WOOD, N. W. 2006. Expanding insights of mitochondrial dysfunction in Parkinson's disease. *Nat Rev Neurosci,* 7, 207-219.

ADAM-VIZI, V. & CHINOPOULOS, C. 2006. Bioenergetics and the formation of mitochondrial reactive oxygen species. *Trends Pharmacol Sci,* 27, 639-45.

AFT, R. L., ZHANG, F. W. & GIUS, D. 2002. Evaluation of 2-deoxy-D-glucose as a chemotherapeutic agent: mechanism of cell death. *Br J Cancer,* 87, 805-12.

ALEXANDER, C., VOTRUBA, M., PESCH, U. E., THISELTON, D. L., MAYER, S., MOORE, A., RODRIGUEZ, M., KELLNER, U., LEO-KOTTLER, B., AUBURGER, G., BHATTACHARYA, S. S. & WISSINGER, B. 2000. OPA1, encoding a dynamin-related GTPase, is mutated in autosomal dominant optic atrophy linked to chromosome 3q28. *Nat Genet,* 26, 211-5.

ALMEIDA, A., ALMEIDA, J., BOLANOS, J. P. & MONCADA, S. 2001. Different responses of astrocytes and neurons to nitric oxide: the role of glycolytically generated ATP in astrocyte protection. *Proc Natl Acad Sci U S A,* 98, 15294-9.

ALMEIDA, A., MONCADA, S. & BOLANOS, J. P. 2004. Nitric oxide switches on glycolysis through the AMP protein kinase and 6-phosphofructo-2-kinase pathway. *Nat Cell Biol,* 6, 45-51.

AMATI-BONNEAU, P., VALENTINO, M. L., REYNIER, P., GALLARDO, M. E., BORNSTEIN, B., BOISSIERE, A., CAMPOS, Y., RIVERA, H., DE LA ALEJA, J. G., CARROCCIA, R., IOMMARINI, L., LABAUGE, P., FIGARELLA-BRANGER, D., MARCORELLES, P., FURBY, A., BEAUVAIS, K., LETOURNEL, F., LIGUORI, R., LA MORGIA, C., MONTAGNA, P., LIGUORI, M., ZANNA, C., RUGOLO, M., COSSARIZZA, A., WISSINGER, B., VERNY, C., SCHWARZENBACHER, R., MARTIN, M. A., ARENAS, J., AYUSO, C., GARESSE, R., LENAERS, G., BONNEAU, D. & CARELLI, V. 2008. OPA1 mutations induce mitochondrial DNA instability and optic atrophy 'plus' phenotypes. *Brain,* 131, 338-51.

ARISMENDI-MORILLO, G. 2009. Electron microscopy morphology of the mitochondrial network in human cancer. *The International Journal of Biochemistry & Cell Biology,* 41, 2062-2068.

ARISMENDI-MORILLO, G. 2011. Electron microscopy morphology of the mitochondrial network in gliomas and their vascular microenvironment. *Biochim Biophys Acta,* 1807, 602-8.

ARISMENDI-MORILLO, G. J. & CASTELLANO-RAMIREZ, A. V. 2008. Ultrastructural mitochondrial pathology in human astrocytic tumors: potentials implications pro-therapeutics strategies. *Journal of electron microscopy,* 57, 33-39.

ARNOULT, D., GRODET, A., LEE, Y. J., ESTAQUIER, J. & BLACKSTONE, C. 2005. Release of OPA1 during apoptosis participates in the rapid and complete release of cytochrome c and subsequent mitochondrial fragmentation. *J Biol Chem,* 280, 35742-50.

ASTRUP, A., ANDERSEN, T., CHRISTENSEN, N. J., BULOW, J., MADSEN, J., BREUM, L. & QUAADE, F. 1990. Impaired glucose-induced thermogenesis and arterial norepinephrine response persist after weight reduction in obese humans. *Am J Clin Nutr,* 51, 331-7.

AUTRET, A. & MARTIN, S. J. 2010. Bcl-2 family proteins and mitochondrial fission/fusion dynamics. *Cell Mol Life Sci,* 67, 1599-606.

AZIM, H., AZIM, H. A., JR. & ESCUDIER, B. 2010. Targeting mTOR in cancer: renal cell is just a beginning. *Target Oncol,* 5, 269-80.

AZOULAY-ZOHAR, H., ISRAELSON, A., ABU-HAMAD, S. & SHOSHAN-BARMATZ, V. 2004. In self-defence: hexokinase promotes voltage-dependent anion channel closure and prevents mitochondria-mediated apoptotic cell death. *Biochemical Journal,* 377, 347.

BACH, D., NAON, D., PICH, S., SORIANO, F. X., VEGA, N., RIEUSSET, J., LAVILLE, M., GUILLET, C., BOIRIE, Y., WALLBERG-HENRIKSSON, H., MANCO, M., CALVANI, M., CASTAGNETO, M., PALACIN, M., MINGRONE, G., ZIERATH, J. R., VIDAL, H. & ZORZANO, A. 2005. Expression of Mfn2, the Charcot-Marie-Tooth neuropathy type 2A gene, in human skeletal muscle: effects of type 2 diabetes, obesity, weight loss, and the regulatory role of tumor necrosis factor alpha and interleukin-6. *Diabetes,* 54, 2685-93.

BACH, D., PICH, S., SORIANO, F. X., VEGA, N., BAUMGARTNER, B., ORIOLA, J., DAUGAARD, J. R., LLOBERAS, J., CAMPS, M., ZIERATH, J. R., RABASA-LHORET, R., WALLBERG-HENRIKSSON, H., LAVILLE, M., PALACIN, M., VIDAL, H., RIVERA, F., BRAND, M. & ZORZANO, A. 2003. Mitofusin-2 determines mitochondrial network architecture and mitochondrial metabolism. A novel regulatory mechanism altered in obesity. *J Biol Chem,* 278, 17190-7.

BALOH, R. H. 2008. Mitochondrial dynamics and peripheral neuropathy. *Neuroscientist,* 14, 12-8.

BARICAULT, L., SEGUI, B., GUEGAND, L., OLICHON, A., VALETTE, A., LARMINAT, F. & LENAERS, G. 2007. OPA1 cleavage depends on decreased mitochondrial ATP level and bivalent metals. *Exp Cell Res,* 313, 3800-8.

BARSOUM, M. J., YUAN, H., GERENCSER, A. A., LIOT, G., KUSHNAREVA, Y., GRABER, S., KOVACS, I., LEE, W. D., WAGGONER, J., CUI, J., WHITE, A. D., BOSSY, B., MARTINOU, J. C., YOULE, R. J., LIPTON, S. A., ELLISMAN, M. H., PERKINS, G. A. & BOSSY-WETZEL, E. 2006. Nitric oxide-induced mitochondrial fission is regulated by dynamin-related GTPases in neurons. *EMBO J,* 25, 3900-11.

BECHTEL, W. & ABRAHAMSEN, A. 2007. In search of mitochondrial mechanisms: interfield excursions between cell biology and biochemistry. *J Hist Biol,* 40, 1-33.

BECKNER, M. E., GOBBEL, G. T., ABOUNADER, R., BUROVIC, F., AGOSTINO, N. R., LATERRA, J. & POLLACK, I. F. 2005. Glycolytic glioma cells with active glycogen synthase are sensitive to PTEN and inhibitors of PI3K and gluconeogenesis. *Lab Invest,* 85, 1457-1470.

BENARD, G., BELLANCE, N., JAMES, D., PARRONE, P., FERNANDEZ, H., LETELLIER, T. & ROSSIGNOL, R. 2007. Mitochondrial bioenergetics and structural network organization. *J Cell Sci,* 120, 838-48.

BENARD, G., BELLANCE, N., JOSE, C. & ROSSIGNOL, R. 2011. Relationships Between Mitochondrial Dynamics and Bioenergetics. *Mitochondrial Dynamics and Neurodegeneration*, 47.

BERMAN, S. B., CHEN, Y. B., QI, B., MCCAFFERY, J. M., RUCKER, E. B., 3RD, GOEBBELS, S., NAVE, K. A., ARNOLD, B. A., JONAS, E. A., PINEDA, F. J. & HARDWICK, J. M. 2009. Bcl-x L increases mitochondrial fission, fusion, and biomass in neurons. *J Cell Biol,* 184, 707-19.

BIANCHI, C., GENOVA, M. L., PARENTI CASTELLI, G. & LENAZ, G. 2004. The mitochondrial respiratory chain is partially organized in a supercomplex assembly: kinetic evidence using flux control analysis. *J Biol Chem,* 279, 36562-9.

BILLUPS, B. & FORSYTHE, I. D. 2002. Presynaptic mitochondrial calcium sequestration influences transmission at mammalian central synapses. *J Neurosci,* 22, 5840-7.

BLAKER, W. D., GOODRUM, J. F. & MORELL, P. 1981. Axonal transport of the mitochondria-specific lipid, diphosphatidylglycerol, in the rat visual system. *J Cell Biol,* 89, 579-84.

BLASS, J. P. 2000. The mitochondrial spiral. An adequate cause of dementia in the Alzheimer's syndrome. *Ann N Y Acad Sci,* 924, 170-83.

BLEAZARD, W., MCCAFFERY, J. M., KING, E. J., BALE, S., MOZDY, A., TIEU, Q., NUNNARI, J. & SHAW, J. M. 1999. The dynamin-related GTPase Dnm1 regulates mitochondrial fission in yeast. *Nat Cell Biol,* 1, 298-304.

BOEKEMA, E. J. & BRAUN, H. P. 2007. Supramolecular structure of the mitochondrial oxidative phosphorylation system. *J Biol Chem,* 282, 1-4.

BOLANOS, J. P., ALMEIDA, A. & MONCADA, S. 2010. Glycolysis: a bioenergetic or a survival pathway? *Trends Biochem Sci,* 35, 145-9.

BORER, R. A., LEHNER, C. F., EPPENBERGER, H. M. & NIGG, E. A. 1989. Major nucleolar proteins shuttle between nucleus and cytoplasm. *Cell,* 56, 379-390.

BORLONGAN, C. V., KOUTOUZIS, T. K. & SANBERG, P. R. 1997. 3-Nitropropionic acid animal model and Huntington's disease. *Neurosci Biobehav Rev,* 21, 289-93.

BOSSY-WETZEL, E., PETRILLI, A. & KNOTT, A. B. 2008. Mutant huntingtin and mitochondrial dysfunction. *Trends Neurosci,* 31, 609-16.

BRAAK, H., GHEBREMEDHIN, E., RUB, U., BRATZKE, H. & DEL TREDICI, K. 2004. Stages in the development of Parkinson's disease-related pathology. *Cell Tissue Res,* 318, 121-34.

BRADFORD, M. M. 1976. A rapid and sensitive method for the quantitation of microgram quantities of protein utilizing the principle of protein-dye binding. *Anal Biochem,* 72, 248-54.

BRAND, M. D. & NICHOLLS, D. G. 2011. Assessing mitochondrial dysfunction in cells. *Biochem J,* 435, 297-312.

BRANDON, M., BALDI, P. & WALLACE, D. C. 2006. Mitochondrial mutations in cancer. *Oncogene,* 25, 4647-62.

BRUSTOVETSKY, T., BRITTAIN, M. K., SHEETS, P. L., CUMMINS, T. R., PINELIS, V. & BRUSTOVETSKY, N. 2011. KB-R7943, an inhibitor of the

reverse Na+ /Ca2+ exchanger, blocks N-methyl-D-aspartate receptor and inhibits mitochondrial complex I. *Br J Pharmacol,* 162**,** 255-70.

BURBULLA, L. F., KREBIEHL, G. & KRUGER, R. 2010. Balance is the challenge--the impact of mitochondrial dynamics in Parkinson's disease. *Eur J Clin Invest,* 40, 1048-60.

BUSTAMANTE, E. & PEDERSEN, P. L. 1980. Mitochondrial hexokinase of rat hepatoma cells in culture: solubilization and kinetic properties. *Biochemistry,* 19, 4972-7.

CAI, Q. & SHENG, Z. H. 2009. Mitochondrial transport and docking in axons. *Exp Neurol,* 218, 257-67.

CALKINS, M. J., MANCZAK, M., MAO, P., SHIRENDEB, U. & REDDY, P. H. 2011. Impaired mitochondrial biogenesis, defective axonal transport of mitochondria, abnormal mitochondrial dynamics and synaptic degeneration in a mouse model of Alzheimer's disease. *Hum Mol Genet,* 20, 4515-29.

CAMPANELLA, M., CASSWELL, E., CHONG, S., FARAH, Z., WIECKOWSKI, M. R., ABRAMOV, A. Y., TINKER, A. & DUCHEN, M. R. 2008. Regulation of mitochondrial structure and function by the F1Fo-ATPase inhibitor protein, IF1. *Cell Metab,* 8, 13-25.

CANET-AVILES, R. M., WILSON, M. A., MILLER, D. W., AHMAD, R., MCLENDON, C., BANDYOPADHYAY, S., BAPTISTA, M. J., RINGE, D., PETSKO, G. A. & COOKSON, M. R. 2004. The Parkinson's disease protein DJ-1 is neuroprotective due to cysteine-sulfinic acid-driven mitochondrial localization. *Proc Natl Acad Sci U S A,* 101, 9103-8.

CANEVARI, L., CLARK, J. B. & BATES, T. E. 1999. beta-Amyloid fragment 25-35 selectively decreases complex IV activity in isolated mitochondria. *FEBS Lett,* 457, 131-4.

CAPALDI, R. A., AGGELER, R., GILKERSON, R., HANSON, G., KNOWLES, M., MARCUS, A., MARGINEANTU, D., MARUSICH, M., MURRAY, J., OGLESBEE, D., REMINGTON, S. J. & ROSSIGNOL, R. 2002. A replicating module as the unit of mitochondrial structure and functioning. *Biochim Biophys Acta,* 1555, 192-5.

CARTONI, R., LEGER, B., HOCK, M. B., PRAZ, M., CRETTENAND, A., PICH, S., ZILTENER, J. L., LUTHI, F., DERIAZ, O., ZORZANO, A., GOBELET, C., KRALLI, A. & RUSSELL, A. P. 2005. Mitofusins 1/2 and ERRalpha expression are increased in human skeletal muscle after physical exercise. *J Physiol,* 567, 349-58.

CASARI, G., DE FUSCO, M., CIARMATORI, S., ZEVIANI, M., MORA, M., FERNANDEZ, P., DE MICHELE, G., FILLA, A., COCOZZA, S., MARCONI, R., DURR, A., FONTAINE, B. & BALLABIO, A. 1998. Spastic paraplegia and OXPHOS impairment caused by mutations in paraplegin, a nuclear-encoded mitochondrial metalloprotease. *Cell,* 93, 973-83.

CEREGHETTI, G. M., COSTA, V. & SCORRANO, L. 2010. Inhibition of Drp1-dependent mitochondrial fragmentation and apoptosis by a polypeptide antagonist of calcineurin. *Cell Death Differ,* 17, 1785-94.

CEREGHETTI, G. M., STANGHERLIN, A., MARTINS DE BRITO, O., CHANG, C. R., BLACKSTONE, C., BERNARDI, P. & SCORRANO, L. 2008. Dephosphorylation by calcineurin regulates translocation of Drp1 to mitochondria. *Proc Natl Acad Sci U S A,* 105, 15803-8.

CHANCE, B., SIES, H. & BOVERIS, A. 1979. Hydroperoxide metabolism in mammalian organs. *Physiol Rev,* 59, 527-605.

CHANG, C. R. & BLACKSTONE, C. 2007. Cyclic AMP-dependent protein kinase phosphorylation of Drp1 regulates its GTPase activity and mitochondrial morphology. *J Biol Chem,* 282, 21583-7.

CHANG, C. R. & BLACKSTONE, C. 2010. Dynamic regulation of mitochondrial fission through modification of the dynamin-related protein Drp1. *Ann N Y Acad Sci,* 1201, 34-9.

CHANG, D. T. & REYNOLDS, I. J. 2006. Differences in mitochondrial movement and morphology in young and mature primary cortical neurons in culture. *Neuroscience,* 141, 727-36.

CHANG, D. T., RINTOUL, G. L., PANDIPATI, S. & REYNOLDS, I. J. 2006. Mutant huntingtin aggregates impair mitochondrial movement and trafficking in cortical neurons. *Neurobiol Dis,* 22, 388-400.

CHEN, H. & CHAN, D. C. 2009. Mitochondrial dynamics--fusion, fission, movement, and mitophagy--in neurodegenerative diseases. *Hum Mol Genet,* 18, R169-76.

CHEN, H., CHOMYN, A. & CHAN, D. C. 2005. Disruption of fusion results in mitochondrial heterogeneity and dysfunction. *J Biol Chem,* 280, 26185-92.

CHEN, H., DETMER, S. A., EWALD, A. J., GRIFFIN, E. E., FRASER, S. E. & CHAN, D. C. 2003. Mitofusins Mfn1 and Mfn2 coordinately regulate mitochondrial fusion and are essential for embryonic development. *J Cell Biol,* 160, 189-200.

CHEN, H., MCCAFFERY, J. M. & CHAN, D. C. 2007. Mitochondrial fusion protects against neurodegeneration in the cerebellum. *Cell,* 130, 548-62.

CHEN, H., VERMULST, M., WANG, Y. E., CHOMYN, A., PROLLA, T. A., MCCAFFERY, J. M. & CHAN, D. C. 2010. Mitochondrial fusion is required for mtDNA stability in skeletal muscle and tolerance of mtDNA mutations. *Cell,* 141, 280-9.

CHEN, K. H., GUO, X., MA, D., GUO, Y., LI, Q., YANG, D., LI, P., QIU, X., WEN, S., XIAO, R. P. & TANG, J. 2004. Dysregulation of HSG triggers vascular proliferative disorders. *Nat Cell Biol,* 6, 872-83.

CHERNYAK, B. V., IZYUMOV, D. S., LYAMZAEV, K. G., PASHKOVSKAYA, A. A., PLETJUSHKINA, O. Y., ANTONENKO, Y. N., SAKHAROV, D. V., WIRTZ, K. W. & SKULACHEV, V. P. 2006. Production of reactive oxygen species in mitochondria of HeLa cells under oxidative stress. *Biochim Biophys Acta,* 1757, 525-34.

CHIARA, F., CASTELLARO, D., MARIN, O., PETRONILLI, V., BRUSILOW, W. S., JUHASZOVA, M., SOLLOTT, S. J., FORTE, M., BERNARDI, P. & RASOLA, A. 2008. Hexokinase II detachment from mitochondria triggers apoptosis through the permeability transition pore independent of voltage-dependent anion channels. *PLoS One,* 3, e1852.

CHICHE, J., ROULEAU, M., GOUNON, P., BRAHIMI-HORN, M. C., POUYSSEGUR, J. & MAZURE, N. M. 2010. Hypoxic enlarged mitochondria protect cancer cells from apoptotic stimuli. *J Cell Physiol,* 222, 648-57.

CHO, D. H., NAKAMURA, T., FANG, J., CIEPLAK, P., GODZIK, A., GU, Z. & LIPTON, S. A. 2009. S-nitrosylation of Drp1 mediates beta-amyloid-related mitochondrial fission and neuronal injury. *Science,* 324, 102-5.

CHOI, W. S., PALMITER, R. D. & XIA, Z. 2011. Loss of mitochondrial complex I activity potentiates dopamine neuron death induced by microtubule dysfunction in a Parkinson's disease model. *J Cell Biol,* 192, 873-82.

CIPOLAT, S., MARTINS DE BRITO, O., DAL ZILIO, B. & SCORRANO, L. 2004. OPA1 requires mitofusin 1 to promote mitochondrial fusion. *Proc Natl Acad Sci U S A,* 101, 15927-32.

CIPOLAT, S., RUDKA, T., HARTMANN, D., COSTA, V., SERNEELS, L., CRAESSAERTS, K., METZGER, K., FREZZA, C., ANNAERT, W., D'ADAMIO, L., DERKS, C., DEJAEGERE, T., PELLEGRINI, L., D'HOOGE, R., SCORRANO, L. & DE STROOPER, B. 2006. Mitochondrial rhomboid PARL regulates cytochrome c release during apoptosis via OPA1-dependent cristae remodeling. *Cell,* 126, 163-75.

COLIN, E., ZALA, D., LIOT, G., RANGONE, H., BORRELL-PAGES, M., LI, X. J., SAUDOU, F. & HUMBERT, S. 2008. Huntingtin phosphorylation acts as a molecular switch for anterograde/retrograde transport in neurons. *EMBO J,* 27, 2124-34.

CREAGH, E. M. & MARTIN, S. J. 2003. Cell stress-associated caspase activation: intrinsically complex? *Sci STKE,* 2003, pe11.

CRIBBS, J. T. & STRACK, S. 2007. Reversible phosphorylation of Drp1 by cyclic AMP-dependent protein kinase and calcineurin regulates mitochondrial fission and cell death. *EMBO Rep,* 8, 939-44.

CULMSEE, C., MONNIG, J., KEMP, B. E. & MATTSON, M. P. 2001. AMP-activated protein kinase is highly expressed in neurons in the developing rat brain and promotes neuronal survival following glucose deprivation. *J Mol Neurosci,* 17, 45-58.

CUNNINGHAM, J. T., RODGERS, J. T., ARLOW, D. H., VAZQUEZ, F., MOOTHA, V. K. & PUIGSERVER, P. 2007. mTOR controls mitochondrial oxidative function through a YY1-PGC-1alpha transcriptional complex. *Nature,* 450, 736-40.

DANG, C. V., LE, A. & GAO, P. 2009. MYC-induced cancer cell energy metabolism and therapeutic opportunities. *Clin Cancer Res,* 15, 6479-83.

DAUER, W. & PRZEDBORSKI, S. 2003. Parkinson's disease: mechanisms and models. *Neuron,* 39, 889-909.

DAVEY, G. P., CANEVARI, L. & CLARK, J. B. 1997. Threshold effects in synaptosomal and nonsynaptic mitochondria from hippocampal CA1 and paramedian neocortex brain regions. *J Neurochem,* 69, 2564-70.

DAVEY, G. P. & CLARK, J. B. 1996. Threshold effects and control of oxidative phosphorylation in nonsynaptic rat brain mitochondria. *J Neurochem,* 66, 1617-24.

DAVEY, G. P., PEUCHEN, S. & CLARK, J. B. 1998. Energy thresholds in brain mitochondria. Potential involvement in neurodegeneration. *J Biol Chem,* 273, 12753-7.

DE BRITO, O. M. & SCORRANO, L. 2008a. Mitofusin 2 tethers endoplasmic reticulum to mitochondria. *Nature,* 456, 605-10.

DE BRITO, O. M. & SCORRANO, L. 2008b. Mitofusin 2: a mitochondria-shaping protein with signaling roles beyond fusion. *Antioxid Redox Signal,* 10, 621-33.

DE BRITO, O. M. & SCORRANO, L. 2009. Mitofusin-2 regulates mitochondrial and endoplasmic reticulum morphology and tethering: the role of Ras. *Mitochondrion,* 9, 222-6.

DE MOURA, M. B., DOS SANTOS, L. S. & VAN HOUTEN, B. 2010. Mitochondrial dysfunction in neurodegenerative diseases and cancer. *Environmental and molecular mutagenesis,* 51, 391-405.

DE VOS, K. J., ALLAN, V. J., GRIERSON, A. J. & SHEETZ, M. P. 2005. Mitochondrial function and actin regulate dynamin-related protein 1-dependent mitochondrial fission. *Curr Biol,* 15, 678-83.

DEBERARDINIS, R. J., MANCUSO, A., DAIKHIN, E., NISSIM, I., YUDKOFF, M., WEHRLI, S. & THOMPSON, C. B. 2007. Beyond aerobic glycolysis: transformed cells can engage in glutamine metabolism that exceeds the requirement for protein and nucleotide synthesis. *Proc Natl Acad Sci U S A,* 104, 19345-50.

DELETTRE, C., GRIFFOIN, J. M., KAPLAN, J., DOLLFUS, H., LORENZ, B., FAIVRE, L., LENAERS, G., BELENGUER, P. & HAMEL, C. P. 2001. Mutation spectrum and splicing variants in the OPA1 gene. *Hum Genet,* 109, 584-91.

DELETTRE, C., LENAERS, G., GRIFFOIN, J. M., GIGAREL, N., LORENZO, C., BELENGUER, P., PELLOQUIN, L., GROSGEORGE, J., TURC-CAREL, C., PERRET, E., ASTARIE-DEQUEKER, C., LASQUELLEC, L., ARNAUD, B., DUCOMMUN, B., KAPLAN, J. & HAMEL, C. P. 2000. Nuclear gene OPA1, encoding a mitochondrial dynamin-related protein, is mutated in dominant optic atrophy. *Nat Genet,* 26, 207-10.

DENG, H., DODSON, M. W., HUANG, H. & GUO, M. 2008. The Parkinson's disease genes pink1 and parkin promote mitochondrial fission and/or inhibit fusion in Drosophila. *Proc Natl Acad Sci U S A,* 105, 14503-8.

DESAI, A. & MITCHISON, T. J. 1997. Microtubule polymerization dynamics. *Annu Rev Cell Dev Biol,* 13, 83-117.

DESAI, B. N., MYERS, B. R. & SCHREIBER, S. L. 2002. FKBP12-rapamycin-associated protein associates with mitochondria and senses osmotic stress via mitochondrial dysfunction. *Proc Natl Acad Sci U S A,* 99, 4319-24.

DETMER, S. A. & CHAN, D. C. 2007. Complementation between mouse Mfn1 and Mfn2 protects mitochondrial fusion defects caused by CMT2A disease mutations. *J Cell Biol,* 176, 405-14.

DHANKHAR, R., DAHIYA, K., SINGH, V., SANGWAN, L. & KAUSHAL, V. 2010. Nitric Oxide And Cancer. *Journal of Clinical and Diagnostic Research,* 4, 2550-2559.

DLASKOVA, A., CLARKE, K. J. & PORTER, R. K. 2010. The role of UCP 1 in production of reactive oxygen species by mitochondria isolated from brown adipose tissue. *Biochim Biophys Acta,* 1797**,** 1470-6.

D'SOUZA, G. G., WAGLE, M. A., SAXENA, V. & SHAH, A. 2011. Approaches for targeting mitochondria in cancer therapy. *Biochim Biophys Acta,* 1807, 689-96.

DUVEZIN-CAUBET, S., JAGASIA, R., WAGENER, J., HOFMANN, S., TRIFUNOVIC, A., HANSSON, A., CHOMYN, A., BAUER, M. F., ATTARDI, G., LARSSON, N. G., NEUPERT, W. & REICHERT, A. S. 2006. Proteolytic processing of OPA1 links mitochondrial dysfunction to alterations in mitochondrial morphology. *J Biol Chem,* 281, 37972-9.

ECHTAY, K. S., ESTEVES, T. C., PAKAY, J. L., JEKABSONS, M. B., LAMBERT, A. J., PORTERO-OTIN, M., PAMPLONA, R., VIDAL-PUIG, A. J., WANG, S., ROEBUCK, S. J. & BRAND, M. D. 2003. A signalling role for 4-hydroxy-2-nonenal in regulation of mitochondrial uncoupling. *EMBO J,* 22**,** 4103-10.

ECHTAY, K. S., ROUSSEL, D., ST-PIERRE, J., JEKABSONS, M. B., CADENAS, S., STUART, J. A., HARPER, J. A., ROEBUCK, S. J., MORRISON, A., PICKERING, S., CLAPHAM, J. C. & BRAND, M. D. 2002. Superoxide activates mitochondrial uncoupling proteins. *Nature,* 415**,** 96-9.

EIGENBRODT, E., KALLINOWSKI, F., OTT, M., MAZUREK, S. & VAUPEL, P. 1998. Pyruvate kinase and the interaction of amino acid and carbohydrate metabolism in solid tumors. *Anticancer research,* 18, 3267.

ELSTROM, R. L., BAUER, D. E., BUZZAI, M., KARNAUSKAS, R., HARRIS, M. H., PLAS, D. R., ZHUANG, H., CINALLI, R. M., ALAVI, A., RUDIN, C. M. & THOMPSON, C. B. 2004. Akt stimulates aerobic glycolysis in cancer cells. *Cancer Res,* 64**,** 3892-9.

EURA, Y., ISHIHARA, N., OKA, T. & MIHARA, K. 2006. Identification of a novel protein that regulates mitochondrial fusion by modulating mitofusin (Mfn) protein function. *J Cell Sci,* 119, 4913-25.

EURA, Y., ISHIHARA, N., YOKOTA, S. & MIHARA, K. 2003. Two mitofusin proteins, mammalian homologues of FZO, with distinct functions are both required for mitochondrial fusion. *J Biochem,* 134, 333-44.

EXNER, N., TRESKE, B., PAQUET, D., HOLMSTROM, K., SCHIESLING, C., GISPERT, S., CARBALLO-CARBAJAL, I., BERG, D., HOEPKEN, H. H., GASSER, T., KRUGER, R., WINKLHOFER, K. F., VOGEL, F., REICHERT, A. S., AUBURGER, G., KAHLE, P. J., SCHMID, B. & HAASS, C. 2007. Loss-of-function of human PINK1 results in mitochondrial pathology and can be rescued by parkin. *J Neurosci,* 27, 12413-8.

FASANO, M., BERGAMASCO, B. & LOPIANO, L. 2007. The proteomic approach in Parkinson's disease. *Proteomics Clin Appl,* 1, 1428-35.

FIGUEROA-ROMERO, C., INIGUEZ-LLUHI, J. A., STADLER, J., CHANG, C. R., ARNOULT, D., KELLER, P. J., HONG, Y., BLACKSTONE, C. & FELDMAN, E. L. 2009. SUMOylation of the mitochondrial fission protein Drp1 occurs at multiple nonconsensus sites within the B domain and is linked to its activity cycle. *FASEB J,* 23, 3917-27.

FLEMING, S. M., ZHU, C., FERNAGUT, P. O., MEHTA, A., DICARLO, C. D., SEAMAN, R. L. & CHESSELET, M. F. 2004. Behavioral and immunohistochemical effects of chronic intravenous and subcutaneous infusions of varying doses of rotenone. *Exp Neurol,* 187, 418-29.

FLISS, H. & GATTINGER, D. 1996. Apoptosis in ischemic and reperfused rat myocardium. *Circ Res,* 79, 949-56.

FRANK, S., GAUME, B., BERGMANN-LEITNER, E. S., LEITNER, W. W., ROBERT, E. G., CATEZ, F., SMITH, C. L. & YOULE, R. J. 2001. The role of dynamin-related protein 1, a mediator of mitochondrial fission, in apoptosis. *Dev Cell,* 1, 515-25.

FRANSSON, A., RUUSALA, A. & ASPENSTROM, P. 2003. Atypical Rho GTPases have roles in mitochondrial homeostasis and apoptosis. *J Biol Chem,* 278, 6495-502.

FREY, P. A. 1996. The Leloir pathway: a mechanistic imperative for three enzymes to change the stereochemical configuration of a single carbon in galactose. *FASEB J,* 10, 461-70.

FREZZA, C., CIPOLAT, S., MARTINS DE BRITO, O., MICARONI, M., BEZNOUSSENKO, G. V., RUDKA, T., BARTOLI, D., POLISHUCK, R. S., DANIAL, N. N., DE STROOPER, B. & SCORRANO, L. 2006. OPA1 controls apoptotic cristae remodeling independently from mitochondrial fusion. *Cell,* 126, 177-89.

FUJIKAWA, M. & YOSHIDA, M. 2010. A sensitive, simple assay of mitochondrial ATP synthesis of cultured mammalian cells suitable for high-throughput analysis. *Biochem Biophys Res Commun,* 401, 538-43.

GABALDON, T. & HUYNEN, M. A. 2007. From endosymbiont to host-controlled organelle: the hijacking of mitochondrial protein synthesis and metabolism. *PLoS Comput Biol,* 3, e219.

GANDRE-BABBE, S. & VAN DER BLIEK, A. M. 2008. The novel tail-anchored membrane protein Mff controls mitochondrial and peroxisomal fission in mammalian cells. *Mol Biol Cell,* 19, 2402-12.

GAO, W., PU, Y., LUO, K. Q. & CHANG, D. C. 2001. Temporal relationship between cytochrome c release and mitochondrial swelling during UV-induced apoptosis in living HeLa cells. *J Cell Sci,* 114, 2855-62.

GAREDEW, A., ANDREASSI, C. & MONCADA, S. 2012. Mitochondrial Dynamics, Biogenesis, and Function Are Coordinated with the Cell Cycle by APC/C(CDH1). *Cell Metab,* 15, 466-79.

GASSER, T. 2007. Update on the genetics of Parkinson's disease. *Mov Disord,* 22 Suppl 17, S343-50.

GEGG, M. E., COOPER, J. M., CHAU, K. Y., ROJO, M., SCHAPIRA, A. H. & TAANMAN, J. W. 2010. Mitofusin 1 and mitofusin 2 are ubiquitinated in a PINK1/parkin-dependent manner upon induction of mitophagy. *Hum Mol Genet,* 19, 4861-70.

GEISLER, S., HOLMSTROM, K. M., SKUJAT, D., FIESEL, F. C., ROTHFUSS, O. C., KAHLE, P. J. & SPRINGER, W. 2010. PINK1/Parkin-mediated mitophagy is dependent on VDAC1 and p62/SQSTM1. *Nat Cell Biol,* 12, 119-31.

GERMAIN, M., MATHAI, J. P., MCBRIDE, H. M. & SHORE, G. C. 2005. Endoplasmic reticulum BIK initiates DRP1-regulated remodelling of mitochondrial cristae during apoptosis. *EMBO J,* 24, 1546-56.

GILKERSON, R. W., SCHON, E. A., HERNANDEZ, E. & DAVIDSON, M. M. 2008. Mitochondrial nucleoids maintain genetic autonomy but allow for functional complementation. *J Cell Biol,* 181, 1117-28.

GISPERT, S., RICCIARDI, F., KURZ, A., AZIZOV, M., HOEPKEN, H. H., BECKER, D., VOOS, W., LEUNER, K., MULLER, W. E., KUDIN, A. P., KUNZ, W. S., ZIMMERMANN, A., ROEPER, J., WENZEL, D., JENDRACH, M., GARCIA-ARENCIBIA, M., FERNANDEZ-RUIZ, J., HUBER, L., ROHRER, H., BARRERA, M., REICHERT, A. S., RUB, U., CHEN, A., NUSSBAUM, R. L. & AUBURGER, G. 2009. Parkinson phenotype in aged PINK1-deficient mice is accompanied by progressive mitochondrial dysfunction in absence of neurodegeneration. *PLoS One,* 4, e5777.

GLATER, E. E., MEGEATH, L. J., STOWERS, R. S. & SCHWARZ, T. L. 2006. Axonal transport of mitochondria requires milton to recruit kinesin heavy chain and is light chain independent. *J Cell Biol,* 173, 545-57.

GOMES, L. C., DI BENEDETTO, G. & SCORRANO, L. 2011. During autophagy mitochondria elongate, are spared from degradation and sustain cell viability. *Nat Cell Biol,* 13, 589-98.

GRAY, M. W., BURGER, G. & LANG, B. F. 1999. Mitochondrial evolution. *Science,* 283, 1476-81.

GRIFFIN, E. E., GRAUMANN, J. & CHAN, D. C. 2005. The WD40 protein Caf4p is a component of the mitochondrial fission machinery and recruits Dnm1p to mitochondria. *J Cell Biol,* 170, 237-48.

GU, M., GASH, M. T., MANN, V. M., JAVOY-AGID, F., COOPER, J. M. & SCHAPIRA, A. H. 1996. Mitochondrial defect in Huntington's disease caudate nucleus. *Ann Neurol,* 39, 385-9.

GUILLERY, O., MALKA, F., LANDES, T., GUILLOU, E., BLACKSTONE, C., LOMBES, A., BELENGUER, P., ARNOULT, D. & ROJO, M. 2008. Metalloprotease-mediated OPA1 processing is modulated by the mitochondrial membrane potential. *Biol Cell,* 100, 315-25.

GUILLET, V., GUEGUEN, N., CARTONI, R., CHEVROLLIER, A., DESQUIRET, V., ANGEBAULT, C., AMATI-BONNEAU, P., PROCACCIO, V., BONNEAU, D., MARTINOU, J. C. & REYNIER, P. 2011. Bioenergetic defect associated with mKATP channel opening in a mouse model carrying a mitofusin 2 mutation. *FASEB J.*

GULHATI, P., BOWEN, K. A., LIU, J., STEVENS, P. D., RYCHAHOU, P. G., CHEN, M., LEE, E. Y., WEISS, H. L., O'CONNOR, K. L., GAO, T. & EVERS, B. M. 2011. mTORC1 and mTORC2 regulate EMT, motility, and metastasis of colorectal cancer via RhoA and Rac1 signaling pathways. *Cancer Res,* 71, 3246-56.

HACKENBROCK, C. R. 1966. Ultrastructural bases for metabolically linked mechanical activity in mitochondria. I. Reversible ultrastructural changes with change in metabolic steady state in isolated liver mitochondria. *J Cell Biol,* 30, 269-97.

HACKENBROCK, C. R. 1968. Ultrastructural bases for metabolically linked mechanical activity in mitochondria. II. Electron transport-linked ultrastructural transformations in mitochondria. *J Cell Biol,* 37, 345-69.

HACKENBROCK, C. R., REHN, T. G., WEINBACH, E. C. & LEMASTERS, J. J. 1971. Oxidative phosphorylation and ultrastructural transformation in mitochondria in the intact ascites tumor cell. *J Cell Biol,* 51, 123-37.

HAJEK, P., CHOMYN, A. & ATTARDI, G. 2007. Identification of a novel mitochondrial complex containing mitofusin 2 and stomatin-like protein 2. *J Biol Chem,* 282, 5670-81.

HALES, K. G. & FULLER, M. T. 1997. Developmentally regulated mitochondrial fusion mediated by a conserved, novel, predicted GTPase. *Cell,* 90, 121-9.

HAM, A. J. & LIEBLER, D. C. 1995. Vitamin E oxidation in rat liver mitochondria. *Biochemistry,* 34, 5754-61.

HAN, X. J., LU, Y. F., LI, S. A., KAITSUKA, T., SATO, Y., TOMIZAWA, K., NAIRN, A. C., TAKEI, K., MATSUI, H. & MATSUSHITA, M. 2008. CaM kinase I alpha-induced phosphorylation of Drp1 regulates mitochondrial morphology. *J Cell Biol,* 182, 573-85.

HANAHAN, D. & WEINBERG, R. A. 2000. The hallmarks of cancer. *Cell,* 100, 57-70.

HANAHAN, D. & WEINBERG, R. A. 2011. Hallmarks of cancer: the next generation. *Cell,* 144, 646-74.

HARDER, Z., ZUNINO, R. & MCBRIDE, H. 2004. Sumo1 conjugates mitochondrial substrates and participates in mitochondrial fission. *Curr Biol,* 14, 340-5.

HAYASHI, J., OHTA, S., KAGAWA, Y., TAKAI, D., MIYABAYASHI, S., TADA, K., FUKUSHIMA, H., INUI, K., OKADA, S., GOTO, Y. & ET AL. 1994. Functional and morphological abnormalities of mitochondria in human cells containing mitochondrial DNA with pathogenic point mutations in tRNA genes. *J Biol Chem,* 269, 19060-6.

HEAZLEWOOD, J. L., MILLAR, A. H., DAY, D. A. & WHELAN, J. 2003. What makes a mitochondrion? *Genome Biol,* 4, 218.

HENNESSY, B. T., SMITH, D. L., RAM, P. T., LU, Y. & MILLS, G. B. 2005. Exploiting the PI3K/AKT pathway for cancer drug discovery. *Nat Rev Drug Discov,* 4, 988-1004.

HERMANN, G. J., THATCHER, J. W., MILLS, J. P., HALES, K. G., FULLER, M. T., NUNNARI, J. & SHAW, J. M. 1998. Mitochondrial fusion in yeast requires the transmembrane GTPase Fzo1p. *J Cell Biol,* 143, 359-73.

HERRERO-MENDEZ, A., ALMEIDA, A., FERNANDEZ, E., MAESTRE, C., MONCADA, S. & BOLANOS, J. P. 2009. The bioenergetic and antioxidant status of neurons is controlled by continuous degradation of a key glycolytic enzyme by APC/C-Cdh1. *Nat Cell Biol,* 11, 747-52.

HERTZ, L. 2004. The astrocyte-neuron lactate shuttle: a challenge of a challenge. *J Cereb Blood Flow Metab,* 24, 1241-8.

HIRAI, K., ALIEV, G., NUNOMURA, A., FUJIOKA, H., RUSSELL, R. L., ATWOOD, C. S., JOHNSON, A. B., KRESS, Y., VINTERS, H. V., TABATON, M., SHIMOHAMA, S., CASH, A. D., SIEDLAK, S. L., HARRIS,

P. L., JONES, P. K., PETERSEN, R. B., PERRY, G. & SMITH, M. A. 2001. Mitochondrial abnormalities in Alzheimer's disease. *J Neurosci,* 21, 3017-23.

HIROKAWA, N. & TAKEMURA, R. 2004. Kinesin superfamily proteins and their various functions and dynamics. *Exp Cell Res,* 301, 50-9.

HOLDEN, H. M., RAYMENT, I. & THODEN, J. B. 2003. Structure and function of enzymes of the Leloir pathway for galactose metabolism. *J Biol Chem,* 278, 43885-8.

HOLLENBECK, P. J. & SAXTON, W. M. 2005. The axonal transport of mitochondria. *J Cell Sci,* 118, 5411-9.

HONG, S. & PEDERSEN, P. L. 2008. ATP Synthase and the Actions of Inhibitors Utilized To Study Its Roles in Human Health, Disease, and Other Scientific Areas. *Microbiology and Molecular Biology Reviews,* 72, 590-641.

HOPPINS, S., EDLICH, F., CLELAND, M. M., BANERJEE, S., MCCAFFERY, J. M., YOULE, R. J. & NUNNARI, J. 2011. The soluble form of Bax regulates mitochondrial fusion via MFN2 homotypic complexes. *Mol Cell,* 41, 150-60.

HUANG, P., GALLOWAY, C. A. & YOON, Y. 2011. Control of mitochondrial morphology through differential interactions of mitochondrial fusion and fission proteins. *PLoS One,* 6, e20655.

HUDSON, G., AMATI-BONNEAU, P., BLAKELY, E. L., STEWART, J. D., HE, L., SCHAEFER, A. M., GRIFFITHS, P. G., AHLQVIST, K., SUOMALAINEN, A., REYNIER, P., MCFARLAND, R., TURNBULL, D. M., CHINNERY, P. F. & TAYLOR, R. W. 2008. Mutation of OPA1 causes dominant optic atrophy with external ophthalmoplegia, ataxia, deafness and multiple mitochondrial DNA deletions: a novel disorder of mtDNA maintenance. *Brain,* 131, 329-37.

HURLEY, R. L., ANDERSON, K. A., FRANZONE, J. M., KEMP, B. E., MEANS, A. R. & WITTERS, L. A. 2005. The Ca2+/calmodulin-dependent protein kinase kinases are AMP-activated protein kinase kinases. *J Biol Chem,* 280, 29060-6.

HWA, J. J., HILLER, M. A., FULLER, M. T. & SANTEL, A. 2002. Differential expression of the Drosophila mitofusin genes fuzzy onions (fzo) and dmfn. *Mech Dev,* 116, 213-6.

INOKI, K., ZHU, T. & GUAN, K. L. 2003. TSC2 mediates cellular energy response to control cell growth and survival. *Cell,* 115, 577-90.

ISHIHARA, N., EURA, Y. & MIHARA, K. 2004. Mitofusin 1 and 2 play distinct roles in mitochondrial fusion reactions via GTPase activity. *J Cell Sci,* 117, 6535-46.

ISHIHARA, N., FUJITA, Y., OKA, T. & MIHARA, K. 2006. Regulation of mitochondrial morphology through proteolytic cleavage of OPA1. *EMBO J,* 25, 2966-77.

ISHIHARA, N., NOMURA, M., JOFUKU, A., KATO, H., SUZUKI, S. O., MASUDA, K., OTERA, H., NAKANISHI, Y., NONAKA, I., GOTO, Y., TAGUCHI, N., MORINAGA, H., MAEDA, M., TAKAYANAGI, R., YOKOTA, S. & MIHARA, K. 2009. Mitochondrial fission factor Drp1 is essential for embryonic development and synapse formation in mice. *Nat Cell Biol,* 11, 958-66.

JACINTO, E., LOEWITH, R., SCHMIDT, A., LIN, S., RUEGG, M. A., HALL, A. & HALL, M. N. 2004. Mammalian TOR complex 2 controls the actin cytoskeleton and is rapamycin insensitive. *Nat Cell Biol,* 6, 1122-8.

JEYARAJU, D. V., CISBANI, G. & PELLEGRINI, L. 2009. Calcium regulation of mitochondria motility and morphology. *Biochim Biophys Acta,* 1787, 1363-73.

JEZEK, P., PLECITA-HLAVATA, L., SMOLKOVA, K. & ROSSIGNOL, R. 2010. Distinctions and similarities of cell bioenergetics and the role of mitochondria in hypoxia, cancer, and embryonic development. *Int J Biochem Cell Biol,* 42, 604-22.

JI, J. & ZHENG, P. S. 2010. Activation of mTOR signaling pathway contributes to survival of cervical cancer cells. *Gynecol Oncol,* 117, 103-8.

JIN, J., MEREDITH, G. E., CHEN, L., ZHOU, Y., XU, J., SHIE, F. S., LOCKHART, P. & ZHANG, J. 2005. Quantitative proteomic analysis of mitochondrial proteins: relevance to Lewy body formation and Parkinson's disease. *Brain Res Mol Brain Res,* 134, 119-38.

JOHNSON, K. A. & WALL, J. S. 1983. Structure and molecular weight of the dynein ATPase. *J Cell Biol,* 96, 669-78.

JOHNSON, R. J., PEREZ-POZO, S. E., SAUTIN, Y. Y., MANITIUS, J., SANCHEZ-LOZADA, L. G., FEIG, D. I., SHAFIU, M., SEGAL, M., GLASSOCK, R. J., SHIMADA, M., RONCAL, C. & NAKAGAWA, T. 2009. Hypothesis: Could Excessive Fructose Intake and Uric Acid Cause Type 2 Diabetes? *Endocrine Reviews,* 30, 96-116.

JORGENSEN, S. B., RICHTER, E. A. & WOJTASZEWSKI, J. F. 2006. Role of AMPK in skeletal muscle metabolic regulation and adaptation in relation to exercise. *J Physiol,* 574, 17-31.

JOSE, C., BELLANCE, N. & ROSSIGNOL, R. 2011. Choosing between glycolysis and oxidative phosphorylation: a tumor's dilemma? *Biochim Biophys Acta,* 1807, 552-61.

JOSHI, D. C. & BAKOWSKA, J. C. 2011. Determination of Mitochondrial Membrane Potential and Reactive Oxygen Species in Live Rat Cortical Neurons. *J Vis Exp,* e2704.

KAASIK, A., SAFIULINA, D., CHOUBEY, V., KUUM, M., ZHARKOVSKY, A. & VEKSLER, V. 2007. Mitochondrial swelling impairs the transport of organelles in cerebellar granule neurons. *J Biol Chem,* 282, 32821-6.

KAGEYAMA, Y., ZHANG, Z. & SESAKI, H. 2011. Mitochondrial division: molecular machinery and physiological functions. *Curr Opin Cell Biol,* 23, 427-34.

KARBOWSKI, M., ARNOULT, D., CHEN, H., CHAN, D. C., SMITH, C. L. & YOULE, R. J. 2004a. Quantitation of mitochondrial dynamics by photolabeling of individual organelles shows that mitochondrial fusion is blocked during the Bax activation phase of apoptosis. *J Cell Biol,* 164, 493-9.

KARBOWSKI, M., JEONG, S. Y. & YOULE, R. J. 2004b. Endophilin B1 is required for the maintenance of mitochondrial morphology. *J Cell Biol,* 166, 1027-39.

KARBOWSKI, M., LEE, Y. J., GAUME, B., JEONG, S. Y., FRANK, S., NECHUSHTAN, A., SANTEL, A., FULLER, M., SMITH, C. L. & YOULE, R. J. 2002. Spatial and temporal association of Bax with mitochondrial fission sites, Drp1, and Mfn2 during apoptosis. *J Cell Biol,* 159, 931-8.

KARBOWSKI, M., NEUTZNER, A. & YOULE, R. J. 2007. The mitochondrial E3 ubiquitin ligase MARCH5 is required for Drp1 dependent mitochondrial division. *J Cell Biol,* 178, 71-84.

KARBOWSKI, M., NORRIS, K. L., CLELAND, M. M., JEONG, S. Y. & YOULE, R. J. 2006. Role of Bax and Bak in mitochondrial morphogenesis. *Nature,* 443, 658-62.

KAYALAR, C., ROSING, J. & BOYER, P. D. 1977. An alternating site sequence for oxidative phosphorylation suggested by measurement of substrate binding patterns and exchange reaction inhibitions. *J Biol Chem,* 252, 2486-91.

KEENEY, P. M., XIE, J., CAPALDI, R. A. & BENNETT, J. P., JR. 2006. Parkinson's disease brain mitochondrial complex I has oxidatively damaged subunits and is functionally impaired and misassembled. *J Neurosci,* 26, 5256-64.

KILBRIDE, S. M., FARRELLY, A. M., BONNER, C., WARD, M. W., NYHAN, K. C., CONCANNON, C. G., WOLLHEIM, C. B., BYRNE, M. M. & PREHN, J. H. 2010. AMP-activated protein kinase mediates apoptosis in response to bioenergetic stress through activation of the pro-apoptotic Bcl-2 homology domain-3-only protein BMF. *J Biol Chem,* 285, 36199-206.

KILBRIDE, S. M., TELFORD, J. E., TIPTON, K. F. & DAVEY, G. P. 2008. Partial inhibition of complex I activity increases Ca-independent glutamate release rates from depolarized synaptosomes. *J Neurochem,* 106, 826-34.

KIM, J. M., BAE, H. R., PARK, B. S., LEE, J. M., AHN, H. B., RHO, J. H., YOO, K. W., PARK, W. C., RHO, S. H., YOON, H. S. & YOO, Y. H. 2003. Early mitochondrial hyperpolarization and intracellular alkalinization in lactacystin-induced apoptosis of retinal pigment epithelial cells. *J Pharmacol Exp Ther,* 305, 474-81.

KIM, J., KUNDU, M., VIOLLET, B. & GUAN, K. L. 2011. AMPK and mTOR regulate autophagy through direct phosphorylation of Ulk1. *Nat Cell Biol,* 13, 132-41.

KNORRE, D., OJOVAN, S., SAPRUNOVA, V., SOKOLOV, S., BAKEEVA, L. & SEVERIN, F. 2008. Mitochondrial matrix fragmentation as a protection mechanism of yeast Saccharomyces cerevisiae. *Biochemistry (Moscow),* 73, 1254-1259.

KNOTT, A. B., PERKINS, G., SCHWARZENBACHER, R. & BOSSY-WETZEL, E. 2008. Mitochondrial fragmentation in neurodegeneration. *Nat Rev Neurosci,* 9, 505-18.

KOOPMAN, W. J., VERKAART, S., VISCH, H. J., VAN DER WESTHUIZEN, F. H., MURPHY, M. P., VAN DEN HEUVEL, L. W., SMEITINK, J. A. & WILLEMS, P. H. 2005a. Inhibition of complex I of the electron transport chain causes O2-. -mediated mitochondrial outgrowth. *Am J Physiol Cell Physiol,* 288, C1440-50.

KOOPMAN, W. J., VISCH, H. J., VERKAART, S., VAN DEN HEUVEL, L. W., SMEITINK, J. A. & WILLEMS, P. H. 2005b. Mitochondrial network complexity and pathological decrease in complex I activity are tightly correlated in isolated human complex I deficiency. *Am J Physiol Cell Physiol,* 289, C881-90.

KOSHIBA, T., DETMER, S. A., KAISER, J. T., CHEN, H., MCCAFFERY, J. M. & CHAN, D. C. 2004. Structural basis of mitochondrial tethering by mitofusin complexes. *Science,* 305, 858-62.

KREBIEHL, G., RUCKERBAUER, S., BURBULLA, L. F., KIEPER, N., MAURER, B., WAAK, J., WOLBURG, H., GIZATULLINA, Z., GELLERICH, F. N., WOITALLA, D., RIESS, O., KAHLE, P. J., PROIKAS-CEZANNE, T. & KRUGER, R. 2010. Reduced basal autophagy and impaired mitochondrial dynamics due to loss of Parkinson's disease-associated protein DJ-1. *PLoS One,* 5, e9367.

KUZNETSOV, S. A. & GELFAND, V. I. 1986. Bovine brain kinesin is a microtubule-activated ATPase. *Proc Natl Acad Sci U S A,* 83, 8530-4.

LAI, J. C. & CLARK, J. B. 1979. Preparation of synaptic and nonsynaptic mitochondria from mammalian brain. *Methods Enzymol,* 55, 51-60.

LANDES, T., EMORINE, L. J., COURILLEAU, D., ROJO, M., BELENGUER, P. & ARNAUNE-PELLOQUIN, L. 2010. The BH3-only Bnip3 binds to the dynamin Opa1 to promote mitochondrial fragmentation and apoptosis by distinct mechanisms. *EMBO Rep,* 11, 459-65.

LANDES, T. & MARTINOU, J. C. 2011. Mitochondrial outer membrane permeabilization during apoptosis: the role of mitochondrial fission. *Biochim Biophys Acta,* 1813, 540-5.

LANGSTON, J. W., FORNO, L. S., TETRUD, J., REEVES, A. G., KAPLAN, J. A. & KARLUK, D. 1999. Evidence of active nerve cell degeneration in the substantia nigra of humans years after 1-methyl-4-phenyl-1,2,3,6-tetrahydropyridine exposure. *Ann Neurol,* 46, 598-605.

LEE, S. B., KIM, J. J., CHUNG, J. S., LEE, M.-S., LEE, K.-H., KIM, B. S. & DO YOO, Y. 2011. Romo1 is a negative-feedback regulator of Myc. *Journal of Cell Science,* 124, 1911-1924.

LEE, Y. J., JEONG, S. Y., KARBOWSKI, M., SMITH, C. L. & YOULE, R. J. 2004. Roles of the mammalian mitochondrial fission and fusion mediators Fis1, Drp1, and Opa1 in apoptosis. *Mol Biol Cell,* 15, 5001-11.

LEGROS, F., LOMBES, A., FRACHON, P. & ROJO, M. 2002. Mitochondrial fusion in human cells is efficient, requires the inner membrane potential, and is mediated by mitofusins. *Mol Biol Cell,* 13, 4343-54.

LEGROS, F., MALKA, F., FRACHON, P., LOMBES, A. & ROJO, M. 2004. Organization and dynamics of human mitochondrial DNA. *J Cell Sci,* 117, 2653-62.

LESAGE, S. & BRICE, A. 2009. Parkinson's disease: from monogenic forms to genetic susceptibility factors. *Hum Mol Genet,* 18, R48-59.

LI, H., CHEN, Y., JONES, A. F., SANGER, R. H., COLLIS, L. P., FLANNERY, R., MCNAY, E. C., YU, T., SCHWARZENBACHER, R., BOSSY, B., BOSSY-WETZEL, E., BENNETT, M. V., PYPAERT, M., HICKMAN, J. A., SMITH, P. J., HARDWICK, J. M. & JONAS, E. A. 2008. Bcl-xL induces Drp1-dependent synapse formation in cultured hippocampal neurons. *Proc Natl Acad Sci U S A,* 105, 2169-74.

LI, Z., OKAMOTO, K., HAYASHI, Y. & SHENG, M. 2004. The importance of dendritic mitochondria in the morphogenesis and plasticity of spines and synapses. *Cell,* 119, 873-87.

LIESA, M., BORDA-D'AGUA, B., MEDINA-GOMEZ, G., LELLIOTT, C. J., PAZ, J. C., ROJO, M., PALACIN, M., VIDAL-PUIG, A. & ZORZANO, A. 2008. Mitochondrial fusion is increased by the nuclear coactivator PGC-1beta. *PLoS One,* 3, e3613.

LIGON, L. A. & STEWARD, O. 2000. Role of microtubules and actin filaments in the movement of mitochondria in the axons and dendrites of cultured hippocampal neurons. *J Comp Neurol,* 427, 351-61.

LIN, X., ZHANG, F., BRADBURY, C. M., KAUSHAL, A., LI, L., SPITZ, D. R., AFT, R. L. & GIUS, D. 2003. 2-Deoxy-D-glucose-induced cytotoxicity and radiosensitization in tumor cells is mediated via disruptions in thiol metabolism. *Cancer Res,* 63, 3413-7.

LIOT, G., BOSSY, B., LUBITZ, S., KUSHNAREVA, Y., SEJBUK, N. & BOSSY-WETZEL, E. 2009. Complex II inhibition by 3-NP causes mitochondrial fragmentation and neuronal cell death via an NMDA- and ROS-dependent pathway. *Cell Death Differ,* 16, 899-909.

LIU, Q. A. & SHIO, H. 2008. Mitochondrial morphogenesis, dendrite development, and synapse formation in cerebellum require both Bcl-w and the glutamate receptor delta2. *PLoS Genet,* 4, e1000097.

LIU, X., WEAVER, D., SHIRIHAI, O. & HAJNOCZKY, G. 2009. Mitochondrial /`kiss-and-run/': interplay between mitochondrial motility and fusion-fission dynamics. *EMBO J,* 28, 3074-3089.

LUTZ, A. K., EXNER, N., FETT, M. E., SCHLEHE, J. S., KLOOS, K., LAMMERMANN, K., BRUNNER, B., KURZ-DREXLER, A., VOGEL, F., REICHERT, A. S., BOUMAN, L., VOGT-WEISENHORN, D., WURST, W., TATZELT, J., HAASS, C. & WINKLHOFER, K. F. 2009. Loss of parkin or PINK1 function increases Drp1-dependent mitochondrial fragmentation. *J Biol Chem,* 284, 22938-51.

LYAMZAEV, K. G., IZYUMOV, D. S., AVETISYAN, A. V., YANG, F., PLETJUSHKINA, O. Y. & CHERNYAK, B. V. 2004. Inhibition of mitochondrial bioenergetics: the effects on structure of mitochondria in the cell and on apoptosis. *Acta Biochim Pol,* 51, 553-62.

MA, W., SUNG, H. J., PARK, J. Y., MATOBA, S. & HWANG, P. M. 2007. A pivotal role for p53: balancing aerobic respiration and glycolysis. *J Bioenerg Biomembr,* 39, 243-6.

MACASKILL, A. F., RINHOLM, J. E., TWELVETREES, A. E., ARANCIBIA-CARCAMO, I. L., MUIR, J., FRANSSON, A., ASPENSTROM, P., ATTWELL, D. & KITTLER, J. T. 2009. Miro1 is a calcium sensor for glutamate receptor-dependent localization of mitochondria at synapses. *Neuron,* 61, 541-55.

MAJEWSKI, N., NOGUEIRA, V., ROBEY, R. B. & HAY, N. 2004. Akt inhibits apoptosis downstream of BID cleavage via a glucose-dependent mechanism involving mitochondrial hexokinases. *Mol Cell Biol,* 24, 730-40.

MALKA, F., GUILLERY, O., CIFUENTES-DIAZ, C., GUILLOU, E., BELENGUER, P., LOMBES, A. & ROJO, M. 2005. Separate fusion of outer and inner mitochondrial membranes. *EMBO Rep,* 6, 853-9.

MANCZAK, M., CALKINS, M. J. & REDDY, P. H. 2011. Impaired mitochondrial dynamics and abnormal interaction of amyloid beta with mitochondrial protein Drp1 in neurons from patients with Alzheimer's disease: implications for neuronal damage. *Hum Mol Genet,* 20, 2495-509.

MARGINEANTU, D. H., GREGORY COX, W., SUNDELL, L., SHERWOOD, S. W., BEECHEM, J. M. & CAPALDI, R. A. 2002. Cell cycle dependent morphology changes and associated mitochondrial DNA redistribution in mitochondria of human cell lines. *Mitochondrion,* 1, 425-35.

MAJEWSKI, N., NOGUEIRA, V., ROBEY, R. B. & HAY, N. 2004. Akt inhibits apoptosis downstream of BID cleavage via a glucose-dependent mechanism involving mitochondrial hexokinases. *Mol Cell Biol,* 24, 730-40.

MARROQUIN, L. D., HYNES, J., DYKENS, J. A., JAMIESON, J. D. & WILL, Y. 2007. Circumventing the Crabtree effect: replacing media glucose with galactose increases susceptibility of HepG2 cells to mitochondrial toxicants. *Toxicol Sci,* 97, 539-47.

MARSIN, A. S., BERTRAND, L., RIDER, M. H., DEPREZ, J., BEAULOYE, C., VINCENT, M. F., VAN DEN BERGHE, G., CARLING, D. & HUE, L. 2000. Phosphorylation and activation of heart PFK-2 by AMPK has a role in the stimulation of glycolysis during ischaemia. *Curr Biol,* 10, 1247-55.

MARTINOU, J. C. & YOULE, R. J. 2011. Mitochondria in apoptosis: Bcl-2 family members and mitochondrial dynamics. *Dev Cell,* 21, 92-101.

MATHUPALA, S. P., KO, Y. H. & PEDERSEN, P. L. 2009. Hexokinase-2 bound to mitochondria: cancer's stygian link to the "Warburg Effect" and a pivotal target for effective therapy. *Semin Cancer Biol,* 19, 17-24.

MATHUPALA, S. P., KO, Y. H. & PEDERSEN, P. L. 2010. The pivotal roles of mitochondria in cancer: Warburg and beyond and encouraging prospects for effective therapies. *Biochim Biophys Acta,* 1797, 1225-30.

MATOBA, S., KANG, J. G., PATINO, W. D., WRAGG, A., BOEHM, M., GAVRILOVA, O., HURLEY, P. J., BUNZ, F. & HWANG, P. M. 2006. p53 regulates mitochondrial respiration. *Science,* 312, 1650-3.

MATTENBERGER, Y., JAMES, D. I. & MARTINOU, J. C. 2003. Fusion of mitochondria in mammalian cells is dependent on the mitochondrial inner membrane potential and independent of microtubules or actin. *FEBS Lett,* 538, 53-9.

MERKWIRTH, C., DARGAZANLI, S., TATSUTA, T., GEIMER, S., LOWER, B., WUNDERLICH, F. T., VON KLEIST-RETZOW, J. C., WAISMAN, A., WESTERMANN, B. & LANGER, T. 2008. Prohibitins control cell proliferation and apoptosis by regulating OPA1-dependent cristae morphogenesis in mitochondria. *Genes Dev,* 22, 476-88.

MEYER, H., VITAVSKA, O. & WIECZOREK, H. 2011. Identification of an animal sucrose transporter. *Journal of Cell Science,* 124, 1984.

MINGRONE, G., MANCO, M., CALVANI, M., CASTAGNETO, M., NAON, D. & ZORZANO, A. 2005. Could the low level of expression of the gene encoding skeletal muscle mitofusin-2 account for the metabolic inflexibility of obesity? *Diabetologia,* 48, 2108-14.

MISKO, A., JIANG, S., WEGORZEWSKA, I., MILBRANDT, J. & BALOH, R. H. 2010. Mitofusin 2 is necessary for transport of axonal mitochondria and interacts with the Miro/Milton complex. *J Neurosci,* 30, 4232-40.

MITCHELL, P. 1961. Coupling of phosphorylation to electron and hydrogen transfer by a chemi-osmotic type of mechanism. *Nature,* 191, 144-8.

MITHOFER, K., SANDY, M. S., SMITH, M. T. & DI MONTE, D. 1992. Mitochondrial poisons cause depletion of reduced glutathione in isolated hepatocytes. *Arch Biochem Biophys,* 295**,** 132-6.

MODICA-NAPOLITANO, J. S. & SINGH, K. K. 2002. Mitochondria as targets for detection and treatment of cancer. *Expert Rev Mol Med,* 4, 1-19.

MONCADA, S. & BOLANOS, J. P. 2006. Nitric oxide, cell bioenergetics and neurodegeneration. *J Neurochem,* 97**,** 1676-89.

MONTESSUIT, S., SOMASEKHARAN, S. P., TERRONES, O., LUCKEN-ARDJOMANDE, S., HERZIG, S., SCHWARZENBACHER, R., MANSTEIN, D. J., BOSSY-WETZEL, E., BASANEZ, G., MEDA, P. & MARTINOU, J. C. 2010. Membrane remodeling induced by the dynamin-related protein Drp1 stimulates Bax oligomerization. *Cell,* 142, 889-901.

MOORE, B. A., GONZALEZ AVILES, G. D., LARKINS, C. E., HILLMAN, M. J. & CASPARY, T. 2010. Mitochondrial retention of Opa1 is required for mouse embryogenesis. *Mamm Genome,* 21, 350-60.

MORAN, M., RIVERA, H., SANCHEZ-ARAGO, M., BLAZQUEZ, A., MERINERO, B., UGALDE, C., ARENAS, J., CUEZVA, J. M. & MARTIN, M. A. 2010. Mitochondrial bioenergetics and dynamics interplay in complex I-deficient fibroblasts. *Biochim Biophys Acta,* 1802, 443-53.

MORTIBOYS, H., THOMAS, K. J., KOOPMAN, W. J., KLAFFKE, S., ABOU-SLEIMAN, P., OLPIN, S., WOOD, N. W., WILLEMS, P. H., SMEITINK, J. A., COOKSON, M. R. & BANDMANN, O. 2008. Mitochondrial function and morphology are impaired in parkin-mutant fibroblasts. *Ann Neurol,* 64, 555-65.

MOZDY, A. D., MCCAFFERY, J. M. & SHAW, J. M. 2000. Dnm1p GTPase-mediated mitochondrial fission is a multi-step process requiring the novel integral membrane component Fis1p. *J Cell Biol,* 151, 367-80.

MUNTANÉ, J. & DE LA MATA, M. 2010. Nitric oxide and cancer. *World Journal of Hepatology,* 2, 337.

NAKAMURA, N., KIMURA, Y., TOKUDA, M., HONDA, S. & HIROSE, S. 2006. MARCH-V is a novel mitofusin 2- and Drp1-binding protein able to change mitochondrial morphology. *EMBO Rep,* 7, 1019-22.

NARENDRA, D., TANAKA, A., SUEN, D. F. & YOULE, R. J. 2008. Parkin is recruited selectively to impaired mitochondria and promotes their autophagy. *J Cell Biol,* 183, 795-803.

NARENDRA, D., TANAKA, A., SUEN, D. F. & YOULE, R. J. 2009. Parkin-induced mitophagy in the pathogenesis of Parkinson disease. *Autophagy,* 5, 706-8.

NEDERGAARD, J., GOLOZOUBOVA, V., MATTHIAS, A., ASADI, A., JACOBSSON, A. & CANNON, B. 2001. UCP1: the only protein able to mediate adaptive non-shivering thermogenesis and metabolic inefficiency. *Biochim Biophys Acta,* 1504**,** 82-106.

NEHLIG, A. & COLES, J. A. 2007. Cellular pathways of energy metabolism in the brain: is glucose used by neurons or astrocytes? *Glia,* 55, 1238-50.

NEUSPIEL, M., ZUNINO, R., GANGARAJU, S., RIPPSTEIN, P. & MCBRIDE, H. 2005. Activated mitofusin 2 signals mitochondrial fusion, interferes with Bax activation, and reduces susceptibility to radical induced depolarization. *J Biol Chem,* 280, 25060-70.

NICHOLLS, D. G. 1977. The effective proton conductance of the inner membrane of mitochondria from brown adipose tissue. Dependency on proton electrochemical potential gradient. *Eur J Biochem,* 77, 349-56.

NICHOLLS, D. G. & BUDD, S. L. 2000. Mitochondria and neuronal survival. *Physiol Rev,* 80, 315-60.

NICHOLLS, D. G. & LINDBERG, O. 1973. Brown-adipose-tissue mitochondria. The influence of albumin and nucleotides on passive ion permeabilities. *Eur J Biochem,* 37, 523-30.

NICHOLLS, D. G. & RIAL, E. 1999. A history of the first uncoupling protein, UCP1. *J Bioenerg Biomembr,* 31, 399-406.

NOJI, H., YASUDA, R., YOSHIDA, M. & KINOSITA, K., JR. 1997. Direct observation of the rotation of F1-ATPase. *Nature,* 386, 299-302.

NUNNARI, J., MARSHALL, W. F., STRAIGHT, A., MURRAY, A., SEDAT, J. W. & WALTER, P. 1997. Mitochondrial transmission during mating in Saccharomyces cerevisiae is determined by mitochondrial fusion and fission and the intramitochondrial segregation of mitochondrial DNA. *Mol Biol Cell,* 8, 1233-42.

OELKRUG, R., KUTSCHKE, M., MEYER, C. W., HELDMAIER, G. & JASTROCH, M. 2010. Uncoupling protein 1 decreases superoxide production in brown adipose tissue mitochondria. *J Biol Chem,* 285, 21961-8.

OLICHON, A., BARICAULT, L., GAS, N., GUILLOU, E., VALETTE, A., BELENGUER, P. & LENAERS, G. 2003. Loss of OPA1 perturbates the mitochondrial inner membrane structure and integrity, leading to cytochrome c release and apoptosis. *J Biol Chem,* 278, 7743-6.

OLICHON, A., EMORINE, L. J., DESCOINS, E., PELLOQUIN, L., BRICHESE, L., GAS, N., GUILLOU, E., DELETTRE, C., VALETTE, A., HAMEL, C. P., DUCOMMUN, B., LENAERS, G. & BELENGUER, P. 2002. The human dynamin-related protein OPA1 is anchored to the mitochondrial inner membrane facing the inter-membrane space. *FEBS Lett,* 523, 171-6.

ONYANGO, I. G. 2008. Mitochondrial dysfunction and oxidative stress in Parkinson's disease. *Neurochem Res,* 33, 589-97.

OTERA, H. & MIHARA, K. 2011. Discovery of the membrane receptor for mitochondrial fission GTPase Drp1. *Small Gtpases,* 2, 167-172.

OTERA, H., WANG, C., CLELAND, M. M., SETOGUCHI, K., YOKOTA, S., YOULE, R. J. & MIHARA, K. 2010. Mff is an essential factor for mitochondrial recruitment of Drp1 during mitochondrial fission in mammalian cells. *J Cell Biol,* 191, 1141-58.

OWEN, J. B. & BUTTERFIELD, D. A. 2010. Measurement of oxidized/reduced glutathione ratio. *Methods Mol Biol,* 648, 269-77.

PALACINO, J. J., SAGI, D., GOLDBERG, M. S., KRAUSS, S., MOTZ, C., WACKER, M., KLOSE, J. & SHEN, J. 2004. Mitochondrial dysfunction and oxidative damage in parkin-deficient mice. *J Biol Chem,* 279, 18614-22.

PANDOLFI, P. P. 2008. P-TEN exciting years: from the cytosol to the nucleus and back to keep cancer at bay. *Oncogene,* 27, 5386.

PALMER, C. S., OSELLAME, L. D., LAINE, D., KOUTSOPOULOS, O. S., FRAZIER, A. E. & RYAN, M. T. 2011. MiD49 and MiD51, new components of the mitochondrial fission machinery. *EMBO Rep,* 12, 565-73.

PARK, Y. Y., LEE, S., KARBOWSKI, M., NEUTZNER, A., YOULE, R. J. & CHO, H. 2010. Loss of MARCH5 mitochondrial E3 ubiquitin ligase induces cellular senescence through dynamin-related protein 1 and mitofusin 1. *J Cell Sci,* 123, 619-26.

PARKER, W. D., JR., PARKS, J. K. & SWERDLOW, R. H. 2008. Complex I deficiency in Parkinson's disease frontal cortex. *Brain Res,* 1189, 215-8.

PARONE, P. A., DA CRUZ, S., TONDERA, D., MATTENBERGER, Y., JAMES, D. I., MAECHLER, P., BARJA, F. & MARTINOU, J. C. 2008. Preventing mitochondrial fission impairs mitochondrial function and leads to loss of mitochondrial DNA. *PLoS One,* 3, e3257.

PASTORINO, J. G., SHULGA, N. & HOEK, J. B. 2002. Mitochondrial binding of hexokinase II inhibits Bax-induced cytochrome c release and apoptosis. *J Biol Chem,* 277, 7610-8.

PATTERSON, G. H. & LIPPINCOTT-SCHWARTZ, J. 2002. A photoactivatable GFP for selective photolabeling of proteins and cells. *Science,* 297, 1873-7.

PEDERSEN, P. L., MATHUPALA, S., REMPEL, A., GESCHWIND, J. F. & KO, Y. H. 2002. Mitochondrial bound type II hexokinase: a key player in the growth and survival of many cancers and an ideal prospect for therapeutic intervention. *Biochim Biophys Acta,* 1555, 14-20.

PENNEY, J. B., JR., VONSATTEL, J. P., MACDONALD, M. E., GUSELLA, J. F. & MYERS, R. H. 1997. CAG repeat number governs the development rate of pathology in Huntington's disease. *Ann Neurol,* 41, 689-92.

PENSO, J. & BEITNER, R. 1998. Clotrimazole and bifonazole detach hexokinase from mitochondria of melanoma cells. *Eur J Pharmacol,* 342, 113-7.

PETERSEN, K. F., BEFROY, D., DUFOUR, S., DZIURA, J., ARIYAN, C., ROTHMAN, D. L., DIPIETRO, L., CLINE, G. W. & SHULMAN, G. I. 2003. Mitochondrial dysfunction in the elderly: possible role in insulin resistance. *Science,* 300, 1140-2.

PETROS, A. M., OLEJNICZAK, E. T. & FESIK, S. W. 2004. Structural biology of the Bcl-2 family of proteins. *Biochim Biophys Acta,* 1644, 83-94.

PETROS, J. A., BAUMANN, A. K., RUIZ-PESINI, E., AMIN, M. B., SUN, C. Q., HALL, J., LIM, S., ISSA, M. M., FLANDERS, W. D., HOSSEINI, S. H., MARSHALL, F. F. & WALLACE, D. C. 2005. mtDNA mutations increase tumorigenicity in prostate cancer. *Proceedings of the National Academy of Sciences of the United States of America,* 102, 719-724.

PICH, S., BACH, D., BRIONES, P., LIESA, M., CAMPS, M., TESTAR, X., PALACIN, M. & ZORZANO, A. 2005. The Charcot-Marie-Tooth type 2A gene product,

Mfn2, up-regulates fuel oxidation through expression of OXPHOS system. *Hum Mol Genet,* 14, 1405-15.

PITTS, K. R., YOON, Y., KRUEGER, E. W. & MCNIVEN, M. A. 1999. The dynamin-like protein DLP1 is essential for normal distribution and morphology of the endoplasmic reticulum and mitochondria in mammalian cells. *Mol Biol Cell,* 10, 4403-17.

PLECITA-HLAVATA, L., LESSARD, M., SANTOROVA, J., BEWERSDORF, J. & JEZEK, P. 2008. Mitochondrial oxidative phosphorylation and energetic status are reflected by morphology of mitochondrial network in INS-1E and HEP-G2 cells viewed by 4Pi microscopy. *Biochim Biophys Acta,* 1777, 834-46.

PLETJUSHKINA, O. Y., LYAMZAEV, K. G., POPOVA, E. N., NEPRYAKHINA, O. K., IVANOVA, O. Y., DOMNINA, L. V., CHERNYAK, B. V. & SKULACHEV, V. P. 2006. Effect of oxidative stress on dynamics of mitochondrial reticulum. *Biochim Biophys Acta,* 1757, 518-24.

POMPELLA, A., VISVIKIS, A., PAOLICCHI, A., DE TATA, V. & CASINI, A. F. 2003. The changing faces of glutathione, a cellular protagonist. *Biochem Pharmacol,* 66, 1499-503.

POOLE, A. C., THOMAS, R. E., ANDREWS, L. A., MCBRIDE, H. M., WHITWORTH, A. J. & PALLANCK, L. J. 2008. The PINK1/Parkin pathway regulates mitochondrial morphology. *Proc Natl Acad Sci U S A,* 105, 1638-43.

POOLE, A. C., THOMAS, R. E., YU, S., VINCOW, E. S. & PALLANCK, L. 2010. The mitochondrial fusion-promoting factor mitofusin is a substrate of the PINK1/parkin pathway. *PLoS One,* 5, e10054.

PORTER, R. K. 2008. Uncoupling protein 1: a short-circuit in the chemiosmotic process. *J Bioenerg Biomembr,* 40, 457-61.

RADAD, K., RAUSCH, W. D. & GILLE, G. 2006. Rotenone induces cell death in primary dopaminergic culture by increasing ROS production and inhibiting mitochondrial respiration. *Neurochem Int,* 49, 379-86.

RADAK, Z., ZHAO, Z., GOTO, S. & KOLTAI, E. 2011. Age-associated neurodegeneration and oxidative damage to lipids, proteins and DNA. *Mol Aspects Med.*

RAGAN, C. I., WILSON, M. T., DARLEY-USMAR, V. M. & LOWE, P. N. 1987. Assays of Individual Mitochondrial Enzymes. *In:* DARLEY-USMAR, V. M., RICKWOOD, D. & WILSON, M. T. (eds.) *Mitochondria, A Practical Approach*, pp 79-112. Oxford: IRL Press at Oxford University Press.

RAMBOLD, A. S., KOSTELECKY, B. & LIPPINCOTT-SCHWARTZ, J. 2011. Together we are stronger: Fusion protects mitochondria from autophagosomal degradation. *Autophagy,* 7.

REDDY, P. H., TRIPATHI, R., TROUNG, Q., TIRUMALA, REDDY, T. P., ANEKONDA, V., SHIRENDEB, U. P., CALKINS, M. J., REDDY, A. P., MAO, P. & MANCZAK, M. 2011. Abnormal mitochondrial dynamics and synaptic degeneration as early events in Alzheimer's disease: Implications to mitochondria-targeted antioxidant therapeutics. *Biochim Biophys Acta.*

REITZER, L. J., WICE, B. M. & KENNELL, D. 1979. Evidence that glutamine, not sugar, is the major energy source for cultured HeLa cells. *The Journal of biological chemistry,* 254, 2669-76.

RHEINWALD, J. G. & GREEN, H. 1974. Growth of cultured mammalian cells on secondary glucose sources. *Cell,* 2, 287-93.

ROBEY, R. B. & HAY, N. 2006. Mitochondrial hexokinases, novel mediators of the antiapoptotic effects of growth factors and Akt. *Oncogene,* 25, 4683-96.

RODRIGUEZ-RODRIGUEZ, P., FERNANDEZ, E., ALMEIDA, A. & BOLANOS, J. P. 2012. Excitotoxic stimulus stabilizes PFKFB3 causing pentose-phosphate pathway to glycolysis switch and neurodegeneration. *Cell Death Differ.*

ROJO, M., LEGROS, F., CHATEAU, D. & LOMBES, A. 2002. Membrane topology and mitochondrial targeting of mitofusins, ubiquitous mammalian homologs of the transmembrane GTPase Fzo. *J Cell Sci,* 115, 1663-74.

ROSSIGNOL, R., FAUSTIN, B., ROCHER, C., MALGAT, M., MAZAT, J. P. & LETELLIER, T. 2003. Mitochondrial threshold effects. *Biochem J,* 370, 751-62.

ROSSIGNOL, R., GILKERSON, R., AGGELER, R., YAMAGATA, K., REMINGTON, S. J. & CAPALDI, R. A. 2004. Energy substrate modulates mitochondrial structure and oxidative capacity in cancer cells. *Cancer Res,* 64, 985-93.

ROVINI, A., SAVRY, A., BRAGUER, D. & CARRÉ, M. 2011. Microtubule-targeted agents: when mitochondria become essential to chemotherapy. *Biochimica et Biophysica Acta (BBA)-Bioenergetics.*

SAFIULINA, D., VEKSLER, V., ZHARKOVSKY, A. & KAASIK, A. 2006. Loss of mitochondrial membrane potential is associated with increase in mitochondrial volume: physiological role in neurones. *J Cell Physiol,* 206, 347-53.

SÁNCHEZ-ARAGÓ, M., CHAMORRO, M. & CUEZVA, J. M. 2010. Selection of cancer cells with repressed mitochondria triggers colon cancer progression. *Carcinogenesis,* 31, 567.

SÁNCHEZ-CENIZO, L., FORMENTINI, L., ALDEA, M., ORTEGA, Á. D., GARCÍA-HUERTA, P., SÁNCHEZ-ARAGÓ, M. & CUEZVA, J. M. 2010. Up-regulation of the ATPase Inhibitory Factor 1 (IF1) of the Mitochondrial H+-ATP Synthase in Human Tumors Mediates the Metabolic Shift of Cancer Cells to a Warburg Phenotype. *Journal of Biological Chemistry,* 285, 25308-25313.

SANTEL, A. & FULLER, M. T. 2001. Control of mitochondrial morphology by a human mitofusin. *J Cell Sci,* 114, 867-74.

SAOTOME, M., SAFIULINA, D., SZABADKAI, G., DAS, S., FRANSSON, A., ASPENSTROM, P., RIZZUTO, R. & HAJNOCZKY, G. 2008. Bidirectional Ca2+-dependent control of mitochondrial dynamics by the Miro GTPase. *Proc Natl Acad Sci U S A,* 105, 20728-33.

SATO, S., MURATA, A., ORIHARA, T., SHIRAKAWA, T., SUENAGA, K., KIGOSHI, H. & UESUGI, M. 2011. Marine natural product aurilide activates the OPA1-mediated apoptosis by binding to prohibitin. *Chem Biol,* 18, 131-9.

SAUVANET, C., DUVEZIN-CAUBET, S., DI RAGO, J. P. & ROJO, M. 2010. Energetic requirements and bioenergetic modulation of mitochondrial morphology and dynamics. *Semin Cell Dev Biol,* 21, 558-65.

SCHIEKE, S. M., PHILLIPS, D., MCCOY, J. P., JR., APONTE, A. M., SHEN, R. F., BALABAN, R. S. & FINKEL, T. 2006. The mammalian target of rapamycin (mTOR) pathway regulates mitochondrial oxygen consumption and oxidative capacity. *J Biol Chem,* 281**,** 27643-52.

SCHON, E. A. & GILKERSON, R. W. 2010. Functional complementation of mitochondrial DNAs: mobilizing mitochondrial genetics against dysfunction. *Biochim Biophys Acta,* 1800, 245-9.

SCHON, E. A. & PRZEDBORSKI, S. 2011. Mitochondria: the next (neurode)generation. *Neuron,* 70, 1033-53.

SCHUBERT, D. 2005. Glucose metabolism and Alzheimer's disease. *Ageing Res Rev,* 4**,** 240-57.

SMITH, A. C., BRUCE, C. R. & DYCK, D. J. 2005. AMP kinase activation with AICAR simultaneously increases fatty acid and glucose oxidation in resting rat soleus muscle. *J Physiol,* 565**,** 537-46.

SCORRANO, L., ASHIYA, M., BUTTLE, K., WEILER, S., OAKES, S. A., MANNELLA, C. A. & KORSMEYER, S. J. 2002. A distinct pathway remodels mitochondrial cristae and mobilizes cytochrome c during apoptosis. *Dev Cell,* 2, 55-67.

SEMENZA, G. L. 2010. Defining the role of hypoxia-inducible factor 1 in cancer biology and therapeutics. *Oncogene,* 29, 625-34.

SEMENZATO, M., COGLIATI, S. & SCORRANO, L. 2011. Prohibitin(g) cancer: aurilide and killing by Opa1-dependent cristae remodeling. *Chem Biol,* 18, 8-9.

SESAKI, H., SOUTHARD, S. M., YAFFE, M. P. & JENSEN, R. E. 2003. Mgm1p, a dynamin-related GTPase, is essential for fusion of the mitochondrial outer membrane. *Mol Biol Cell,* 14, 2342-56.

SHERIDAN, C., DELIVANI, P., CULLEN, S. P. & MARTIN, S. J. 2008. Bax- or Bak-induced mitochondrial fission can be uncoupled from cytochrome C release. *Mol Cell,* 31, 570-85.

SHERIDAN, C. & MARTIN, S. J. 2010. Mitochondrial fission/fusion dynamics and apoptosis. *Mitochondrion,* 10, 640-8.

SHIN-BUEHRING, Y., LEITNER, H., HENSELEIT, H., WIRTZ, A., HAAS, B. & SCHAUB, J. 1979. Characteristics of galactokinase and galactose-1-phosphate uridyltransferase in cultivated fibroblasts and amniotic fluid cells. *Human Genetics,* 48, 31-37.

SHIRENDEB, U. P., CALKINS, M., MANCZAK, M., ANEKONDA, V., DUFOUR, B., MCBRIDE, J. L., MAO, P. & REDDY, P. H. 2011. Mutant huntingtin's interaction with mitochondrial protein Drp1 impairs mitochondrial biogenesis and causes defective axonal transport and synaptic degeneration in Huntington's disease. *Human Molecular Genetics.*

SIEVERS, C., BILLIG, G., GOTTSCHALK, K. & RUDEL, T. 2010. Prohibitins are required for cancer cell proliferation and adhesion. *PLoS One,* 5, e12735.

SMIGRODZKI, R., PARKS, J. & PARKER, W. D. 2004. High frequency of mitochondrial complex I mutations in Parkinson's disease and aging. *Neurobiol Aging,* 25, 1273-81.

SMIRNOVA, E., GRIPARIC, L., SHURLAND, D. L. & VAN DER BLIEK, A. M. 2001. Dynamin-related protein Drp1 is required for mitochondrial division in mammalian cells. *Mol Biol Cell,* 12, 2245-56.

SMIRNOVA, E., SHURLAND, D. L., RYAZANTSEV, S. N. & VAN DER BLIEK, A. M. 1998. A human dynamin-related protein controls the distribution of mitochondria. *J Cell Biol,* 143, 351-8.

SMOLKOVA, K., PLECITA-HLAVATA, L., BELLANCE, N., BENARD, G., ROSSIGNOL, R. & JEZEK, P. 2011. Waves of gene regulation suppress and then restore oxidative phosphorylation in cancer cells. *Int J Biochem Cell Biol,* 43, 950-68.

SOLAINI, G., SGARBI, G. & BARACCA, A. 2011. Oxidative phosphorylation in cancer cells. *Biochim Biophys Acta,* 1807, 534-42.

SONG, W., CHEN, J., PETRILLI, A., LIOT, G., KLINGLMAYR, E., ZHOU, Y., POQUIZ, P., TJONG, J., POULADI, M. A., HAYDEN, M. R., MASLIAH, E., ELLISMAN, M., ROUILLER, I., SCHWARZENBACHER, R., BOSSY, B., PERKINS, G. & BOSSY-WETZEL, E. 2011. Mutant huntingtin binds the mitochondrial fission GTPase dynamin-related protein-1 and increases its enzymatic activity. *Nat Med,* 17, 377-82.

SONG, Z., CHEN, H., FIKET, M., ALEXANDER, C. & CHAN, D. C. 2007. OPA1 processing controls mitochondrial fusion and is regulated by mRNA splicing, membrane potential, and Yme1L. *J Cell Biol,* 178, 749-55.

SONG, Z., GHOCHANI, M., MCCAFFERY, J. M., FREY, T. G. & CHAN, D. C. 2009. Mitofusins and OPA1 mediate sequential steps in mitochondrial membrane fusion. *Mol Biol Cell,* 20, 3525-32.

STOJANOVSKI, D., KOUTSOPOULOS, O. S., OKAMOTO, K. & RYAN, M. T. 2004. Levels of human Fis1 at the mitochondrial outer membrane regulate mitochondrial morphology. *J Cell Sci,* 117, 1201-10.

STRAUSS, M., HOFHAUS, G., SCHRODER, R. R. & KUHLBRANDT, W. 2008. Dimer ribbons of ATP synthase shape the inner mitochondrial membrane. *EMBO J,* 27, 1154-60.

SUEN, D. F., NORRIS, K. L. & YOULE, R. J. 2008. Mitochondrial dynamics and apoptosis. *Genes Dev,* 22, 1577-90.

SUN, Q., CHEN, X., MA, J., PENG, H., WANG, F., ZHA, X., WANG, Y., JING, Y., YANG, H., CHEN, R., CHANG, L., ZHANG, Y., GOTO, J., ONDA, H., CHEN, T., WANG, M. R., LU, Y., YOU, H., KWIATKOWSKI, D. & ZHANG, H. 2011. Mammalian target of rapamycin up-regulation of pyruvate kinase isoenzyme type M2 is critical for aerobic glycolysis and tumor growth. *Proc Natl Acad Sci U S A,* 108, 4129-34.

SUN, M. G., WILLIAMS, J., MUNOZ-PINEDO, C., PERKINS, G. A., BROWN, J. M., ELLISMAN, M. H., GREEN, D. R. & FREY, T. G. 2007. Correlated three-dimensional light and electron microscopy reveals transformation of mitochondria during apoptosis. *Nat Cell Biol,* 9, 1057-65.

SWERDLOW, R. H. 2009a. Mitochondrial Medicine and the Neurodegenerative Mitochondriopathies. *Pharmaceuticals (Basel),* 2, 150-167.

SWERDLOW, R. H. 2009b. The neurodegenerative mitochondriopathies. *J Alzheimers Dis,* 17, 737-51.

SZCZEPANOWSKA, J., ZABLOCKI, K. & DUSZYNSKI, J. 2004. Influence of a mitochondrial genetic defect on capacitative calcium entry and mitochondrial organization in the osteosarcoma cells. *FEBS Lett,* 578, 316-22.

TAKEDA, Y., PEREZ-PINZON, M. A., GINSBERG, M. D. & SICK, T. J. 2004. Mitochondria consume energy and compromise cellular membrane potential by reversing ATP synthetase activity during focal ischemia in rats. *J Cereb Blood Flow Metab,* 24, 986-92.

TAN, A. R., CAI, A. Y., DEHESHI, S. & RINTOUL, G. L. 2011. Elevated intracellular calcium causes distinct mitochondrial remodelling and calcineurin-dependent fission in astrocytes. *Cell Calcium,* 49, 108-14.

TATSUTA, T., MODEL, K. & LANGER, T. 2005. Formation of membrane-bound ring complexes by prohibitins in mitochondria. *Mol Biol Cell,* 16, 248-59.

TELFORD, J. E., KILBRIDE, S. M. & DAVEY, G. P. 2009. Complex I is rate-limiting for oxygen consumption in the nerve terminal. *J Biol Chem,* 284, 9109-14.

TIEU, Q. & NUNNARI, J. 2000. Mdv1p is a WD repeat protein that interacts with the dynamin-related GTPase, Dnm1p, to trigger mitochondrial division. *J Cell Biol,* 151, 353-66.

TONDERA, D., CZAUDERNA, F., PAULICK, K., SCHWARZER, R., KAUFMANN, J. & SANTEL, A. 2005. The mitochondrial protein MTP18 contributes to mitochondrial fission in mammalian cells. *J Cell Sci,* 118, 3049-59.

TONDERA, D., GRANDEMANGE, S., JOURDAIN, A., KARBOWSKI, M., MATTENBERGER, Y., HERZIG, S., DA CRUZ, S., CLERC, P., RASCHKE, I., MERKWIRTH, C., EHSES, S., KRAUSE, F., CHAN, D. C., ALEXANDER, C., BAUER, C., YOULE, R., LANGER, T. & MARTINOU, J. C. 2009. SLP-2 is required for stress-induced mitochondrial hyperfusion. *EMBO J,* 28, 1589-600.

TONDERA, D., SANTEL, A., SCHWARZER, R., DAMES, S., GIESE, K., KLIPPEL, A. & KAUFMANN, J. 2004. Knockdown of MTP18, a novel phosphatidylinositol 3-kinase-dependent protein, affects mitochondrial morphology and induces apoptosis. *J Biol Chem,* 279, 31544-55.

TRIMMER, P. A., SWERDLOW, R. H., PARKS, J. K., KEENEY, P., BENNETT, J. P., JR., MILLER, S. W., DAVIS, R. E. & PARKER, W. D., JR. 2000. Abnormal mitochondrial morphology in sporadic Parkinson's and Alzheimer's disease cybrid cell lines. *Exp Neurol,* 162, 37-50.

TURRENS, J. F. 2003. Mitochondrial formation of reactive oxygen species. *J Physiol,* 552, 335-44.

TWIG, G., ELORZA, A., MOLINA, A. J., MOHAMED, H., WIKSTROM, J. D., WALZER, G., STILES, L., HAIGH, S. E., KATZ, S., LAS, G., ALROY, J., WU, M., PY, B. F., YUAN, J., DEENEY, J. T., CORKEY, B. E. & SHIRIHAI, O. S. 2008a. Fission and selective fusion govern mitochondrial segregation and elimination by autophagy. *EMBO J,* 27, 433-46.

TWIG, G., HYDE, B. & SHIRIHAI, O. S. 2008b. Mitochondrial fusion, fission and autophagy as a quality control axis: the bioenergetic view. *Biochim Biophys Acta,* 1777, 1092-7.

UO, T., KINOSHITA, Y. & MORRISON, R. S. 2005. Neurons exclusively express N-Bak, a BH3 domain-only Bak isoform that promotes neuronal apoptosis. *J Biol Chem,* 280, 9065-73.

VAN LAAR, V. S. & BERMAN, S. B. 2009. Mitochondrial dynamics in Parkinson's disease. *Exp Neurol,* 218, 247-56.

VANDER HEIDEN, M. G., CANTLEY, L. C. & THOMPSON, C. B. 2009. Understanding the Warburg effect: the metabolic requirements of cell proliferation. *Science,* 324, 1029.

VAUGHN, A. E. & DESHMUKH, M. 2008. Glucose metabolism inhibits apoptosis in neurons and cancer cells by redox inactivation of cytochrome c. *Nat Cell Biol,* 10, 1477-83.

WAGNER, K., PERSCHIL, I., FICHTER, C. D. & VAN DER LAAN, M. 2010. Stepwise Assembly of Dimeric F1Fo-ATP Synthase in Mitochondria Involves the Small Fo-Subunits k and i. *Molecular Biology of the Cell,* 21, 1494-1504.

WALLACE, D. C. 1999. Mitochondrial diseases in man and mouse. *Science,* 283, 1482-8.

WANG, X. & SCHWARZ, T. L. 2009. The mechanism of Ca2+ -dependent regulation of kinesin-mediated mitochondrial motility. *Cell,* 136, 163-74.

WANG, X., SU, B., FUJIOKA, H. & ZHU, X. 2008a. Dynamin-like protein 1 reduction underlies mitochondrial morphology and distribution abnormalities in fibroblasts from sporadic Alzheimer's disease patients. *Am J Pathol,* 173, 470-82.

WANG, X., SU, B., LEE, H. G., LI, X., PERRY, G., SMITH, M. A. & ZHU, X. 2009a. Impaired balance of mitochondrial fission and fusion in Alzheimer's disease. *J Neurosci,* 29, 9090-103.

WANG, X., SU, B., SIEDLAK, S. L., MOREIRA, P. I., FUJIOKA, H., WANG, Y., CASADESUS, G. & ZHU, X. 2008b. Amyloid-beta overproduction causes abnormal mitochondrial dynamics via differential modulation of mitochondrial fission/fusion proteins. *Proc Natl Acad Sci U S A,* 105, 19318-23.

WANG, X., SU, B., ZHENG, L., PERRY, G., SMITH, M. A. & ZHU, X. 2009b. The role of abnormal mitochondrial dynamics in the pathogenesis of Alzheimer's disease. *J Neurochem,* 109 Suppl 1, 153-9.

WARBURG, O. 1956. On respiratory impairment in cancer cells. *Science,* 124, 269-70.

WASIAK, S., ZUNINO, R. & MCBRIDE, H. M. 2007. Bax/Bak promote sumoylation of DRP1 and its stable association with mitochondria during apoptotic cell death. *J Cell Biol,* 177, 439-50.

WATERHAM, H. R., KOSTER, J., VAN ROERMUND, C. W., MOOYER, P. A., WANDERS, R. J. & LEONARD, J. V. 2007. A lethal defect of mitochondrial and peroxisomal fission. *N Engl J Med,* 356, 1736-41.

WEIHOFEN, A., THOMAS, K. J., OSTASZEWSKI, B. L., COOKSON, M. R. & SELKOE, D. J. 2009. Pink1 Forms a Multiprotein Complex with Miro and Milton, Linking Pink1 Function to Mitochondrial Trafficking†. *Biochemistry,* 48, 2045-2052.

WESTERMANN, B. 2010. Mitochondrial fusion and fission in cell life and death. *Nat Rev Mol Cell Biol,* 11, 872-84.

WILLERS, I. M. & CUEZVA, J. M. 2011. Post-transcriptional regulation of the mitochondrial H(+)-ATP synthase: a key regulator of the metabolic phenotype in cancer. *Biochim Biophys Acta,* 1807, 543-51.

WU, M., NEILSON, A., SWIFT, A. L., MORAN, R., TAMAGNINE, J., PARSLOW, D., ARMISTEAD, S., LEMIRE, K., ORRELL, J., TEICH, J., CHOMICZ, S. & FERRICK, D. A. 2007. Multiparameter metabolic analysis reveals a close link between attenuated mitochondrial bioenergetic function and enhanced glycolysis dependency in human tumor cells. *Am J Physiol Cell Physiol,* 292, C125-36.

YALCIN, A., TELANG, S., CLEM, B. & CHESNEY, J. 2009. Regulation of glucose metabolism by 6-phosphofructo-2-kinase/fructose-2,6-bisphosphatases in cancer. *Exp Mol Pathol,* 86, 174-9.

YAMAGUCHI, R., LARTIGUE, L., PERKINS, G., SCOTT, R. T., DIXIT, A., KUSHNAREVA, Y., KUWANA, T., ELLISMAN, M. H. & NEWMEYER, D. D. 2008. Opa1-mediated cristae opening is Bax/Bak and BH3 dependent, required for apoptosis, and independent of Bak oligomerization. *Mol Cell,* 31, 557-69.

YAMAGUCHI, H. & WANG, H. G. 2001. The protein kinase PKB/Akt regulates cell survival and apoptosis by inhibiting Bax conformational change. *Oncogene,* 20, 7779-86.

YAO, J., CHEN, S., CADENAS, E. & BRINTON, R. D. 2011a. Estrogen protection against mitochondrial toxin-induced cell death in hippocampal neurons: antagonism by progesterone. *Brain Res,* 1379, 2-10.

YAO, J., CHEN, S., MAO, Z., CADENAS, E. & BRINTON, R. D. 2011b. 2-Deoxy-D-glucose treatment induces ketogenesis, sustains mitochondrial function, and reduces pathology in female mouse model of Alzheimer's disease. *PLoS One,* 6, e21788.

YOSHIDA, M., MUNEYUKI, E. & HISABORI, T. 2001. ATP synthase--a marvellous rotary engine of the cell. *Nat Rev Mol Cell Biol,* 2, 669-77.

YU, M., ZHOU, Y., SHI, Y., NING, L., YANG, Y., WEI, X., ZHANG, N., HAO, X. & NIU, R. 2007. Reduced mitochondrial DNA copy number is correlated with tumor progression and prognosis in Chinese breast cancer patients. *IUBMB Life,* 59, 450-7.

YU, T., ROBOTHAM, J. L. & YOON, Y. 2006. Increased production of reactive oxygen species in hyperglycemic conditions requires dynamic change of mitochondrial morphology. *Proceedings of the National Academy of Sciences of the United States of America,* 103, 2653-2658.

ZABLOCKAITE, D., GENDVILIENE, V., MARTISIENE, I. & JUREVICIUS, J. 2007. Effect of oxidative phosphorylation uncoupler FCCP and F1F0-ATPase inhibitor oligomycin on the electromechanical activity of human myocardium. *Adv Med Sci,* 52, 89-93.

ZALA, D., COLIN, E., RANGONE, H., LIOT, G., HUMBERT, S. & SAUDOU, F. 2008. Phosphorylation of mutant huntingtin at S421 restores anterograde and retrograde transport in neurons. *Hum Mol Genet,* 17, 3837-46.

ZANNA, C., GHELLI, A., PORCELLI, A. M., KARBOWSKI, M., YOULE, R. J., SCHIMPF, S., WISSINGER, B., PINTI, M., COSSARIZZA, A., VIDONI, S., VALENTINO, M. L., RUGOLO, M. & CARELLI, V. 2008. OPA1 mutations associated with dominant optic atrophy impair oxidative phosphorylation and mitochondrial fusion. *Brain,* 131, 352-67.

ZEEVALK, G. D., RAZMPOUR, R. & BERNARD, L. P. 2008. Glutathione and Parkinson's disease: is this the elephant in the room? *Biomed Pharmacother,* 62, 236-49.

ZEITELHOFER, M., VESSEY, J. P., THOMAS, S., KIEBLER, M. & DAHM, R. 2009. Transfection of cultured primary neurons via nucleofection. *Curr Protoc Neurosci,* Chapter 4, Unit4 32.

ZHANG, J., LIU, W., LIU, J., XIAO, W., LIU, L., JIANG, C., SUN, X., LIU, P., ZHU, Y., ZHANG, C. & CHEN, Q. 2010. G-protein beta2 subunit interacts with mitofusin 1 to regulate mitochondrial fusion. *Nat Commun,* 1, 101.

ZHANG, Y., GAO, X. & MICHAEL GARAVITO, R. 2011. Biochemical characterization of human dynamin-like protein 1. *J Biochem.*

ZHANG, Y., ZHANG, X., PARK, T. S. & GIDDAY, J. M. 2005. Cerebral endothelial cell apoptosis after ischemia-reperfusion: role of PARP activation and AIF translocation. *J Cereb Blood Flow Metab,* 25, 868-77.

ZHAO, J., LIU, T., JIN, S., WANG, X., QU, M., UHLEN, P., TOMILIN, N., SHUPLIAKOV, O., LENDAHL, U. & NISTER, M. 2011. Human MIEF1 recruits Drp1 to mitochondrial outer membranes and promotes mitochondrial fusion rather than fission. *EMBO J,* 30, 2762-78.

ZIVIANI, E., TAO, R. N. & WHITWORTH, A. J. 2010. Drosophila parkin requires PINK1 for mitochondrial translocation and ubiquitinates mitofusin. *Proc Natl Acad Sci U S A,* 107, 5018-23.

ZORZANO, A., LIESA, M. & PALACIN, M. 2009. Role of mitochondrial dynamics proteins in the pathophysiology of obesity and type 2 diabetes. *Int J Biochem Cell Biol,* 41, 1846-54.

ZOU, H., LI, Y., LIU, X. & WANG, X. 1999. An APAF-1.cytochrome c multimeric complex is a functional apoptosome that activates procaspase-9. *J Biol Chem,* 274, 11549-56.

ZUCHNER, S., MERSIYANOVA, I. V., MUGLIA, M., BISSAR-TADMOURI, N., ROCHELLE, J., DADALI, E. L., ZAPPIA, M., NELIS, E., PATITUCCI, A., SENDEREK, J., PARMAN, Y., EVGRAFOV, O., JONGHE, P. D., TAKAHASHI, Y., TSUJI, S., PERICAK-VANCE, M. A., QUATTRONE, A., BATTALOGLU, E., POLYAKOV, A. V., TIMMERMAN, V., SCHRODER, J. M. & VANCE, J. M. 2004. Mutations in the mitochondrial GTPase mitofusin 2 cause Charcot-Marie-Tooth neuropathy type 2A. *Nat Genet,* 36, 449-51.